Katholieke
Universiteit
Leuven

FACULTEIT DER WETENSCHAPPEN
Departement Scheikunde
Afdeling Coördinatiechemie

Mesomorphism and Optical Properties of Peripherally Substituted Phthalocyanines: Influence of Chain Length, Linking Group and Central Metal Ion

Promotor
Prof. Dr. K. Binnemans

Proefschrift ingediend voor het
behalen van de graad van Doctor
in de Wetenschappen
Jurgen Sleven

2002

Leden van de examencommissie

4 oktober 2002

Promotor:	Prof. Dr. K. Binnemans
Overige juryleden:	Prof. Dr. A. Ceulemans (Katholieke Universiteit Leuven)
	Prof. Dr. W. Dehaen (Katholieke Universiteit Leuven)
	Dr. B. Donnio (IPCMS, Straatsburg, Frankrijk)
	Prof. Dr. C. Görller-Walrand (Katholieke Universiteit Leuven)
	Prof. Dr. J. Hofkens (Katholieke Universiteit Leuven)
	Prof. Dr. G. Maes (Katholieke Universiteit Leuven)

Afdeling Coördinatiechemie, Departement Scheikunde, Faculteit Wetenschappen
Katholieke Universiteit Leuven

Dankwoord

Voor u ligt de vrucht van mijn vier jaren durende ontdekkingstocht doorheen de wereld van de vloeibaar-kristallijne ftalocyanines. Zoals menig doctoraat was dit geen tocht zonder hindernissen. Toch was het zonder meer een zeer boeiende periode, zowel op wetenschappelijk als persoonlijk gebied. Aan het einde van deze vier jaren rest er mij enkel nog de dankbare taak om de mensen te vermelden die dit alles mede mogelijk maakten.

Allereerst wens ik Prof. Dr. Christiane-Görller-Walrand te bedanken voor de mogelijkheid om, na een kleine onderbreking, alsnog mijn doctoraat aan te kunnen vatten in haar onderzoeksgroep. Op een gedeelde eerste plaats komt echter ook Prof. Dr. Koen Binnemans wiens wetenschappelijke ijver en gedrevenheid mij met de jaren meer respect heeft doen afdwingen. Ik voel me dan ook bevoorrecht om als een van de eersten te mogen promoveren onder zijn directe supervisie. Met plezier denk ik terug aan mijn 'pionierstijd' wanneer we in 1998 nog met slechts drie doctorandi (zelfs vrije) dagen doorbrachten met het herinrichten van de eerste labo's met het oog op de synthese van onze vloeibare kristallen. Ondertussen groeide de groep 'lichtjes' aan en dit bracht dan ook weer meer organisatorische problemen met zich mee die dienden aangepakt, waar ik graag mijn steentje aan heb proberen bijdragen.

Uiteraard is het wetenschappelijk werk in deze thesis niet louter het resultaat van de inzet van één iemand en daarom wens ik ook een aantal mensen in het bijzonder te bedanken. Petra Bloemen, Liesbet Jongen en Leen Van Nerum van onze afdeling voor het uitvoeren van de (niet altijd evidente) CHN, IR en TGA metingen. Mijn neef, Daniël Nelis en zijn promotor Prof. Jules Mullens van het Limburgs Universitair Centrum voor de TGA-analyses. Dr. Geert Baggerman van het laboratorium voor Ontwikkelingsfysiologie en Moleculaire Biologie (Prof. A. De Loof) voor de MALDI-TOF analyses en Ing. René de Boer voor de andere massaspectra. Dr. Dirk Hinz at the University of Köln in Germany (Prof. Gerd Meyer) for some of the XRD-measurements. Je tiens à remercier Prof. Daniel Guillon pour l'opportunité qui m'a été offerte de pouvoir effectuer mes analyses XRD à l'IPCMS à Strasbourg. Et encore un grand merci à Dr. Bertrand Donnio et aux autres là-bas pour les bons conseils et le temps agréable passé parmi vous.

Ook bedank ik mijn thesisstudenten Judith, Thomas en Bert voor hun bijdrage aan dit project.

Ook ben ik veel dank verschuldigd aan Rita, Firmin en Linda voor de ondersteuning bij alle kleine en grote administratieve en logistieke problemen. Voor de financiële zekerheid gedurende mijn doctoraatsjaren ben ik een grote blijk van dank verschuldigd aan het IWT en allen die me hierop voorbereidden, in het bijzonder Rik, wiens ervaringen en (wan)smaak voor humor een bijzondere stimulans vormden. Tenslotte bedank ik ook de andere labogenoten voor wie mijn ‘groene chemie’ ook moeilijk onopgemerkt kon blijven.

Een laatste (en niet te onderschatten) factor die bijgedragen heeft tot het resultaat dat nu voor u ligt vormen de mensen die samen met mij de afgelopen jaren buiten de labo-uren het leven op allerlei manieren zoveel aangenamer maakten. Hierbij denk ik aan de harde kern van de Kloosterlaan, de vrienden van thuis, de jong-KVCV’ers en eenieder die mijn sympathieën voor sport, de betere grooves en het leven deelde: keep the vibe alive ! Mijn ouders die mij steunden van het begin tot het einde: bedankt voor alles !! En tenslotte, Pascale, ook jij bedankt voor je liefdevol begrip en aanpassingsvermogen aan mijn bioritme, wat deze laatste (belastende) maanden toch een pak lichter maakten.

Table of Contents

List of abbreviations and acronyms

B	B-band or Soret band
Col_h	hexagonal columnar mesophase
Col_{ho}	ordered hexagonal columnar mesophase
Col_{hd}	disordered hexagonal columnar mesophase
Col_o	oblique hexagonal columnar mesophase
Col_r	rectangular columnar mesophase
Col_{ro}	ordered rectangular columnar mesophase
Col_{rd}	disordered rectangular columnar mesophase
Col_t	tetragonal columnar mesophase
CHN	elemental microanalysis (CHN-analysis)
Cr	crystalline phase
DBN	1,5-diazabicyclo[4.3.0]non-5-ene
DBU	1,5-diazabicyclo[5.4.0]undec-7-ene
DCM	dichloromethane
Dec	decomposition
DMAE	dimethylethanolamine
DMF	dimethylformamide
DSC	differential scanning calorimetry
I	isotropic liquid
IR	infrared spectroscopy
MALDI-TOF	matrix-assisted laser desorption ionisation time-of-flight mass spectrometry
MCD	magnetic circular dichroism spectroscopy

NMR	nuclear magnetic resonance
PcH_2	metal-free unsubstituted phthalocyanine
Pc	phthalocyanine
Pc_2Ln	bis(phthalocyaninato)lanthanide(III) sandwich complex
PcM	phthalocyanine transition metal complex
POM	polarising optical microscopy
Q	Q-band
TGA	thermogravimetric analysis
UV/VIS	ultraviolet/visible spectroscopy
XRD	X-ray diffraction

Chapter 1

INTRODUCTION

Phthalocyanines (Figure 1) form a colourful class of macrocyclic compounds, attracting the attention of many scientists. Some of these compounds – especially the metal containing phthalocyanines – play an important role in industrial activity and in society. Soon after the accidental discovery of Cu(II)-phthalocyanine in 1927, metallophthalocyanines came into use as blue and green dyes [DeDvon27]. Every year, thousands of tons of phthalocyanine material are being produced for the use in the textile industry as dyes, in the printing industry as pigments for inks, in the fuel industry as a catalyst for the removal of sulphur and in xerography as a photoconductor [MosTho63, Lev65, LezLev96, McK98].

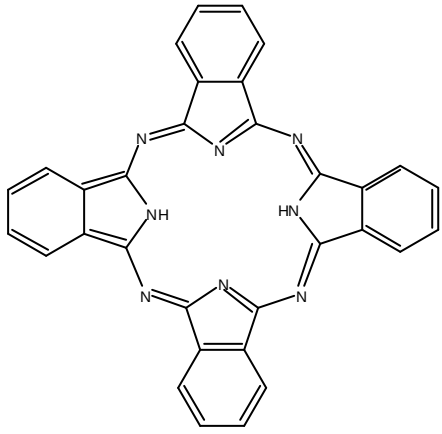

Figure 1 - Structure of the phthalocyanine molecule

Other applications for phthalocyanine compounds are found in the fields of non-linear optics (NLO), catalysis, electronic (bio)sensors, photovoltaic solar cells, optical data storage, lubricants, photo- and radiosensitizers for treatment of cancer, protein inhibitors… [VidFic98, McK98, Alivan99, RodSou99, Eic00, PriRai00].

The loss of the central hydrogen atoms results in the formation of a phthalocyanine dianion (Pc^{2-}), which can bind a metal ion and hence form metal complexes. Many different (transition) metal complexes have been synthesised over the years, giving rise to compounds with different physical and chemical properties. The trivalent lanthanide ions form with phthalocyanines (Pc) complexes of the type Pc_2Ln, where the lanthanide ion is sandwiched between two phthalocyanine rings (Figure 2). Compounds of this type are only known since the middle 1960's [KirMos65] and they have awoken the interest of chemists because of their electrochromic properties i.e. an electrochemically induced colour change. When a thin film of Pc_2Lu (Pc = phthalocyanine) deposited on an electrode is submersed in an electrolyte, the colour of the complex will vary (red, green, blue) according to the cell potential.

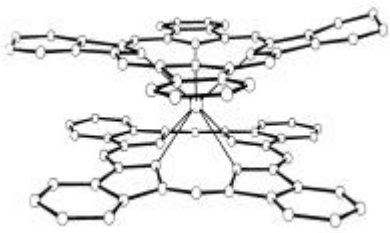

Figure 2 - Structure of the lanthanide metal sandwich complex

When substituents are placed on the Pc-ring (Figure 3), not only the solubility of the compounds increases [HanHai93], but supramolecular organisation can be achieved too. Liquid-crystalline behaviour of phthalocyanines was first demonstrated in an alkoxymethyl-substituted Cu(II)-phthalocyanine in 1982 by

Simon and co-workers [PieSim82]. The aromatic phthalocyanine core can be considered as the core of a discotic mesogen forming a supramolecular organisation and exhibiting columnar mesophases. The transition from the solid state to the liquid-crystalline phase (melting point) corresponds to the melting of the flexible side chains. The aromatic cores keep their positional and orientational order. The transition from the mesophase to the isotropic liquid (clearing point) corresponds to the breakdown of the columns.

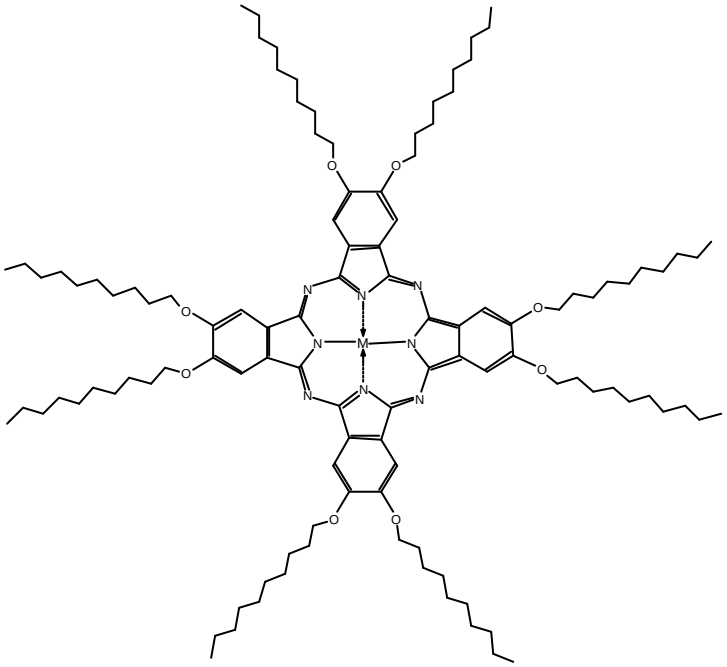

Figure 3 - Liquid-crystalline phthalocyanine complex

Liquid-crystalline phthalocyanines offer the possibility of combining the opto-electronic properties of the phthalocyanines with the orientational control of conventional liquid-crystal systems. The columnar architecture of the mesophase suggested the possibility to use them as anisotropic electric conductors. Charge

transport along the columns would be facilitated by the substantial π-π orbital overlap of the aromatic cores, whereas the molten alkyl chains would hinder the electric conductivity perpendicular to the columnar axes. Since the discovery of the first liquid-crystalline phthalocyanine, various mesogenic phthalocyanines have been prepared, but with a limited variation for the central metal ion: mainly the copper(II) ion was used.

Simon *et al*. also were the first to investigate the liquid-crystalline octa-alkoxy substituted phthalocyanine lutetium(III) complex in 1985 [PieSim85]. Since then only a few papers have been published on this class of metallomesogens and moreover, most studies of liquid-crystalline Pc_2Ln compounds have been restricted to Lu(III) as the metal ion [BinGör02]. Liquid-crystalline phthalocyanines are being investigated for potential use in the field of molecular electronics [SimSir89, SimBas93, vanPic94]. The columns formed by the discotic molecules can be regarded as submicroscopic wires. Bis(phthalocyaninato) lutetium(III) also shows semi-conductive properties [AndHol85, MaiGui87].

In spite of the wide interest in this type of compounds, as mentioned above, so far only a limited number of liquid-crystalline phthalocyanine complexes have been studied. In this work we will describe the synthesis and thermal behaviour of octa-substituted phthalocyanine ligands and their complexes with different transition metal and lanthanide ions. We are interested in the systematic study of the influence of the central metal ion, the substituent type and the chain length on the thermal behaviour and optical properties. Three types of substituents were examined: alkoxy, alkyl and alkoxymethyl chains. The thermal behaviour was studied by optical microscopy, DSC, TGA-DTA and small angle X-ray diffraction experiments. Optical properties were investigated by absorption and MCD-spectroscopy. Although we were primarily interested in their thermal and optical properties, our compounds might become useful as thin films in the field of electrochromism, (bio)sensors, NLO, …

References

[Alivan99] H. Ali, J.E. van Lier, *Chem. Rev.*, **99**, 2379, 1999.

[AndHol85] J.J. André, K. Holczer, P. Petit, M.T. Riou, C. Clarisse, R. Even, M. Fourmigue, J. Simon, *Chem. Phys. Lett.*, **115**, 463, 1985.

[BinGör02] K. Binnemans, C. Görller-Walrand, *Chem. Rev.*, **102**, 2303, 2002.

[DeDvon27] H. de Diesbach, E. von der Weid, *Helv. Chim. Acta*, **10**, 886, 1927.

[Eic00] H. Eichhorn, *J. Porphyr. Phthalocya*., **4**, 88, 2000.

[HanHai93] M. Hanack, P. Haisch, H. Lehmann, L.R. Subramanian, *Synthesis*, 387, 1993.

[KirMos65] I.S. Kirin, P.N. Moskalev, Y.A. Makashev, *Russ. J. Inorg. Chem.*, **10**, 1065, 1965.

[LezLev96] C.C. Leznoff, A.B.P Lever , *Phthalocyanines, Properties and Applications*, Vols 1-4, VCH Weinheim, 1989.

[Lev65] A.B.P. Lever, *Adv. Inorg. Chem Radiochem.*, **7,** 27, 1965.

[MaiGui87] M. Maitrot, G. Guillaud, B. Boudjema, J.J. André, H. Strzelecka, J. Simon en R. Even, *Chem. Phys. Lett.*, **133**, 59, 1987.

[McK98] N.B. McKeown, *Phthalocyanine Materials: Synthesis, Structure and Function*, Cambridge University Press, 1998.

[MosTho63] F.H. Moser, A.L. Thomas, *Phthalocyanine Compounds*, Reinhold Publishing Corporation, 1963.

[PieSim82] C. Piechocki, J. Simon, A. Skoulios, D. Guillon, P. Weber, *J. Am. Chem. Soc.*, **104**, 5245, 1982.

[PieSim85] C. Piechocki, J. Simon, *J. Chem. Soc. Chem. Commun*., 259, 1985.

[PriRai00] S.A. Priola, A. Raines, W.S. Caughey, *Science*, **287**, 1503, 2000.

[RodSou99] M.L. Rodríguez-Méndez, J. Souto, R. de Saja, J. Martínez, J.A. de Saja, *Sensors and Actuators B*, **58**, 544, 1999.

[SimBas93] J. Simon, P. Bassoul, "Phthalocyanine based Liquid Crystals: Towards Submicronic Devices" in *Phthalocyanines, Properties and Applications*, Vol 3, eds. C.C. Leznoff en A.B.P. Lever, VCH Weinheim, 1993.

[SimSir89] J. Simon, C. Sirlin, *Pure & Appl. Chem.*, **61**, 1625, 1989.

[vanPic94] C.F. van Nostrum, S.J. Picken, R.J.M. Nolte, *Angew. Chem. Int. Ed. Engl.*, **33**, 2173, 1994.

[VidFic98] C. Videlot, D. Fichou, F. Garnier, *Mol. Cryst. Liq. Cryst.*, **322**, 319, 1998.

Chapter 2

LITERATURE OVERVIEW

2.1 Phthalocyanines

Unlike the structurally related porphyrins, phthalocyanines do not occur in nature. Moreover they were one of the first macrocycles that were synthesised in the laboratory. Because of their striking resemblance with hemes and chlorophyll, phthalocyanines are being used as models for these biomolecules. The molecular structure of the metal-free, unsubstituted phthalocyanine molecule is depicted in Figure 4. The twenty-eight reactive sites of the phthalocyanine have been numbered. A phthalocyanine molecule consists of four pyrrole-units or can be considered as the condensation product of four iso-indole groups. Other common names in nomenclature are: tetrabenzotetraazoporphyrin or tetrabenzo-porphyrazine.

There are sixteen possible sites for macrocycle substitution associated with the four benzo-subunits. The eight peripheral and eight non-peripheral hydrogen atoms can be replaced by various inorganic and organic substituents. Substitution in the eight peripheral positions (2,3,9,10,16,17,23,24-substituted phthalocyanines) with long chains yields more readily soluble phthalocyanines than the unsubstituted phthalocyanines (which almost do not dissolve in common organic solvents like dichloromethane or acetone). Most common substituents are alkyl (C_xH_{2x+1}), alkoxy (OC_xH_{2x+1}) or alkoxymethyl ($CH_2OC_xH_{2x+1}$) chains as will be illustrated later on in this chapter [GuiSko83, PieSim85, vanNee88, OhtJac88, SimBas93, EngBas93, SchWar94, ClaMcK95].

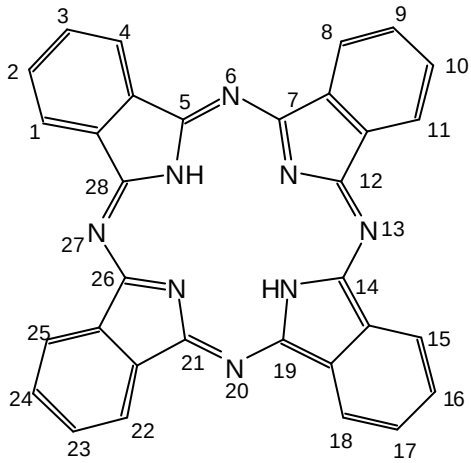

Figure 4 - Molecular representation of the metal-free, unsubstituted phthalocyanine; the reactive sites have been numbered according to the commonly accepted convention

The two hydrogen atoms in the central cavity can be replaced by metal ions (phthalocyanine can be regarded as a very weak dibasic acid). Hence a metallophthalocyanine is created. Figure 5 shows the Cu(II)-phthalocyanine.

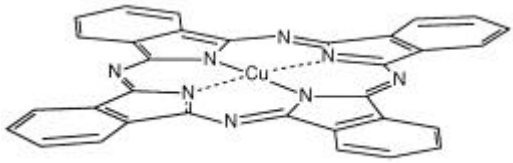

Figure 5 - Cu(II)-phthalocyanine

The next paragraphs will give a synopsis of the history and the applications of phthalocyanines as well as a short overview of the possible ways of preparing phthalocyanine ligands and complexes.

2.1.1 The history of phthalocyanine

Phthalocyanine, like many other synthetic products, was discovered by serendipity, rather than by a breakthrough in a targeted research scheme [Elv99, Gre99, McK99]. During the synthesis of *ortho*-cyanobenzamide starting from phthalimide and acetic acid (Scheme 1), Braun and Tcherniac (South Metropolitan Gas Company, London) noticed in 1907 a dark, insoluble impurity [BraTch07].

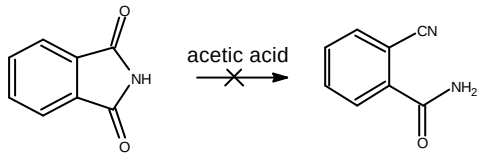

Scheme 1 – Attempted synthesis of ortho-cyanobenzamide by Braun and Tcherniac (1907)

Unfortunately, they did not pay further attention to this observation. In 1927 de Diesbach and von der Weid (Université de Fribourg, Switzerland) observed a very stable blue product that was formed in a 23 % yield during the reaction of *ortho*-dibromobenzene with copper(I) cyanide in boiling pyridine, the aim being the synthesis of the corresponding *ortho*-dinitrile (Scheme 2).

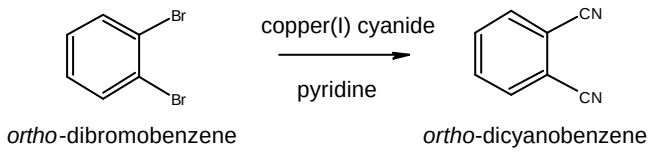

Scheme 2 - Synthesis of ortho-dicyanobenzene by de Diesbach and von der Weid (1927)

The elemental analysis of that time corresponded to that of the (unknown) copper phthalocyanine complex. Furthermore the stability of the product in alkaline media, in concentrated sulphuric acid and under heating was witnessed. Their results were published and the article ended with a plea for further investigation of

this remarkable new substance: '*Retenues par d'autres travaux, nous serions heureux si les collègues plus spécialisés dans l'étude des sels complexes voudraient bien éclaircir la constitution et les causes de la stabilité des nouveaux produits*' [DeDvon27]. In spite of their request, the full elucidation of phthalocyanine was the result of yet another 'accident' in 1928 on an industrial site of Scottish Dyes Ltd. in Grangemouth. On the site, phthalimide was made starting from phthalic anhydride. A plant chemist (A.G. Dandridge) noticed a blue colour around the charge hole, presuming a contamination with a blue pigment (dibromo-indanthrone) produced on the site next-door. Nevertheless the material was investigated and found to be an entirely different iron-containing compound. The chemists of Scottish Dyes (Dandridge, Dunworth, Thomas, and Drescher) soon discovered a crack in the glass reaction vessel that was surrounded by an outer steel casing. A synthesis was then carried out with phthalic anhydride, ammonia and iron filings, and it yielded the blue impurity. The potential of the stable iron-containing product was acknowledged and in 1929 a patent was granted to ICI, who had acquired Scottish Dyes earlier on that year [DanDre29]. In order to understand the structure of the mysterious compound, a sample was sent to Professor Reginald Linstead at Imperial College (London). He devoted a series of papers to the elucidation of the structure of phthalocyanine and the synthesis of some of its metal derivatives [Lin34, LinLow34a, LinLow34b, ByrLin34, DenLin34a, DenLin34b]. The structure Linstead proposed (based on elemental analysis, ebullioscopic molecular mass determination and oxidative degradation) was later confirmed by Robertson using X-ray diffraction. This was the first organic compound to have its structure confirmed by this technique [Rob35, Rob36a, Rob36b, Rob37, Rob40].

Linstead was also the first to use the name '*phthalocyanine*'. With this name he denoted the origin from phthalic anhydride and its derivatives (*phthalo* comes from the Greek *nafta*, meaning rock oil) and the dominating blue colour (*cyanine* which is the Greek for blue). Taking into account that already a long time before the

discovery by Braun en Tcherniac, research was done on phthalocyanine precursors like phthalonitrile and phthalimide at temperatures of 100 to 200 °C, it is most likely that they were not the first to have accidentally synthesised phthalocyanine, but they were the first to report on it. Figure 6 gives a schematic overview of the history of the phthalocyanines.

1819	discovery of naphthalene by Kidd
1821	naphthalene gets its name
1836	discovery of *ortho*-phthalic acid by Laurent
1907	accidental discovery of phthalocyanine by Braun and Tcherniac
1927	- de Diesbach and von der Weid discover copper(II) phthalocyanine by accident - patent phthalocyanine production process
1928	'accident' leading to the 'final' discovery of iron phthalocyanine at Scottish Dyes Inc.
1933	- first use of name “phthalocyanine” by Linstead - formula found by means of chemical methods by Linstead
1935	- X-ray structure determination of Pc by Robertson - industrial scale production of PcCu (ICI)
1936	- first double-decker Pc: Pc_2Sn - industrial scale production by I.G. Farbenindustrie, Ludwigshafen
1937	Du Pont starts producing Pc compounds
1949	Standard Ultramarine & Colour Company starts production Pc
1973	electronic structure of MPc mapped by Schaffer *et al.* [SchGou73]
1982	synthesis of the first liquid-crystalline phthalocyanine compound
1986	synthesis of Pc containing crown ethers
1990	calculation of electronic structure of PcH_2 by Orti *et al.* [OrtBré90]

Figure 6 - History of phthalocyanines

2.1.2 Applications of phthalocyanine

After the elucidation of its structure, phthalocyanine soon became eminent in the industrial production of pigments. ICI developed Monastral Blue (copper phthalocyanine) in 1935, what even resulted in a headline in the New York Times. Later that decade, IG Farbenindustrie in Ludwigshafen and the Du Pont Company in Deepwater Point (New Jersey) also started with the production of copper(II) phthalocyanine. The development of water-soluble dyes based on sulphonated phthalocyanines lead to applications in the textile branch. Still today many thousands of tons of phthalocyanine are produced in order to meet with the worldwide demand for blue and green dyes and pigments that are used in inks, textiles, car paint, plastics and photography [MosTho63, Lev65, LezLev96, McK98]. Continued industrial and academic interest in modified phthalocyanines has led to new applications in different fields, including hi-tech areas: semi-conductors, photoconductivity, electronic (bio)sensors, optical data storage, nonlinear optics, electrochromism, lubricants, catalysis, photodynamic therapy for treatment of cancer and protein inhibitors as anti-scrapie drugs [AndHol85, MaiGui87, SimSir89, SilLuk91, SimBas93, vanPic94, McK98, Alivan99, Eic00, PriRai00].

2.1.3 Synthesis of phthalocyanine

Scheme 3 gives an overview of different precursors that can be used for the synthesis of metal-free phthalocyanines. The most common precursor used in the laboratory synthesis is phthalonitrile (1,2-dicyanobenzene) [LezLev96]. In an intermediate step the phthalonitrile can first be converted into diiminoisoindoline, by reaction with ammonia. Next, the diiminoisoindoline will condense relatively easy to PcH_2 (by refluxing in a high-boiling alcohol). Reaction of the phthalonitrile in a melt with hydroquinone as a reductans forms a second synthesis path. Another possibility is the use of a strong organic base (e.g.

1,8-diazabicyclo[5.4.0]undec-7-ene (DBU) or 1,5-diazabicyclo[4.3.0]non-5-ene (DBN)) in a melt or with pentanol as a solvent [TomSai80, OliSmi87, WöhSch92]. Cyclotetramerisation in 2-dimethyl-aminoethanol (DMAE) also was suggested [BraGra70].

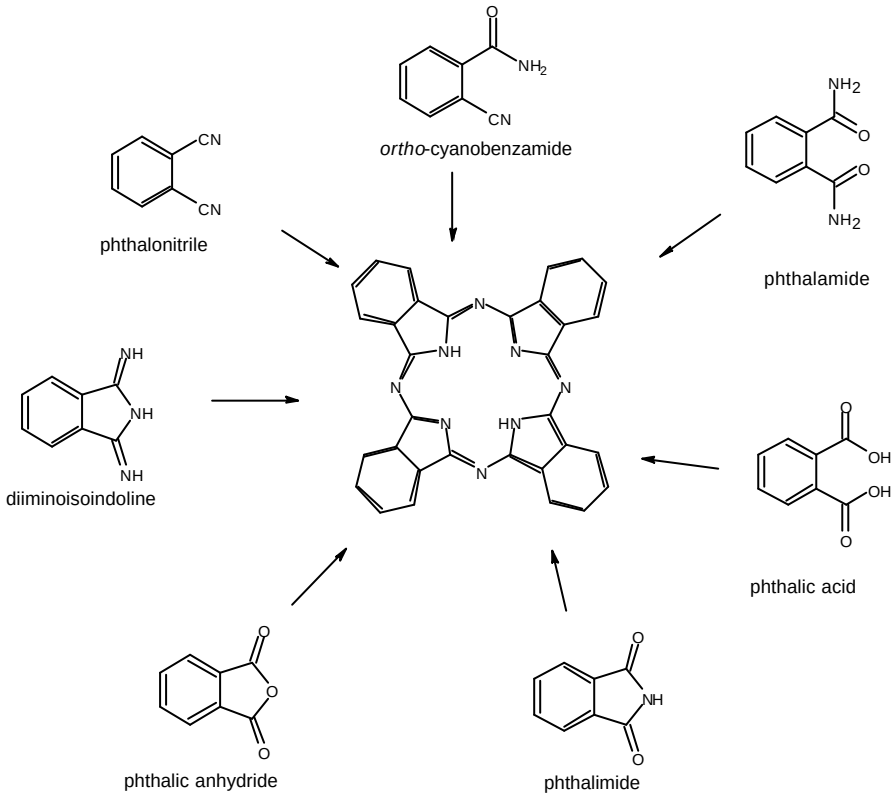

Scheme 3 - Synthetic pathways for the synthesis of PcH_2

Other precursors that can be used are: ortho-cyanobenzamide, phthalimide, phthalic acid and phthalic anhydride. For the three last precursors, urea is used as a nitrogen donor. An alternative is the synthesis of a lithium metal complex (template synthesis) followed by demetallation in a dilute acidic solution.

The synthesis of phthalocyanine metal complexes can also be approached in several different ways. A first major distinction is made between a chelating reaction and a template synthesis. In the former, a metal ion replaces the two hydrogen or lithium atoms bound to the pyrrole nitrogens [Pie82]. The use of Li_2Pc is preferred because it is more soluble in for example acetone, while PcH_2 requires the use of a high-boiling aromatic solvent as chloronaphthalene.

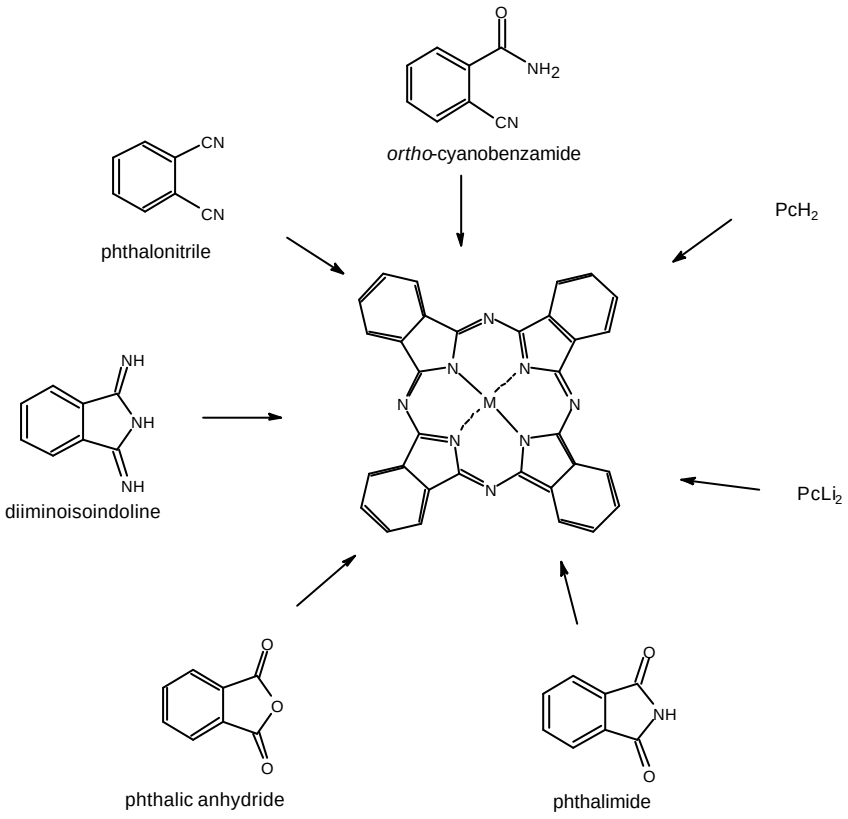

Scheme 4 - Pathways for the synthesis of metallophthalocyanine

The template synthesis takes advantage of the so-called template effect: *'a chemical template organises an assembly of atoms, with respect to one or more geometric loci, in order to achieve a particular linking of atoms'* [ShrAtk95, GerAri99]. In the case of the phthalocyanine complex, the geometric 'locus' is formed by the metal ion. It serves as the mould for the precursor building blocks, forming through a series of condensation reactions a macrocyclic compound. Both kinetic and thermodynamic forces can drive the template effect. For the synthesis of phthalocyanines, the thermodynamic effect is often regarded to be prevailing.

Scheme 4 shows the possible precursors that can be used. The precursor is mixed with an excess of the template ion (thus $n_{ion} > 1/4\ n_{precursor}$). The reaction can take place in a solvent like dimethylamino-ethanol (DMAE) or in a melt with urea and ammonium molybdate as a catalyst.

Tomodo *et al.* systematically investigated a number of parameters for the synthesis of phthalocyanines from phthalonitrile: presence of light (UV or daylight), temperature, reaction time, solvent and atmosphere [TomHib76]. They found the best yields using pentanol and stirring the mixture at reflux temperature in the presence of daylight. It has to be mentioned that they did come across moderate yields at room temperature when illuminating with UV-light. By these findings they suggested the importance of UV/VIS light in the mechanism.

During the course of our research project, Linaje *et al.* even reported on the multivariate analysis (Taguchi method) they performed on the synthetic procedure and purification methods of the lutetium bisphthalocyanine [LinQui00].

Also, recently microwave synthesis was found successful as an alternative energy source to activate the reaction [Sha98, Ung99, LiuLee01, VilHam01]. Advantages of this method are the shorter reaction times (<20 min vs. >2 h for conventional energy sources) and the generally higher yield. Electrochemical synthesis has also been proven useful [PetPli89, KhaBla99].

2.2 Metallophthalocyanines

So far, over seventy different metal ions have been used to synthesise metallophthalocyanines (Figure 7) [BarDen36, BarFry38, McK98]. The choice of the central metal ion can strongly affect the physical properties of the complex. In general, the phthalocyanine ligand is present as the dianion Pc^{2-}, but the macrocyclic ring can both be oxidised and reduced. Most cations are held firmly in the central cavity of the phthalocyanine ligand. Removing them can only be done by destroying the macrocycle.

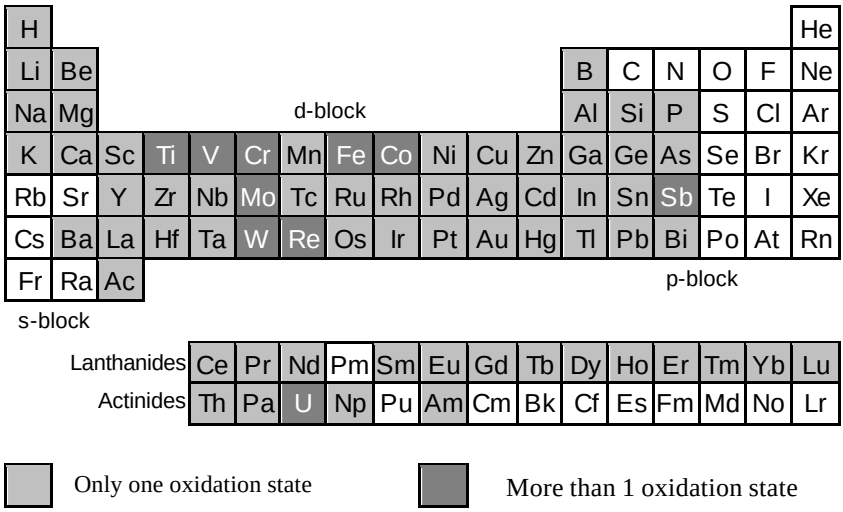

Figure 7 - Overview of known phthalocyanine metal complexes

2.2.1 Phthalocyanines chelated with s-block elements

Phthalocyanine will ligate two cations when the metal ion has as oxidation state +1 (Li^+, Na^+, K^+). Since they cannot fit both in the central cavity, the ring conformation will be disturbed from planar to a concave form. Because the stacking of concave molecules is less efficient than for planar molecules, the

solubility in polar solvents will increase. Bivalent ions s-block elements (e.g. Be^{2+}, Ca^{2+}) fit in the cavity and will not cause a significant distortion of the macrocycle.

2.2.2 Phthalocyanines chelated with d-block elements

The use of metal ions with oxidation states higher than +2 will yield complexes with axial ligands/counterions to equilibrate the charge balance (e.g. Ru^{4+}, Figure 8). This will also enhance the solubility.

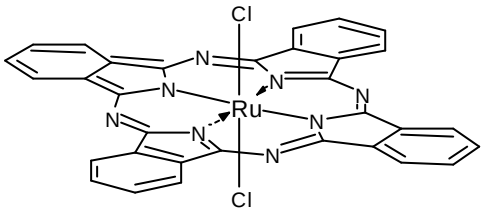

Figure 8 - Axially substituted RuPc

2.2.3 Phthalocyanines chelated with p-block elements

Axial substitution is also observed for the Si(IV), Ge(IV) and Sn(IV) Pc's. Some p-block ions are too big (> 0.8 Å) to fit in the cavity (e.g. Pb^{2+}, Sn^{2+}) and are situated above the plane of the phthalocyanine ring. The use of cations like Sn^{4+} will yield phthalocyanine complexes with five iminoisoindoline units instead of four, and a so-called super-phthalocyanine is formed [KraFer88]. A metallophthalocyanine with only three iminoisoindoline units – a subphthalocyanine – is formed by a template synthesis around a (small) borane ion [KobSud90]. Both a sub- and a super-phthalocyanine are represented in Figure 9.

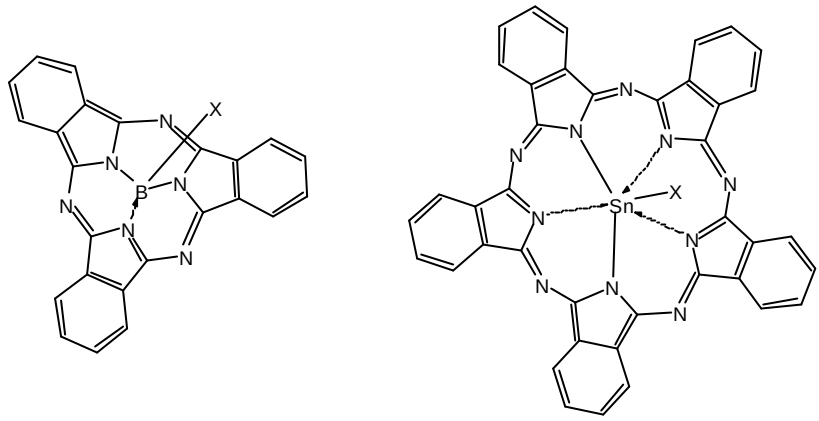

Figure 9 - Sub-phthalocyanine (left) and super-phthalocyanine (right)

2.2.4 Phthalocyanines chelated with lanthanides

The diameter of the trivalent lanthanide ions is too large to make them fit in the cavity of the tetra-iminoisoindoline macrocycle. These ions will form dimers with the lanthanide ion 'sandwiched' between two phthalocyanine ligands. The lutetium bisphthalocyanine is depicted in Figure 10.

Herr was one of the first to acknowledge the stability of the rare earth phthalocyanine complexes, which he used to isolate isotopes [HerGöt50, Her53]. Lanthanide bisphthalocyanines are still being studied because of their semi-conductive and electrochromic properties [CorGra79, ChaMar81, Mar82, MaiGui87]. Deposited as a thin film on an electrode, immersed in an electrolyte, lutetium(III)bisphthalocyanine exhibits five colours (violet, blue, green, yellow, red) when the voltage of the cell is varied between –1.5 and +1.5 V [MosKir72, NicGal77].

Since all four of the pyrrole hydrogens have disappeared and the ion is in a trivalent state, one of the ligands must carry only one negative charge. This problem has been the subject of intensive discussions throughout the years.

Kirin *et al*. initially obtained a blue and a green fraction by purification of a rare earth phthalocyanine by column chromatography. They identified the blue compound as the Pc_2LnH dimer by elemental analysis and suggested that the green compound was a monophthalocyanine LnPcCl, based upon its optical spectrum compared to other metal phthalocyanines. No satisfying elemental analysis results were obtained for this hypothesis, though. Acid-base reactions were explained by use of an unstable hydrogen atom [KirMos65, KirMos67, MosKir80]. MacKay *et al*. reported that both the blue and the green form were bisphthalocyanines, interconverting in different solvent environments, but again no reliable elemental analysis results were obtained [MacBoa74].

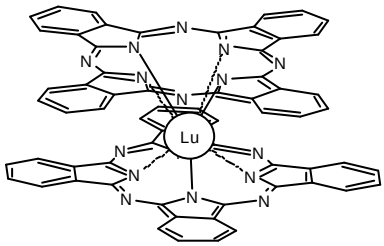

Figure 10 - Lutetium bisphthalocyanine

Nicholson *et al*. also proposed $LuPc_2H$ as the formula for the green product and appointed the colour transitions to faradaic processes, though in a later publication they turned to the Pc_2Ln formula [NicPiz79, NicPiz80, NicPiz81, NicWei84]. Corker *et al*. obtained lutetium bisphthalocyanine as a green compound for which they suggested the formula $[LuPc_2H]^+A^-$, A^- being an unidentified anion. They also showed that the blue and violet species could be obtained from the latter by electrochemical reduction, while a yellow-reddish compound was formed by oxidation [CorGra79]. Kasuga *et al*. demonstrated by X-ray photoelectron spectroscopy in 1980 that all eight central nitrogen atoms are chemically equivalent. Therefore, if an extra hydrogen atom would be present in the dimer, it

would not bind strongly to any of the nitrogen atoms in the complex [KasTsu80]. Based on magnetic susceptibility measurements and ESR spectroscopy Chang *et al*. concluded that the formula Pc_2Ln is favoured. The measurements indicated the presence of an unpaired electron for each Pc_2Ln molecule. Moreover the results confirmed that the radical is situated on the macrocyclic rings and not on the lanthanide ion. The complex can be represented as $Pc^{2-}Ln^{3+}Pc^{-\bullet}$ [ChaMar81]. Yamana *et al*. proposed a hydrogen-bonded polymer structure for the dimers, the proton located between the $[Pc_2Ln]H^+$ molecules [YamTsu82]. On the other hand, Colins *et al*. could not find the extra hydrogen by a thorough mass spectral analysis [ColSch82]. The multiplicity of opinions on the green compound and the inherent uncertainty on the blue, violet, yellow and red forms inspired L'Her *et al*. to investigate the electrochemical properties of the compound. They concluded that the transitions between the different forms are reversible mono-electronic redox reactions and no proton exchange is coupled to these reactions. Hence, they confirmed the conclusions drawn by Chang *et al*. [LheCoz85]. The representation of the green dimer as $Pc^{2-}Ln^{3+}Pc^{-\bullet}$ is now accepted. The lanthanide ion is sandwiched between the two phthalocyanine ligands. One ring is rotated by 45° with respect to the other. The interplanar distance between the two planes formed by the eight nitrogen atoms is 2.69 Å. Both macrocycles are strongly deformed and are both convex [DecMou85]. Consequently, the coordination polyhedron is a (distorted) square antiprism. By altering the reaction times and the reactant ratios, a triple-decker lanthanide compound (Pc_3Ln_2) could also be obtained [KasAnd86, MsaRon86].

2.2.5 Phthalocyanines chelated with actinides

Around the large uranyl cation (UO^{2+}) the template synthesis will yield, as for the Sn^{4+} cation, a super-phthalocyanine [DayMar74, MarSto78, CueSto80, CueMar81].

2.3 Liquid crystals

Liquid crystals are omni-present in modern society: the displays of watches, game-consoles, notebooks, mobile phones, digital cameras … Today, displays based on the liquid-crystalline technology form more than a concurrent to the classical cathode-ray tube (CRT) screens. Less well known is the fact that liquid crystals also play a dominant role in soaps, detergents and in living structures, where their function seems to be fundamental in the control of biochemical processes.

2.3.1 What are liquid crystals ?

A phase consists of a homogeneous, macroscopic volume of matter, separated by well-defined surfaces. By tradition, matter is thought of as being present in one of the following phases: a solid, a liquid or a gas. The solid phase was discovered to be present in a crystalline state or in a glassy state (a *glass*). Usually when a liquid is cooled to below its melting point, crystals form and it solidifies, but sometimes the liquid can be *supercooled* and remain fluid below its melting point because there are no nucleation sites to initiate the crystallisation. If the viscosity strongly increases as the liquid is cooled further it may never crystallise, and eventually become an amorphous solid. The molecules then have a disordered arrangement but sufficient cohesion to maintain some rigidity. This state is often called an amorphous solid or *glass*. A liquid to crystal transition is a thermodynamic one, i.e. the crystal is energetically more favourable than the liquid below the melting point. The glass transition is purely kinetic, i.e. the disordered glassy state does not have enough kinetic energy to overcome the potential energy barriers required for movement of the molecules along one another. The molecules of the glass take on a fixed but disordered arrangement.

The main difference between the solid (glass and crystal) phases and the liquid phase is the presence or absence of the three types of large-amplitude motion: translation, rotation and internal motion. The crystalline state is characterised by a

three-dimensional molecular positional and oriental order. The centres of gravity of the molecules are located on the knots of three-dimensional Bravais' networks and thus every crystalline structure is defined by a space group. The molecular order of the liquid is short-range with a complete loss of both positional and orientational order as the molecules are free to move randomly in all the directions of the space. Hence the liquid state is said to be isotropic. Phases existing between the solid state and the liquid phase were found. These phases were called *mesophases*, from the Greek 'mesos = in the middle', compounds showing the mesophase are called *mesogens*. These mesophases are: the *liquid crystalline state*, the *plastic crystalline state* and the *conformationally disordered state*. All these mesophases have their glassy equivalent, so we come to the schematic representation in Figure 11 as proposed by Wunderlich [Wun99]. The mesophases are characterised by an increase of disorder relative to a crystal and by the presence of distinct amounts of large-amplitude molecular motion. The mesophase material is referred to as the *mesogen*.

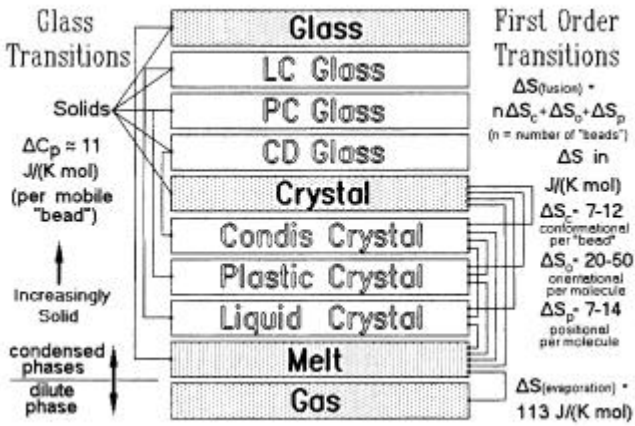

Figure 11 - Schematic representation of the classical phases and the mesophases (transitions are indicated by the connecting lines); after[Wun99]

Conformationally disordered crystals, discovered in 1975, show positional and orientational order of the molecule as a whole, but are partially or fully conformationally disordered and mobile. Polyethylene can exist as a conformationally disordered crystal.

Plastic crystals, first recognised in the 1930's, are related to the classical crystals, because they have full positional order. The molecules of plastic crystals are almost spherical and they are able to rotate at a given transition temperature. Because of the rotation, the crystals have weakly bound molecules and hence the crystals deform easily: they are plastic. Fullerene (C_{60}), HBr, and camphor are examples of molecules with a plastic crystalline phase.

The *liquid-crystalline state* was the first intermediate phase that was given the name *mesophase*. This was done by Friedel in 1922 [Fri22] to describe liquid crystals since an Austrian botanist Reinitzer first reported them upon in 1888 [Rei88]. He was investigating the melting behaviour of an organic substance related to cholesterol (cholesterol benzoate as later was determined), and observed the melting of the compound into a cloudy liquid at 145.5 °C and the clearing at 178.5 °C. Between 1850 and 1888, different researchers in different research fields (chemistry, biology, medicine, physics) had come across the same phenomenon, where materials behaved 'strangely' at temperatures near their melting points (e.g. 1850: Heintz found that magnesium tetradecanoate melted from a solid to a cloudy liquid at 52 °C, changed at 58 °C to an opaque and at 62.5 °C to a clear liquid [Hei55]). Nevertheless, it was Reinitzer who recognised the existence of a new phase of matter.

Lehmann and Vorländer proposed the term *liquid crystal* because this phase strongly resembles the liquid phase (fluidity), but maintains a degree of orientational order (anisotropy). Hence, liquid crystals can be viewed as orientationally ordered liquids or positionally disordered crystals. They possess the fluidal properties of liquids and the anisotropic properties of solids (optical, magnetical and electric anisotropy). Yet, the name *liquid crystal* is more

appropriate because e.g. for the cholesteryl myristate the latent heat of clearing is much smaller (±30 J/g) than for the melting process (±250 J/g). Figure 12 shows a time axis with the most important developments in the field of liquid crystal research.

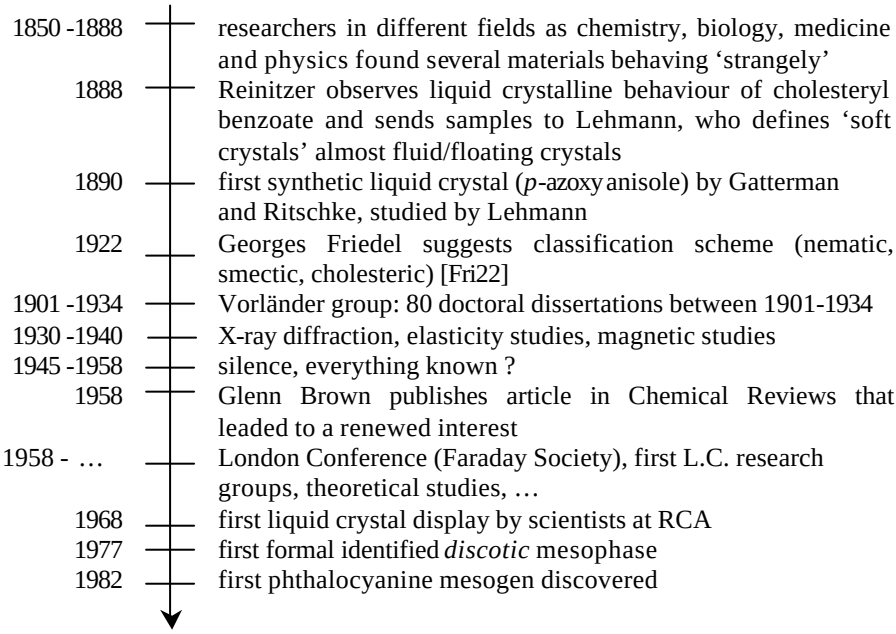

Figure 12 - Schematic history of liquid crystals

Liquid crystals show unique properties: they respond to much weaker electric and magnetic fields than solids, liquids or gases. Other important properties that make liquid crystals useful in high-tech devices are their birefringence, viscosity and elasticity.

2.3.2 Classification of the mesophases

The classification of liquid crystals can be approached in different ways: the method of inducing the mesophases, the symmetry of the mesophases and the

molecular structure of the mesogens. We will first discuss the classification of liquid crystals based on the way the mesophase is induced. Afterwards, we will give a structural classification of the mesogens that are induced by heat.

2.3.2.1 Lyotropic and thermotropic liquid crystals

Mesomorphism can originate from the combined action of a solvent and temperature or from the effect of temperature solely. In the former case, the term *lyotropic mesomorphism* is used and the compounds are called lyotropic liquid crystals. The order of the liquid-crystalline phase is disrupted by solvent action. The temperature also influences the phase transition, but only in combination with a suitable solvent. Lyotropic liquid crystals contain a hydrophobic (water repellent) part and a hydrophilic part (water attracting). For this reason they are called amphiphiles or surfactants. The driving force in forming the mesophase is the minimisation of electrostatic interactions.

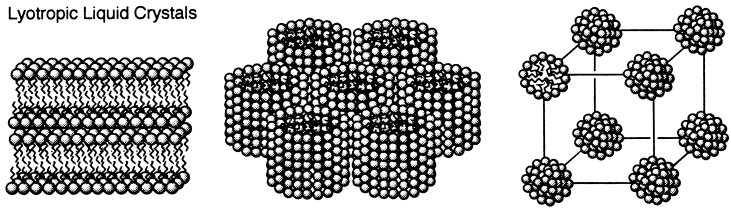

Figure 13 - Lyotropic liquid crystalline phases: lamellar (left), hexagonal (middle) and cubic mesophase (right)

There are two types of lyotropic mesophases: type I ('oil in water') or type II ('water in oil'). For a type I lyotropic molecule, the hydrophobic parts will organise in a way the interaction with the water(like) solvent is avoided and the hydrophilic part show a maximum contact with the water(like) solvent. The principles of self-organisation are identical for type I and II. Looking at the symmetry of the mesophases, five different groups can be distinguished: the

nematic (N), the lamellar (L_a), the bicontinuous cubic (V), the hexagonal (H) and the micellar cubic (I) phases. The micellar solution (L) is not a mesophase as it does not show short or long-range order between the micelles and is thus isotropic. Lyotropic liquid crystals are fundamental for living creatures, since a lyotropic mesophase exists in the cell membrane.

Thermotropic liquid crystals enter the mesophase by a change in temperature. By heating a fully ordered molecular crystal (Cr), the thermal motion of the molecules will increase and eventually the vibrations will have an effect on the positions of the atoms. The temperature at which this happens is called the *melting temperature* (T_m). When in addition to the changes in position also the orientational order is lost in the bulk, the isotropic state of matter is achieved (I). If the orientation is retained, a liquid-crystalline phase or mesophase is observed (M). Further heating will still lead to the isotropic (clear) liquid. This temperature is called the *clearing point* (T_m). The melting point from the heating cycle does (often) not coincide with the one from the cooling cycle. Thus, a strong supercooling can be observed while for the clearing point the heating and the cooling cycle in general the same temperature of transition will be observed (sometimes a small undercooling is observed). The transition from a mesophase into the isotropic liquid hence is a reversible process [ColHir97]. This can be represented as follows:

$$\mathrm{Cr} \underset{T_{M2}}{\overset{T_{M1}}{\rightleftharpoons}} \mathrm{M} \underset{T_{C2}}{\overset{T_{C1}}{\rightleftharpoons}} \mathrm{I} \qquad T_{M1} \geq T_{M2} \text{ and } T_{C1} = T_{C2}$$

A distinction has to be made between the monotropic and the enantiotropic liquid crystals. *Enantiotropic* liquid crystals can attain the mesophase by heating and by cooling from the liquid. *Monotropic* liquid crystals can only reach the liquid-crystalline phase by cooling from the isotropic liquid. This is because the mesophase is thermodynamically less stable than the crystal phase. The clearing

point from the isotropic phase into the mesophase is still reversible. The process can be schematically drawn as follows:

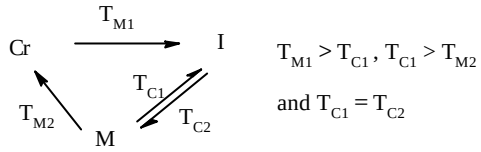

Many liquid crystals show more than one mesophase on going from the crystalline phase into the isotropic liquid. The transitions between mesophases are reversible processes. The presence of more than one type of mesophase is called *polymorphism*:

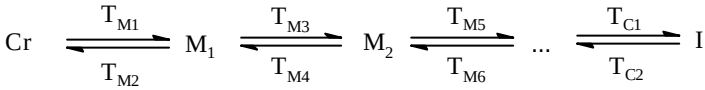

Mesophases that are formed on subsequent cooling from a first mesophase can have *paramorphotic* textures. This means that the textures have features of the preceding phase.

2.3.2.2 Classification system of thermotropic liquid crystals

Thermotropic liquid crystals are classified into two main groups by the structure of their constituting molecules: mesophases formed by calamitic molecules and mesophases formed by discotic molecules.

A. MESOPHASES FORMED BY CALAMITIC MOLECULES

Calamitics are rod-like molecules and they can form different mesophases. Looking at the order in the mesophase, a further distinction can be made between nematic and smectic mesophases.

A.1 Nematic mesophases

The *nematic* mesophase (notation: N) is the least ordered of all thermotropic mesophases. In this mesophase all molecules are oriented with their long molecular axis on average in the same direction (denoted by the director ñ) but there is no positional correlation. In other words: there is an orientational order in one dimension, but no translational order. A schematic representation is given in Figure 14.

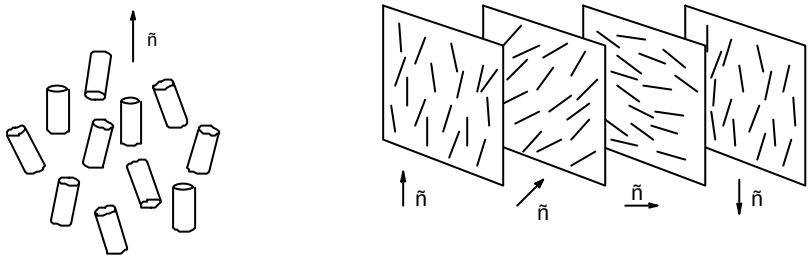

Figure 14 - Left: nematic mesophase (N); right: chiral-nematic mesophase (N)*

The *chiral-nematic* mesophase (notation: N^*) or cholesteric phase is obtained for each enantiomer of a racemic mixture of an optically active material that shows a nematic phase. The director describes a helical path over the planes of nematic ordered molecules. If the helix of an enantiomer twists clockwise, the other enantiomer will twist in the opposite direction. This explains why the racemic mixture will show the nematic mesophase. Figure 14 (right) shows a chiral-nematic mesophase. The distance needed for the director of a chiral-nematic mesophase to make a 360° twist is called the *pitch*.

A.2 Smectic mesophases

The smectic mesophase as opposed to the nematic mesophase also shows some positional order. Generally in a smectic mesophase, the molecules are ordered in

layers, although the degree of organisation strongly differs between the different types of smectic mesophases. A smectic mesophase will usually occur at a lower temperature than a nematic mesophase of the same compound.

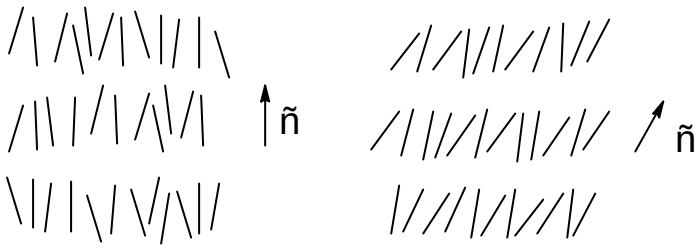

Figure 15 - Left: smectic A mesophase (SmA); right: smectic C mesophase (SmC)

The *smectic A* mesophase (notation: SmA or S_A) is the least ordered of the smectic phases. As for the nematic mesophase there is an orientational order, but in addition a weak, short-distance translational order is responsible for some degree of orientation in layers. The director is placed perpendicular to the layers (Figure 15 - left). In spite of its additional order, the SmA mesophase still has a low viscosity and the molecules can fluctuate up to 20° from the perpendicular direction to the layer planes. The average direction of the molecules though, is perpendicular to these planes.

The *smectic C* mesophase (notation: SmC or S_C) shows an analogy with the SmA mesophase, but on average the molecules are tilted over an angle θ with respect to the perpendicular of the layers (Figure 15 - right). This mesophase is also very fluid and there are no strong attracting forces between the layers. There are a number of other smectic mesophases that we will not discuss here. All of them show an increased viscosity compared to the SmA and SmC mesophases, due to the additional (hexatic) order within the layers. These mesophases (SmB, SmF, SmI) together with the SmA and SmC phases are called the *real smectic mesophases*. On the other hand, smectic mesophases having stronger attracting

forces between the layers are more rigid and are called *crystalline smectic mesophases* or *crystal phases* (E, G, H, J, K, L).

B. MESOPHASES FORMED BY DISCOTIC MOLECULES

The nomenclature of the mesophases formed by discotic molecules has been subject to change during the past few years. The original notation, introduced by Destrade in 1981, used the notation 'D' [DesTin81, DesGas83]. This abbreviation reflects the discotic shape of the composing particles. Naming the mesophases after their shapes is not consequent to the naming of the mesophases of calamitic molecules [Cha93]. These mesophases are named after the order within the mesophase instead of the actual shape of the molecules. Moreover many non-discotic molecules (e.g. dimers) and polymers show 'discotic' mesophases (even the liquid-crystalline phthalocyanines that are subject of our research are strictly speaking not discotic, but cross-shaped). That's why recently the abbreviation 'Col' was suggested, to emphasise the mesophase when the molecules are arranged in columns, instead of the shape of its components. Discotic molecules can have nematic-discotic and columnar mesophases.

B.1 Nematic discotic and nematic columnar mesophases

Thermotropic materials that show these phases are very rare. The nematic discotic mesophase (notation: N_D) is the discotic equivalent of the nematic calamitic mesophase. There is only orientational order parallel to the short molecular axis (Figure 16 - left). This mesophase has a low viscosity. For the nematic columnar mesophase (notation: N_{Col}) a limited number of disc-shaped molecules are stacked together in short columns. These columns then are ordered as the nematic phases (Figure 16 - right).

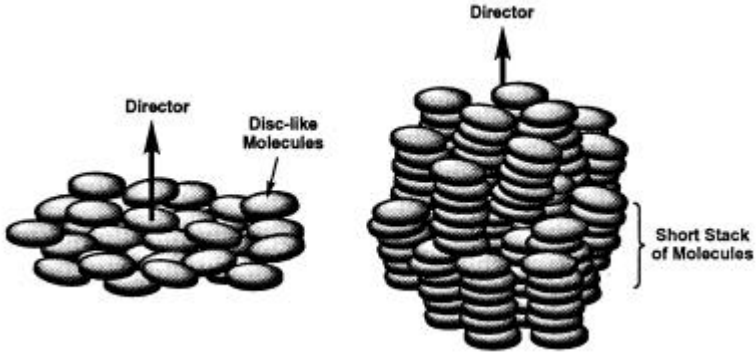

Figure 16 - Nematic discotic mesophases (N_D) and nematic columnar mesophase (N_{Col})

B.2 Columnar mesophases

Columnar mesophases are formed by the stacking of molecules into columns. A distinction is also made by the way the columns are arranged with respect to one another, i.e. the 2D lattice.

The hexagonal columnar mesophase is built up by columns that arrange themselves in a hexagonal fashion (Figure 17). The full name of the mesophase depends on the way the individual molecules are grouped within a column: if they are distributed evenly along the column, the ordered hexagonal columnar mesophase (notation: Col_{ho}) is obtained. If the molecules are stacked irregularly along the column, the disordered hexagonal columnar mesophase (notation: Col_{hd}) is observed.

The ordered hexagonal columnar mesophase cannot be considered as a liquid-crystalline phase without argument. Strictly spoken, structures that show a formal three-dimensional long-range order are called 'disturbed crystals' (although some sources also use the term 'mesophase' here). Only structures with order in less than three dimensions are considered as liquid crystals. On the other hand does the Col_{ho} phase not show any correlation between the positions of the molecules within two neighbouring columns and hence no real bulky crystalline

phase parallel to the axis of the column can be appointed (one could even call the phase a liquid). For obvious reasons, we will not go any further in to this discussion and we will restrict ourselves to the presented nomenclature.

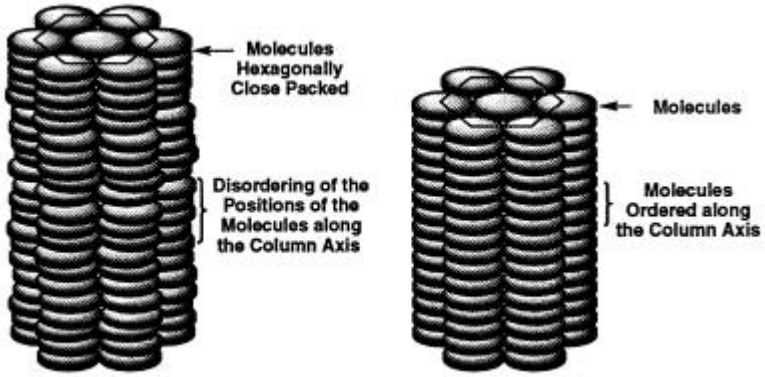

Figure 17 - The disordered hexagonal columnar mesophase Col_{hd} (left) and the ordered hexagonal columnar mesophase Col_{ho} (right)

Whereas for the hexagonal columnar mesophases the columns are packed in a hexagonal lattice with C_6 symmetry (circular columnar section), the molecules of the rectangular columnar mesophase (notation: Col_{rd} (disordered) or Col_{ro} (ordered); Figure 18, left) are packed in a rectangular lattice with C_2 symmetry (ellipsoidal columnar section). For the oblique columnar mesophase, the molecules are packed in a triclinic lattice (they also show an ellipsoidal cross-section; Figure 18, right). For all these mesophases the columns are perpendicular to the two-dimensional lattice.

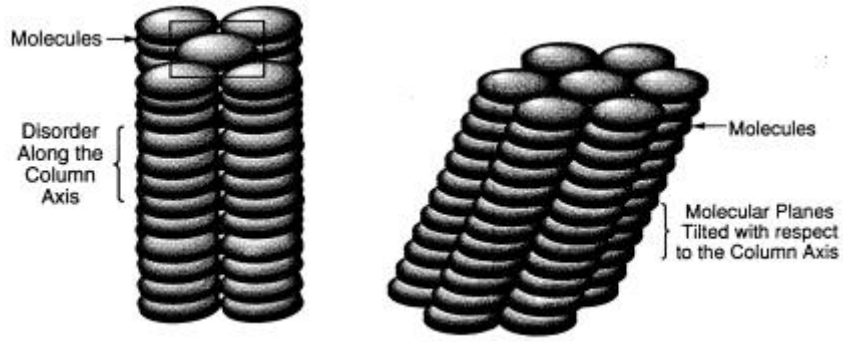

Figure 18 - Disordered rectangular columnar mesophase Col_{rd} (left) and oblique columnar mesophase Col_o (right)

2.3.3 Molecular structural demands for thermotropic liquid crystals

Intermolecular forces and the molecular structure are the two most important aspects that determine whether or not a liquid-crystalline phase is formed. Weak dispersive forces (weaker than the intermolecular forces in solids) are operating between the molecules in a mesophase. These forces are necessary for the orientational order. If they are not present, the molecules can move around freely and an isotropic state is observed. In order to maximise these forces they have to be directional. This can be obtained by designing structurally anisotropic molecules. We will distinguish between the calamitic and the columnar mesophases.

Calamitic mesophases

Rod-like molecules form calamitic mesophases. The general structure can be represented as in Figure 19.

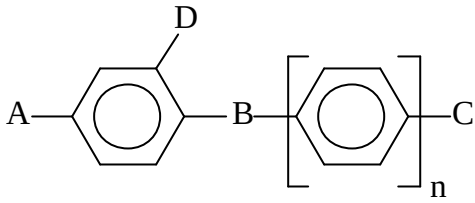

Figure 19 - General structure of a calamitic (rod-like) molecule (A, C = terminal groups, B = connecting group, D = side-group and n usually equals 1 or 2)

There are three requirements that the molecules will have to obey in order to be able to form a calamitic mesophase:

1) They have to be anisotropic in their molecular structure, i.e. have a high aspect ratio (ratio of the molecule length and its width); typically, calamitic molecules have a 13 to 14 Å minimum length ,
2) They have to possess a permanent dipole or have to be readily polarised,
3) The polarisability has to be strongly anisotropic.

From the figure, we can identify two terminal groups (A and C), a linking group (B) and a lateral group (D); n is typically 1 or 2. The linking group is typically one that lengthens the molecule. For the terminal part, groups that extend the length, without increasing the width, stabilise the mesophase. Sometimes, small lateral substituents can also be tolerated and are beneficial. The more the molecule resembles a rod, the stronger the anisotropic dispersive forces and the more stable the mesophase will be. Every combination of A, B, C and D that prolongs the molecule without adding much to the width, will stabilise the mesophase. Figure 20 depicts some rod-like molecules that exhibit calamitic mesophases.

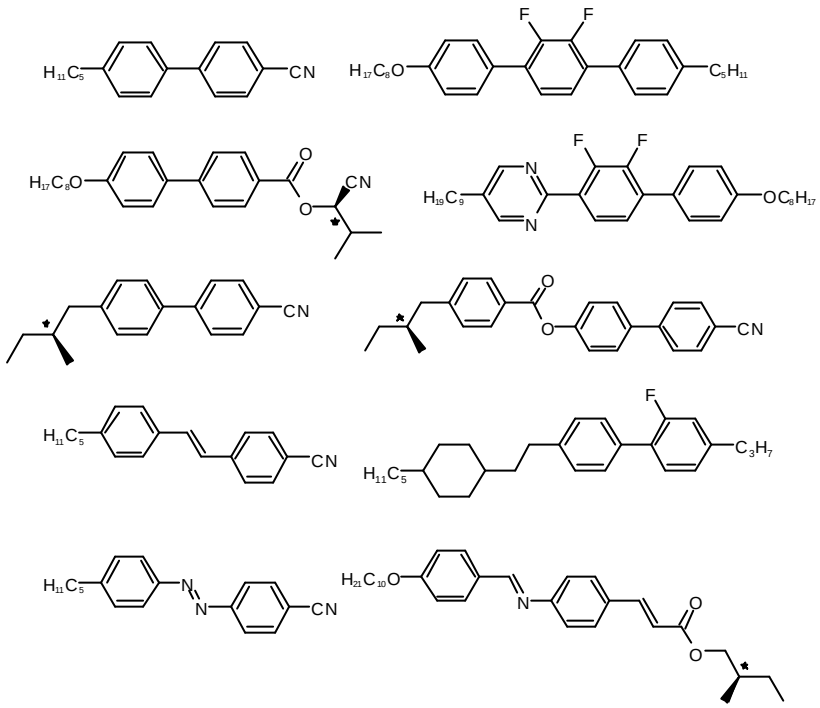

Figure 20 - Rod-like compounds forming calamitic mesophases

Discotic-columnar mesophases

In general, discotic mesophases consist of disc-shaped molecules. The general structure can be considered as a flat core (usually aromatic), surrounded by at least six aliphatic chains. The correlation between the structure and the stability of the mesophase is less defined for the columnar mesophases than for the calamitic mesophases. Figure 21 shows different discotic molecules that give rise to columnar mesophases. It has to be mentioned that recently molecules have been shown to exhibit thermotropic liquid-crystalline behaviour without long terminal substituents. Polarisable chlorine atoms, sulphur atoms and cyano groups play the role as unusual *soft* parts [BarRak98].

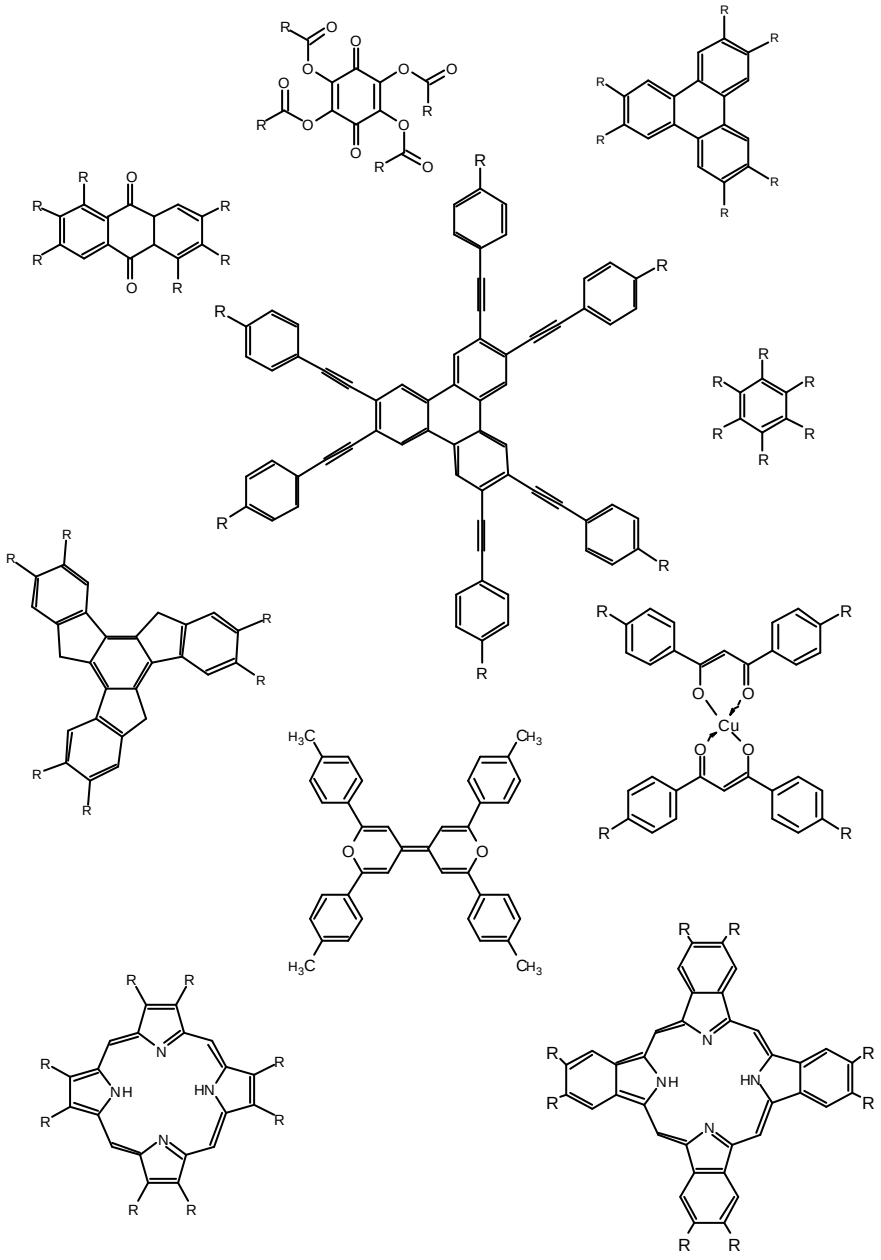

Figure 21 - Discotic liquid crystals forming columnar mesophases

2.3.4 Properties of liquid crystals

Liquid crystals are liquids that possess anisotropic physical properties (birefringence, permittivity, elasticity, viscosity, polarisability …) because of the partial orientational order of the molecules [Col90]. 'Anisotropic' means that the magnitude of the property depends on the direction.

Rod-like molecules for example are more readily polarised along the length of the molecule and less easily along their width. This will cause liquid crystals to demonstrate two main refractive indices and hence *birefringence* is observed when light is sent through such a mesophase. Light polarised parallel to the director has a different index of refraction (that is to say it travels at a different velocity) than light polarised perpendicular to the director. Thus, when light enters a birefringent material, such as a nematic liquid crystal sample, the process is modelled in terms of the light being broken up into the fast (called the ordinary ray) and slow (called the extraordinary ray) components. Because the two components travel at different velocities, the waves get out of phase. When the rays are recombined as they leave the birefringent material, the polarisation state has changed because of this phase difference. This is depicted in Figure 22

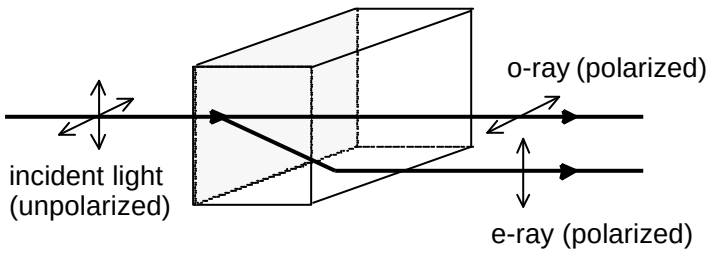

Figure 22 - Birefringence for a nematic mesophase

The birefringence of a material is characterised by the difference, in the indices of refraction for the ordinary and extraordinary rays, *Dn*. To be a little more

quantitative, since the index of refraction of a material is defined as the ratio of the speed of light in a vacuum to that in the material, we have for this case, $n_e = c/V_{\perp}$ and $n_o = c/V_{\wedge}$ for the velocities of a wave travelling perpendicular to the director and polarised parallel and perpendicular to the director, so that the maximum value for the birefringence, $Dn = n_e - n_o$.

The length of the sample is another important parameter because the phase shift increases as long as the light propagates in the birefringent material. Any polarisation state can be produced with the right combination of the birefringence and length parameters.

It is convenient here to introduce the concept of optical path in media since for the above two wave components travelling with different speeds in a birefringent material, the difference in optical paths will lead to a change in the polarisation state of the wave as it progresses through the medium. We define the optical path for a wave travelling a distance L in a crystal as nL so that the optical path difference for the two wave components mentioned above will be $L\cdot(n_e - n_o) = L\cdot Dn$. The resultant phase difference between the two components (the amount by which the slow, extraordinary component lags behind the fast, ordinary one) is just $2\cdot p\cdot L\cdot Dn/\lambda\cdot v$ where λ is the wavelength in vacuum. The resulting light beam at the end of the medium is elliptically polarised.

2.3.5 Characterisation of liquid-crystalline properties

Three important experimental techniques are used to characterise (thermotropic) mesophases: thermo-optical microscopy, differential scanning calorimetry (DSC) and small angle variable temperature X-ray diffraction. Due to the minimal differences in the structures of different liquid-crystalline phases of a compound, the identification can be difficult. Hence, these techniques are often used in combination with each other.

2.3.5.1 Thermo-optical microscopy

An important invention for the study of liquid crystalline phases was the heating stage microscope by Otto Lehmann, a physicist from Karlsruhe (Germany). This microscope allowed the control of the temperature of the sample. In a later stadium, polarisers were added and it has become a piece of standard equipment for every liquid crystal research laboratory. Thermo-optical microscopy is also called polarising optical microscopy (POM). Figure 23 shows the general principle of a thermo-optical microscope.

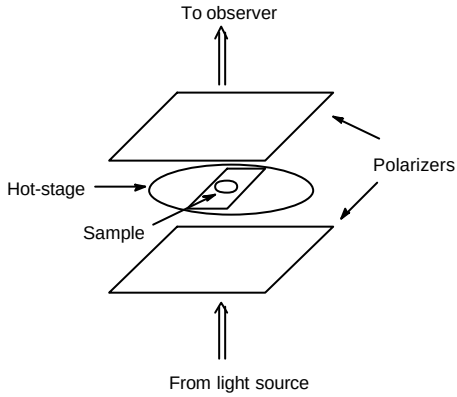

Figure 23 - Thermo-optical microscopy

Consider the case where a liquid crystal sample (embodied in a heating device) is placed between crossed polarisers whose transmission axes are aligned at some angle between the fast and slow direction of the material. Because of the birefringent nature of the sample, the incoming linearly polarised light becomes elliptically polarised. When this ray reaches the second polariser, there is now a component that can pass through, and the viewing field appears bright. For monochromatic light (single frequency), the magnitude of the phase difference is determined by the length and the birefringence of the material. If the sample is very thin, the ordinary and extraordinary components do not get very far out of

phase. Likewise, if the sample is thick, the phase difference can be large. If the phase difference equals 360°, the wave returns to its original polarisation state and is blocked by the second polariser. The size of the phase shift determines the intensity of the transmitted light.

If the transmission axis of the first polariser is parallel to either the ordinary or extraordinary directions, the light is not broken up into components, and no change in the polarisation state occurs. In this case, there is not a transmitted component and the region appears dark.

In a typical liquid crystal, the birefringence and length are not constant over the entire sample. This means that some areas appear light and others appear dark. The light and dark areas denote regions of differing director orientation, birefringence, and length. Moreover, because of the mesogenic defects in the thin sample, a typical pattern (texture) is visible through the ocular of the microscope. The observed texture is characteristic for the type of mesophase.

In general, textures are studied by first heating the sample to an isotropic liquid and by slowly cooling into the mesophase in order to prevent paramorphotic effects. Thermo-optical microscopy is a fast and inexpensive technique for gathering information on the mesophase.

2.3.5.2 Differential Scanning Calorimetry (DSC)

The transitions between the solid and the liquid-crystalline phase, between different liquid-crystalline phases and between the liquid-crystalline phase and the isotropic phase are always accompanied by a change in enthalpy DH (and thus in entropy $DS = DH/T$). DSC determines the power supplied to (or absorbed by) the sample that is proportional to the transition enthalpy. DH and DS can also provide information on the mechanism of the transition. As was discussed earlier, different mesophases have different symmetries and therefore the heat needed for a transition is different. Most liquid crystal-liquid crystal transitions are first order transitions. This means they have a discontinuity in the slope of the free energy G

at the phase changes ($DS = -D(dG/dT)$). For second order transitions, the slope is continuous at the transition, but the gradient of the slope changes.

Large enthalpy changes correspond to a large change of molecular organisation in the structure; such transitions are first order. Examples are: melting transitions, transitions between two mesophases and in some cases the clearing transition. The transition between the SmC and SmA mesophases, when the change in tilt angle of the molecules with respect to the normal of the layer is continuous, is an example of a second order transition.

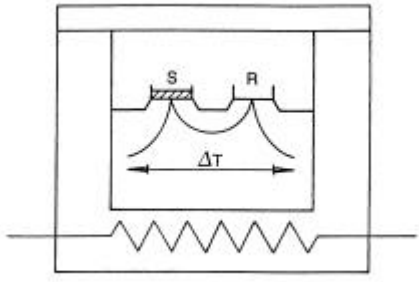

Figure 24 - Schematic drawing of a heat flux DSC cell (S: sample, R: reference)

A heat flux DSC (Figure 24) measures the difference in temperature between the sample and a reference that are heated at the same rate by an oven. Both the sample (a few milligrams) and the reference are held in inert containers or pans (usually aluminium). When the compound inside the sample cell is melting, more heating is required than for the reference cell to reach the same temperature. The sample cell will thus be at a lower temperature than the reference. The difference in heat flow is monitored as a function of the temperature. In this way, transition temperatures can be measured accurately. The DSC profiles are represented by curves of differential temperatures (which are translated to the corresponding heat in mW) versus the time on the abscissa. The area of the transition peaks is proportional to the transition enthalpy *DH*.

2.3.5.3 Small angle variable temperature X-ray diffraction

The most powerful method for mesophase characterisation is small angle X-ray diffraction. This technique is based on the fact that mesophases are periodical and hence diffract light. Applying Bragg's law and other simple crystallographic principles allows the unique determination of the structure of the mesophase (see appendix D). A schematic representation is given in Figure 25. Two (complementary) experimental setups are usually used: one for the long spacings, corresponding to the low-angle region (SAXS) and another designed for wide-angle (WAXS), corresponding to crystal spacings of around 4.5 Å. In synthetic laboratories X-ray diffraction is not often applied because it requires expensive and specialised equipment. The techniques we applied are thoroughly discussed in Appendix D.

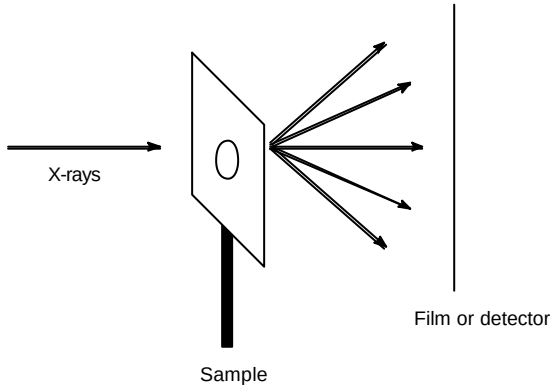

Figure 25 - Schematic representation of the principle of X-ray diffraction

2.3.6 Liquid-crystalline phthalocyanines

As mentioned in the introduction and as can be seen from the tables in Appendices B and C, only a limited number of liquid-crystalline phthalocyanine compounds were synthesised prior to this research [McK98]. In this paragraph we present a

short overview of the most important milestones in the field of liquid-crystalline phthalocyanine research.

The *lyotropic mesomorphism* of a number of phthalocyanine compounds was studied by Usoltseva *et al*. [UsoByk90, UsoByk92, BykUso96, Uso96, Uso97].

Tetra-substituted liquid-crystalline phthalocyanines were investigated only sporadically, due to the difficulty of obtaining a sample containing only one isomer [McKPai84, TreCla95, KonNem97].

Cook *et al*. carried out an extensive study of mesogenic *non-peripherally 1,4,8,11,15,18,22,25-octasubstituted phthalocyanines* (Figure 26) with different types of substituents: alkyl, alkoxy and alkoxymethyl [CooDan87, CooMcK89, CooCra91, CamCoo91, CheDav91, Coo94]. Also branched side-chains and non-uniformly substituted mesogens were the subject of research [CamCoo91, ChaCoo93, HumCla96]. The compounds studied were the metal-free ligands and Cu(II), Ni(II), Zn(II) complexes.

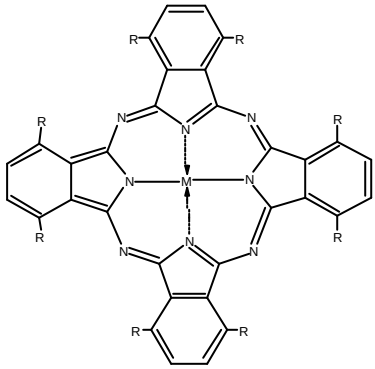

Figure 26 - Schematic representation of a non-peripherally 1,4,8,11,15,18,22,25-octasubstituted phthalocyanine complex (R= C_nH_{2n+1}, OC_nH_{2n+1}, $CH_2OC_nH_{2n+1}$)

As mentioned in the introduction, the most prominent group of liquid-crystalline phthalocyanines are the *peripherally 2,3,9,10,16,17,23,24-octasubstituted*

phthalocyanines. Most of the investigated compounds had the octa-alkoxy substitution pattern [vanNee89, SchWar94]. Mainly Cu(II) was used as the metal, although Co(II), Zn(II), Ni(II), Pt(II), $Si(OH)_2$, Li(I) and Lu(III) complexes have been reported on [SauWeg88, BelSir89, VacDop92, SevUnd93]. For the octa-alkoxymethyl Pc's only nine compounds were investigated [PieSim82, GuiSko83, GuiWeb85, PieSim85, WebGui87, SirBos88, MarLéc91, SimBas93]. The octa-alkyl Pc's form a third main class of mesogens [OhtJac88, NisAzu92, EngBas93, KomOht94, ClaMcK95]. Other types of substituents investigated were: octa-alkoxycarbonyl [DulGit92], octa-oligo(ethyleneoxy) [GuiWeb85, ClaMcK95, ClaHas96, KroKoe97], branched side-chains [ChoLim87, Schvan91, vanBos93, LelPet89, ForSum94], octa-(dioctylaminocarbonyl)methoxy [DurTor93], octa-(dialkylaminocarbonyl)-methoxy [Durdel96], amphiphilic, chiral and crownether substituents [SirBos87, Tou95, van97], alkoxyphenyl compounds [OhtWat91, OhtAzu96], alkoxyphenoxy [HatOht01] and thioalkyl chains [EicWöh97, BanNis00, BanNis01].

A number of other mesogenic (more exotic) compounds have also been reported. We just want to mention: non-uniformly peripherally octa-substituted Pc's with a single poly(oxyethylene) side chain [ClaCoo96], unsymmetrical substituted Pc's [AliCla98].

The peripherally 2,3,9,10,16,17,23,24-octasubstituted phthalocyanines with alkoxy, alkyl and alkoxymethyl side-chains served as a starting point for our examinations. By expanding this range of liquid-crystalline compounds a more thorough understanding of the influence of the linking group, the chain length and the central metal ion on the mesogenic properties becomes available.

2.4 Conclusions

Phthalocyanines (or metallophthalocyanines) have been the continuous subject of research since their accidental discovery. As a proof of this attention only recently (1997) a new international journal was dedicated to phthalocyanines and the related porphyrin molecules (Journal of Porphyrins and Phthalocyanines). Figure 27 illustrates the wide academic interest by showing the number of published articles on phthalocyanines in general (left) and liquid crystalline phthalocyanines (source: Web of Science).

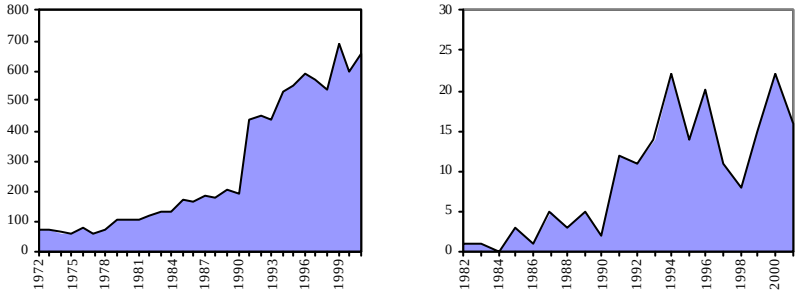

Figure 27 - Number of articles on phthalocyanines published since 1972 (left) and number of article published since 1982 on liquid-crystalline phthalocyanines (right)

Liquid-crystalline metal-containing phthalocyanines (or metallophthalocyanines) have been investigated for over 20 years since the first mesogen was synthesised. However, most complexes that were known prior to this work have the copper(II) ion as the central transition metal ion or lutetium(III) as the central lanthanide ion. The incorporation of other metals and the use of different chain lengths and types might give rise to new properties and applications.

2.5 References

[AliCla98] Z. Ali-Adib, G.J. Clarkson, N.B. McKeown, K.E. Treacher, H.F. Gleeson, A.S. Stennet, *J. Mater. Chem.*, **8**, 2371, 1998.

[Alivan99] H. Ali, J.E. van Lier, *Chem. Rev.*, **99**, 2379, 1999.

[AndHol85] J.J. André, K. Holczer, P. Petit, M.T. Riou, C. Clarisse, R. Even, M. Fourmigue, J. Simon, *Chem. Phys. Lett.*, **115**, 463, 1985.

[BanNis00] K. Ban, K. Nishizawa, K. Ohta, H. Shirai, *J. Mater. Chem.*, **10**, 1083, 2000.

[BanNis01] K. Ban, K. Nishizawa, K. Ohta, A.M. van de Craats, J.M. Warman, I. Yamamoto, H. Shirai, *J. Mater. Chem.*, **11**, 321, 2001.

[BarDen36] P.A Barret, C.E. Dent, R.P. Linstead, *J. Chem. Soc*., 1719, 1936.

[BarFry38] P.A. Barret, D.A. Frye, R.P. Linstead, *J. Chem. Soc.*, 1157, 1938.

[BarRak98] J. Barberá, O.A. Rakitin, M.B. Ros, T. Torroba, *Angew. Chem. Int. Ed*., **37**, 3, 1998.

[BelSir89] Z. Belarbi, C. Sirlin, J. Simon, JJ. Andre, *J. Phys. Chem.*, **93**, 8105, 1989.

[BraGra70] P.J. Brach, S.J. Grammatica, O.A. Ossanna, L. Weinberger, *J. Heterocyclic. Chem.*, **7**, 1403, 1970.

[BraTch07] A. Braun, J. Tcherniac, *Ber. Deut. Chem. Ges.*, **40**, 2709, 1907.

[BykUso96] V.V. Bykova, N.V. Usoltseva, G.A. Ananieva, N.M. Kormilitsyn, A.S. Semeikin, *Bull. Russ. Ac. Sci*., **60**, 558, 1996.

[ByrLin34] G.T. Byrne, R.P. Linstead, A.R. Lowe, *J. Chem. Soc.*, 1017, 1934.

[CamCoo91] A.N. Cammidge, M.J. Cook, K.J. Harrison, N.B. McKeown, *J. Chem. Soc. Perkin Trans. 1*, 3053, 1991.

[Cha93] S. Chandrasekhar, *Liq. Cryst*., **14**, 3, 1993.

[ChaCoo93] I. Chambrier, M.J. Cook, S.J. Cracknell, J. McMurdo, *J. Mater. Chem.*, **3**, 841, 1993.

[ChaMar81] A.T. Chang, J.C. Marchon, *Inorg. Chim. Act*a, **53**, 241, 1981.

[CheDav91] A.S. Cherodian, A.N. Davies, R.M. Richardson, M.J. Cook, N.B. McKeown, A.J. Thomson, J. Feijoo, G. Ungar, K.J. Harrison, *Mol. Cryst. Liq. Cryst.*, **196**, 103, 1991.

[ChoLim87] I. Cho, Y. Lim, *Chem. Lett.*, 2107, 1987.

[ClaCoo96] G.J. Clarkson, A. Cook, N.B. McKeown, K.E. Treacher, Z. Ali-Adib, *Macromolecules*, **29**, 913, 1996.

[ClaHas96] G.J. Clarkson, B.M. Hassan, D.R. Maloney, N.B. McKeown, *Macromolecules*, **29**, 1854, 1996.

[ClaMcK95] G.J. Clarkson, N.B. McKeown and K.E. Treacher, *J. Chem. Soc. Perkin Trans. I*, 1817, 1995.

[ColSch82] G.C.S. Collins, D.J. Schiffrin, *J. Electroanal. Chem.*, **139**, 335, 1982.

[Coo94] M.J. Cook, *J. Mater. Sci. Mater. Elec.*, **5**, 117, 1994.

[CooCra91] M.J. Cook, S.J. Cracknell, K.J. Harrison, *J. Mater. Chem.*, **1**, 703, 1991.

[CooDan87] M.J. Cook, M.F. Daniel, K.J. Harrison, N.B. McKeown, A.J. Thomson, *J. Chem. Soc. Chem. Commun.*, 1086, 1987.

[CooMcK89] M.J. Cook, N.B. McKeown, A.J. Thomson, *Chem. Mat.*, **1**, 287, 1989.

[CorGra79] G.A. Corker, B. Grant, N.J. Clecak, *J. Electrochem. Soc.*, **126**, 1340, 1979.

[CueMar81] E.A. Cuellar, T.J. Marks, *Inorg. Chem.*, **20**, 3766, 1981

[CueSto80] E.A. Cuellar, D.R. Stojakovic, T.J. Marks, *Inorg. Synth.*, **20**, 97, 1980.

[DanDre29] A.G. Dandridge, H.A.E. Drescher, J. Thomas, *Dyes*. British patent 322, 169, 1929.

[DayMar74] V.W. Day, T.J. Marks, W.A. Wachter, *J. Am. Chem. Soc.*, **97**, 4519,1975.

[DecMou85] A. De Cian, M. Moussave, J. Fischer, R. Weiss, *Inorg. Chem.*, **24**, 3162, 1985.

[DeDvon27] H. de Diesbach, E. von der Weid, *Helv. Chim. Acta*, **10**, 886, 1927.

[DenLin34a] C.E. Dent, R.P. Linstead, *J. Chem. Soc.*, 1027, 1934.

[DenLin34b] C.E. Dent, R.P. Linstead, *J. Chem. Soc.*, 1033, 1934.

[DesTin81] C. Destrade, N.H. Tinh, H. Gasparoux, J. Malthête, A.M. Levelut, *Mol. Cryst. Liq. Cryst.*, **71**, 111, 1981.

[DesGas83] C. Destrade, P. Foucher, H. Gasparoux, N.H. Tinh, A.M. Levelut, J. Malthête, *Mol. Cryst. Liq. Cryst.*, **106**, 121, 1984.

[DulGit92] L. Dulog, A. Gittinger, *Mol. Cryst. Liq. Cryst.*, **213**, 31, 1992.

[DurTor93] J.A. Duro, T. Torres, *Chem. Ber.*, **126**, 269, 1993.

[Durdel96] J.A. Duro, G. de la Torre, J. Barbera, J.L. Serrano, T. Torres, *Chem. Mater.*, **8**, 1061, 1996.

[Eic00] H. Eichhorn, *J. Porphyr. Phthalocya*., **4**, 88, 2000.

[EicWöh97] H. Eichhorn, D. Wöhrle, D. Pressner, *Liq. Cryst*., **22**, 643, 1997.

[Elv99] J.A. Elvidge, *J. Porphyr. Phthalocya*., **3**, 392, 1999.

[EngBas93] M.K. Engel, P. Bassoul, L. Bosio, H. Lehmann, M. Hanack and J. Simon, *Liq. Cryst*., **15**, 709, 1993.

[ForSum94] W.T. Ford, L. Sumner, W. Zhu, Y.H. Chang, PJ. Um, K.H. Choi, P.A. Heiney, N.C. Maliszewskyj, *New J. Chem.*, **18**, 495, 1994.

[Fri22] G. Friedel, *Ann. Physique*, **18**, 273, 1922.

[GerAri99] N.V. Gerbeleu, V.B. Arion, J. Burgess, Template Synthesis of Macrocyclic Compounds, Wiley-VCH, Weinheim, 1999.

[Gre99] P. Gregory, *J. Porphyr. Phthalocya*., **3**, 468, 1999.

[GuiSko83] D. Guillon, A. Skoulios, C. Piechocki, J. Simon, P. Weber, *Mol. Cryst. Liq. Cryst*., **100**, 275, 1983.

[GuiWeb85] D. Guillon, P. Weber, A. Skoulios, C. Piechocki, J. Simon, *Mol. Cryst. Liq. Cryst*., **130**, 223, 1985.

[HatOht01] K. Hatsusaka, K. Ohta, I. Yamamoto, H. Shirai, *J. Mater. Chem.*, **11**, 423, 2001.

[Hei55] W. Heintz, *J. Prakt. Chem.*, **66**, 1, 1855.

[Her53] W. Herr, *Angew. Chem.*, **65**, 303, 1953.

[HerGöt50] W. Herr, H. Götte, *Z. Naturforschg.*, **5a**, 29, 1950.

[HumCla96] P. Humberstone, G.J. Clarkson, N.B. McKeown, K.E. Treacher, *J. Mater. Chem.*, **6**, 315, 1996.

[KasAnd86] K. Kasuga, M. Ando, H. Morimoto, M. Ïa, *Chem. Lett.*, 1095, 1986.

[KasTsu80] K. Kasuga, M. Tsutsui, R.C. Petterson, K. Tatsumi, N. Van Opdenbosch, G. Pepe, E.F. Meyer Jr., *J. Am. Chem. Soc.*, **102**, 4836, 1980.

[KhaBla99] B.I. Kharisov, L.M. Blanco, L.M. Torres-Martinez, A. García-Luna, *Ind. Eng. Chem. Res.*, **38**, 2880, 1999.

[KirMos65] I.S. Kirin, P.N. Moskalev, Y.A. Makashev, *Russ. J. Inorg. Chem.*, **10**, 1065, 1965.

[KirMos67] I.S. Kirin, P.N. Moskalev, Y.A. Makashev, *Russ. J. Inorg. Chem.*, **12**, 369, 1967.

[KobSud90] N. Kobayashi, K. Sudo, T. Osa, *Bull. Chem. Soc. Jpn.*, **63**, 571, 1990.

[KomOht94] T. Komatsu, K. Ohta, T. Fujimoto, I. Yamamoto, *J. Mater. Chem.*, **4**, 533, 1994.

[KonNem97] N.V. Kondratenko, V.N. Nemykin, E.A. Lukyanets, N.A. Kostromina, S.V. Volkov, L.M. Yagupolskii, *J. Porphyr. Phthalocya.*, **1**, 341, 1997.

[KraFer88] B. Kraut, G. Ferraudi, *Inorg. Chim. Acta*, **149**, 273, 1988.

[KroKoe97] J.M. Kroon, R.B.M. Koehorst, M. van Dijk, G.M. Sanders, E.J.R. Sudhölter, *J. Mater. Chem.*, **7**, 615, 1997.

[LelPet89] D. Lelievre, M.A. Petit, J. Simon, *Liq. Cryst.*, **4**, 707, 1989.

[Lev65] A.B.P. Lever, *Adv. Inorg. Chem. Radiochem.*, **7,** 27, 1965.

[LezLev96] C.C. Leznoff, A.B.P Lever , *Phthalocyanines, Properties and Applications*, Vols 1-4, VCH Weinheim, 1989.

[LheCoz85] M. L'Her, Y. Cozien, J. Courtot-Coupez, C.R. Acad. Sc. Paris, t.300, Série II, 11, 1985.

[Lin34] R.P. Linstead, *J. Chem. Soc.*, 1016, 1934.

[LinLow34a] R.P. Linstead, A.R. Lowe, *J. Chem. Soc.*, 1022, 1934.

[LinLow34b] R.P. Linstead, A.R. Lowe, *J. Chem. Soc.*, 1031, 1934.

[LinQui00] M. Linaje, M.C. Quintanila, A. Gonzales, J.L. del Valle, G. Alcaide, M.L. Rodriguez-Mendez, *Analyst*, **125**, 341, 2000.

[LiuLee01] L.C. Liu, C.C. Lee, A. Teh Hu, *J. Porphyr. Phthalocya*., **5**, 806, 2001.

[MacBoa74] A.G. MacKay, J.F. Boas, G.J. Troup, *Aust. J. Chem.*, **27**, 955, 1974.

[MaiGui87] M. Maitrot, G. Guillaud, B. Boudjema, J.J. André, H. Strzelecka, J. Simon en R. Even, *Chem. Phys. Lett.*, **133**, 59, 1987.

[Mar82] J.C. Marchon, *J. Electrochem. Soc.*, **129**, 1377, 1982.

[MarLéc91] D. Markovitsi, I. Lécuyer, J. Simon, *J. Phys. Chem.*, **95**, 3620, 1991.

[MarSto78] T.J. Marks, D.R. Stojakovic, *J. Am. Chem. Soc.*, **100**, 1695, 1978.

[McK98] N.B. McKeown, *Phthalocyanine Materials: Synthesis, Structure and Function*, Cambridge University Press, 1998.

[McKPai84] N.B. McKeown, J. Painter, *J. Mater. Chem.*, **4**, 1153, 1984.

[MosKir72] P.N. Moskalev, I.S. Kirin, *Russ. J. Inorg. Chem.*, **46**, 1019, 1972.

[MosKir80] P.N. Moskalev, I.S. Kirin, *Russ. J. Inorg. Chem.*, **16**, 1971, 57.

[MosTho63] F.H. Moser, A.L. Thomas, *Phthalocyanine Compounds*, Reinhold Publishing Corporation, 1963.

[MsaRon86] M. M'sadak, J. Roncali, F. Garnier, *J. Chim. Phys*., **83**, 211, 1986.

[NicGal77] M.M. Nicholson, R.V. Galiardi, U.S. NTIS Report AD-A039596, 1977.

[NicPiz79] M.M. Nicholson, F.A. Pizzarello, *J. Electrochem. Soc.*, **126**, 1490, 1979.

[NicPiz80] M.M. Nicholson, F.A. Pizzarello, *J. Electrochem. Soc.*, **127**, 2617, 1980.

[NicPiz81] M.M. Nicholson, F.A. Pizzarello, *J. Electrochem. Soc.*, **128**, 1740, 1981.

[NicWei84] M.M. Nicholson, J.P. Weismuller, *J. Electrochem. Soc.*, **131**, 2311, 1984.

[NisAzu92] H. Nishi, N. Azuma, K. Kitahara, *J. Heterocycl. Chem.*, **29**, 475, 1992.

[OhtAzu96] K. Ohta, S. Azumane, T. Watanabe, S. Tsukada, I. Yamamoto, *Appl. Organomet. Chem.*, **10**, 623, 1996.

[OhtJac88] K. Ohta, L. Jacquemin, C. Sirlin, L. Bosio and J. Simon, *New. J. Chem.*, **12**, 751, 1988.

[OhtWat91] K. Ohta, T. Watanabe, S. Tanaka, T. Fujimoto, I. Yamamoto, P. Bassoul, N. Kucharczyck, J. Simon, *Liq. Cryst.*, **10**, 357, 1991.

[OliSmi87] S.W. Oliver, T.D. Smith, *J. Chem. Soc. Perkin Trans. 2*, 1579, 1987.

[OrtBré90] E. Orti, J.L. Brédas, C. Clarisse, *J. Chem. Phys.*, **92**, 1228, 1990.

[PetPli89] M.A. Petit, V. Plichon, H. Belkacemi, *New J. Chem.*, **13**, 459, 1989.

[Pie82] C. Piechocki, Thèse Docteur Spécialisé, Strasbourg, 1982.

[PieSim82] C. Piechocki, J. Simon, A. Skoulios, D. Guillon, P. Weber, *J. Am. Chem. Soc.*, **104**, 5245, 1982.

[PieSim85] C. Piechocki, J. Simon, J.J. André, D. Guillon, P. Petit, A. Skoulios, P. Weber, *Chem. Phys. Lett.*, **122**, 124, 1985.

[PriRai00] S.A. Priola, A. Raines, W.S. Caughey, *Science*, 287, 1503, 2000.

[Rei88] F. Reinitzer, *Monatsh. Chem.*, **9**, 421, 1888.

[Rob35] J.M. Robertson, *J. Chem. Soc.*, 615, 1935.

[Rob36a] J.M. Robertson, *J. Chem. Soc.*, 1195, 1936.

[Rob36b] J.M. Robertson, *J. Chem. Soc.*, 1736, 1936.

[Rob37] J.M. Robertson, I. Woodward, *J. Chem. Soc.*, 219, 1937.

[Rob40] J.M. Robertson, *J. Chem. Soc.*, 36, 1940.

[SauWeg88] T. Sauer, G. Wegner, *Mol. Cryst. Liq. Cryst.*, **162**, 97, 1988.

[SchGou73] A.M. Schaffer, M. Gouterman, E.R. Davidson, *Theor. Chim. Acta*., **30**, 9, 1973.

[Schvan91] P.G. Schouten, J.F. Van Der Pol, J.W. Zwikker, W. Drenth, S.J. Picken, *Mol. Cryst. Liq. Cryst.*, **195**, 291, 1991.

[SchWar94] P.G. Schouten, J.W. Warman, M.P. de Haas, C.F. van Nostrum, G.H. Gelinck, R.J.M. Nolte, M.J. Copyn, J.W. Zwikker, M.K. Engel, M. Hanack, Y.H. Chang and W.T. Ford, *J. Am. Chem. Soc.* **116**, 6880, 1994.

[SevUnd93] L.M. Severs, A.E. Underhill, D. Edwards, P. Wight, D. Thetford, *Mol. Cryst. Liq. Cryst.*, **234**, 235, 1993.

[Sha98] A. Shaabani, *J. Chem. Res.*, 672, 1998.

[ShrAtk95] D.F. Shriver, P.W. Atkins, C.H. Langford, *Inorganic Chemistry*, Oxford University Press, 240, 1995.

[SilLuk91] J. Silver, P. Lukes, P. Hey, M.T. Ahmet, *J. Mater. Chem.*, **1**, 881, 1991.

[SimBas93] J. Simon, P. Bassoul, "Phthalocyanine based Liquid Crystals: Towards Submicronic Devices" in *Phthalocyanines, Properties and Applications*, eds. C.C. Leznoff en A.B.P. Lever, VCH Weinheim, Volume 2, 1993.

[SimSir89] J. Simon, C. Sirlin, *Pure & Appl. Chem.*, **61**, 1625, 1989.

[SirBos87] C. Sirlin, L. Bosio, J. Simon, V. Ahsen, E. Yilmazer, O. Bekaroglu, *Chem. Phys. Lett.*, **139**, 362, 1987.

[SirBos88] C. Sirlin, L. Bosio, J. Simon, *Mol. Cryst. Liq. Cryst.*, **155**, 231, 1988.

[TreCla95] K.E. Treacher, G.J. Clarkson, N.B. McKeown, *Mol. Cryst. Liq. Cryst*., **260**, 255, 1995.

[TomHib76] H. Tomoda, E. Hibiya, T. Nakamura, H. Ito, S. Saito, *Chem. Lett*., 1003, 1976.

[TomSai80] H. Tomoda, S. Saito, S. Ogawa, S. Shiraishi, *Chem. Lett*., 1277, 1980.

[Tou95] T. Toupance, PhD thesis, Université de Paris VI, Paris, 1995.

[Ung99] C. Ungurenasu, *Synthesis*, **10**, 1729, 1999.

[UsoByk90] N.V. Usoltseva, V.V. Bykova, N.M. Kormilitsyn, G.A. Ananieva, V.E. Maizlish, *Nuovo Cimento*, **9**, 1237, 1990.

[UsoByk92] N.V. Usoltseva, V.V. Bykova, *Mol. Cryst. Liq. Cryst*., **215**, 89, 1992.

[Uso96] N. Usol'tseva, M*ol. Cryst. Liq. Cryst*., **288**, 201, 1996.

[Uso97] N. Usol'tseva, V. Bykova, A. Semeikin, G. Ananjeva, A. Smirnova, V. Negrimovski, *Mol. Cryst. Liq. Cryst*., **304**, 201, 1997.

[VacDop92] J. Vacus, P. Doppelt, J. Simon, G. Memetzidis, *J. Mater. Chem.*, **2**, 1065, 1992.

[van97] C.F. van Nostrum, *Mol. Cryst. Liq. Cryst*., **302**, 303, 1997.

[vanBos93] C.F. van Nostrum, A.W. Bosman, G.H. Gelinck, S.J. Picken, P.G. Schouten, J.M. Warman, A.J. Schouten, R.J.M. Nolte, *J. Chem. Soc., Chem. Commun*., 1120, 1993.

[vanNee88] J.F. van der Pol, E. Neeleman, J.W. Zwikker, R.J.M. Nolte, W. Drenth, *Recl. Trav. Chim. Pays-Bas*, **107**, 615, 1988.

[vanPic94] C.F. van Nostrum, S.J. Picken, R.J.M. Nolte, *Angew. Chem. Int. Ed. Engl*., **33**, 2173, 1994.

[VilHam01] D. Villemin, M. Hammadi, M. Hachemi, N. Bar, *Molecules*, **6**, 831, 2001.

[WebGui87] P. Weber, D. Guillon, A. Skoulios, *J. Phys. Chem.*, **91**, 2242, 1987.

[WöhSch92] D. Wöhrle, G. Schnurpfeil, G. Knothe, *Dyes and Pigments*, **18**, 91, 1992.

[Wun99] B. Wunderlich, *Thermochim. Acta*, **340**, 37, 1999.

[YamTsu82] M. Yamana, M. Tsutsui, J.S. Ham, *J. Chem. Phys.*, **76**, 2761, 1982.

Chapter 3

METHODOLOGY

3.1 Synthesis

This section deals with the synthetic pathways we followed during the synthetic part of this research project. Because different methods are broadly described in literature, we combined the experience of several researchers in order to obtain our compounds.

3.1.1 Synthesis of the precursors

For the **alkoxy compounds** (Scheme 5), during the first step, catechol was alkylated via a Williamson etherification reaction with two equivalents of the desired alkyl bromide, two equivalents of potassium hydroxide and a drop of a phase-transfer catalyst (Aliquat 336).

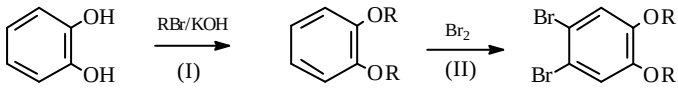

Scheme 5 – Pathway of synthesis for the 1,2-dicyano-4,5-bisalkoxy benzene precursors

In the second step the bisalkylated product was brominated in dichloromethane [MasSir87]. No catalyst was required because of the presence of activating alkoxy substituents.

The **alkyl precursors** (Scheme 6) were synthesised by first reacting *ortho*-dichlorobenzene with a Grignard reagents of the desired chain length in the presence of a catalytic amount of dichloro[1.3-bis(diphenylphosphino)-ethane]nickel(II) [TamSum76, KumTam78]. The second step consisted of the bromination of this compound [CamHil85, OhtJac88].

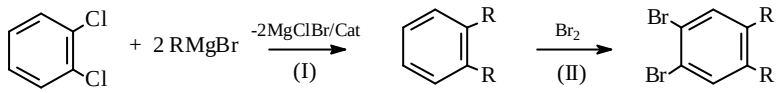

Scheme 6 - Pathway of synthesis for the 1,2-dicyano-4,5-bisalkyl benzene precursors

The **alkoxymethyl precursors** were synthesised by substitution of *ortho*-xylene with bromine [WisAns55, HanBec87], followed by a radical bromination of the two methyl groups of the 1,2-dibromo-4,5-dimethylbenzene with *N*-bromosuccinimide (NBS) in CCl_4 with benzoylperoxide as the initiator [PawHan80]. The alkoxy groups were introduced by the reaction of the tetra-bromo compound with the corresponding alcoholate (Scheme 7) [Pie85].

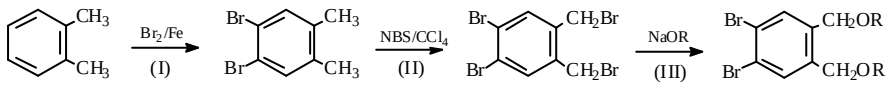

Scheme 7 - Pathway of synthesis for the 1,2-dicyano-4,5-bisalkoxymethyl benzene precursors

The third step for the three types of side-chains consisted of a Rosenmund-Von Braun substitution reaction of the bromo groups by cyano groups (Scheme 8). The dibromo compounds were refluxed with copper(I) cyanide in *N,N*-dimethylformamide (DMF) [EllRom87].

Scheme 8 – Rosenmund-Von Braun substitution reaction

As already pointed out by Severs *et al.* [SevUnd93] a minor impurity can contaminate the final phthalocyanine product. It was therefore necessary that these interferences were completely removed. This was done by column chromatography.

3.1.2 Synthesis of the phthalocyanine ligands

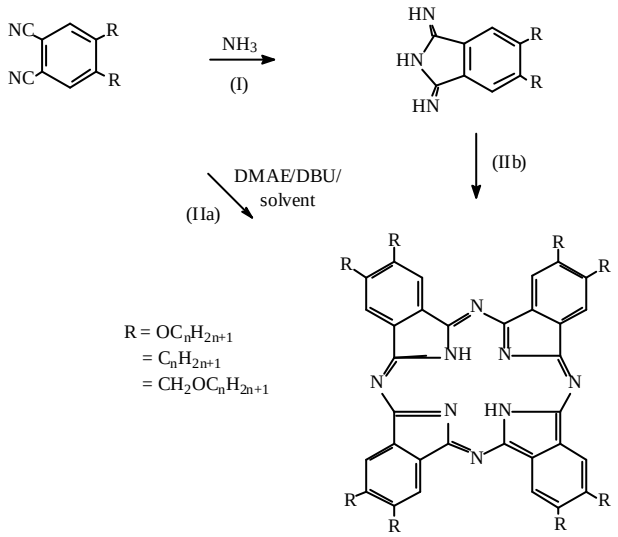

Scheme 9 – Schematic scheme for the synthesis of phthalocyanine ligands

The phthalocyanine is obtained by cyclotetramerisation of the phthalonitrile (step IIa Scheme 9) [VanNee88, WöhSch92] or by first synthesising the iminoisoindoline (step I, IIb) [SchLeh90]. Since the pathway via the

iminoisoindoline requires special precautions for using ammonia as a gas, this step was omitted. Moreover, the overall yield of the phthalocyanine end product was not heavily affected by using the shortcut via the phthalonitrile. The cyclotetramerisation was performed in either dimethylethanolamine (DMAE), 1-pentanol or in 1-hexanol with 1,5-diazabicyclo[5.4.0]undec-7-ene (DBU) as the base. Theoretically, the condensation of four phthalonitrile or iminoisoindoline subunits can only lead to an anti-aromatic macrocyclic structure bearing only 16 p-electrons. It is therefore necessary that a reducing agent is present [YanLin80, PetPli89]. Dimethylethanolamine is an optimal solvent in this case, since it operates as the reducing agent and is a high-boiling solvent at the same time.

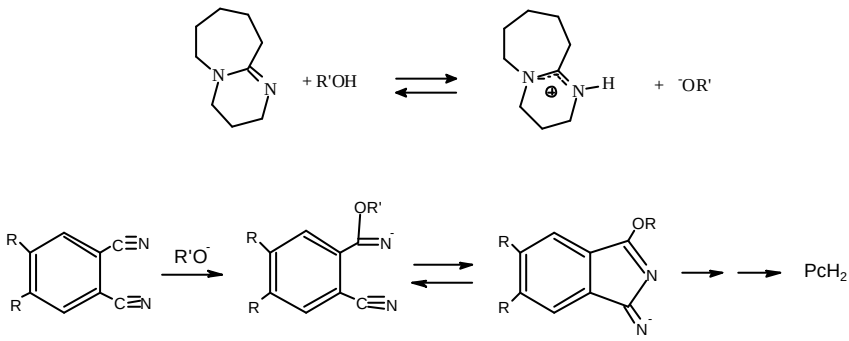

Scheme 10 - Mechanism for phthalocyanine synthesis in a higher alcohol with DBU

The reaction with DBU (or DBN) in a higher alcohol (typically 1-pentanol or 1-hexanol) is generally found to lead to higher yields, especially for the metal complexes [TomSai80]. The DBU molecule acts as a proton acceptor for the alcohol. The mechanism proceeds according to the representation in Scheme 10 [OliSmi87].

3.1.3 Synthesis of the phthalocyanine transition metal complexes

For the synthesis of the transition metal complexes a template type reaction was used (Scheme 11). The disubstituted phthalonitrile was refluxed together with the metal salt in a minimum amount of 2-(dimethylamino)ethanol or 1-pentanol during 48 hours under nitrogen.

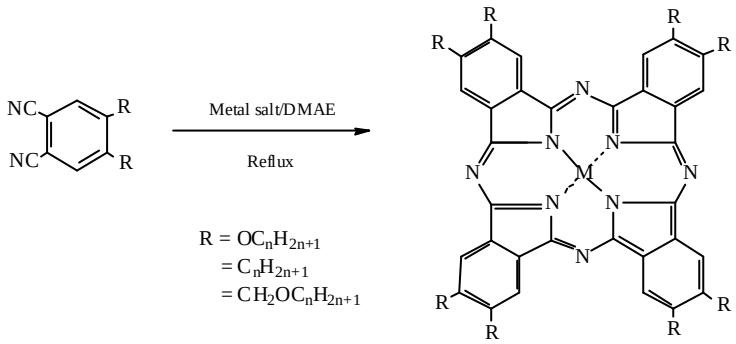

Scheme 11 – Schematic representation of the synthesis of the phthalocyanine transition metal complexes

The mechanism for the template synthesis is shown in Scheme 12. The alcoholate ions play a key role in the synthesis. They initiate the nucleophilic attack on the imide group. The phthalonitriles thus form dimers that group two by two around the metal ion. The presence of the dimers was proven by Gaspard *et al.* [GasMai87]. In the last condensation step, the alcoholate is eliminated and oxidised to an aldehyde. This step frees two electrons that make the macrocycle aromatic (18 π-electrons). The proton is trapped by yet another alcoholate molecule:

$$\text{-OR'} + \text{-N=} \rightarrow \text{RHO} + H^+ + \text{-N=} + 2\,e^-$$

This mechanism justifies the use of 0.5 mol equivalents of DBU for each phthalonitrile.

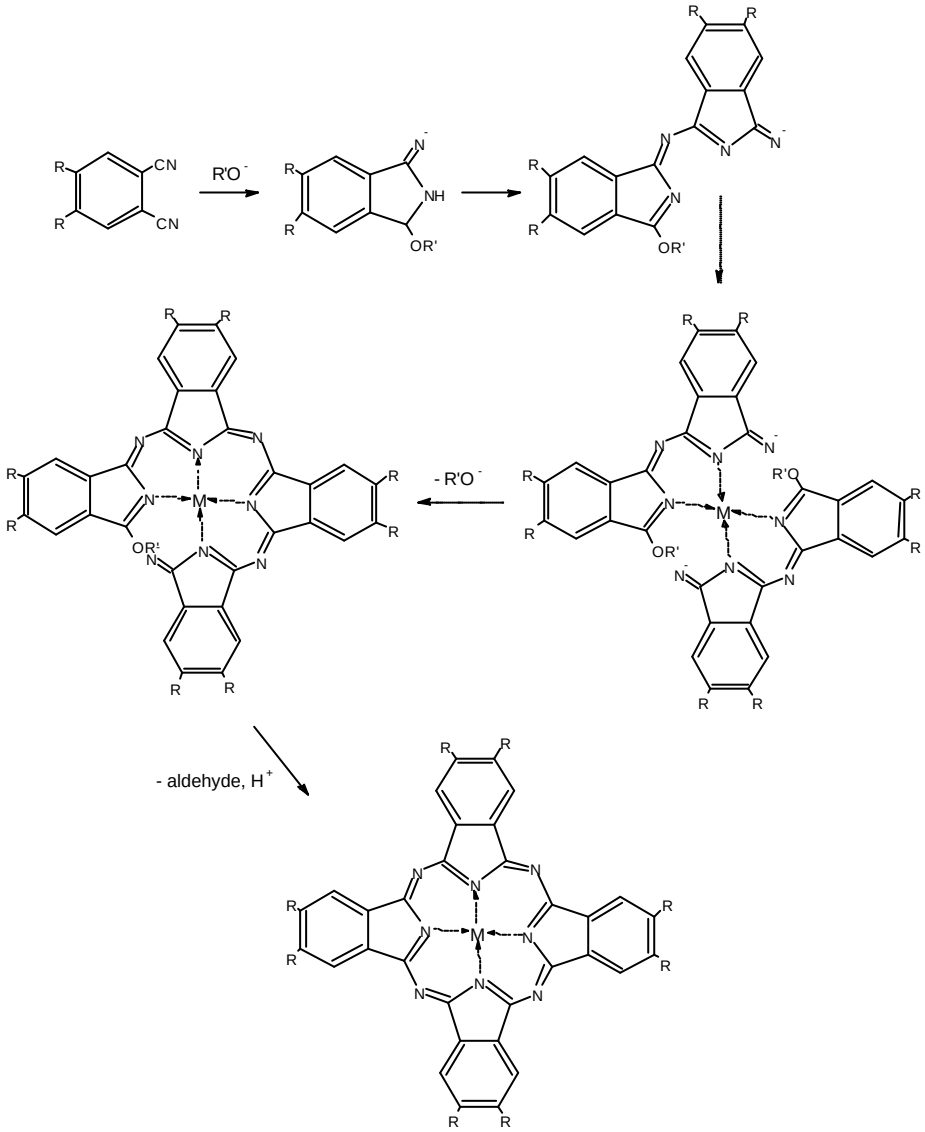

Scheme 12 – Mechanism for the template synthesis of metallophthalocyanines

3.1.4 Synthesis of phthalocyanine lanthanide complexes

3.1.4.1 Octa-substituted phthalocyanine lanthanide complexes

The sandwich complexes containing rare-earth ions (La-Lu, except Pm) were prepared by the template reaction of four phthalonitrile precursors with a lanthanide salt. Scheme 2 shows the reaction for the octa-alkoxy substituted lanthanide bisphthalocyanines. Another route is refluxing the ligand in a high-boiling solvent like 1-chloronaphthalene in the presence of a lanthanide salt [JonHun94]. Deprotonation of H_2Pc in 1-pentanol with potassium pentanolate yields the Pc^{2-} dianon that can be complexed with the lanthanide salt to give the Pc_2Ln complex [PieSim85]. The template reaction, for which we have chosen, consists of a reaction of the phthalonitrile with 1/8 equivalent of lanthanide acetate salt in the presence of ½ equivalent of DBU in 1-hexanol (Scheme 13) [BelSir89] (Jiang *et al.* used 1/16 equivalent lanthanide salt and 1-pentanol as the solvent [JiaLiu97]).

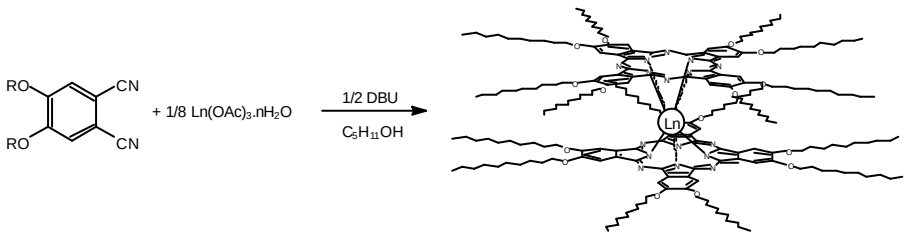

Scheme 13 - Schematic scheme for the synthesis of the bis(octa-alkoxy phthalocyaninato) lanthanide complexes

After a reaction time of twenty hours, the mixture was dissolved in a minimum amount of chloroform and the product is precipitated in methanol and filtered. Further purification to separate the complex from phthalonitrile oligomers and the

metal-free ligand, was done by multiple column chromatography over silicagel, size exclusion chromatography and recrystallisation in ethyl acetate.

3.1.4.2 Unsubstituted phthalocyanine lanthanide complexes

We also synthesised the series (La-Lu, except Pm) of unsubstituted bis(phthalocyaninato) lanthanide(III) complexes. The optical properties of these complexes are used in Chapter 6 for comparison with the spectra of the substituted compounds. As a precursor we used phthalonitrile, which we mixed thoroughly with 1/8 equivalent of the lanthanide salt, urea and a catalytic amount of ammonium molybdate. The mixture (without solvent) was placed in a large tube and this tube was positioned without a cover in a commercial microwave oven (AEG Micromat 110, 2450 MHz). The mixture was irradiated for ten minutes at maximum power (1200 W). A blue-green colour appeared during the reaction time and after cooling, the product was ground to a powder. The excess phthalonitrile was removed by Soxhlet extraction with acetone, ethyl acetate and acetonitrile for eight hours each. The residue was dissolved in methanol and further separated by column chromatography.

Our attempts in synthesising octa-substituted phthalocyanine compounds by means of microwave radiation were not successful, probably due to the demolition of the side-chains. Further research in this area and the use of a more professional microwave source (with better control of the parameters) might yield better results.

3.2 References

[BelSir89] Z. Belarbi, C. Sirlin, J. Simon and J.J. André, *J. Phys. Chem.*, **93**, 8105, 1989.

[CamHil85] M.J. Camenzind, C.L. Hill, *J. Heterocyclic Chem.*, **22**, 575, 1985.

[EllRom87] G.P. Ellis, T.M. Romney-Alexander, *Chem. Rev.*, **87**, 779, 1987.

[GasMai87] S. Gaspard, P. Maillard, *Tetrahedron*, **43**, 1083, 1978.

[HanBec87] M. Hanack, A. Beck, H. Lehmann, *Synthesis*, 703, 1987.

[JiaLiu97] J. Jiang, R.C.W. Liu, T.C.W. Mak, T.W.D. Chan, D.K.P. Ng, *Polyhedron*, **16**, 515, 1997.

[JonHun94] R. Jones, R.A. Hunter and K. Davidson, *Thin Solid Films*, **250**, 249, 1994.

[KumTam78] M. Kumada, K. Tamao, K. Sumitani, *Org. Synth.*, **58**, 127, 1978.

[MasSir87] D. Masurel, C. Sirlin, J. Simon, *New J. Chem.*, **11**, 455, 1987.

[OhtJac88] K. Ohta, L. Jacquemin, C. Sirlin, L. Bosio, J. Simon, *New J. Chem.*, **12**, 751, 1988.

[OliSmi87] S.W. Oliver, T.D. Smith, *J. Chem. Soc. Perkin Trans. 2*, 1579, 1987.

[PawHan80] G. Pawlowski, M. Hanack, *Synthesis*, 287, 1980.

[PetPli89] M.A. Petit, V. Plichon, H. Belkacemi, *New J. Chem.*, **13**, 459, 1989.

[Pie85] C. Piechocki, PhD thesis, Université de Paris VI, 288, 1985.

[PieSim85] C. Piechocki, J. Simon, J.J. André, D. Guillon, P. Petit, A. Skoulios, P. Weber, *Chem. Phys. Lett.*, **122**, 124, 1985.

[SchLeh90] H. Schultz, H. Lehmann, M. Rein, M. Hanack, *Struct.Bond.*, **74**, 41, 1990.

[SevUnd93] L.M. Severs, A.E. Underhill, D. Edwards, P. Wight, D. Thetford, *Mol. Cryst. Liq. Cryst.*, **234**, 235, 1993.

[TamSum76] K. Tamao, K. Sumitani, Y. Kiso, M. Zembayashi, A. Fujioka, S. Kodama, I. Nakajima, A. Minato, M. Kumada, *Bull. Chem. Soc. Jpn*., **49**, 1958, 1976.

[TomSai80] H. Tomoda, S. Saito, S. Ogawa, S. Shiraishi, *Chem. Lett*., 1277, 1980.

[VanNee88] J.F. van der Pol, E. Neeleman, J.W. Zwikker, R.J.M. Nolte, W. Drenth, *Recl. Trav. Chim. Pays-Bas*, **107**, 615, 1988.

[WisAns55] W.A. Wisansky, S. Ansbacher, *Org. Syn. Coll. Vol. 3*,148, 1955.

[WöhSch92] D. Wöhrle, G. Schnurpfeil, G. Knothe, *Dyes and Pigments*, **18**, 91, 1992.

[YanLin80] C.H. Yang, S.F. Lin, H.L. Chen, C.T. Chang, *Inorg. Chem.*, **19**, 3541, 1980.

Chapter 4

EXPERIMENTAL SECTION

4.1 Characterisation

All the intermediate products, phthalocyanine ligands and complexes were characterised by ^{1}H-NMR, mass spectroscopy, IR-spectroscopy and CHN microanalysis. The complexes were characterised by MALDI-TOF mass spectroscopy, UV/VIS spectroscopy and CHN microanalysis. The mesomorphic properties were studied by DSC, TGA, POM and XRD. UV/VIS and MCD were used to measure the optical properties of our compounds. The following paragraphs give an overview in detail of the used instruments.

4.1.1 ^{1}H-NMR

All ^{1}H NMR spectra were recorded on a Bruker Avance 300 spectrometer (300 MHz) using $CDCl_3$ as solvent and tetramethylsilane (TMS) as the internal standard. The abbreviations used for the description of the spectra are: s, singlet; d, doublet; t, triplet; b, broad; m, multiplet. All chemical shifts are given in ppm relative to TMS.

4.1.2 CHN

Elemental analyses (CHN) were performed on a CE-Instrument EA-1110 elemental analyser.

4.1.3 IR

IR spectra have been obtained on a Bruker IFS66 FTIR-spectrometer. The KBr-pellet technique was used to measure the samples. The abbreviations used for the description of the intensities of the transitions are: w (weak), m (medium) en s (strong).

4.1.4 UV/VIS

UV-VIS spectra have been measured on a Shimadzu UV-3100 spectrophotometer.

4.1.5 MCD

MCD spectra were recorded on an AVIV 62 DS CD-spectrometer, extended with an electromagnet (1 Tesla).

4.1.6 DSC

Differential scanning calorimetry (DSC) measurements were done on a Mettler-Toledo DSC821e module (scan rate 10 °C min^{-1} under a helium flow).

4.1.7 Microscopy

Optical textures of the mesophases were observed with an Olympus BX60 polarising microscope equipped with a Linkam THMS600 hot stage and a Linkam TMS93 programmable temperature controller.

4.1.8 TGA

Thermogravimetric analyses were performed with a Polymer Laboratories STA1000H TG-DTA apparatus, using a static air atmosphere or with a TA Instruments Hi-Res TGA 2950 Thermogravimetric Analyser (argon flow). The experiments on the latter instrument were carried out in the high-resolution mode.

The principle used was that when a reaction started, the heating rate was decreased in accordance to the mass loss. The maximum heating rate was set at 10 °C min^{-1}. As a consequence, the temperatures at which the transitions occurred were better defined. In order to identify the evolved gasses, TG-MS experiments were performed by coupling a TG 951-2000 thermogravimeter (TA Instruments) to a quadrupole mass spectrometer (Model Thermolab of VG Fisons Instruments), using a flexible heated silica lined steel capillary and a molecular leak. Platinum cups were used as sample holder. The analyses were done at IMO, Laboratory of Inorganic and Physical Chemistry, Limburgs Universitair Centrum by Daniël Nelis under the supervision of Prof. Jules Mullens.

4.1.9 XRD

X-ray diffractograms were recorded by Dr. Dirk Hinz at the University of Köln in Germany (Prof. Gerd Meyer) and at the Institut de Physique et Chimie des Matériaux de Strasbourg (ICPMS) in France. We give a short description of the instruments at both institutions. Details can be found in Appendix D.

Köln: High temperature X-ray diffraction was measured on a STOE Transmission Powder Diffractometer System STADI P, with a high temperature attachment version 0.65.1 (temperature range from room temperature to 1000 °C). Monochromatic Cu $K_{\alpha 1}$ radiation (λ = 1.5406 Å) was obtained with the aid of a curved germanium primary monochromator. Diffracted X-rays were measured by a linear Position Sensitive Detector (PSD). The sample was placed in a quartz glass capillary (outer diameter 0.3 mm, wall thickness 0.01 mm) and spinned during the measurement. In general, data were collected in the range $1 < 2\theta < 40°$.

Strasbourg: The XRD patterns were obtained with two different experimental set-ups, the crude powder was filled in Lindemann capillaries of 1 mm diameter. A linear monochromatic Cu-Ka_1 beam (λ = 1.5405Å) was obtained using a Guinier camera with a sealed-tube generator (900 W) and a Debye-Scherrer camera

equipped with a bent quartz monochromator and an electric oven. A first set of diffraction patterns was registered with a curved counter "Inel CPS 120" associated with a data acquisition computer system; periodicities up to 60 Å can be measured, and the sample temperature is controlled within ±0.05°C. The two other sets of diffraction patterns were registered on an image plate. With the Guinier camera, periodicities up to 90 Å can be measured (the sample temperature is controlled within ±0.3°C). The other set up, periodicities up to 300Å can be measured, and the cell parameters were calculated from the position of the reflection at the smallest Bragg angle, which was in all cases the most intense. In each case, exposure times were varied from 1 to 24 hours depending on the mesophase being observed and upon the specific reflections being sought (weaker reflections obviously taking longer exposure times).

4.1.10 Mass spectroscopy

Mass spectra of the organic precursors were recorded on a low-resolution electron-impact Hewlett-Packard 5989A for low molecular mass substances. For the phthalocyanines a Micromass Quattro II (triple quadrupole) was used. The complexes (except for the unsubstituted Pc_2Ln) were determined by MALDI-TOF measurements on a VG Tofspec SE (Micromass, UK) equipped with a N_2-laser (337 nm). The MALDI-TOF measurements were done by Dr. Geert Baggerman of the laboratory for Developmental Physiology and Molecular Biology (Prof. A. De Loof).

4.2 Synthesis precursors

4.2.1 1,2-dicyano-4,5-bisalkoxy benzene precursors

We synthesised compounds with chain lengths ranging from $-OC_4H_9$ to $-OC_{20}H_{42}$ in order to study the effect of the chain length on the mesomorphic behaviour. The

synthesis of the bis(alkoxy)benzenes was done by means of a Williamson ether synthesis, via a phase transfer mechanism: catechol was heated during 3 hours at 120 °C under N_2-atmosphere together with the (liquid) bromoalkane and the base (KOH). A catalytic amount of Aliquat 336 was also added. For the longer chain lengths (starting from $C_{17}H_{35}Br$) the bromoalkanes were no longer liquid at room temperature, so we melted them first in the erlenmeyer before adding the other reactants. Purification was done by recrystallisation in acetone. Most products were pure after one or more recrystallisations (the purity was checked by ^{1}H-NMR, CHN-analysis and TLC). For a number of shorter chain lengths (-OC_4H_9 to -OC_8H_{17}) the reaction product was liquid and they were purified by distillation *in vacuo*.

The Williamson-synthesis was followed by a bromination of the bisalkylated catechol in the 4- and 5-positions. The product was dissolved in dichloromethane (DCM) and placed in an ice bath. A solution of bromine in DCM was slowly added and after complete addition the mixture was stirred for 2 hours. The organic layer was then washed with a saturated sodium metabisulfite solution, a saturated sodium hydrogen carbonate solution and with water. After drying and evaporation of the solvent the product was purified by recrystallisation in acetone. For some compounds the TLC gave evidence for the presence of monobrominated product. Hence, the compound was brominated a second time with an appropriate equivalent of bromine. Nevertheless, a chromatographic separation over silicagel with ethyl acetate in *n*-hexane was sometimes necessary. This procedure was also needed for the liquid dibrominated bisalkoxybenzenes (-OC_4H_9 and -OC_6H_{13}).

Though for most chain lengths we obtained good yields for steps one and two (usually over > 80 %), a bottleneck in our synthesis was the Rosenmund-Von Braun reaction for the formation of the dicyano compounds [EllRom87]. The reaction was done by refluxing the dibromobis(alkoxy)benzene in dimethylformamide (DMF) during 6 hours under nitrogen atmosphere in the presence of a slight excess of CuCN (ratio CuCN/dibrominated product: 2.7).

After cooling the mixture was poured into an ammonium hydroxide solution that was stirred for a day in order to remove the excess of copper(II) ions by complexing them. This is of utmost importance to prevent the formation of copper phthalocyanine in the next cyclotetramerisation step. Next, the solution was filtered and the residue was washed extensively with DCM. The organic layer is separated and washed with water. After drying and evaporation of the solvent, TLC showed that we obtained a mixture of dicyanobenzene, the monosubstituted product and the initial compound. In some cases an additional reaction with CuCN favoured the formation of the wanted compound, but we still ended up with a mixture. Repeated recrystallisation in hexane leads to the pure product, but in low yields. A labour-intensive separation by column chromatography over silica with toluene as the eluent was done. The yields for the Rosenmund-Von Braun reaction were almost never higher than 60 %.

Table 1 gives an overview of the yields of all the intermediate and end products. As mentioned above, the first two steps gave in general good yields (> 60%). The third step only gave a moderate yield (20-50 %).

Table 1 - Yields of the three consecutive synthesis steps for the bis(alkoxy)dicyanobenzene precursors

Compound	Step I (%)	Step II (%)	Step III (%)	Compound	Step I (%)	Step II (%)	Step III (%)
$-OC_4H_9$	10	91	51	$-OC_{13}H_{27}$	69	90	43
$-OC_5H_{11}$	93	85	33	$-OC_{14}H_{29}$	20	86	44
$-OC_6H_{13}$	81	72	51	$-OC_{15}H_{31}$	44	93	34
$-OC_7H_{15}$	90	92	21	$-OC_{16}H_{33}$	79	91	49
$-OC_8H_{17}$	61	79	37	$-OC_{17}H_{35}$	68	88	27
$-OC_9H_{19}$	66	82	28	$-OC_{18}H_{37}$	52	98	17
$-OC_{10}H_{21}$	80	92	29	$-OC_{19}H_{39}$	82	45	39
$-OC_{11}H_{23}$	54	88	21	$-OC_{20}H_{41}$	76	97	2.5
$-OC_{12}H_{25}$	70	94	61				

Here, we only describe the synthesis of the precursor with two -$OC_{10}H_{21}$ side chains. For the synthesis of the other chain lengths the same analytical techniques were used to ensure the purity of the compounds. Tables 2 to 4 show the elemental analysis results for the intermediate bis(alkoxy)benzenes, dibromo-bis(alkoxy)benzenes and the dicyanobis(alkoxy)benzenes respectively.

Table 2 - Elemental analysis data for the bis(alkoxy)benzene intermediates

Chain length	Compound	Calculated			Found		
		C (%)	H (%)	N (%)	C (%)	H (%)	N (%)
4	$C_{14}H_{22}O_2$	75.63	9.97	—	75.39	9.49	—
5	$C_{16}H_{26}O_2$	76.75	10.47	—	76.38	10.35	—
6	$C_{18}H_{30}O_2$	77.65	10.86	—	77.33	10.70	—
7	$C_{20}H_{34}O_2$	78.38	11.18	—	78.26	11.06	—
8	$C_{22}H_{38}O_2$	78.99	11.45	—	78.64	11.10	—
9	$C_{24}H_{42}O_2$	79.50	11.68	—	79.42	11.62	—
10	$C_{26}H_{46}O_2$	79.94	11.87	—	79.72	11.84	—
11	$C_{28}H_{50}O_2$	80.32	12.04	—	80.32	12.03	—
12	$C_{30}H_{54}O_2$	80.65	12.18	—	80.32	12.08	—
13	$C_{32}H_{58}O_2$	80.95	12.31	—	80.82	12.29	—
14	$C_{34}H_{62}O_2$	81.21	12.43	—	80.88	12.34	—
15	$C_{36}H_{66}O_2$	81.44	12.53	—	81.23	12.24	—
16	$C_{38}H_{70}O_2$	81.65	12.62	—	81.54	12.54	—
17	$C_{40}H_{74}O_2$	81.84	12.71	—	81.58	12.77	—
18	$C_{42}H_{78}O_2$	82.02	12.78	—	81.86	12.88	—
19	$C_{44}H_{82}O_2$	82.17	12.85	—	82.09	12.61	—
20	$C_{46}H_{86}O_2$	82.32	12.92	—	82.16	12.88	—

Synthesis of 1,2-bis(decyloxy)benzene

From a mixture of 22 g (0.2 mol) of catechol, 88.5 g of 1-bromodecane (0.4 mol), 26.5 g of potassium hydroxide (0.4 mol) and 1 mL of Aliquat 336 phase transfer catalyst, oxygen was removed by repeated evacuation followed by admission of

nitrogen. Next, the mixture was heated at 100 °C in a dry nitrogen atmosphere with stirring. After 8 hours, 250 mL of water and 100 mL of dichloromethane were added. The organic layer was separated and the aqueous layer extracted three times with 50 mL of ether. The combined organic layers were washed with 200 mL of water, dried over $MgSO_4$ and concentrated. The residue was recrystallised from acetone. Yield: 80% (62 g); m.p. 41 °C. MS *m/z:* 390 (M^+). IR (KBr): 3000-2750 (alkyl); 1500 (aryl); 750 (*o*-substituted benzene) cm^{-1}. ^{1}H-NMR δ ($CDCl_3$): 0.88 (t, 6H, CH_3), 1.27 (m, 24H, CH_2), 1.80 (m, 4H, CH_2), 3.99 (t, 4H, OCH_2), 6.88 (s, 4H, Ar). CHN-analysis: $C_{26}H_{46}O_2$ (390.64). Calcd (%): C, 79.94; H, 11.87. Found (%): C, 79.72; H, 11.84.

Table 3 - Elemental analysis data for the dibromobis(alkoxy)benzene intermediates

Chain length	Compound	Calculated			Found		
		C (%)	H (%)	N (%)	C (%)	H (%)	N (%)
4	$C_{14}H_{20}O_2Br_2$	44.24	5.30	—	43.82	5.20	—
5	$C_{16}H_{24}O_2Br_2$	47.08	5.93	—	46.78	5.91	—
6	$C_{18}H_{28}O_2Br_2$	49.56	6.50	—	49.54	6.38	—
7	$C_{20}H_{32}O_2Br_2$	51.74	6.95	—	51.61	6.87	—
8	$C_{22}H_{36}O_2Br_2$	53.67	7.37	—	53.12	7.26	—
9	$C_{24}H_{40}O_2Br_2$	55.39	7.75	—	55.45	7.80	—
10	$C_{26}H_{44}O_2Br_2$	56.94	8.09	—	57.19	8.16	—
11	$C_{28}H_{48}O_2Br_2$	58.34	8.39	—	58.85	8.46	—
12	$C_{30}H_{52}O_2Br_2$	59.60	8.67	—	59.20	8.55	—
13	$C_{32}H_{56}O_2Br_2$	60.76	8.93	—	60.85	9.08	—
14	$C_{34}H_{60}O_2Br_2$	61.81	9.15	—	62.14	9.23	—
15	$C_{36}H_{64}O_2Br_2$	62.78	9.37	—	62.80	9.35	—
16	$C_{38}H_{68}O_2Br_2$	63.68	9.56	—	63.60	9.52	—
17	$C_{40}H_{72}O_2Br_2$	64.50	9.74	—	64.99	9.98	—
18	$C_{42}H_{76}O_2Br_2$	65.27	9.91	—	66.03	10.27	—
19	$C_{44}H_{80}O_2Br_2$	65.98	10.07	—	66.09	10.29	—
20	$C_{46}H_{84}O_2Br_2$	66.65	10.21	—	66.73	10.28	—

Synthesis of 1,2-dibromo-4,5-bis(decyloxy)benzene

To a solution of 20 g (0.05 mol) of 1,2-bis(decyloxy)benzene in 100 mL of dichloromethane, a solution of 5.1 mL (0.10 mol) of bromine in 15 mL of dichloromethane was added over circa 1 hour, the first half at 0 °C, the second half at room temperature. The mixture was stirred over night at room temperature. The reaction mixture was washed with sat'd $Na_2S_2O_5$, sat'd $NaHCO_3$, and twice with water. The extract was dried over $MgSO_4$ and evaporated to dryness. Purification was done by recrystallisation from acetone. Yield: 92% (26 g); m.p. 42 °C. MS *m/z:* 548 (M^+). IR (KBr): 3000-2750 (alkyl); 1500 (aryl); 750 (*o*-substituted benzene) cm^{-1}. ^{1}H-NMR δ ($CDCl_3$): 0.88 (t, 6H, CH_3), 1.27 (m, 24H, CH_2), 1.77 (m, 4H, CH_2), 3.94 (t, 4H, OCH_2), 7.06 (s, 2H, Ar). CHN-analysis: $C_{26}H_{44}O_2Br_2$ (548.43). Calcd (%): C, 56.94; H, 8.09. Found (%): C, 57.19; H, 8.16.

Synthesis of 1,2-dicyano-4,5-bis(decyloxy)benzene

A mixture of 25.4 g (0.05 mol) of 1,2-dibromo-4,5-bis(decyloxy)benzene and 12.1 g (0.14 mol) of CuCN was heated at reflux in 100 mL of DMF for 6 hours under an atmosphere of dry nitrogen. After leaving to cool to room temperature, the reaction mixture was poured in an aqueous ammonia solution (25%, 1L) and stirred for 62 hours. The mixture was filtered, the water phase extracted with DCM and the remaining solid was poured into an aqueous ethylene diamine solution and stirred for 12 hours. After filtration, the solid was washed with water, dissolved in dichloromethane, filtrated and evaporated to dryness. The crude product was purified by column chromatography over SiO_2 (eluent: chloroform) and recrystallised from hexane. Yield: 29% (5.3 g); m.p. 106 °C. MS *m/z*: 440 (M^+). IR (KBr): 2750-3000 (alkyl); 2240 (CN); 1500 (aryl); 750 (o-substituted benzene) cm^{-1}. ^{1}H-NMR δ ($CDCl_3$): 0.88 (t, 6H, CH_3), 1.27 (m, 24H, CH_2), 1.86 (m, 4H, CH_2), 4.05 (t, 4H, OCH_2), 7.11 (s, 2H, Ar). CHN-analysis: $C_{28}H_{44}O_2N_2$

(440.66). Calcd (%): C, 76.32; H, 10.06; N, 6.36. Found (%): C, 76.18; H, 10.05; N, 6.19.

Table 4 - Elemental analysis data for the dicyanobis(alkoxy)benzene intermediates

Chain length	Compound	Calculated			Found		
		C (%)	H (%)	N (%)	C (%)	H (%)	N (%)
4	$C_{16}H_{20}N_2O_2$	70.56	7.40	10.29	70.19	7.37	10.15
5	$C_{18}H_{24}N_2O_2$	71.97	8.05	9.33	71.88	8.05	9.27
6	$C_{20}H_{28}N_2O_2$	73.14	8.59	8.53	73.00	8.58	8.47
7	$C_{22}H_{32}N_2O_2$	74.12	9.05	7.86	74.08	9.05	7.84
8	$C_{24}H_{36}N_2O_2$	74.96	9.44	7.28	74.65	9.40	7.22
9	$C_{26}H_{40}N_2O_2$	75.68	9.77	6.79	75.39	9.73	6.67
10	$C_{28}H_{44}N_2O_2$	76.32	10.06	6.36	76.18	10.05	6.19
11	$C_{30}H_{48}N_2O_2$	76.87	10.32	5.98	76.58	10.28	5.85
12	$C_{32}H_{52}N_2O_2$	77.37	10.55	5.64	77.12	10.44	5.51
13	$C_{34}H_{56}N_2O_2$	77.81	10.76	5.34	77.54	10.69	5.21
14	$C_{36}H_{60}N_2O_2$	78.21	10.94	5.07	78.10	10.89	4.97
15	$C_{38}H_{64}N_2O_2$	78.57	11.10	4.82	78.12	11.04	4.73
16	$C_{40}H_{68}N_2O_2$	78.89	11.25	4.60	78.78	11.23	4.46
17	$C_{42}H_{72}N_2O_2$	79.19	11.39	4.40	78.94	11.28	4.35
18	$C_{44}H_{76}N_2O_2$	79.46	11.52	4.21	78.70	11.44	4.01
19	$C_{46}H_{80}N_2O_2$	79.71	11.63	4.04	79.68	11.61	3.86
20	$C_{48}H_{84}N_2O_2$	79.94	11.74	3.88	77.92	11.49	3.53

4.2.2 1,2-dicyano-4,5-bisalkyl benzene precursors

For the alkyl precursors, we restricted the synthesis to six different chain lengths. We had to deal with some initial problems when facing the Grignard-like reaction. In spite of the rigorous conditions we were working under, we did not or only partly succeed in obtaining the bisalkylated products. The use of THF instead of ether as the solvent and reagents from various suppliers did not improve the outcome. Nevertheless, working under less strict circumstances (no dry solvents,

glassware used without preliminary heating) did yield the desired compounds in an acceptable yield. A dilute acid solution was added to the reaction product and the water layer was extracted with dichloromethane (DCM). The organic layer was dried and evaporated. The products were liquid for the shorter chain lengths but solid starting from chain length -$C_{14}H_{29}$. For the liquids purification was done by means of silica column chromatography with heptane as the eluent and by recrystallisation in heptane for the solids.

The bromination also yielded products that were solid starting from -$C_{14}H_{29}$. The compounds were all purified by silica column chromatography with heptane as the eluent.

The cooled reaction mixture after the Rosenmund-Von Braun reaction was poured out in a 25% ethylene diamine solution and was left stirring for 24 hours in order to remove any excess copper ions by chelating. The solution was filtered and the residue was thoroughly washed with DCM. The organic solution obtained from this procedure was washed with water. After drying and evaporation we obtained in most cases a mixture of the dibromo-bis(alkyl)benzene, the mononitrile and the desired product (based on TLC).

Table 5 - Yields of the three consecutive synthesis steps for the bis(alkyl)dicyanobenzene precursors

Compound	Step I (%)	Step II (%)	Step III (%)
-C_7H_{15}	58	82	15
-C_8H_{17}	43	87	13
-$C_{12}H_{25}$	67	89	23
-$C_{14}H_{29}$	43	79	10
-$C_{16}H_{33}$	65	56	22
-$C_{18}H_{37}$	68	45	16

The purification had to be performed by means of labour-extensive silica column chromatography with toluene as the eluent. For chain lengths below -$C_{12}H_{25}$ multiple column chromatography was necessary. The yields for the substitution reaction were never higher than 25 %. Additional reaction of the monophthalonitrile increased the final yield. Table 5 gives an overview of the yields we obtained for the different intermediate steps.

The synthesis of the precursor with two -$C_{12}H_{25}$ side chains is described below. For the synthesis of the other chain lengths the same analytical techniques were used to ensure the purity of the compounds. Tables 6 to 8 show the elemental analysis results for the intermediate bis(alkyl)benzenes, dibromobis(alkyl)-benzenes and the dicyanobis(alkyl)benzenes respectively.

Table 6 - Elemental analysis data for the bis(alkyl)benzene intermediates

Chain length	Compound	Calculated			Found		
		C (%)	H (%)	N (%)	C (%)	H (%)	N (%)
7	$C_{20}H_{34}$	87.52	12.49	—	87.35	12.31	—
8	$C_{22}H_{38}$	87.34	12.66	—	87.13	12.33	—
12	$C_{30}H_{54}$	86.88	13.12	—	86.75	12.88	—
14	$C_{34}H_{62}$	86.73	13.27	—	86.56	12.98	—
16	$C_{38}H_{70}$	86.61	13.39	—	86.60	13.03	—
18	$C_{42}H_{78}$	86.52	13.48	—	86.50	13.40	—

Synthesis of 1,2-bis(dodecyl)benzene

Magnesium turnings (23 g; 0.95 mol) were dried by heating them in a three-neck flask under nitrogen atmosphere in order to activate the magnesium. After cooling dry diethyl ether (400 mL) were added. A mixture of bromododecane (228 mL; 0.95 mol) in 200 mL of ether was added slowly over a period of an hour. Afterwards the mixture was refluxed during 1.5 hour. After cooling in an ice bath, dichloro[1.3-bis(diphenylphosphino)-ethane]nickel(II) catalyst (0.75 g) was added.

A solution of dichlorobenzene (42 mL; 0.4 mol) in 250 mL dry diethyl ether was added gradually over a few minutes. The mixture was stirred during 1 hour at room temperature and is refluxed for a period of 10 hours afterwards. After cooling in an ice bath, the mixture was hydrolysed with a dilute solution of HCl. The desired product was separated by extraction with diethyl ether. After drying on $MgSO_4$ and evaporation of the solvent an oily liquid was obtained. Purification was done by means of column chromatography with silica as the stationary phase and *n*-hexane as the eluent. Yield: 67% (112.5 g). MS *m/z:* 415 (M^+). R_f (*n*-hexane): 0.61. ^{1}H-NMR ($CDCl_3$) δ: 0.88 (t, 6H, CH_3), 1.26 (b, 36H, CH_2), 1.54 (m, 4H, β-CH_2), 2.59 (t, 4H, a-CH_2), 7.20 (s, 4H, Ar). CHN-analysis: $C_{30}H_{54}$ (414.75). Calcd (%): C, 86.88; H, 13.12. Found (%): C, 86.75; H, 12.88.

Table 7 - Elemental analysis data for the dibromobis(alkyl)benzene intermediates

Chain length	Compound	Calculated			Found		
		C (%)	H (%)	N (%)	C (%)	H (%)	N (%)
7	$C_{20}H_{32}Br_2$	55.57	7.46	—	55.51	7.37	—
8	$C_{22}H_{36}Br_2$	57.40	7.88	—	56.89	7.96	—
12	$C_{30}H_{52}Br_2$	62.93	9.15	—	62.16	9.27	—
14	$C_{34}H_{60}Br_2$	64.96	9.62	—	64.83	9.51	—
16	$C_{38}H_{68}Br_2$	66.65	10.01	—	66.43	9.88	—
18	$C_{42}H_{76}Br_2$	68.09	10.34	—	67.67	10.31	—

Synthesis of 1,2-dibromo-4,5-bis(dodecyl)benzene

A solution of bromine (25.8 mL; 0.5 mol) in 250 mL of CCl_4 was slowly added to an ice-cooled solution of 1,2-bis(dodecyl)benzene (112.5 g; 0.27 mol) in 250 mL of CH_2Cl_2, with 0.75 g of iron filings and 0.150 g of I_2. The mixture was stirred during 10 hours at room temperature. The excess bromine was neutralised by adding a saturated solution of sodium metabisulfite ($Na_2S_2O_5$). The organic layer was washed with a 10% NaOH solution and with water. After drying over $MgSO_4$

and evaporation of the solvent, the purification was performed by column chromatography with silica as the stationary phase and *n*-hexane as the eluent. Yield: 89% (134.7 g). R_f (*n*-heptane): 0.62. MS *m/z:* 573 (M^+). ^{1}H-NMR ($CDCl_3$) δ: 0.88 (t, 6H, CH_3), 1.26 (b, 36H, CH_2), 1.52 (m, 4H, β-CH_2), 2.50 (t, 4H, α-CH_2), 7.35 (s, 2H, Ar). CHN-analysis: $C_{30}H_{52}Br_2$ (572.54). Calcd (%): C, 62.93; H, 9.15. Found (%): C, 62.16; H, 9.27.

Table 8 - Elemental analysis data for the dicyanobis(alkyl)benzene intermediates

Chain length	Compound	Calculated			Found		
		C (%)	H (%)	N (%)	C (%)	H (%)	N (%)
7	$C_{22}H_{32}N_2$	81.43	9.94	8.63	81.09	9.79	8.54
8	$C_{24}H_{36}N_2$	81.76	10.29	7.95	82.28	10.53	7.84
12	$C_{32}H_{52}N_2$	82.70	11.28	6.03	82.77	11.53	5.75
14	$C_{36}H_{60}N_2$	83.01	11.61	5.38	82.78	11.44	5.14
16	$C_{40}H_{68}N_2$	83.27	11.88	4.86	83.23	11.81	4.93
18	$C_{44}H_{76}N_2$	83.48	12.10	4.42	83.39	12.01	4.21

Synthesis of 1,2-dicyano-4,5-bis(dodecyl)benzene

1,2-dibromo-4,5-bis(dodecyloxy)benzene (25 g; 0.044 mol) and CuCN (11.73 g; 0.13 mol) in 400 mL of DMF were heated at 155 °C during 5 hours under an argon atmosphere. The reaction mixture was filtered and the residue is washed extensively with dichloromethane. The combined organic layers were treated with ethylenediamine during 24 hours. The organic layer was separated and washed with water. After drying over $MgSO_4$ and evaporation of the solvent, the product was purified by column chromatography with silica as the stationary phase and toluene as the eluent. Yield: 23% (5 g); m.p.: 31 °C. MS *m/z:* 465 (M^+). R_f (toluene): 0.68. ^{1}H-NMR ($CDCl_3$) δ: 0.90 (t, 6H, CH_3), 1.28 (b, 40H, CH_2), 4.05 (t, 4H, α-CH_2), 7.45 (s, 2H, Ar). CHN-analysis: $C_{32}H_{52}N_2$ (464.77). Calcd (%): C, 82.70; H, 11.28; N, 6.03. Found (%): C, 82.77; H, 11.53; N, 5.75.

4.2.3 1,2-dicyano-4,5-bisalkoxymethyl benzene precursors

For the alkoxymethyl-type precursors, we restricted ourselves to three chain lengths: $-CH_2OC_8H_{17}$, $-CH_2OC_{12}H_{25}$ and $-CH_2OC_{16}H_{33}$. For the first common step for all chain lengths, the bromination on the aromatic ring of the *o*-xylene had to be executed in the presence of a catalytic amount of iron and a iodide crystal because of the deactivating methyl groups. As soon as the iodide colour had disappeared, the bromine was added to the cooled mixture (±10 °C) at such a rate that the temperature remained constant. The evolving HBr fumes were collected in a gas washing flask filled with a basic sodium hydroxide solution by leading a nitrogen stream over the reaction mixture. After the addition of the bromine, the reaction mixture was stirred another 48 hours at room temperature. The organic mixture was washed with a dilute solution of sodium metabisulfite ($Na_2S_2O_5$) in order to remove the excess of bromine. The layers were separated and the organic layer was consecutively washed twice with water. The organic layer was then dried and the solvent evaporated. As the yellowish oil was cooled in the refrigerator, crystallisation occurred. The white solid was filtered over a cold Büchner funnel and the precipitate was washed with petroleum ether. By sequential evaporating, cooling the filtrate, filtering and collecting the crystals the yield of the reaction could be increased. The combined (lachrymatory) solids were consecutively dried *in vacuo*.

The second common step was the side-chain bromination. This was done by mixing the dibromo compound with *N*-bromosuccinimide (NBS) and benzoylperoxide as the initiator in CCl_4. The mixture was refluxed and the start of the radical reaction could be observed by a sudden intensification of the reflux. The succinimide collects at the top of the solution. After the slowing down of the reaction was noticed, the mixture was refluxed for another hour. The mixture was cooled, filtrated and evaporated. By adding warm petroleum ether (30-60°C) some remaining succinimide was precipitated. The succinimide was filtered off and the

filtrate was again evaporated. The obtained oil was cooled in the refrigerator and crystallisation occurred. The yellow-white solid was filtered over a cold Büchner funnel and the precipitate was washed with petroleum ether. As for the dibromo-*o*-xylene, by sequential evaporating, cooling and filtration the yield of the reaction could be increased. Next, the combined (lachrymatory) solids were dried *in vacuo*.

The introduction of the side-chains was done by a nucleophilic substitution. By using a protic solvent and a large excess of the alcohol of the desired chain length satisfying yields were obtained. First the alcohol was transformed into the alcoholate by adding it to a solution of *t*-BuO$^-$K$^+$ in *tert*-butylalcohol. The tetrabromo derivate was added slowly and the mixture was refluxed for another 48 hours under inert atmosphere. The mixture was poured in water and neutralised with a dilute HCl solution. After extraction, drying and evaporation, the excess *tert*-buytlalcohol was removed by distillation *in vacuo*. Further purification was done by column chromatography in silica and $CHCl_3$ as the eluent. The product with chain length -$CH_2OC_8H_{17}$ was liquid, whereas the other chain lengths were solids.

The fourth step, the Rosenmund-Von Braun reaction, was carried out as described for the other two precursor-types. Purification by silica column chromatography yielded a solid for all three chain lengths. Table 9 gives an overview of the yields we obtained for the different intermediate steps.

Table 9 - Yields of the last two synthesis steps for the bis(alkoxymethyl)dicyanobenzene precursors

Compound	Step I (%)	Step II (%)
-$CH_2OC_8H_{17}$	33	36
-$CH_2OC_{12}H_{25}$	40	30
-$CH_2OC_{16}H_{33}$	42	41

The synthesis of the starting compound 4,5-bis(bromomethyl)-1,2-dibromobenzene and the precursor with two -$CH_2OC_{16}H_{33}$ side chains is described below. For the synthesis of the other chain lengths the same analytical techniques were used to ensure the purity of the compounds. Tables 10 and 11 show the elemental analysis results for the intermediate dibromobis(alkoxymethyl)benzenes and the dicyanobis(alkoxymethyl)benzenes respectively.

Synthesis of 1,2-dibromo-4,5-dimethylbenzene

o-Xylene (244 mL) was dissolved in 200 mL of CCl_4. The mixture was cooled to 5°C and iron powder and a iodide crystal were added. Bromine (211 mL) was added whilst keeping the temperature under 10°C. The mixture was stirred another 48 hours at room temperature. Washing with a dilute solution of sodium metabisulfite ($Na_2S_2O_5$) removed the excess of bromine. The organic layer was washed twice with water. After drying and evaporating, the obtained yellowish oil was cooled in the refrigerator. The white solid was filtered and washed with petroleum ether (30-60°C). The solid was dried *in vacuo*. Yield: 87% (458.3 g); m.p.: 85°C. MS *m/z:* 264 (M^+). ^{1}H-NMR ($CDCl_3$) δ: 2.17 (s, 6H, CH_3), 7.35 (s, 2H, Ar). CHN-analysis: $C_8H_8Br_2$ (263.96). Calcd (%): C, 36.40; H, 3.05. Found (%): C, 36.44; H, 3.06.

Synthesis of 4,5-bis(bromomethyl)-1,2-dibromobenzene

25 g of 1,2-dibromo-4,5-dimethylbenzene, 33.7 g of *N*-bromosuccinimide and 315 mg of benzoylperoxide were boiled to reflux in 100 mL of CCl_4. After the reaction slowed down, the mixture was stirred for another hour. After cooling, the succinimide was filtered of and the filtrate was evaporated. Treatment of the oil with boiling petroleum ether yielded additional succinimide, which was removed by filtration. After evaporating, the oil was cooled in the refrigerator. The white solid was filtered and washed with petroleum ether. The solid was dried *in vacuo*.

Yield: 32% (12.7 g); m.p.: 88°C. MS *m/z:* 422 (M^+). ^{1}H-NMR ($CDCl_3$) δ: 4.53 (s, 4H, CH_2), 7.62 (s, 2H, Ar). CHN-analysis: $C_8H_6Br_4$ (421.83). Calcd (%): C, 22.78; H, 1.43. Found (%): C, 22.51; H, 1.60.

Table 10 - Elemental analysis data for the dibromobis(alkoxymethyl)benzene intermediates

Chain length	Compound	Calculated			Found		
		C (%)	H (%)	N (%)	C (%)	H (%)	N (%)
8	$C_{24}H_{40}O_2Br_2$	55.39	7.75	—	55.21	7.56	—
12	$C_{32}H_{56}O_2Br_2$	60.76	8.92	—	60.52	8.63	—
16	$C_{40}H_{72}O_2Br_2$	64.50	9.74	—	64.36	9.57	—

Synthesis of 4,5-bis(hexadecyloxymethyl)-1,2-dibromobenzene

18.6 g of K were introduced in 250 mL of tert-butanol. When the potassium had reacted with the solvent, 232 g of hexadecanol were added. 40 g of 4,5-bis(bromomethyl)-1,2-dibromobenzene were added slowly over half an hour. The mixture was refluxed for 48 hours under an inert atmosphere. After cooling, the mixture was poured in water and neutralised by a dilute HCl solution. CH_2Cl_2 was added and the organic layer was washed with water. After drying, filtration and evaporation, the purification of the compound was done by means of column chromatography with silica as the stationary phase and *n*-heptane/toluene (1/1) as the eluent. Yield: 42% (23.4 g).; m.p.: 53°C. R_f (*n*-heptane/toluene-1/1): 0.37. MS *m/z:* 745 (M^+). ^{1}H-NMR ($CDCl_3$) δ: 0.90 (t, 6H, CH_3), 1.27 (b, 52H, CH_2), 1.60 (m, 4H, β-CH_2), 3.48 (t, 4H., α-CH_2), 4.47 (s, 4H, Ar-CH_2), 7.66 (s, 2H, Ar). CHN-analysis: $C_{40}H_{72}O_2Br_2$ (744.81). Calcd (%): C, 64.50; H, 9.74. Found (%): C, 64.36; H, 9.57.

Table 11 - Elemental analysis data for the dicyanobis(alkoxymethyl)benzene intermediates

Chain length	Compound	Calculated			Found		
		C (%)	H (%)	N (%)	C (%)	H (%)	N (%)
8	$C_{26}H_{40}O_2N_2$	75.68	9.77	6.79	75.43	9.63	6.62
12	$C_{34}H_{56}O_2N_2$	77.81	10.76	5.34	77.68	10.84	5.16
16	$C_{42}H_{72}O_2N_2$	79.19	11.39	4.40	79.32	11.52	4.33

Synthesis of 4,5-bis(hexadecyloxymethyl)-1,2-dicyanobenzene

15 g of 4,5-bis(hexadecyloxymethyl)-1,2-dibromobenzene and 5.4 g of CuCN were added to 100 mL of DMF. The mixture was stirred for 6 hours at 150°C. After cooling and evaporation, a 25% solution of ethylenediamine was added and the whole was stirred for 30 minutes at 80°C. The mixture was extracted with CH_2Cl_2 and the combined organic layers were dried. After evaporation, the purification of the compound was done by means of column chromatography with silica as the stationary phase and CH_2Cl_2 as the eluent. Yield: 41% (12.8 g); m.p.: 86°C. R_f (CH_2Cl_2): 0.60. MS *m/z:* 673 (M^+). ^{1}H-NMR ($CDCl_3$) δ: 0.88 (t, 6H, CH_3), 1.26 (b, 52H, CH_2), 1.65 (m, 4H, β-CH_2), 3.53 (t, 4H, α-CH_2), 4.52 (s, 4H, Ar-CH_2), 7.90 (s, 2H, Ar). CHN-analysis: $C_{42}H_{72}O_2N_2$ (673.03). Calcd (%): C, 79.19; H, 11.39; N, 4.40. Found (%): C, 79.32; H, 11.52; N, 4.33.

4.3 Synthesis of ligands

The cyclotetramerisation reaction was done by refluxing the disubstituted phthalonitrile in a minimal amount of 2-(dimethylamino)ethanol (DMAE) during 78 hours under nitrogen atmosphere. After cooling the mixture was dissolved in a minimal amount of chloroform and poured in a beaker with acetone. The phthalocyanine coagulated and the precipitate was filtered over a glass sinter (porosity 4) and washed with acetone and ethanol. The ligands were also purified

by column chromatography over silicagel with chloroform as the eluent. The final product was dried *in vacuo*.

4.3.1 Octa-alkoxy phthalocyanines

Table 12 gives an overview of the yields of the ligands for the different chain lengths. The low yields probably are due to the formation of phthalonitrile oligomers. The elemental analysis did produce good results, except for some compounds. This is rather unusual for this type of compounds, as in literature generally deviations of often more than 1 % from the calculated value are found [ForSum94, GuyPon94, JiaLiu97]. The CHN-data are represented in Table 13.

Table 12 - Yields for the octa-alkoxy phthalocyanine ligands

Compound	Yield (%)	Compound	Yield (%)
$(C_4H_9O)_8PcH_2$	49	$(C_{13}H_{27}O)_8PcH_2$	10
$(C_5H_{11}O)_8PcH_2$	50	$(C_{14}H_{29}O)_8PcH_2$	23
$(C_6H_{13}O)_8PcH_2$	22	$(C_{15}H_{31}O)_8PcH_2$	21
$(C_7H_{15}O)_8PcH_2$	8	$(C_{16}H_{33}O)_8PcH_2$	33
$(C_8H_{17}O)_8PcH_2$	15	$(C_{17}H_{35}O)_8PcH_2$	14
$(C_9H_{19}O)_8PcH_2$	12	$(C_{18}H_{37}O)_8PcH_2$	27
$(C_{10}H_{21}O)_8PcH_2$	17	$(C_{19}H_{39}O)_8PcH_2$	17
$(C_{11}H_{23}O)_8PcH_2$	10	$(C_{20}H_{41}O)_8PcH_2$	13
$(C_{12}H_{25}O)_8PcH_2$	15		

The ^{1}H-NMR-spectrum of pure octa-butyloxy substituted phthalocyanine is depicted in Figure 28. The typical peak between -4 en -3 ppm is caused by the deshielded inner protons of the phthalocyanine ligand. The other peaks can be attributed to the non-peripheral protons (singlet at 7.96 ppm), the α-H's of the alkoxy chains (triplet at 4.46 ppm) and the other protons of the aliphatic chain (multiplets between 2.3 and 1.2 ppm).

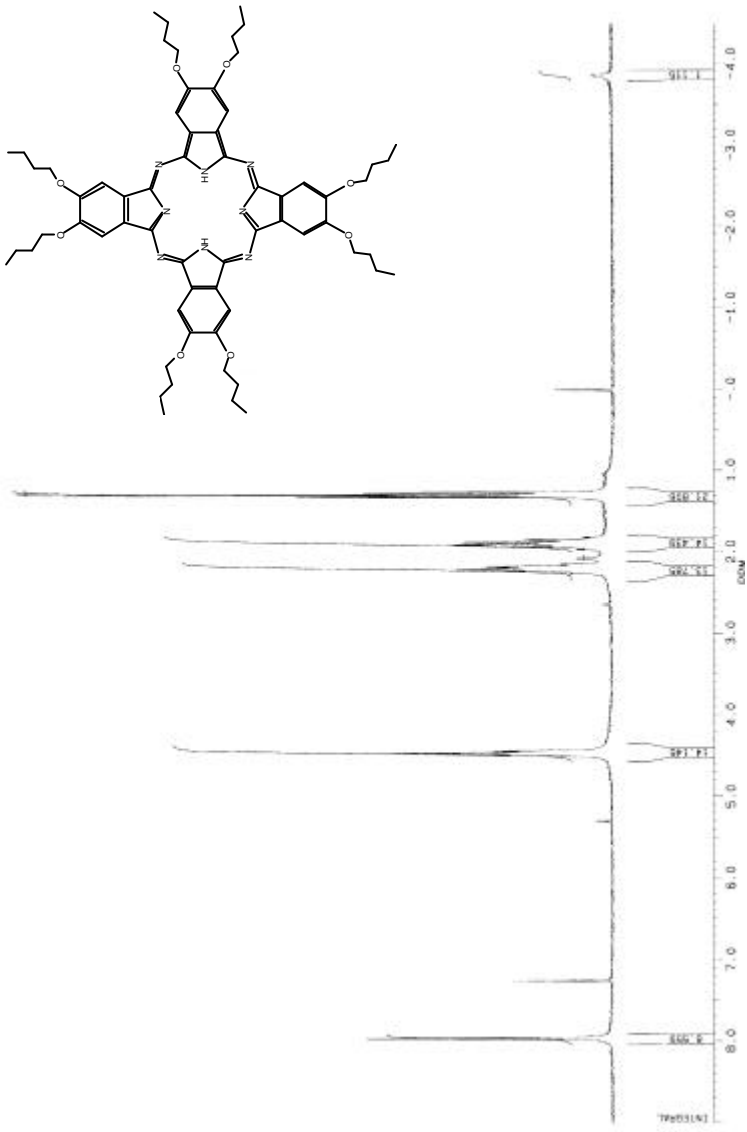

Figure 28 - ^{1}H-NMR-spectrum of the octa-butyloxy phthalocyanine ligand

Table 13 - Elemental analysis data for the octa-alkoxy phthalocyanine ligands

	Calculated			Found		
Compound	C (%)	H (%)	N (%)	C (%)	H (%)	N (%)
$(C_4H_9O)_8PcH_2$	70.43	7.57	10.27	69.80	7.54	10.13
$(C_5H_{11}O)_8PcH_2$	71.85	8.21	9.31	71.38	8.17	9.20
$(C_6H_{13}O)_8PcH_2$	73.02	8.73	8.52	73.03	8.70	8.32
$(C_7H_{15}O)_8PcH_2$	74.01	9.18	7.85	73.61	9.10	7.75
$(C_8H_{17}O)_8PcH_2$	74.86	9.55	7.28	74.09	9.46	7.29
$(C_9H_{19}O)_8PcH_2$	75.59	9.88	6.78	74.78	9.85	6.78
$(C_{10}H_{21}O)_8PcH_2$	76.23	10.16	6.35	76.10	9.86	6.12
$(C_{11}H_{23}O)_8PcH_2$	76.79	10.42	5.97	76.15	10.45	5.62
$(C_{12}H_{25}O)_8PcH_2$	77.29	10.64	5.63	76.94	10.59	5.59
$(C_{13}H_{27}O)_8PcH_2$	77.74	10.84	5.33	77.54	10.33	5.02
$(C_{14}H_{29}O)_8PcH_2$	78.14	11.02	5.06	77.85	11.07	4.89
$(C_{15}H_{31}O)_8PcH_2$	78.50	11.18	4.82	78.67	11.02	4.72
$(C_{16}H_{33}O)_8PcH_2$	78.83	11.33	4.60	78.10	11.10	4.63
$(C_{17}H_{35}O)_8PcH_2$	79.12	11.46	4.39	78.75	11.35	4.54
$(C_{18}H_{37}O)_8PcH_2$	79.40	11.58	4.21	78.78	11.10	4.75
$(C_{19}H_{39}O)_8PcH_2$	79.65	11.70	4.04	79.10	11.83	3.55
$(C_{20}H_{41}O)_8PcH_2$	79.88	11.80	3.88	79.02	11.14	3.16

Synthesis of 2,3,9,10,16,17,23,24-Octa(decyloxy)phthalocyanine

A solution of 1 g (7.98 mmol) of 4,5-dicyano-1,2-bis(decyloxy)benzene in 1 mL of 2-(diethylamino)ethanol was heated at reflux for 78 h in a dry nitrogen atmosphere. After leaving to cool to room temperature, the mixture was diluted with 20 mL of chloroform and then poured in 125 mL of acetone. The precipitate was filtrated on a Gooch-filter with porosity 4. Purification was done by recrystallising twice from ethyl acetate. Yield: 26% (0.26 g). MS *m/z*: 1764 (M^+). IR (KBr): 3300 (NH), 2900-2800 (CH), 1270 (ArO), 1095 (ArOC) cm^{-1}. ^{1}H-NMR δ ($CDCl_3$): -3.21 (b, 2H, NH), 0.97 (t, 24 H, CH_3), 1.43 (m, 112H, CH_2), 2.17 (m, 16H, β-CH_2), 4.49

(m, 16H, OCH_2), 8.30 (s, 8H, Ar). Analysis: $C_{112}H_{178}O_8N_8$ (1764.66). Calcd (%): C, 76.23; H, 10.16; N, 6.35. Found (%): C, 76.10; H, 9.86; N, 6.12. UV/VIS ($CHCl_3$) λ_{max}/nm: 704, 667, 647, 604, 427, 350, 297.

4.3.2 Octa-alkyl phthalocyanines

The mixture obtained from the cyclotetramerisation reaction was refluxed in hot ethanol in order to remove the DMAE solvent molecules. After cooling, the ligand was filtered over a Gooch-filter with porosity 4. The resulting product was purified by multiple column chromatography with silica as the stationary phase and chloroform as the eluent. After evaporation of the chloroform the ligand was coagulated by pouring the compound – dissolved in a minimum amount of chloroform – in methanol. This mixture was filtered and the resulting green-blue product was dried in a desiccator. Table 14 shows the different yields for the ligands we prepared. The elemental analysis results are given in Table 15. These results were not satisfying even after multiple chromatography, but this is quite usual as mentioned in 4.3.1.

Table 14 - Yields for the octa-alkoxy phthalocyanine ligands

Compound	Yield (%)
$(C_7H_{15})_8PcH_2$	10
$(C_8H_{17})_8PcH_2$	4
$(C_{12}H_{25})_8PcH_2$	16
$(C_{14}H_{29})_8PcH_2$	8
$(C_{16}H_{33})_8PcH_2$	12
$(C_{18}H_{37})_8PcH_2$	11

Synthesis of 2,3,9,10,16,17,23,24-octa(dodecyl)phthalocyanine

0.750 g (1.6 mmol) of 1,2-dicyano-4,5-bis(dodecyl)benzene in 1 mL of *N*,*N*-dimethylaminoethanol was refluxed during 15 hours. The reaction mixture was

treated with 40 mL of hot ethanol to remove the solvent and other soluble polar products. Purification was done by column chromatography with silica as the stationary phase and chloroform as the eluent. Yield: 16% (120 mg). MS *m/z:* 1861 (M^+). R_f (CH_2Cl_2/CCl_4): 0.43. CHN-analysis: $C_{128}H_{210}N_8$ (1861.09). Calcd (%): C, 82.61; H, 11.37; N, 6.03. Found (%): C, 80.77; H, 11.53; N, 5.75.

Table 15 - Elemental analysis data for the octa-alkyl phthalocyanine ligands (values between brackets are the calculated values)

	Calculated			Found		
Compound	C (%)	H (%)	N (%)	C (%)	H (%)	N (%)
$(C_7H_{15})_8$ PcH_2	81.30	10.08	8.62	79.82	9.95	8.37
$(C_8H_{17})_8$ PcH_2	81.65	10.42	7.93	77.29	10.19	8.28
$(C_{12}H_{25})_8PcH_2$	82.61	11.37	6.03	80.77	11.53	5.75
$(C_{14}H_{29})_8$ PcH_2	82.93	11.70	5.37	81.98	11.56	5.30
$(C_{16}H_{33})_8$ PcH_2	83.19	11.70	5.37	82.58	11.53	5.01
$(C_{18}H_{37})_8$ PcH_2	83.41	12.17	4.42	82.78	11.98	4.35

4.3.3 Octa-alkoxymethyl phthalocyanines

The synthesis is equal to that for the alkoxy and alkyl compounds. Table 16 shows the different yields for the ligands we prepared. The elemental analysis results are given in Table 16.

Table 16 - Yields for the octa-alkoxymethyl phthalocyanine ligands

Compound	Yield (%)
$(C_8H_{17}OCH_2)_8PcH_2$	16
$(C_{12}H_{24}OCH_2)_8PcH_2$	22
$(C_{16}H_{33}OCH_2)_8PcH_2$	10

Synthesis of 2,3,9,10,16,17,23,24-octa(hexadecyloxymethyl)phthalocyanine

100 mg (0.26 mmol) of 1,2-dicyano-4,5-bis(hexadecyloxymethyl)benzene in 0.5 mL of *N,N*-dimethylaminoethanol was refluxed during 15 hours. The reaction mixture was treated with 25 mL of hot ethanol to remove the solvent and other soluble polar products. The compound was filtered and the residue was purified by column chromatography with alumina as the stationary phase and chloroform as the eluent. Yield: 10 % (10 mg). MS m/z: 2548.8 (M^+). R_f ($CHCl_3$): 0.60 . CHN-analysis: $C_{168}H_{530}O_8N_8$ (2548). Calcd (%): C, 79.11; H, 11.47; N, 4.40. Found (%): C, 78.82; H, 11.33; N, 4.13.

Table 17 - Elemental analysis data for the octa-alkoxymethyl phthalocyanine ligands (values between brackets are the calculated values)

	Calculated			Found		
Compound	C (%)	H (%)	N (%)	C (%)	H (%)	N (%)
$(C_8H_{17}OCH_2)_8\ PcH_2$	75.58	9.89	6.78	74.98	9.83	6.66
$(C_{12}H_{24}OCH_2)_8PcH_2$	77.72	10.85	5.34	77.53	10.79	5.17
$(C_{16}H_{33}OCH_2)_8\ PcH_2$	79.11	11.47	4.40	78.82	11.33	4.13

4.4 Synthesis phthalocyanine transition metal complexes

The octasubstituted phthalocyanine transition metal complexes were synthesised via a template reaction between one equivalent of metal chloride and four equivalents 1,2-dicyano-4,5-bis(alkoxy)benzene using 2-(dimethylamino)ethanol as the solvent, in the presence of half an equivalent of the sterically hindered base 1,8-diazabicyclo[5.4.0]undec-7-ene (DBU) [VanNee88]. The crude products were purified by column chromatography and recrystallisation. By dissolving the pure product in a minimum amount of chloroform and coagulation in methanol, a fine powder was obtained. Finally, the product was dried in a dessicator overnight.

For most of the complexes, it was not possible to obtain accurate data for CHN microanalysis. As mentioned in 4.4.1, such problems are recognised. The reason for this problem remains unclear at this point, but it is probably due to the formation of refractory materials like carbides, nitrides and oxides that only decompose at very high temperatures. Therefore, the metal complexes were identified by MALDI-TOF mass spectrometry and the purity was checked by UV/VIS spectroscopy and MALDI-TOF. Purity control can be done by UV/VIS spectroscopy, because the spectrum of the cobalt(II) phthalocyanine is markedly different from the spectrum of the corresponding metal free phthalocyanine (different splitting of the Q-band, see Chapter 5). The latter compound is the main impurity formed during the reaction. The absence of the ligands peak in the MALDI-TOF spectrum confirmed the purity.

4.4.1 Octa-alkoxy phthalocyanine transition metal complexes

We synthesised transition metal complexes with Zn^{2+}, Cu^{2+}, Ni^{2+}, Co^{2+} and VO^{2+} as the central metal ions. All complexes were prepared for chain lengths 8, 12 and 16. For the cobalt(II) phthalocyanines the alkoxy chain length was also varied between C_4H_9O and $C_{18}H_{37}O$. The reactions with the vanadium(II) chloride salts differed from the other template reactions. Soon after the start of the reaction, the mixture turned black, probably due to the oxidation of the vanadium(II) chloride to the oxovanadium(IV) (VO^{2+}) cation. After a few hours the colour of the reaction mixture changes to green, when the phthalocyanine complex is being formed. The presence of the vanadyl cation, rather than the vanadium(II) ion in the complexes is confirmed by MALDI-TOF mass spectrometry and by IR through the presence of a V=O stretching frequency (992 cm^{-1} for the octa-octyloxy compound, 993 cm^{-1} for the octa-dodecyloxy compound and 995 cm^{-1} for the octa-hexadecyloxy compound).

^{1}H-NMR-spectra could not be recorded due to the paramagnetism of most of the transition metal ions. The IR spectra of all the compounds are virtually identical.

At 2850/2920 (s) cm^{-1} de C-H stretch is found, at 1610 (m) cm^{-1} the aromatic C=C stretch, at 1275 (s) cm^{-1} the Ar-O bending and at 1095 (s) cm^{-1} the Ar-O-C bending. Because of the absence of the characteristic absorption band at 1008 cm^{-1}, due to a N-H vibration, we can be sure that no metal-free phthalocyanine is present. Figure 29 shows the IR-spectra of the $(C_{12}H_{25}O)_8PcZn$ complex (left) and the corresponding ligand (right).

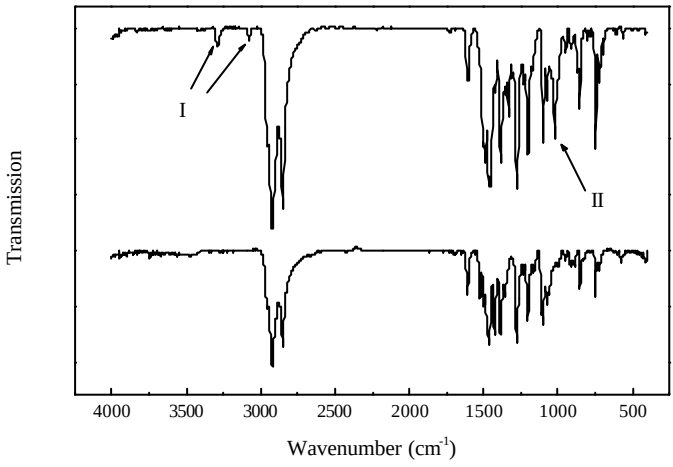

Figure 29 - IR-spectra of $(C_{11}H_{23}O)_8PcH_2$ (top) and $(C_{11}H_{23}O)_8PcCo$ (bottom); I: N-H stretching vibrations, II: N-H skeletal vibration

Table 18 shows the results of the CHN-analysis. Because of the bad results, we based the purity check on mass and UV/VIS spectroscopy as mentioned in the introduction. Complexes that could not be measured by means of the low-resolution electron-impact mass spectrometer (ionisation problems due to the high molecular mass) were determined by MALDI-TOF-analysis. A typical MALDI-TOF spectrum for the $(C_8H_{17}O)_8PcZn$ complex is given in Figure 30.

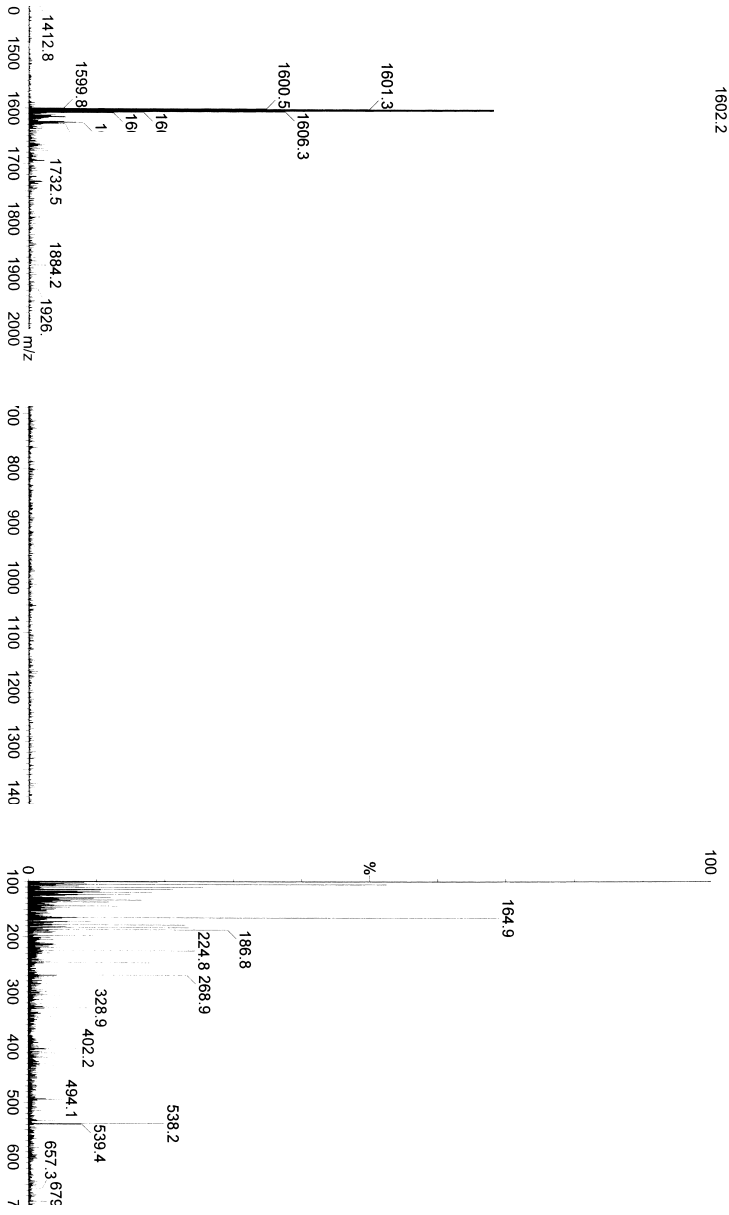

Figure 30 - MALDI-TOF spectrum of the $(C_8H_{17}O)_8PcZn$ complex

Table 18 - CHN-analysis results of the octa-alkoxy substituted phthalocyanine transition metal complexes (/: no analysis because of insufficient sample)

	Calculated			Found		
Compound	C (%)	H (%)	N (%)	C (%)	H (%)	N (%)
$(C_8H_{17}O)_8PcZn$	74.90	10.21	5.46	71.38	10.33	5.08
$(C_8H_{17}O)_8PcCu$	74.97	10.22	5.46	71.65	10.19	5.10
$(C_8H_{17}O)_8PcNi$	75.15	10.25	5.48	69.93	9.68	4.94
$(C_8H_{17}O)_8PcVO$	74.85	10.21	5.46	72.11	10.03	5.09
$(C_{12}H_{25}O)_8PcZn$	71.90	9.05	6.99	70.07	8.97	6.67
$(C_{12}H_{25}O)_8PcCu$	71.98	9.06	7.00	62.55	8.04	5.90
$(C_{12}H_{25}O)_8PcNi$	72.20	9.09	7.02	68.83	8.84	6.59
$(C_{12}H_{25}O)_8PcVO$	71.83	9.04	6.98	66.93	8.67	6.36
$(C_{16}H_{33}O)_8PcZn$	76.83	10.96	4.48	74.80	10.94	4.23
$(C_{16}H_{33}O)_8PcCu$	76.88	10.97	4.48	72.44	10.59	4.16
$(C_{16}H_{33}O)_8PcNi$	77.03	10.99	4.49	73.69	10.76	4.32
$(C_{16}H_{33}O)_8PcVO$	76.78	10.95	4.48	/	/	/
$(C_4H_9O)_8PcCo$	66.94	7.02	9.76	59.92	6.09	8.14
$(C_5H_{11}O)_8PcCo$	68.60	7.68	8.89	57.39	6.61	7.19
$(C_6H_{13}O)_8PcCo$	70.00	8.22	8.16	67.34	8.18	7.66
$(C_7H_{15}O)_8PcCo$	71.18	8.69	7.55	69.66	8.92	7.23
$(C_8H_{17}O)_8PcCo$	72.19	9.09	7.02	52.24	6.78	4.84
$(C_9H_{19}O)_8PcCo$	73.07	9.43	6.55	71.62	9.73	6.25
$(C_{10}H_{21}O)_8PcCo$	73.85	9.74	6.15	72.84	10.12	5.92
$(C_{11}H_{23}O)_8PcCo$	74.53	10.01	5.79	70.59	10.01	5.33
$(C_{12}H_{25}O)_8PcCo$	75.14	10.25	5.48	65.73	9.15	4.65
$(C_{13}H_{27}O)_8PcCo$	75.69	10.46	5.19	72.71	10.72	3.92
$(C_{14}H_{29}O)_8PcCo$	76.18	10.65	4.93	62.66	9.26	3.86
$(C_{15}H_{31}O)_8PcCo$	76.62	10.83	4.70	75.31	11.29	4.60
$(C_{16}H_{33}O)_8PcCo$	77.03	10.99	4.49	54.97	8.11	2.97
$(C_{17}H_{35}O)_8PcCo$	77.40	11.13	4.30	59.80	8.39	3.93
$(C_{18}H_{37}O)_8PcCo$	77.74	11.27	4.12	76.22	11.63	4.13

Table 19 - MALDI-TOF results of the octa-alkoxy substituted phthalocyanine transition metal complexes

Compound	Formula	M (isotopic)	M (found)
$(C_8H_{17}O)_8PcZn$	$C_{96}H_{144}O_8N_8Zn$	1601.04	1602.2
$(C_8H_{17}O)_8PcCu$	$C_{96}H_{144}O_8N_8Cu$	1600.04	1599.7
$(C_8H_{17}O)_8PcNi$	$C_{96}H_{144}O_8N_8Ni$	1595.05	1596.1
$(C_8H_{17}O)_8PcVO$	$C_{96}H_{144}O_9N_8V$	1604.05	1603.8
$(C_{12}H_{25}O)_8PcZn$	$C_{128}H_{208}O_8N_8Zn$	2049.54	2050.8
$(C_{12}H_{25}O)_8PcCu$	$C_{128}H_{208}O_8N_8Cu$	2048.54	2049.0
$(C_{12}H_{25}O)_8PcNi$	$C_{128}H_{208}O_8N_8Ni$	2043.55	2043.6
$(C_{12}H_{25}O)_8PcVO$	$C_{128}H_{208}O_9N_8V$	2052.55	2050.8
$(C_{16}H_{33}O)_8PcZn$	$C_{160}H_{272}O_8N_8Zn$	2498.04	2496.9
$(C_{16}H_{33}O)_8PcCu$	$C_{160}H_{272}O_8N_8Cu$	2497.04	2497.2
$(C_{16}H_{33}O)_8PcNi$	$C_{160}H_{272}O_8N_8Ni$	2492.05	2490.7
$(C_{16}H_{33}O)_8PcVO$	$C_{160}H_{272}O_9N_8V$	2501.05	2501.1
$(C_4H_9O)_8PcCo$	$C_{64}H_{80}O_8N_8Co$	1147.54	1147.1
$(C_5H_{11}O)_8PcCo$	$C_{72}H_{96}O_8N_8Co$	1259.67	1257.9
$(C_6H_{13}O)_8PcCo$	$C_{80}H_{112}O_8N_8Co$	1371.79	1370.8
$(C_7H_{15}O)_8PcCo$	$C_{88}H_{128}O_8N_8Co$	1483.92	1481.5
$(C_8H_{17}O)_8PcCo$	$C_{96}H_{144}O_8N_8Co$	1596.04	1596.0
$(C_9H_{19}O)_8PcCo$	$C_{104}H_{160}O_8N_8Co$	1708.17	1707.2
$(C_{10}H_{21}O)_8PcCo$	$C_{112}H_{176}O_8N_8Co$	1820.29	1819.3
$(C_{11}H_{23}O)_8PcCo$	$C_{120}H_{192}O_8N_8Co$	1932.42	1929.3
$(C_{12}H_{25}O)_8PcCo$	$C_{128}H_{208}O_8N_8Co$	2044.54	2043.6
$(C_{13}H_{27}O)_8PcCo$	$C_{136}H_{224}O_8N_8Co$	2156.67	2154.6
$(C_{14}H_{29}O)_8PcCo$	$C_{144}H_{240}O_8N_8Co$	2268.79	2267.2
$(C_{15}H_{31}O)_8PcCo$	$C_{152}H_{256}O_8N_8Co$	2380.92	2380.8
$(C_{16}H_{33}O)_8PcCo$	$C_{160}H_{272}O_8N_8Co$	2493.04	2492.0
$(C_{17}H_{35}O)_8PcCo$	$C_{168}H_{288}O_8N_8Co$	2605.17	2604.3
$(C_{18}H_{37}O)_8PcCo$	$C_{176}H_{304}O_8N_8Co$	2717.30	2715.1

The yields of the complexes are shown in Table 20. The yields of the vanadyl compounds are in general lower than for the other transition metal ions.

Table 20 – Yields of the octa-alkoxy phthalocyanine transition metal complexes

Compound	Yield (%)	Compound	Yield (%)
$(C_8H_{17}O)_8PcZn$	40	$(C_6H_{13}O)_8PcCo$	28
$(C_8H_{17}O)_8PcCu$	15	$(C_7H_{15}O)_8PcCo$	34
$(C_8H_{17}O)_8PcNi$	29	$(C_8H_{17}O)_8PcCo$	9
$(C_8H_{17}O)_8PcVO$	12	$(C_9H_{19}O)_8PcCo$	34
$(C_{12}H_{25}O)_8PcZn$	46	$(C_{10}H_{21}O)_8PcCo$	24
$(C_{12}H_{25}O)_8PcCu$	48	$(C_{11}H_{23}O)_8PcCo$	36
$(C_{12}H_{25}O)_8PcNi$	38	$(C_{12}H_{25}O)_8PcCo$	16
$(C_{12}H_{25}O)_8PcVO$	29	$(C_{13}H_{27}O)_8PcCo$	40
$(C_{16}H_{33}O)_8PcZn$	39	$(C_{14}H_{29}O)_8PcCo$	26
$(C_{16}H_{33}O)_8PcCu$	20	$(C_{15}H_{31}O)_8PcCo$	22
$(C_{16}H_{33}O)_8PcNi$	33	$(C_{16}H_{33}O)_8PcCo$	8
$(C_{16}H_{33}O)_8PcVO$	4	$(C_{17}H_{35}O)_8PcCo$	20
$(C_4H_9O)_8PcCo$	12	$(C_{18}H_{37}O)_8PcCo$	42
$(C_5H_{11}O)_8PcCo$	29		

Synthesis of 2,3,9,10,16,17,23,24-octa(dodecyloxy)MPc; M = Zn, Cu, Ni, Co, VO

1 g (2 mmol) of 1,2-dicyano-4,5-bis(dodecyloxy)benzene, 0.54 mmol of the metal salt ($ZnCl_2$, $CuCl_2 \cdot 2H_2O$, $NiCl_2 \cdot 6H_2O$, $CoCl_2 \cdot 6H_2O$, VCl_2), 5 mL of 2-(dimethylamino)ethanol and 4 drops of DBU were refluxed at 150 °C during 48 hours under a nitrogen atmosphere. The mixture was diluted with 10 mL of $CHCl_3$ and poured into 50 mL of acetone. The precipitate was filtered over a Gooch-filter with porosity 4 and washed with acetone, methanol and ethyl acetate. Further purification was done by column chromatography over (neutral) Al_2O_3 with $CHCl_3$

as the eluent. Recrystallisation in ethyl acetate yielded a powder that after filtration was dried in a dessicator.

4.4.2 Octa-alkyl phthalocyanines transition metal complexes

We synthesised transition metal complexes with Zn^{2+}, Cu^{2+}, Ni^{2+}, Co^{2+} and VO^{2+} as the central metal ions. Complexes were prepared for chain lengths 8, 12, 14 and 16. For the cobalt(II) phthalocyanines a selection of alkyl chain lengths between C_7H_{15} and $C_{16}H_{33}O$ was prepared. The reaction mixtures were treated similar to the octa-alkoxy transition metal complexes (the vanadium complexes also showed the behaviour mentioned in 4.4.1).

Again, no satisfying elemental analysis could be obtained; the problems were analogous to the ones discussed in 4.3.1. Table 21 shows the yields of the complexes that were synthesised whereas Table 22 and Table 23 show the elemental analysis and MALDI-TOF results.

Table 21 - Yields of the octa-alkyl phthalocyanine transition metal complexes

Compound	Yield (%)	Compound	Yield (%)
$(C_8H_{17})_8PcZn$	7	$(C_{16}H_{33})_8PcNi$	22
$(C_8H_{17})_8PcCu$	15	$(C_{16}H_{33})_8PcVO$	6
$(C_{12}H_{25})_8PcZn$	19	$(C_{18}H_{37})_8PcCo$	6
$(C_{12}H_{25})_8PcCu$	16	$(C_7H_{15})_8PcCo$	3
$(C_{12}H_{25})_8PcNi$	15	$(C_8H_{17})_8PcCo$	8
$(C_{14}H_{29})_8PcZn$	10	$(C_{12}H_{25})_8PcCo$	16
$(C_{14}H_{29})_8PcCu$	14	$(C_{14}H_{29})_8PcVO$	8
$(C_{14}H_{29})_8PcNi$	9	$(C_{14}H_{29})_8PcCo$	16
$(C_{16}H_{33})_8PcZn$	12	$(C_{16}H_{33})_8PcCo$	13
$(C_{16}H_{33})_8PcCu$	18		

Synthesis of 2,3,9,10,16,17,23,24-octa(dodecyl)MPc; M = Zn, Cu, Ni, Co, VO

0.82 g (2 mmol) of 1,2-dicyano-4,5-bis(dodecyl)benzene, 0.54 mmol of the metal salt ($ZnCl_2$, $CuCl_2 \cdot 2H_2O$, $NiCl_2 \cdot 6H_2O$, $CoCl_2 \cdot 6H_2O$, VCl_2), 5 mL of *n*-heptanol and 4 drops of DBU were refluxed at 150 °C during 48 hours under a nitrogen atmosphere. The reaction mixture was diluted with 10 mL of $CHCl_3$ and poured into 50 mL of acetone. The coagulated precipitate was filtered over a Gooch-filter with porosity 4 and washed with acetone, methanol and ethyl acetate. The compounds were purified by column chromatography on silica as the solid phase with $CHCl_3$ as the eluent. Coagulation of the evaporated product was done with methanol in chloroform. The final powder was dried in a dessicator.

Table 22 - CHN-analysis results of the octa-alkyl substituted phthalocyanine transition metal complexes

	Calculated			Found		
Compound	C (%)	H (%)	N (%)	C (%)	H (%)	N (%)
$(C_8H_{17})_8PcZn$	78.14	9.84	7.59	77.38	10.77	7.26
$(C_8H_{17})_8PcCu$	78.24	9.85	7.60	77.63	10.72	7.27
$(C_{12}H_{25})_8PcZn$	79.89	10.89	5.82	77.99	12.53	5.63
$(C_{12}H_{25})_8PcCu$	79.96	10.90	5.83	78.83	11.09	5.52
$(C_{12}H_{25})_8PcNi$	80.16	10.93	5.84	77.53	10.86	5.43
$(C_{14}H_{29})_8PcCu$	80.55	11.27	5.22	80.30	11.34	5.01
$(C_{14}H_{29})_8PcNi$	80.74	11.29	5.23	79.67	11.23	4.91
$(C_{14}H_{29})_8PcVO$	80.43	11.25	5.21	78.73	11.24	4.87
$(C_{16}H_{33})_8PcZn$	80.97	11.55	4.72	78.64	11.69	4.50
$(C_{16}H_{33})_8PcCu$	81.03	11.56	4.73	79.03	11.27	4.52
$(C_{16}H_{33})_8PcNi$	81.20	11.58	4.73	79.36	11.54	4.25
$(C_{16}H_{33})_8PcVO$	80.92	11.54	4.72	79.33	11.51	4.53
$(C_7H_{15})_8PcCo$	77.89	9.51	8.25	75.78	9.98	6.73
$(C_8H_{17})_8PcCo$	78.48	9.88	7.36	74.97	10.59	6.84
$(C_{12}H_{25})_8PcCo$	80.15	10.93	5.84	76.64	12.73	4.0
$(C_{14}H_{29})_8PcCo$	80.73	11.29	5.23	78.77	11.56	4.94
$(C_{16}H_{33})_8PcCo$	80.49	11.48	4.69	79.58	13.10	4.61
$(C_{18}H_{37})_8PcCo$	81.51	11.89	4.32	83.44	14.42	0.57

Table 23 - MALDI-TOF results of the octa-alkyl substituted phthalocyanine transition metal complexes

Compound	Formula	M (isotopic)	M (found)
$(C_8H_{17})_8PcZn$	$C_{96}H_{144}N_8Zn$	1473.1	1473.0
$(C_8H_{17})_8PcCu$	$C_{96}H_{144}N_8Cu$	1472.1	1471.9
$(C_{12}H_{25})_8PcZn$	$C_{128}H_{208}N_8Zn$	1921.6	1921.5
$(C_{12}H_{25})_8PcCu$	$C_{128}H_{208}N_8Cu$	1920.6	1920.4
$(C_{12}H_{25})_8PcNi$	$C_{128}H_{208}N_8Ni$	1915.6	1915.5
$(C_{14}H_{29})_8PcZn$	$C_{144}H_{240}N_8Zn$	2145.8	2145.7
$(C_{14}H_{29})_8PcCu$	$C_{144}H_{240}N_8Zn$	2144.8	2145.1
$(C_{14}H_{29})_8PcNi$	$C_{144}H_{240}N_8Zn$	2139.8	2140.7
$(C_{14}H_{29})_8PcVO$	$C_{144}H_{240}ON_8V$	2148.8	2146.7
$(C_{16}H_{33})_8PcZn$	$C_{160}H_{272}N_8Zn$	2370.1	2370.0
$(C_{16}H_{33})_8PcCu$	$C_{160}H_{272}N_8Cu$	2367.1	2366.0
$(C_{16}H_{33})_8PcNi$	$C_{160}H_{272}N_8Ni$	2364.1	2363.8
$(C_{16}H_{33})_8PcVO$	$C_{160}H_{272}ON_8V$	2373.1	2372.9
$(C_7H_{15})_8PcCo$	$C_{88}H_{128}N_8Co$	1356.0	1355.9
$(C_8H_{17})_8PcCo$	$C_{96}H_{144}N_8Co$	1468.1	1467.9
$(C_{12}H_{25})_8PcCo$	$C_{128}H_{208}N_8Co$	1916.6	1916.5
$(C_{14}H_{29})_8PcCo$	$C_{144}H_{240}N_8Co$	2140.8	2140.0
$(C_{16}H_{33})_8PcCo$	$C_{160}H_{272}N_8Co$	2365.1	2364.9
$(C_{18}H_{37})_8PcCo$	$C_{176}H_{304}N_8Co$	2591.4	2589.1

4.4.3 Octa-alkoxymethyl phthalocyanines transition metal complexes

The same procedures and remarks as for the octa-alkoxy and the octa-alkyl complexes hold for the octa-alkoxymethyl transition metal complexes. Table 24 shows the yields for the complexes that were synthesised whereas Table 25 and Table 26 show the CHN elemental analysis and MALDI-TOF results. No vanadium complexes were prepared because of the small amount of precursor that was available.

Table 24 - Yields of the octa-alkoxymethyl phthalocyanine transition metal complexes

Compound	Yield (%)	Compound	Yield (%)
$(C_8H_{17}OCH_2)_8PcZn$	10	$(C_{12}H_{24}OCH_2)_8PcNi$	18
$(C_8H_{17}OCH_2)_8PcCu$	15	$(C_{12}H_{24}OCH_2)_8PcCo$	21
$(C_8H_{17}OCH_2)_8PcNi$	26	$(C_{16}H_{33}OCH_2)_8PcZn$	15
$(C_8H_{17}OCH_2)_8PcCo$	27	$(C_{16}H_{33}OCH_2)_8PcCu$	23
$(C_{12}H_{24}OCH_2)_8PcZn$	30	$(C_{16}H_{33}OCH_2)_8PcNi$	23
$(C_{12}H_{24}OCH_2)_8PcCu$	12	$(C_{16}H_{33}OCH_2)_8PcCo$	16

Table 25 - CHN-analysis results of the octa-alkyl substituted phthalocyanine transition metal complexes

	Calculated			Found		
Compound	C (%)	H (%)	N (%)	C (%)	H (%)	N (%)
$(C_8H_{17}OCH_2)_8PcZn$	72.85	9.41	6.54	71.46	9.22	6.10
$(C_8H_{17}OCH_2)_8PcCu$	72.89	9.42	6.54	72.63	9.01	5.57
$(C_8H_{17}OCH_2)_8PcNi$	73.10	9.45	6.56	72.88	9.06	5.88
$(C_8H_{17}OCH_2)_8PcCo$	73.06	9.44	6.56	72.46	9.33	6.13
$(C_{12}H_{24}OCH_2)_8PcZn$	75.50	10.44	5.18	75.20	9.76	5.02
$(C_{12}H_{24}OCH_2)_8PcCu$	75.53	10.45	5.18	75.18	9.53	4.65
$(C_{12}H_{24}OCH_2)_8PcNi$	75.71	10.47	5.20	75.02	9.88	4.85
$(C_{12}H_{24}OCH_2)_8PcCo$	75.67	10.47	5.19	74.35	9.18	4.33
$(C_{16}H_{33}OCH_2)_8PcZn$	77.24	11.12	4.29	76.66	10.75	3.29
$(C_{16}H_{33}OCH_2)_8PcCu$	77.27	11.13	4.29	77.01	10.55	3.96
$(C_{16}H_{33}OCH_2)_8PcNi$	77.41	11.15	4.30	77.23	10.65	4.01
$(C_{16}H_{33}OCH_2)_8PcCo$	77.38	11.14	4.30	76.68	10.99	4.23

Synthesis of 2,3,9,10,16,17,23,24-octa(hexadecyloxymethyl)MPc; M = Zn, Cu, Ni, Co

100 mg (0.26 mmol) of 1,2-dicyano-4,5-bis(hexadecyloxymethyl)benzene, 0.10 mmol of the metal salt ($ZnCl_2$, $CuCl_2{\cdot}2H_2O$, $NiCl_2{\cdot}6H_2O$, $CoCl_2{\cdot}6H_2O$), 0.5 mL of *n*-heptanol and 1

drops of DBU were refluxed at 150 °C during 48 hours under a nitrogen atmosphere. The reaction mixture was diluted with 1 mL of $CHCl_3$ and poured into 20 mL of acetone. The coagulated precipitate is filtered over a small Gooch-filter with porosity 4 and washed with acetone, methanol and ethyl acetate. The compounds were purified by column chromatography on silica with $CHCl_3$ as the eluent, and precipitated with methanol in chloroform. The product was filtered and dried in a dessicator.

Table 26 - MALDI-TOF results for the octa-alkyl substituted phthalocyanine transition metal complexes

Compound	Formula	M (isotopic)	M (found)
$(C_8H_{17}OCH_2)_8PcZn$	$C_{104}H_{160}O_8N_8Zn$	1713.2	1713.6
$(C_8H_{17}OCH_2)_8PcCu$	$C_{104}H_{160}O_8N_8Cu$	1712.2	1712.6
$(C_8H_{17}OCH_2)_8PcNi$	$C_{104}H_{160}O_8N_8Ni$	1707.2	1707.6
$(C_8H_{17}OCH_2)_8PcCo$	$C_{104}H_{160}O_8N_8Co$	1708.2	1709.1
$(C_{12}H_{24}OCH_2)_8PcZn$	$C_{136}H_{224}O_8N_8Zn$	2161.7	2162.1
$(C_{12}H_{24}OCH_2)_8PcCu$	$C_{136}H_{224}O_8N_8Cu$	2160.7	2161.1
$(C_{12}H_{24}OCH_2)_8PcNi$	$C_{136}H_{224}O_8N_8Ni$	2155.7	2156.2
$(C_{12}H_{24}OCH_2)_8PcCo$	$C_{136}H_{224}O_8N_8Co$	2156.7	2157.2
$(C_{16}H_{33}OCH_2)_8PcZn$	$C_{168}H_{288}O_8N_8Zn$	2610.2	2610.7
$(C_{16}H_{33}OCH_2)_8PcCu$	$C_{168}H_{288}O_8N_8Cu$	2609.2	2609.6
$(C_{16}H_{33}OCH_2)_8PcNi$	$C_{168}H_{288}O_8N_8Ni$	2604.2	2604.8
$(C_{16}H_{33}OCH_2)_8PcCo$	$C_{168}H_{288}O_8N_8Co$	2605.2	2605.8

4.5 Synthesis of bis(phthalocyaninato) lanthanide(III) complexes

We only synthesised lanthanide(III) complexes for the octa-alkoxy substituted compounds, because for both other types only a small amount of precursor material was prepared, and the reactions did sometimes only yield a brown (oligomer) mixture. The synthesis of the unsubstituted lanthanide(III) complexes by means of

microwave radiation is also described here, because we will use these compounds in Chapter 6.

4.5.1 Octa-alkoxy phthalocyanines lanthanide complexes

The sandwich complexes containing rare-earth ions were prepared by a template reaction of four phthalonitrile precursors with a lanthanide ion. The reaction consisted of thoroughly mixing the disubstituted phthalonitrile with 1/8 equivalent of the lanthanide(III) acetate salt. The mixture was heated at 150°C for twenty hours in the presence of ½ equivalent of DBU in 1-hexanol [BelSir89]. After cooling, the mixture was dissolved in a minimum amount of chloroform and the product was precipitated in methanol and filtered. Further purification was done by column chromatography, size exclusion chromatography and recrystallisation. The purification of the reaction mixture was done by multiple column chromatography on silica with chloroform as the eluent, followed by size exclusion chromatography on Bio-Rad Bio-Beads S-X3 as the eluent and recrystallisation in ethyl acetate. During column chromatography, two bands (blue and green) eluted from the column. We only collected the green (cation radical) fractions from the purification steps. Table 27 gives an overview of the yields of the octa-alkoxy substituted bisphthalocyaninato lanthanide(III) complexes that were synthesised. Some of the chain lengths did not yield the complex as indicated in the table.

Again, the elemental analysis did not always yield satisfying results (for most samples it was also not possible do perform an elemental analysis because of the low overall yield). Hence, no table with CHN-results is displayed and we judged purely based on the MALDI-TOF measurement to proceed with the purification to the point where chromatography resulted in one single band of which the UV/VIS spectrum was consistent with that of a double-decker. Figure 31 shows the MALDI-TOF spectrum for the $[(C_{14}H_{29}O)_8Pc]_2Er$ complex.

Table 27 - Yields of the octa-alkoxy phthalocyanine lanthanide(III) complexes

Compound	Yield (%)	Compound	Yield (%)
$[(C_{12}H_{25}O)_8Pc]_2La$	0	$[(C_5H_{11}O)_8Pc]_2Er$	3
$[(C_{12}H_{25}O)_8Pc]_2Ce$	0	$[(C_6H_{13}O)_8Pc]_2Er$	11
$[(C_{12}H_{25}O)_8Pc]_2Pr$	11	$[(C_7H_{15}O)_8Pc]_2Er$	0
$[(C_{12}H_{25}O)_8Pc]_2Nd$	17	$[(C_8H_{17}O)_8Pc]_2Er$	0
$[(C_{12}H_{25}O)_8Pc]_2Sm$	0	$[(C_9H_{19}O)_8Pc]_2Er$	9
$[(C_{12}H_{25}O)_8Pc]_2Eu$	23	$[(C_{10}H_{21}O)_8Pc]_2Er$	24
$[(C_{12}H_{25}O)_8Pc]_2Gd$	3	$[(C_{11}H_{23}O)_8Pc]_2Er$	0
$[(C_{12}H_{25}O)_8Pc]_2Tb$	21	$[(C_{12}H_{25}O)_8Pc]_2Er$	8
$[(C_{12}H_{25}O)_8Pc]_2Dy$	16	$[(C_{13}H_{27}O)_8Pc]_2Er$	0
$[(C_{12}H_{25}O)_8Pc]_2Ho$	8	$[(C_{14}H_{29}O)_8Pc]_2Er$	9
$[(C_{12}H_{25}O)_8Pc]_2Er$	15	$[(C_{15}H_{31}O)_8Pc]_2Er$	16
$[(C_{12}H_{25}O)_8Pc]_2Tm$	16	$[(C_{16}H_{33}O)_8Pc]_2Er$	10
$[(C_{12}H_{25}O)_8Pc]_2Yb$	7	$[(C_{18}H_{37}O)_8Pc]_2Er$	27
$[(C_{12}H_{25}O)_8Pc]_2Lu$	21	$[(C_{19}H_{39}O)_8Pc]_2Er$	5
$[(C_4H_9O)_8Pc]_2Er$	16	$[(C_{20}H_{41}O)_8Pc]_2Er$	0

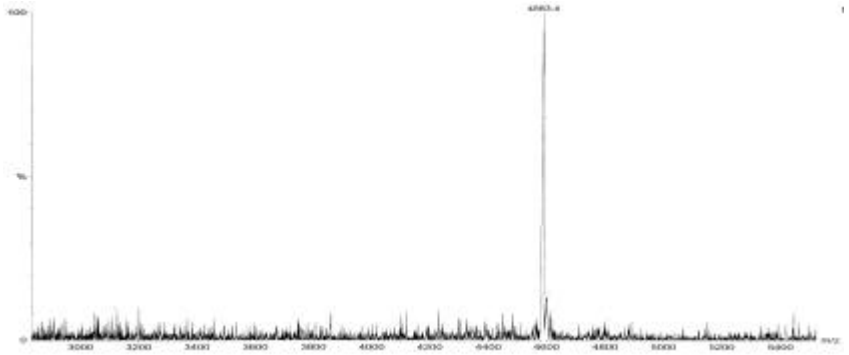

Figure 31 - MALDI-TOF spectrum for the $[(C_{14}H_{29}O)_8Pc]Er$ complex

Table 28 - MALDI-TOF results of the octa-alkoxy substituted bis(phthalocyaninato) lanthanide(III) metal complexes (/ = synthesis did not yield the complex)

Compound	Formula	M (isotopic)	M (found)
$[(C_{12}H_{25}O)_8Pc]_2La$	$C_{256}H_{416}O_{16}N_{16}La$	4110.1	/
$[(C_{12}H_{25}O)_8Pc]_2Ce$	$C_{256}H_{416}O_{16}N_{16}Ce$	4111.1	/
$[(C_{12}H_{25}O)_8Pc]_2Pr$	$C_{256}H_{416}O_{16}N_{16}Pr$	4112.1	4111.4
$[(C_{12}H_{25}O)_8Pc]_2Nd$	$C_{256}H_{416}O_{16}N_{16}Nd$	4113.1	4114.8
$[(C_{12}H_{25}O)_8Pc]_2Sm$	$C_{256}H_{416}O_{16}N_{16}Sm$	4123.1	/
$[(C_{12}H_{25}O)_8Pc]_2Eu$	$C_{256}H_{416}O_{16}N_{16}Eu$	4124.1	4123.2
$[(C_{12}H_{25}O)_8Pc]_2Gd$	$C_{256}H_{416}O_{16}N_{16}Gd$	4129.1	4128.9
$[(C_{12}H_{25}O)_8Pc]_2Tb$	$C_{256}H_{416}O_{16}N_{16}Tb$	4130.1	4129.8
$[(C_{12}H_{25}O)_8Pc]_2Dy$	$C_{256}H_{416}O_{16}N_{16}Dy$	4135.2	4135.6
$[(C_{12}H_{25}O)_8Pc]_2Ho$	$C_{256}H_{416}O_{16}N_{16}Ho$	4136.2	4136.5
$[(C_{12}H_{25}O)_8Pc]_2Er$	$C_{256}H_{416}O_{16}N_{16}Er$	4137.2	4137.5
$[(C_{12}H_{25}O)_8Pc]_2Tm$	$C_{256}H_{416}O_{16}N_{16}Tm$	4140.2	4139.5
$[(C_{12}H_{25}O)_8Pc]_2Yb$	$C_{256}H_{416}O_{16}N_{16}Yb$	4145.2	4145.9
$[(C_{12}H_{25}O)_8Pc]_2Lu$	$C_{256}H_{416}O_{16}N_{16}Lu$	4146.2	4146.8
$[(C_4H_9O)_8Pc]_2Er$	$C_{128}H_{160}O_{16}N_{16}Er$	2343.2	2341.1
$[(C_5H_{11}O)_8Pc]_2Er$	$C_{144}H_{192}O_{16}N_{16}Er$	2567.4	2567.9
$[(C_6H_{13}O)_8Pc]_2Er$	$C_{160}H_{224}O_{16}N_{16}Er$	2791.7	2792.8
$[(C_7H_{15}O)_8Pc]_2Er$	$C_{176}H_{256}O_{16}N_{16}Er$	3015.9	/
$[(C_8H_{17}O)_8Pc]_2Er$	$C_{192}H_{288}O_{16}N_{16}Er$	3240.2	/
$[(C_9H_{19}O)_8Pc]_2Er$	$C_{208}H_{320}O_{16}N_{16}Er$	3464.4	3466.1
$[(C_{10}H_{21}O)_8Pc]_2Er$	$C_{224}H_{352}O_{16}N_{16}Er$	3668.7	3668.8
$[(C_{11}H_{23}O)_8Pc]_2Er$	$C_{240}H_{384}O_{16}N_{16}Er$	3912.9	/
$[(C_{12}H_{25}O)_8Pc]_2Er$	$C_{256}H_{416}O_{16}N_{16}Er$	4137.2	4137.5
$[(C_{13}H_{27}O)_8Pc]_2Er$	$C_{272}H_{448}O_{16}N_{16}Er$	4361.4	/
$[(C_{14}H_{29}O)_8Pc]_2Er$	$C_{288}H_{480}O_{16}N_{16}Er$	4585.7	4583.4
$[(C_{15}H_{31}O)_8Pc]_2Er$	$C_{304}H_{512}O_{16}N_{16}Er$	4809.9	4808.6
$[(C_{16}H_{33}O)_8Pc]_2Er$	$C_{320}H_{544}O_{16}N_{16}Er$	5034.2	5032.7
$[(C_{18}H_{37}O)_8Pc]_2Er$	$C_{352}H_{608}O_{16}N_{16}Er$	5482.7	5478.7
$[(C_{19}H_{39}O)_8Pc]_2Er$	$C_{368}H_{640}O_{16}N_{16}Er$	5706.9	5705.8
$[(C_{20}H_{41}O)_8Pc]_2Er$	$C_{384}H_{632}O_{16}N_{16}Er$	5931.2	/

Synthesis of bis[2,3,9,10,16,17,23,24-octa(decyloxy)Pc]Er

A mixture of 1 g (2.27 mmol) of 1,2-dicyano-4,5-bis(decyloxy)benzene, 135.3 mg (0.30 mmol) of erbium acetate and 0.05 mL (1.3 mmol) of 1,8-diazabicyclo[5.4.0]undec-7-ene was stirred in 6 mL of 1-hexanol under refluxing during 20 hours. After evaporation to dryness, the green residue was dissolved in few millilitres of chloroform and reprecipitated by addition of methanol. Yield: 30 % of crude product. The crude product was purified by chromatography on silica and size exclusion chromatography on Bio-Rad Bio-Beads S-X3 (eluent: $CHCl_3$). The green (neutral) fractions were collected. Yield: 24% (green compound). MS *m/z*: 3669 (M^+). UV/VIS: ($CHCl_3$) λ_{max}/nm : 682, 612, 495, 370.

4.5.2 Unsubstituted phthalocyanine lanthanide complexes

From column chromatography over silicagel with methanol as the eluent we observed for all Pc_2Ln complexes a blue and a green fraction. Being the neutral form (as was mentioned in 2.2.4) only the green fractions were collected. Table 29 shows the yields for the complexes across the lanthanide series (except Pm).

Table 29 - Yields of the unsubstituted phthalocyanine lanthanide(III) complexes

Compound	Yield (%)	Compound	Yield (%)
Pc_2La	13	Pc_2Tb	45
Pc_2Ce	22	Pc_2Dy	54
Pc_2Pr	16	Pc_2Ho	23
Pc_2Nd	33	Pc_2Er	65
Pc_2Sm	34	Pc_2Tm	52
Pc_2Eu	27	Pc_2Yb	78
Pc_2Gd	18	Pc_2Lu	72

The yields for the reactions were rather high on average, although they are not quasi-quantitative as Villemin *et al*. observed for a number of metal complexes [VilHam01], using a resembling setup. Moreover, it was difficult to obtain reproducible results

Again, the elemental analysis did give satisfying results (Table 30) and the purity was judged from the mass spectral data (electron impact, Table 31), IR and the UV/VIS spectrum, consistent with that of the green (neutral) double-decker.

Table 30 - CHN-analysis results of the unsubstituted phthalocyanine lanthanide(III) complexes

	Calculated			Found		
Compound	C (%)	H (%)	N (%)	C (%)	H (%)	N (%)
Pc_2La	66.02	2.77	19.26	64.83	3.20	17.60
Pc_2Ce	65.97	2.77	19.24	67.03	3.18	18.63
Pc_2Pr	65.91	2.77	19.23	66.55	2.78	18.11
Pc_2Nd	65.85	2.77	19.21	65.90	3.15	18.46
Pc_2Sm	65.29	2.74	19.05	66.39	3.14	18.62
Pc_2Eu	65.24	2.74	19.03	65.57	3.05	18.38
Pc_2Gd	64.96	2.73	18.95	61.64	2.54	16.47
Pc_2Tb	64.91	2.73	18.94	58.07	2.46	14.64
Pc_2Dy	64.63	2.71	18.86	61.40	2.51	16.29
Pc_2Ho	64.58	2.71	18.84	62.36	2.56	16.90
Pc_2Er	64.53	2.71	18.82	64.05	2.66	18.00
Pc_2Tm	64.36	2.70	18.78	60.98	2.55	18.01
Pc_2Yb	64.09	2.69	18.70	59.09	1.92	18.22
Pc_2Lu	64.04	2.69	18.70	62.58	2.44	16.36

The elemental analysis problem was discussed with the firm of the elemental analyser apparatus. After numerous experiments on their behalf, no good results could be obtained either (even when increasing the furnace temperature).

Table 31 - Mass spectral data for the unsubstituted bis(phthalocyaninato) lanthanide(III) metal complexes

Compound	Formula	M (isotopic)	M (found)
Pc_2La	$C_{64}H_{32}N_{16}La$	1163.2	1163.4
Pc_2Ce	$C_{64}H_{32}N_{16}Ce$	1164.2	1164.3
Pc_2Pr	$C_{64}H_{32}N_{16}Pr$	1165.2	1165.3
Pc_2Nd	$C_{64}H_{32}N_{16}Nd$	1166.2	1167.1
Pc_2Sm	$C_{64}H_{32}N_{16}Sm$	1176.2	1176.4
Pc_2Eu	$C_{64}H_{32}N_{16}Eu$	1177.2	1177.2
Pc_2Gd	$C_{64}H_{32}N_{16}Gd$	1182.2	1182.2
Pc_2Tb	$C_{64}H_{32}N_{16}Tb$	1183.2	1183.2
Pc_2Dy	$C_{64}H_{32}N_{16}Dy$	1188.2	1187.2
Pc_2Ho	$C_{64}H_{32}N_{16}Ho$	1189.2	1189.2
Pc_2Er	$C_{64}H_{32}N_{16}Er$	1190.2	1190.6
Pc_2Tm	$C_{64}H_{32}N_{16}Tm$	1193.2	1193.1
Pc_2Yb	$C_{64}H_{32}N_{16}Yb$	1198.2	1198.3
Pc_2Lu	$C_{64}H_{32}N_{16}Lu$	1199.2	1199.3

Synthesis of Pc_2Er

A mixture of 2 g (16 mmol) of 1,2-dicyanobenzene, 670 mg (2 mmol) of erbium acetate, 4.69 g (80 mmol) of urea and 140 mg of ammonium molybdate were profoundly ground together in order to obtain a fine powder. The reaction mixture was irradiated during 10 minutes in a commercial microwave oven (1200W, 2450 MHz). The resulting solid was ground and extracted by Soxhlet extraction with acetone, ethyl acetate and acetonitrile for eight hours each. Yield: 65 % of crude product. The crude product was purified by chromatography on silica with methanol as the eluent. Yield: 24% (502 mg, green compound). MS *m/z*: 1190.6 (M^+). UV/VIS: ($CHCl_3$) λ_{max}/nm : 664 (single Q-band), 495.5. IR: 3047 (νC-H), 1606 (νC-C), 1504 (νC-N), 1450, 1322 (νC-C), 1062 (ßC-H), 946, 885 (γC-H), 811, 778, 729, 562, 499.

4.6 Conclusions

We have synthesised a number of peripherally octa-substituted phthalocyanine ligands, transition metal and lanthanide complexes. In general, the complexes were less soluble than the ligands. Three parameters were varied: the chain length, the linking group to the phthalocyanine core and the central metal ion.

A major problem was the purity check of the synthesised complexes. The elemental analysis did only in rare cases yield satisfactory results and adding a combustion catalyst to the CHN-sample did not improve this outcome. Further investigation of the instrumental parameters by the firm of the elemental analyser apparatus on our compounds did not yield a better result either. Nevertheless, from literature survey, this is a well-known problem for these types of macrocyclic compounds. In general, the C content was less than the calculated value. This is probably due to the formation of nitrides (under reducing and anhydrous conditions), carbides and oxides that only decompose at very high temperatures. The problem was overcome by judging the purity based on the compound's MALDI-TOF, IR and UV/VIS spectra.

The overall yield for the octa-substituted synthesised ligands and complexes was in general very low (20 % at the best). The aim of our research however was not to optimise the synthetic pathway. Nevertheless, a recent technique that uses microwave radiation as the energy source during the cyclotetramerisation yielded promising results in preliminary tests [Sha98, VilHam01]. We succeeded in obtaining the unsubstituted phthalocyanine lanthanide complexes (Ln: La-Lu, except Pm) with this technique. Nevertheless, a further refinement of our synthesis method is desired because of the irreproducible yields and lack of control of the parameters of the (commercial) microwave oven. Our first attempts in synthesising peripherally substituted metallophthalocyanines with this technique were unsuccessful, although in literature soluble complexes with relatively short chain lengths were prepared [Ung99, LiuLee01].

4.7 References

[BelSir89] Z. Belarbi, C. Sirlin, J. Simon and J.J. André, *J. Phys. Chem.*, **93**, 8105, 1989.

[EllRom87] G.P. Ellis, T.M. Romney-Alexander, *Chem. Rev.*, **87**, 779, 1987.

[ForSum94] W.T. Ford, L. Sumner, W. Zhu, Y.H. Chang, PJ. Um, K.H. Choi, P.A. Heiney, N.C. Maliszewskyj, *New J. Chem.*, **18**, 495, 1994.

[GuyPon94] F. Guyon, A. Pondaven, P. Guenot, M. L'Her, *Inorg. Chem.*, **33**, 4787, 1994.

[JiaLiu97] J. Jiang, R.C.W. Liu, T.C.W. Mak, T.W.D. Chan, D.K.P. Ng, *Polyhedron*, **16**, 515, 1997.

[LiuLee01] L.C. Liu, C.C. Lee, A. Teh Hu, *J. Porphyr. Phthalocya.*, **5**, 806, 2001.

[Sha98] A. Shaabani, *J. Chem. Res.*, 672, 1998.

[Ung99] C. Ungurenasu, *Synthesis*, **10**, 1729, 1999.

[VanNee88] J.F. van der Pol, E. Neeleman, J.W. Zwikker, R.J.M. Nolte, W. Drenth, *Recl. Trav. Chim. Pays-Bas*, **107**, 615, 1988.

[VilHam01] D. Villemin, M. Hammadi, M. Hachemi, N. Bar, *Molecules*, **6**, 831, 2001.

Chapter 5

THERMAL PROPERTIES

5.1 Differential Scanning Calorimetry (DSC)

In order to determine the Differential Scanning Calorimeter's optimal operating conditions for our type of compounds, preliminary experiments were performed on the octa-dodecyloxy phthalocyanine ligand. We investigated only the influence of sample size and the heating rate on DSC measurements. Other parameters (pan material, gas flow rate, and type of gas) were held constant. Both the sample weight and heating rate influence the outcome of the DSC-curve significantly. With increasing sample weight and/or heating rate the peak sizes and temperature gradients become larger but the resolution decreases. Finding an optimal ratio between sensitivity and resolution is essential.

The influence of the heating rate is illustrated in Figure 32 whereas the thermographic data are summarised in Table 32. An improved sensitivity is noticed for the higher scan rates.

Table 32 - DSC-data showing effect of the variation of the heating rate on transition temperatures and intensities for the octa-dodecyloxy substituted phthalocyanine ligand

Heating rate (°C/min)	Onset (°C)	Peak (°C)	Peak height (mW)	ΔH (kJ/mol)
10	87	91	6.3	109
5	87	92	2.2	102
2	86	93	0.34	101

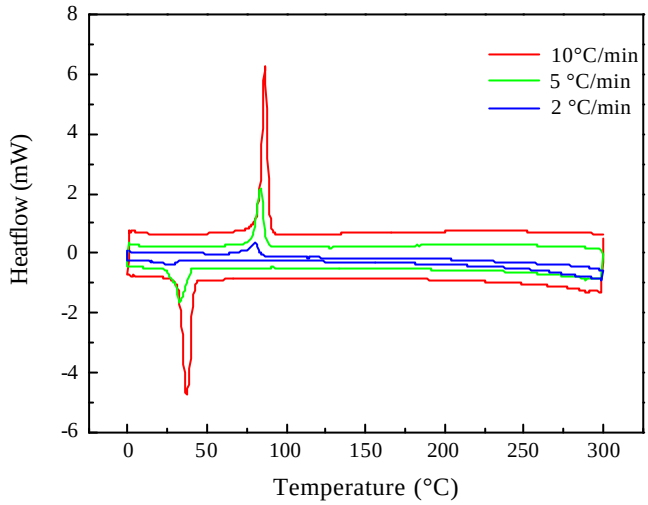

Figure 32 - DSC-graphs showing effect of the variation of the heating rate on transition temperatures and intensities for the octa-dodecyloxy substituted phthalocyanine ligand

Figure 33 shows the influence of the sample size on the DSC-thermograms for the octa-dodecyloxy substituted phthalocyanine. The data can be found in Table 33. As expected the sensitivity improves on increasing weight.

Table 33 - DSC-data showing effect of the variation of the sample size on transition temperatures and intensities for the octa-dodecyloxy substituted phthalocyanine ligand

Sample mass (mg)	Onset (°C)	Peak (°C)	Peak height (mW)	?H (kJ/mol)
10.3	87	93	16.7	93
6.2	87	93	9.3	96
3.1	87	92	1.4	101

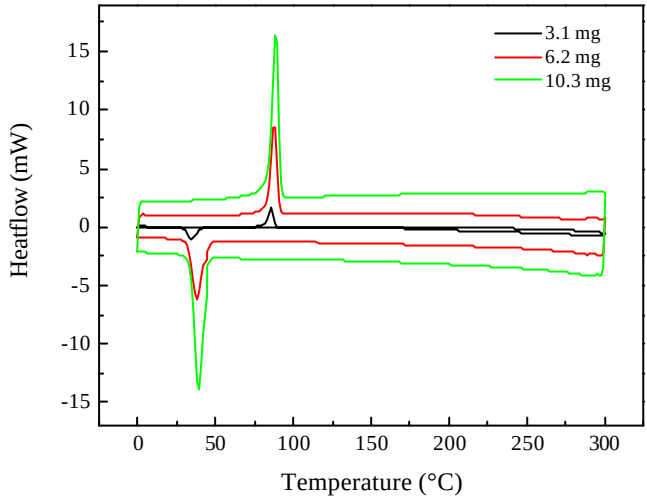

Figure 33 - DSC-graphs showing effect of the variation of the sample size on transition temperatures and intensities for the octa-dodecyloxy substituted phthalocyanine ligand

Since only one mesophase was observed (sometimes a crystal-crystal transition was measured, which is not visible by POM) and the melting and clearing points are separated rather far away, the resolution problem is of less importance for our samples. For some of the complexes synthesis did yield moderate amounts of product, hence we choose to use between 1 and 5 milligrams of sample to obtain an acceptable sensitivity. The heating rate was set to 10°C/min, a standard setting for most liquid crystalline research.

All DSC-thermographic data in this chapter were collected at peak position during a second heating run. We have to remark that references mentioned in Appendix A-C in general do not indicate the parameters used during the thermal analysis and hence comparison with literature data is sometimes difficult.

Figure 34 shows a typical DSC thermogram for one of the compounds we synthesised: the octa-hexadecyl phthalocyanine cobalt(II) complex. The DSC

thermograms of the other products were similar to this one. The sharpness of the melting point gives an indication that the sample is pure. The clearing point enthalpy is much smaller than the melting enthalpy, because for the mesophase to isotropic transition the structural rearrangement of the molecules is far more relevant than for the solid-to-mesophase transition. As mentioned in 2.3.2.1 a stronger undercooling is observed for the melting point than for the clearing point.

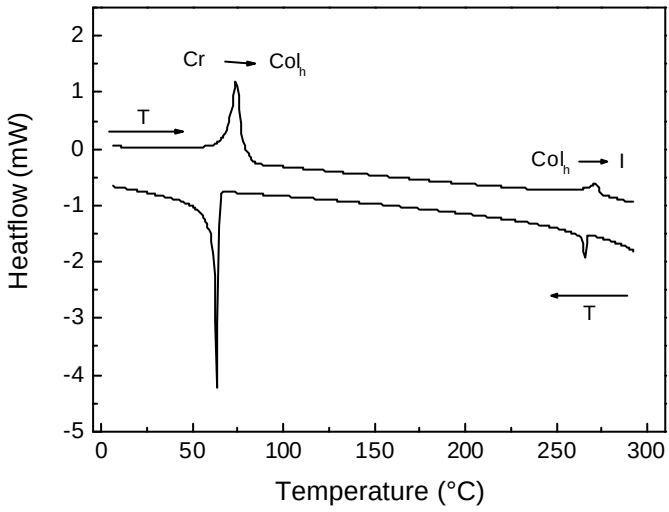

Figure 34 - DSC-thermogram for a second heating and cooling run of the octa-hexadecyl phthalocyanine cobalt(II) complex

5.2 Ligands

5.2.1 Octa-alkoxy phthalocyanines

All our compounds exhibit a wide mesophase range (Table 34). From Figure 35 it can be seen that both the melting point and the clearing point decrease with

increasing chain length. For chain lengths from OC_6H_{13} to OC_8H_{17} the clearing of the mesophase could not be detected by DSC measurements and the clearing point was measured by microscopy. Ligands with chain lengths from OC_4H_9 to OC_5H_{11} decomposed before the clearing point could be observed. This is also illustrated by the TGA thermogram for the octa-butyloxy substituted phthalocyanine (Figure 36). From this graph it is clear that thermal decomposition starts at 300 °C.

Table 34 - Mesomorphism of the octa-alkoxy substituted phthalocyanines (†: observed by polarising microscopy; Dec = decomposition before clearing to the isotropic liquid)

	Melting point			Clearing point
Compound	Transition temperature (°C)	ΔH_m ($kJmol^{-1}$)	ΔS_m ($JK^{-1}mol^{-1}$)	Transition temperature (°C)
$(C_4H_9O)_8PcH_2$	160	8.3	19	Dec
$(C_5H_{11}O)_8PcH_2$	122	37	94	Dec
$(C_6H_{13}O)_8PcH_2$	97	49	132	330†
$(C_7H_{15}O)_8PcH_2$	93	54	147	340†
$(C_8H_{17}O)_8PcH_2$	95	70	190	368†
$(C_9H_{19}O)_8PcH_2$	94	70	191	327
$(C_{10}H_{21}O)_8PcH_2$	90	88	242	326
$(C_{11}H_{23}O)_8PcH_2$	83	94	264	303
$(C_{12}H_{25}O)_8PcH_2$	84	95	266	309
$(C_{13}H_{27}O)_8PcH_2$	89	102	282	264
$(C_{14}H_{29}O)_8PcH_2$	69	105	307	242
$(C_{15}H_{31}O)_8PcH_2$	84	128	358	235
$(C_{16}H_{33}O)_8PcH_2$	44	131	413	221
$(C_{17}H_{35}O)_8PcH_2$	49	139	432	210
$(C_{18}H_{37}O)_8PcH_2$	42	145	460	247
$(C_{19}H_{39}O)_8PcH_2$	54	161	492	219
$(C_{20}H_{41}O)_8PcH_2$	39	173	554	150

The transition enthalpies for the clearing point are not given, because these transitions are very weak and sometimes hard to detect.

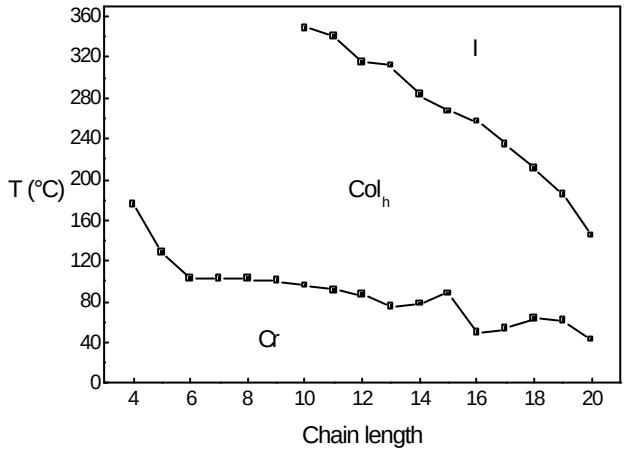

Figure 35 - Influence of the chain length on transition temperatures of the octa-alkoxy substituted phthalocyanines (Cr = crystalline solid, Col_h = hexagonal columnar mesophase, I = isotropic liquid)

The clearing points show a more drastic decrease than the melting points: on going from $OC_{10}H_{21}$ to $OC_{20}H_{41}$ we observed a reduction of the melting point of about 50°C whereas the clearing point decreases by about 175°C. On average, an extra methylene unit reduced the melting point by 6°C and the clearing point by 19°C. This is a common phenomenon for liquid crystals and can be explained based on intermolecular interactions. These interactions are more important for aromatic compounds than for aliphatics and the melting temperatures for the former are always slightly higher than for the latter. When the aliphatic chains get longer, the aromatic character of the compound is decreased in favour of the aliphatic part, and the clearing points will decline. This explanation is not valid for the crystal to mesophase transition, since the initial (or final when cooling) crystalline state is not reproducible, whereas the mesophase and isotropic liquid are always organised in the same manner. Hence, no clear relationship between the chain length and the

melting point can be appointed. We only observe a sharp decline for the melting point of the shorter chain lengths (OC_4H_9 to OC_6H_{13}), and a less-pronounced effect for the longer chains.

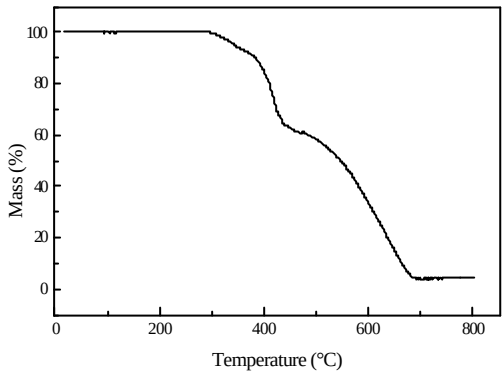

Figure 36 - TGA thermogram of the octa-butyloxy substituted phthalocyanine

As can be seen in Figure 37, the melting enthalpy increases more or less linearly with the chain length, which indicates the similarity of the molecular organisation in the mesophase for the different chain lengths. The linear fit indicates that the melting of the compounds is mainly due to the melting of the peripheral chains.

When the mesomorphic data for the ligands we synthesised are compared with the data obtained by van der Pol *et al.* [vanNee88] we can conclude that for the shorter chain lengths significant differences are observed between our melting points and those obtained by van der Pol (e.g. van der Pol found a melting point of 119°C for the $(C_6H_{13}O)_8PcH_2$ ligand, whereas we observed the melting of the compound at 97°C). Whether this is due to a discrepancy in instrumental parameters or a different thermal history of the sample remains unclear, because the article does not give any details on the way the DSC-measurements were interpreted. For the longer chain lengths ($\geq OC_8H_{17}$) our data are more consistent with those of van der Pol *et al.*

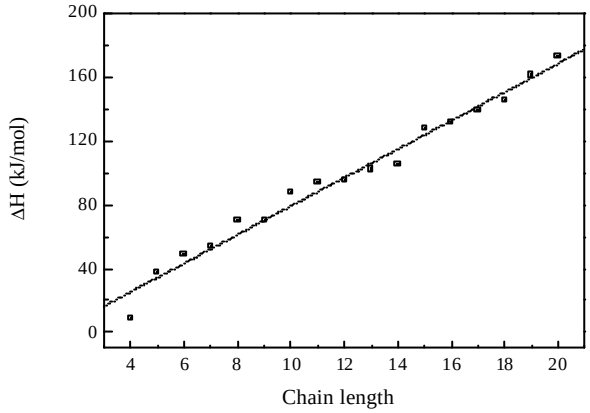

Figure 37 - Variation of the transition enthalpies as a function of the chain length for the melting points of the octa-alkoxy phthalocyanine ligands

In order to elucidate the mesophase structure, we investigated our compounds by polarising optical microscopy. A mosaic texture (pseudo focal-conical) typical for the hexagonal columnar mesophase (Col_h), as observed for the octa-tetradecyloxy phthalocyanine, is shown in Figure 38 (left) [BarRak98]. The mesophases were more viscous for the shorter chain lengths, and became more fluid on heating. Under parallel polarisers snowflake-like structures having a six-fold axis (as indicated by the hexagon in overlay) appeared on cooling from the isotropic liquid (Figure 38, right) as was also reported by van der Pol [vanNee89]. It should be mentioned that the defect textures of columnar mesophases have not been characterised too well so far. Many columnar phases show dendritic growth patterns and fern-like or spine-like textures. The similarity between the textures of the various columnar phases does not allow for the easy identification of the various columnar mesophases.

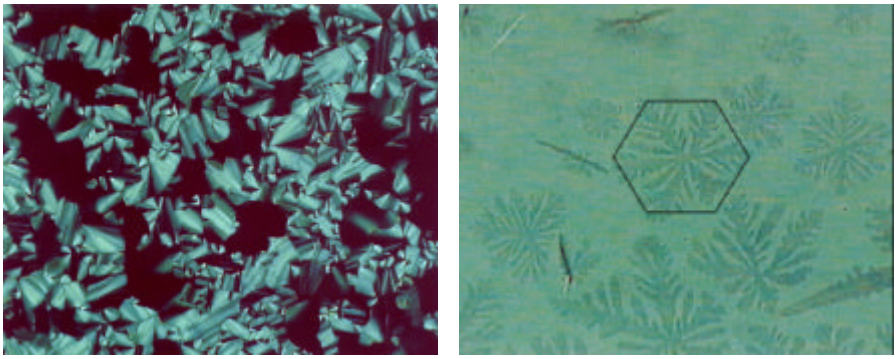

Figure 38 - Textures for the octa-tetradecyloxy substituted phthalocyanine as observed under crossed polarisers (left) and under parallel polarisers (right), both at 290°C and x 200

The hexagonal columnar lattice (Figure 39, bidimensional lattice) is characterised by interplanar distances d_{hkl}. These distances can be mathematically expressed as a function of the lattice parameters a and c and the Miller indices hkl:

$$d_{hkl} = \frac{a}{\sqrt{\frac{4}{3}\cdot(h^2 + k^2 + h\cdot k) + \frac{l^2 \cdot a^2}{c^2}}} \qquad (1)$$

So, we find for the first set of (two-dimensional, $l = 0$) planes:

$$d_{100} = d_{010} = a \cdot \frac{\sqrt{3}}{2}$$

$$d_{110} = a / 2$$

$$d_{200} = \frac{a}{\sqrt{16/3}}$$

$$d_{210} = \frac{a}{\sqrt{28/3}}$$

Hence, the ratios for the sets of planes are: 1, √3, 2, √7, √9...

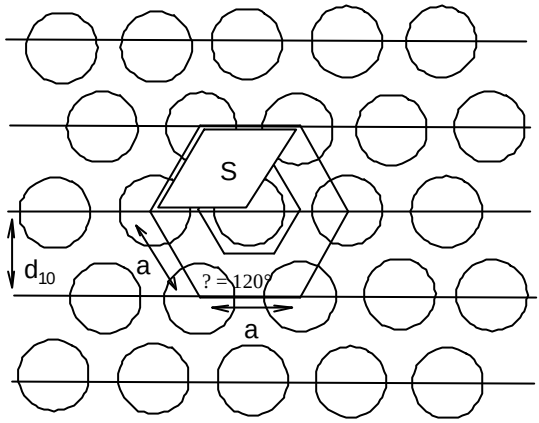

Figure 39 - Schematic representation of the bidimensional hexagonal lattice: the (10) set of planes is shown

The columnar section *S* can be approximated from the lattice area as is illustrated in the representation in Figure 39 . The area of the hexagonal lattice is:

$$S = a \times d_{10} \qquad (2)$$

The relationship between a and d_{10} is given by:

$$d_{10} = d = a \times \sin 60° = a \times (\sqrt{3}/2) \qquad (3)$$

and thus, the unit cell surface:

$$S = (2/\sqrt{3}) \times (d_{10})^2 \qquad (4)$$

X-ray diffraction experiments measurements confirmed the presence of a two-dimensional hexagonal lattice in the mesophase of all our compounds. Figure 40 shows the diffractogram of the $OC_{14}H_{29}$ molecule at 125 °C. The data are summarised in Table 35. The diffractogram showed four Bragg reflections having the reciprocal spacings of $1:\sqrt{3}:\sqrt{4}:\sqrt{7}$, characteristic for a two-dimensional hexagonal lattice as in the hexagonal columnar mesophase. Because we only

observed reflections for *hk0* and *00l* planes we can conclude there is no correlation between the order of the molecules in different columns (if such a relation existed we would be able to define *hkl* planes that intersected all three axes).

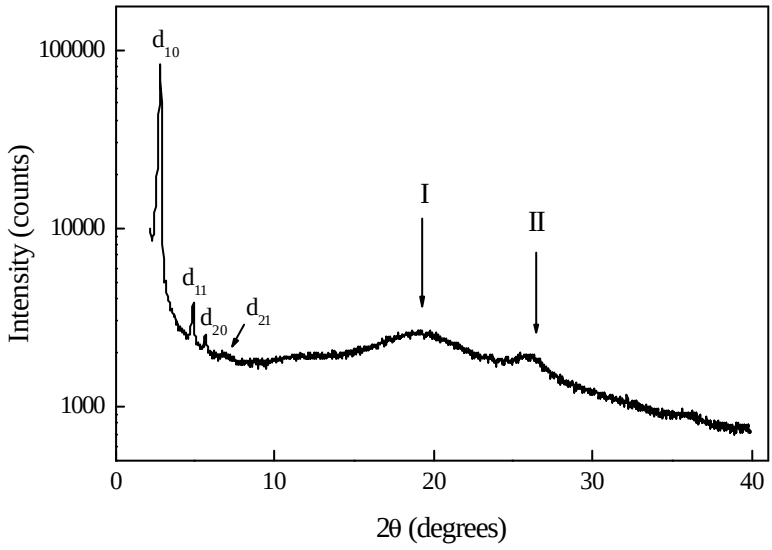

Figure 40 - XRD-diffractogram of the octa-tetradecyloxy phthalocyanine at 125°C

A broad peak at a wider angle (2θ =19°) could also be observed. This peak corresponds to the molten aliphatic chains that are located randomly within the columnar mesophase with an average spacing of 4.6 Å. A less broad peak was found round 3.4 Å, which corresponds to the stacking distance of the phthalocyanine cores within the columns (equal to the van der Waals distance of aromatic compounds). The peak suggests an ordered hexagonal columnar mesophase. The phthalocyanine cores are stacked at regular distances from one another as suggested by Figure 41. The columns are ordered because of the low steric hindrance of the side chains.

These results are similar to the data of the dodecyloxy-substituted phthalocyanine obtained by Ohta [OhtJac88] and van der Pol [vanNee88].

Table 35 - X-ray diffraction data for the octa(tetradecyloxy) phthalocyanine ligand; d_{obs} and d_{calc} are the diffraction spacings which are observed and calculated respectively; calculated value of d_{10} = ¼ (d_{10}+d_{11}√3 + d_{20}√2 + d_{21}√7); I is the intensity of the diffraction signal (VS: very strong, S: strong, M: medium, W: weak, VW: very weak); hk is the indexation of the two-dimensional lattice; a is the lattice parameter, S is the lattice area and p6mm is the 2D space groups of the hexagonal (Col_h) columnar phase

Temperature (°C)	d_{obs} (Å)	I	hk	$d_{calc.}$ (Å)	Mesophase and parameters
125	31.2	VS	10	31.3	Col_h-*p6mm*
	18.0	S	11	18.1	a = 36.0 Å
	15.6	S	20	15.6	S = 1124 Å^2
	11.9	M	21	11.8	
	4.6	halo I	broad		
	3.4	halo II	broad		

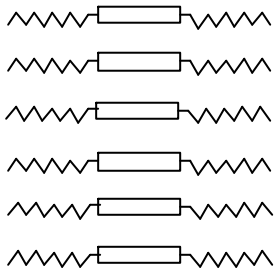

Figure 41 - Side-view of the ordered packing in the hexagonal columnar mesophase for the octa-alkoxy phthalocyanines

We can compare the measured d_{10} (31.1 Å) reflection (which represents the intercolumnar distance) to the calculated molecular dimensions as represented in Figure 42 (left).

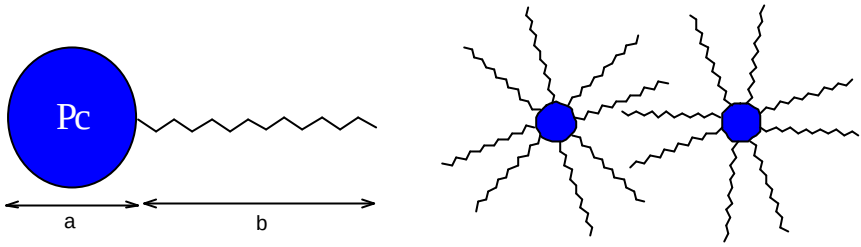

Figure 42 - Schematic representations of the molecular dimensions (left) and interpenetration of neighbouring columns (right)

The length *D* of an octa-tetradecyloxy phthalocyanine molecule is equal to:

$$D = a + 2 \cdot b \qquad (5)$$

where *a* is the length of the unsubstituted Pc (13 Å, fom XRD databases [EngBas93, Tou95]) and *b* is the total side-chain length (17.6 Å, measured from modelling[1]). The chain is almost completely coplanar with the Pc core (provided that the whole chain is in the staggered conformation) because of the Ar-O-CH_2 bond. The calculated value (48.2 Å) is much larger than the measured intercolumnar distance, even when taking into account small angle between the plane of the Pc core and the chain as was done by van der Pol *et al* [vanNee8]. A significant interpenetration of the alkoxy chains of the Pc molecule for neighbouring columns can explain this difference (Figure 42, right). Another explanation can be the increased number of synclinal conformations (which reduces the chain's coplanarity) in the mesophase as was suggested by van der Pol [vanNee88]. A combination of both justifications is also possible, but this will require further study.

The calculated lattice parameter *a* and the hexagonal columnar cross-section *S* are in agreement with those observed in prior research [vanNee88, vanNee89, VacDop92].

[1] We did not take the thermal expansion due to the melting of the chains into account as did Guillon *et al*. [GuiSko83]; they only found a minimal effect.

5.2.2 Octa-alkyl phthalocyanines

The transition temperatures are given in Table 36 and these data are graphically represented in Figure 43. The observed texture with POM is a fan-shaped texture as shown in Figure 44, indicating a hexagonal (disordered) columnar mesophase. Our values and mesophase are in good agreement with the analogue compounds synthesised prior to this work except for the clearing point of $(C_{12}H_{25})_8PcH_2$ which differs over 20°C from the reported value by Ohta *et al.* [OhtJac88, NisUen89, NisAzu92, EngBas93] who all observed a single (disordered hexagonal columnar) mesophase (Col_{hd}). We could not confirm the presence of two distinct phases (Col_{rd} and Col_{hd}) for the $(C_{16}H_{33})_8PcH_2$ ligand. This was observed for this chain length by Clarkson *et al.* [ClaMcK95]. No XRD-measurements were done in order to confirm the presence of such a phase or the order within the columns of the mesophase, because not enough sample could be collected for any of the compounds.

Table 36 - Transition temperatures of the octa-alkyl substituted phthalocyanine ligands (Cr = crystalline phase; Col_h = hexagonal columnar mesophase; I = isotropic phase, Dec = decomposition before clearing to the isotropic liquid)

Compound	Transition temperatures (°C)				
$(C_7H_{15})_8PcH_2$	Cr	192	Col_h	Dec	I
$(C_8H_{17})_8PcH_2$	Cr	180	Col_h	320	I
$(C_{12}H_{25})_8PcH_2$	Cr	120	Col_h	230	I
$(C_{14}H_{29})_8PcH_2$	Cr	128	Col_h	210	I
$(C_{16}H_{33})_8PcH_2$	Cr	103	Col_h	210	I
$(C_{18}H_{37})_8PcH_2$	Cr	101	Col_h	190	I

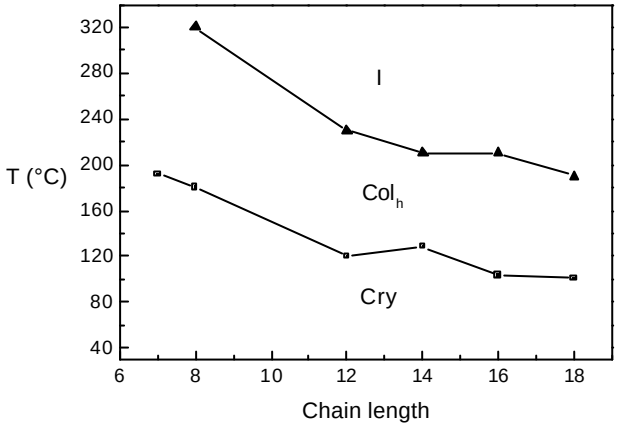

Figure 43 - Influence of the chain length on transition temperatures of the octa-alkyl substituted phthalocyanines (Cr = crystalline solid, Col_h = hexagonal columnar mesophase, I = isotropic liquid)

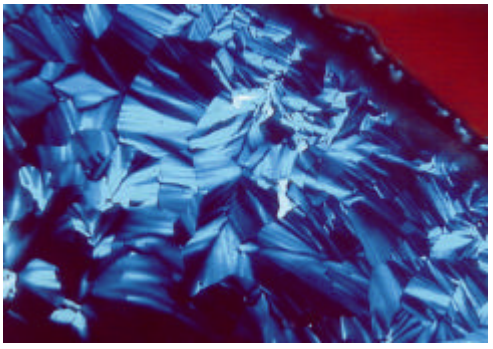

Figure 44 - Fan-shaped texture as observed under crossed polarisers for the octa-tetradecyl substituted phthalocyanine (at 175°C and 100x magnification)

5.2.3 Octa-alkoxymethyl phthalocyanines

The mesomorphic data are given in Table 37 and they are represented in Figure 45. All values are in good agreement with results published earlier on [PieSim82,

GuiSko83, SimBas93]. Optical polarising microscopy again showed textures typical of a hexagonal columnar mesophase. For the octa-alkoxymethyl phthalocyanine ligands no XRD-measurements were done.

Table 37 - Mesomorphic properties of the octa-alkoxy substituted phthalocyanine ligands (Cr = crystalline phase; Col_h = hexagonal columnar mesophase; I = isotropic phase)

	Melting point			Clearing point
Compound	Transition temperature (°C)	ΔH_m ($kJmol^{-1}$)	ΔS_m ($JK^{-1}mol^{-1}$)	Transition temperature (°C)
$(C_8H_{17}OCH_2)_8\ PcH_2$	66	54	159	322
$(C_{12}H_{24}OCH_2)_8PcH_2$	82	114	321	265
$(C_{16}H_{33}OCH_2)_8\ PcH_2$	64	147	436	213

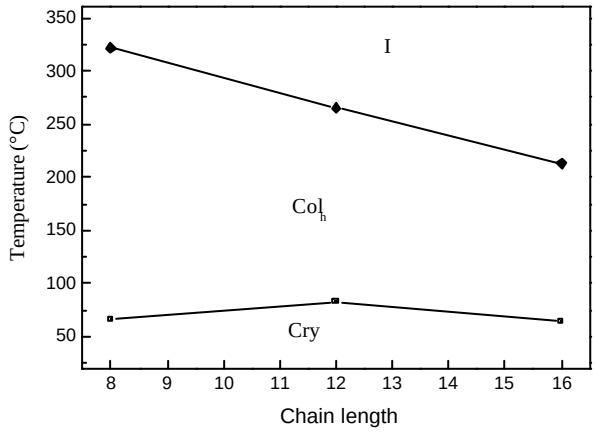

Figure 45 - Influence of the chain length on transition temperatures of the octa-alkoxymethyl substituted phthalocyanines (Cr = crystalline solid, Col_h = hexagonal columnar mesophase, I = isotropic liquid)

5.3 Transition metal complexes

5.3.1 Octa-alkoxy phthalocyanine transition metal complexes

5.3.1.1 Influence of the chain length: homologous series for cobalt(II)

All the cobalt(II) complexes are liquid crystals with a wide mesophase range. The data are given in Table 38. The melting points decrease with increasing chain length of the alkoxy substituents, from 218 °C for the complex with butyloxy substituents to 64 °C for the complex with octadecyloxy substituents (Figure 46). The homologues with chain lengths up to $C_{13}H_{27}O$ decompose above 300 °C without clearing. The clearing point decreases with increasing chain length, from 328 °C for the complex with tetradecyloxy substituents to 266 °C for the complex with octadecyloxy substituents. On average a decrease of 6°C for the melting point and 14°C for the clearing point per extra methylene unit is observed. The same explanations as for the ligands for the influence of the chain length on the mesophase behaviour are in order.

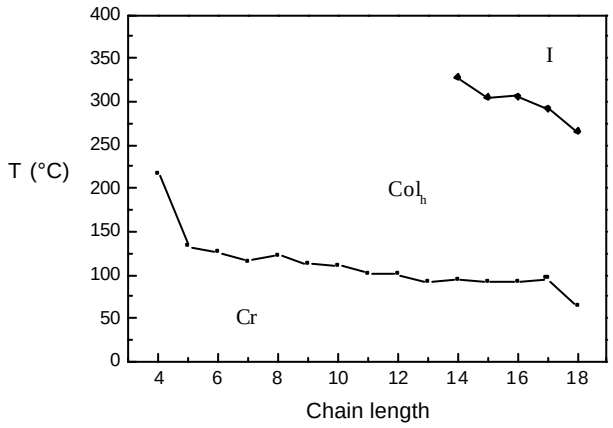

Figure 46 - Influence of the alkoxy chain length on the transition temperatures of the substituted cobalt(II) phthalocyanines (Cr = crystalline solid, Col_h = hexagonal columnar mesophase, I = isotropic liquid)

Table 38 - Mesophase behaviour of the octa(alkoxy)-substituted cobalt(II) phthalocyanine complexes (Dec = decomposition before clearing to the isotropic liquid)

	Melting point			Clearing point
Compound	Transition temperature (°C)	ΔH_m ($kJmol^{-1}$)	ΔS_m ($JK^{-1}mol^{-1}$)	Transition temperature (°C)
$(C_4H_9O)_8PcCo$	218	12	24	Dec
$(C_5H_{11}O)_8PcCo$	133	30	74	Dec
$(C_6H_{13}O)_8PcCo$	126	65	163	Dec
$(C_7H_{15}O)_8PcCo$	116	71	183	Dec
$(C_8H_{17}O)_8PcCo$	123	68	172	Dec
$(C_9H_{19}O)_8PcCo$	112	83	216	Dec
$(C_{10}H_{21}O)_8PcCo$	111	94	245	Dec
$(C_{11}H_{23}O)_8PcCo$	102	94	251	Dec
$(C_{12}H_{25}O)_8PcCo$	101	103	275	Dec
$(C_{13}H_{27}O)_8PcCo$	91	91	250	Dec
$(C_{14}H_{29}O)_8PcCo$	95	106	288	328
$(C_{15}H_{31}O)_8PcCo$	91	106	291	305
$(C_{16}H_{33}O)_8PcCo$	92	82	225	306
$(C_{17}H_{35}O)_8PcCo$	96	232	629	292
$(C_{18}H_{37}O)_8PcCo$	64	120	356	266

The thermal decomposition of the complexes was studied by a thermogravimeter coupled to a mass spectrometer. The TG-thermogram of the cobalt(II) phthalocyanine complex with eight decyloxy chains, $(C_{10}H_{21}O)_8PcCo$, is shown in Figure 47. Thermal decomposition takes place in two distinct steps: one at ca. 300 °C and a sharp step at 600 °C. By TG-MS it could be shown that the decomposition step at 300 °C corresponds to loss of the eight decyl ($C_{10}H_{25}$) chains. Different alkyl fragments between C_2H_5 and $C_{10}H_{25}$ could be observed (Figure 48). The decomposition step at 600 °C corresponds to degradation of the phthalocyanine core (detection of nitrogen in the MS).

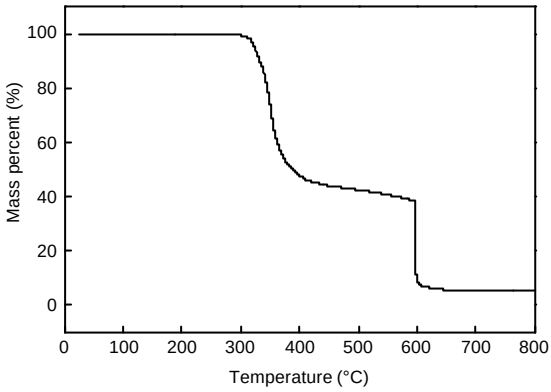

Figure 47 - TG-thermogram of the cobalt(II) complex $(C_{10}H_{21}O)_8PcCo$

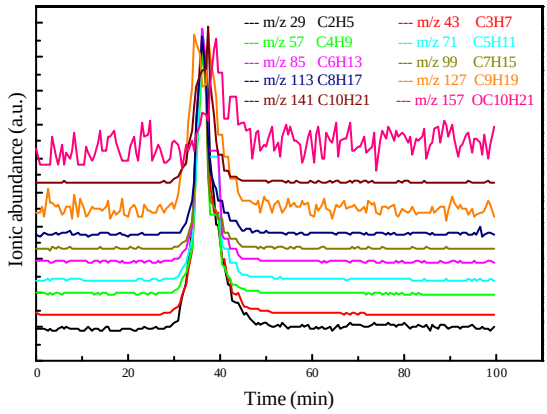

Figure 48 - Decomposition fragments as determined by TG-MS for the cobalt(II) complex $(C_{10}H_{21}O)_8PcCo$

In comparison with the metal-free phthalocyanines, transition temperatures (both melting and clearing point) of the corresponding cobalt(II) phthalocyanines are higher. For instance for the metal-free phthalocyanine with $C_{14}H_{29}O$ chains, the mesophase behaviour (temperatures in °C) is Cr 69 Col_h 242 I, whereas for the

corresponding cobalt(II) complex it is Cr 95 Col_h 328 I. The mesophase stability of the cobalt(II) phthalocyanines is significantly larger than that of the metal-free phthalocyanines. Thus, the metal ion in the central cavity of the phthalocyanine ring has a stabilising effect on the mesophase. On the other hand, the melting temperatures of the cobalt(II) phthalocyanines are very comparable with those of the corresponding copper(II) phthalocyanines. Because for the copper(II) series reported by van der Pol *et al*. only data are available for alkoxy chains up to $C_{12}H_{25}O$ and no clearing points are reported [vanNee88], the clearing points of the copper(II) and cobalt(II) series cannot be compared with one another. However, Ford *et al*. [ForSum94] published data for the copper(II) phthalocyanine with eight octadecyloxy chains, and the transition temperatures of this compound are Cr 52 M 257 I. This is again very comparable with the data for the corresponding cobalt(II) compound: Cr 64 Col_h 266 I.

The textures observed with polarising microscopy between crossed and uncrossed polarisers were similar to those of the corresponding ligands.

The small angle XRD pattern of the compound $(C_{16}H_{33}O)_8PcCo$ at 175 °C is shown in Figure 49. The XRD-data for the same complex at three different temperatures are given in Table 39. The diffractograms for the other compounds were identical. The X-ray patterns consist of: (a) a diffuse scattering halo in the wide angle region, corresponding to the liquid-like disorder of the aliphatic chains, at *ca* 4.4 Å; (b) another, less broad peak around 3.3 Å, which is the stacking distance of the phthalocyanine cores within the columns, (c) up to four sharp, intense reflections in the small angle region, with the reciprocal spacings in the ratio 1:√3:√4:√7, corresponding to the indexation [*hk*] = [10], [11], [20] and [21] (sometimes even [30]). Such features are also characteristic of a two-dimensional hexagonal packing of columns (Col_h). Compared to the ligands the diffractograms show more sharp reflections, what indicates that the mesophases for the complexes are more regularly packed (long-range order). The phase is more disordered within the columns than the corresponding ligands as evident from the less sharp peak in the

wide-angle region (but we still have a hexagonal columnar mesophase). For longer chain lengths and higher temperatures both halos at 3.3 Å and 4.4 Å become less pronounced. This is due to the increased fluctuation of the Pc cores with increasing temperature.

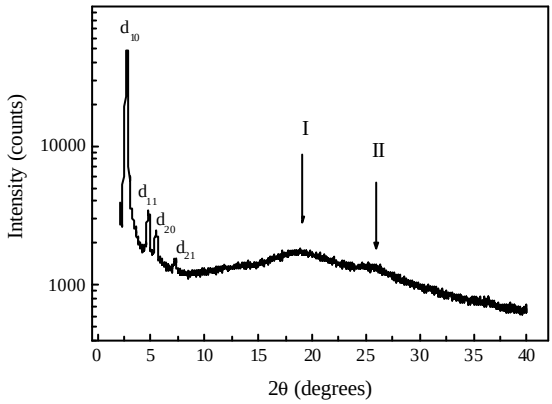

Figure 49 - X-ray diffractogram of cobalt(II) complex ($C_{16}H_{33}O)_8$PcCo at 175 °C

As expected, the lattice parameter *a* increases linearly with the chain length. This is illustrated for the cobalt complexes at 155°C in Figure 50. Moreover, *a* is constant with temperature. The absolute values found for *a* are in good agreement with the data for the copper(II) complexes obtained van der Pol *et al*. [vanNee89].
As a consequence, the hexagonal lattice area *S* is temperature independent for a given chain length in Figure 51 (top) and increases also with chain length as shown in Figure 51 (bottom). By extrapolating the linear fit, we get an approximation for the surface occupied by the Pc ring and the eight oxygen atoms (242 $Å^2$). This value results in diameter of 17.6 Å, which is consistent with 17 Å estimated from CPK models [vanNee89]. These results support the idea that the thermal expansion of the chains occurs on average in the plane perpendicular to the columnar axis and that in the mesophase the Pc core is on average perpendicular to the column axis.

Table 39 - X-ray diffraction data for the octa(hexadecyloxy) phthalocyanine cobalt(II) complex (same legend as Table 35)

Temperature (°C)	d_{obs} (Å)	I	hk	d_{calc} (Å)	Mesophase and parameters
155	33.5	S	10	33.5	Col_h-*p6mm*
	19.2	M	11	19.3	a = 38.7 Å
	16.8	W	20	16.7	S = 1296 Å^2
	4.4	halo I	broad		
	3.3	halo II	broad		
175	33.2	S	10	33.2	Col_h-*p6mm*
	19.2	M	11	19.2	a = 38.3 Å
	16.6	W	20	16.6	S = 1273 Å^2
	12.6	W	21	12.6	
	4.4	halo I	broad		
	3.3	halo II	broad		
200	33.2	S	10	33.4	Col_h-*p6mm*
	19.2	M	11	19.3	a = 38.3 Å
	16.6	W	20	16.7	S = 1273 Å^2
	12.9	W	21	12.6	

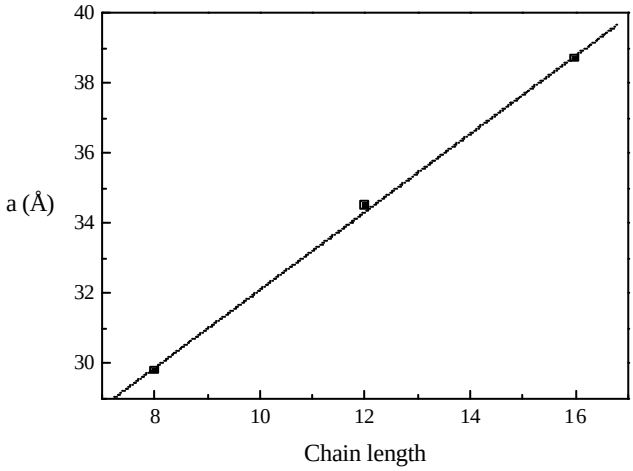

Figure 50 - The variation of the lattice parameter a as a function of the chain length at 155°C

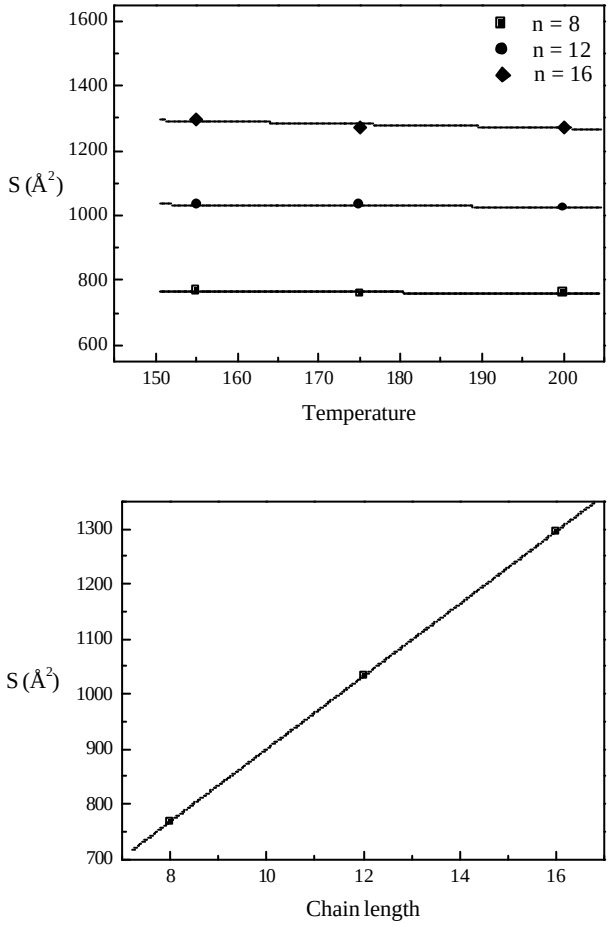

Figure 51 - The variation of the rectangular lattice area S *with the chain length* n *(top) and the temperature* T *(bottom)*

As for the ligands, we can compare the measured d_{10} reflections to the calculated molecular dimensions (modelling), and here also a discrepancy is noticed: e.g. 35.1 Å (calculated) versus 25.8 Å (observed) for the -OC_8H_{17} chain, 44.7 Å vs. 34.5 Å for -$OC_{12}H_{25}$ and 54.4 Å vs. 38.3 Å for -$OC_{16}H_{33}$. The same conclusions as in 5.2.1 can be drawn here.

5.3.1.2 Influence of the central metal ion: Co(II), Ni(II), Cu(II), Zn(II)

An overview of the thermodynamic properties of the phthalocyanine transition metal complexes we synthesised is given in Table 40. Figure 52 shows graphical representations of the influence of the central metal ion on peak temperatures.

Table 40 - Peak values for the melting and clearing points of the synthesised complexes (Dec = decomposition of the sample before clearing to the isotropic liquid)

	Melting point			Clearing point
Compound	Transition temperature (°C)	ΔH_m ($kJmol^{-1}$)	ΔS_m ($JK^{-1}mol^{-1}$)	Transition temperature (°C)
$(C_8H_{17}O)_8PcZn$	135	102	250	Dec
$(C_8H_{17}O)_8PcCu$	123	83	210	Dec
$(C_8H_{17}O)_8PcNi$	110	66	172	Dec
$(C_8H_{17}O)_8PcCo$	123	68	172	Dec
$(C_{12}H_{25}O)_8PcZn$	111	106	276	Dec
$(C_{12}H_{25}O)_8PcCu$	101	97	259	Dec
$(C_{12}H_{25}O)_8PcNi$	83	84	236	Dec
$(C_{12}H_{25}O)_8PcCo$	101	103	275	Dec
$(C_{16}H_{33}O)_8PcZn$	100	149	399	301
$(C_{16}H_{33}O)_8PcCu$	93	125	342	300
$(C_{16}H_{33}O)_8PcNi$	49	106	329	296
$(C_{16}H_{33}O)_8PcCo$	92	61	167	306

All compounds have a quite large mesophase stability range, extending over a range of more than 250 °C. This high stability can be attributed to the strong van der Waals interactions between the alkyl chain and to the π-π interactions between the phthalocyanine cores. The melting points depend on the central metal ion: $Ni^{II} < Cu^{II} \approx Co^{II} < Zn^{II}$. The higher melting point for the Zn(II) complexes might be due to it's preference for five-coordination. The clearing point could only be observed for the compounds with the hexadecyloxy chains, and it was found the nature of the metal ion has a negligible influence on this transition. As for the compounds mentioned before, longer alkoxy chains tend to lower the transition temperatures of the compounds.

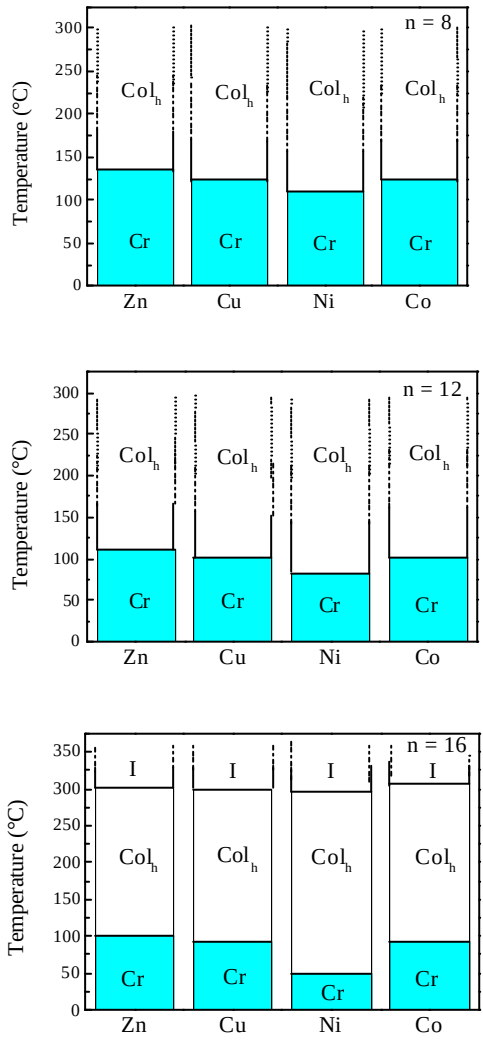

Figure 52 - Graphical representations of the influence of the central metal ion on (peak) transition temperatures for three different alkoxy chain lengths: -OC_8H_{17} (top), - $OC_{12}H_{25}$ (middle) and -$OC_{16}H_{33}$ (bottom) (Cr = crystalline solid, Col_h = hexagonal columnar mesophase, I = isotropic liquid, the dotted lines indicate decomposition of the sample)

The melting points of these metallo-phthalocyanines are also in general higher than that of the corresponding metal-free phthalocyanines. However the melting points of the metal-free phthalocyanine are very comparable with those of the nickel(II) phthalocyanine. In contrast to earlier work by Severs *et al.* where these authors find scattered values for the transition temperatures [SevUnd93], the trends we observe are much smoother. In this respects, our results are in better agreement with those reported by van der Pol *et al.* for the copper(II) phthalocyanines (especially the fact that the compounds with the shorter chain lengths decompose before the clearing point is being reached) [vanNee88, vanNee89].

Small angle X-ray diffraction and polarising optical microscopy measurements confirmed the presence of a two-dimensional hexagonal phase (Col_h). Table 41 shows the XRD-data for the octa(hexadecyloxy) phthalocyanine zinc(II) complex. No further systematic XRD-experiments were performed, but the same conclusions as for the homologous Co(II) series can be drawn.

Table 41 - X-ray diffraction data for the octa(hexadecyloxy) phthalocyanine zinc(II) complex (same legend as Table 35)

T (°C)	d_{obs} (Å)	I	hk	D_{calc} (Å)	Mesophase and parameters
150	32.5	VS	10	32.7	Col_h-*p6mm*
	18.9	S	11	18.9	a = 37.5 Å
	16.4	S	20	16.4	S = 1220 Å^2
	12.4	M	21	12.4	
	4.6	halo I	broad		
	3.4	halo II	broad		
220	32.0	VS	10	32.1	Col_h-*p6mm*
	18.5	S	11	18.5	a = 37.0 Å
	16	S	20	16.0	S = 1182 Å^2
	12.2	M	21	12.1	
	4.7	halo I	broad		
	3.4	halo II	broad		

5.3.1.3 The octa-alkoxy phthalocyanine oxovanadium(IV) complexes

As mentioned in the experimental part, the compounds prepared with vanadium(II)chloride distinguish themselves from the other synthesised complexes by forming a vanadyl complex. This odd behaviour has consequences for the mesophase behaviour. That is why we treat these complexes separately here. All complexes are liquid crystals with a wide mesophase temperature-range. The melting points are nearly chain length independent, since the three compounds melt at around 60°C (Table 42). Repeated heating runs up to 175°C did not affect the position of the peaks either. For all three compounds, the clearing temperature could not be reached before the decomposition of the sample took place in the high temperature domain of the mesophase (onset of decomposition is around 250°C for all the complexes). Note that the enthalpy increases slightly with increasing chain length.

Table 42 - Mesophase behaviour of the octa(alkoxy)-substituted vanadyl phthalocyanine complexes (Cr = crystal, Col_r = rectangular columnar mesophase, Dec = decomposition of the sample before clearing to the isotropic liquid)

Compound	Transition Temperatures (°C)					Melting enthalpy ΔH_m ($kJ\ mol^{-1}$)	Melting entropy ΔS_m ($JK^{-1}mol^{-1}$)
$(C_8H_{17}O)_8PcVO$	Cr	63	Col_r	dec		33	98
$(C_{12}H_{25}O)_8PcVO$	Cr	51	Col_r	dec		53	164
$(C_{16}H_{33}O)_8PcVO$	Cr	60	Col_r	dec		57	171

The texture observed between crossed polarisers of the microscope is depicted in Figure 53 for the same compound, and is characteristic of a columnar mesophase. Before the decomposition process starts, some textural changes could be observed, although it was not possible to assign such changes to the transition to another mesophase.

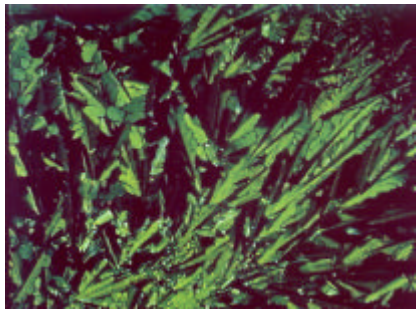

Figure 53 - Texture of the complex $(C_{12}H_{25}O)_8PcVO$ between crossed polarisers at 320 °C (x 200)

In order to clarify the exact nature of the mesophase, X-ray diffraction experiments were carried out for the three complexes at three different temperatures. The XRD patterns at 100 °C are shown in Figure 55 as representative examples.

In the small angle region, two intense fundamental reflections and three higher order reflections were observed. The *hkl* indexation is characteristic of a two-dimensional rectangular packing of columns, and of a rectangular columnar phase (Col_r), with the *c2mm* 2D-space group. The 2D rectangular lattice is characterised by interplanar distances d_{hk}. These distances can be mathematically expressed in function of the lattice parameters *a* and *c* and the Miller indices *hk* (Figure 23).

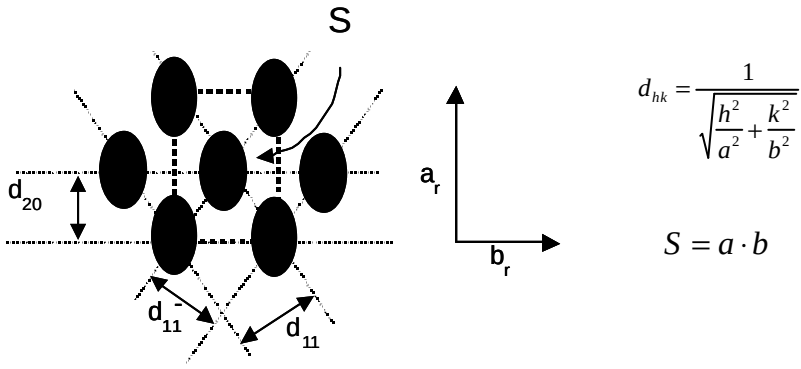

Figure 54 - Schematic representation of the bidimensional rectangular lattice (c2mm)

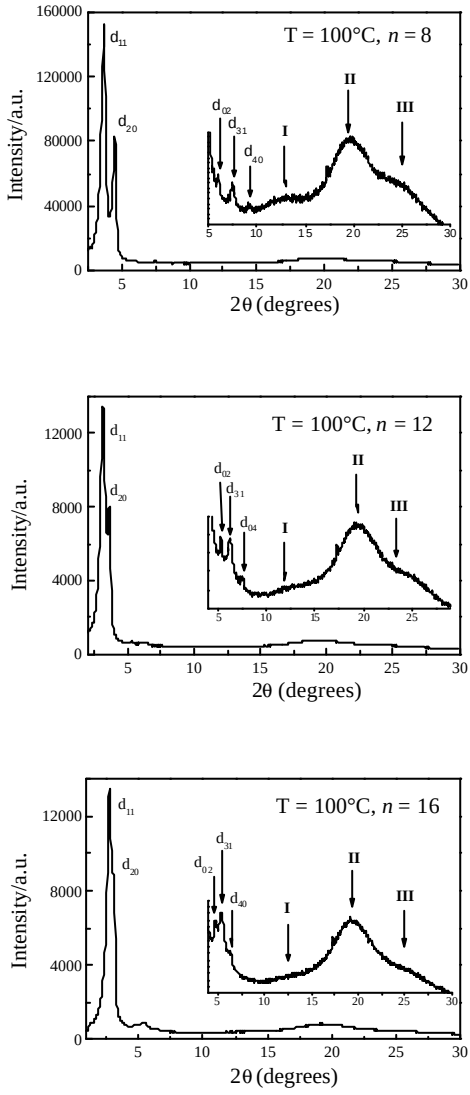

Figure 55 - X-ray diffractograms for the octa(alkoxy)-substituted vanadyl phthalocyanine complexes compounds: -OC_8H_{17} (top), -$OC_{12}H_{25}$ (middle), -$OC_{16}H_{33}$ (bottom) at 100 °C: the inset gives a magnification to show in details diffraction peaks of low intensity

The wide-angle X-ray patterns consist of: (a) a diffuse scattering halo at *ca* 3.5 Å which is the inter-disc stacking periodicity of the phthalocyanine cores along the columns; (b) another, broader halo at around 4.5 Å, corresponding to the liquid-like order of the aliphatic chains, (c) and, a less broad peak at about 7Å, which may indicate the formation of dimers along the axis of the column.

Tables 32-34 list the indexation of the X-ray reflections for our compounds at three temperatures. The phase is disordered since there is no long-range correlation order within the columns as evident from the broadness of the peak at 3.5Å. No modification of the columnar phase structure with temperature could be observed.

Table 43 - X-ray diffraction data for the octa(octyloxy)-substituted vanadyl phthalocyanine complex; d_{obs} and d_{calc} are the diffraction spacings which are observed and calculated respectively; I is the intensity of the diffraction signal (VS: very strong, S: strong, W: weak); hk is the indexation of the 2D lattice; a and b are the lattice parameters, S is the lattice area;C2mm is the 2D space groups of the rectangular (Col_r) columnar phase

Temperature (°C)	d_{obs} (Å)	I	hk	$d_{calc.}$ (Å)	Parameters
100	23.0	VS	11	23.0	Col_r-*C2mm*
	19.5	S	20	18.9	*a* = 39 Å
	14.2	W	02	14.25	*b* = 28.5 Å
	11.95	S	31	11.8	*S* = 1111 Å^2
	9.8	S	40	9.75	
	7.0	halo I	broad		
	4.5	halo II	broad		
	3.5	halo III	broad		
150	23.3	VS	11	23.3	Col_r-*C2mm*
	19.5	S	20	19.5	*a* = 39 Å
	7.0	halo I	broad		*b* = 29 Å
	4.6	halo II	broad		*S* = 1133 Å^2
	3.5	halo III	broad		
200	23.35	VS	11	23.35	Col_r-*C2mm*
	19.9	S	20	19.9	*a* = 39.8 Å
	7.1	halo I	broad		*b* = 28.8 Å
	4.6	halo II	broad		*S* = 1148 Å^2
	3.5	halo III	broad		

Table 44 - X-ray diffraction data for the octa(dodecyloxy)-substituted vanadyl phthalocyanine complex (same legend as Table 43)

Temperature (°C)	d_{obs} (Å)	I	hk	$d_{calc.}$ (Å)	Parameters
100	27.55	VS	11	27.55	Col_r-*C2mm*
	23.85	S	20	23.85	*a* = 47.7 Å
	16.9	W	02	16.9	*b* = 33.75 Å
	14.3	S	31	14.4	*S* = 1610 $Å^2$
	11.8	M	40	11.9	
	7.0	halo I	broad		
	4.5	halo II	broad		
	3.5	halo III	broad		
150	27.3	VS	11	27.3	Col_r-*C2mm*
	23.7	S	20	23.7	*a* = 47.4 Å
	14.3	S	31	14.3	*b* = 33.4 Å
	7.1	halo I	broad		*S* = 1583 $Å^2$
	4.6	halo II	broad		
	3.5	halo III	broad		
200	27.2	VS	11	27.2	Col_r-*C2mm*
	23.85	S	20	23.85	*a* = 47.7 Å
	16.4	W	02	16.55	*b* = 33.1 Å
	14.4	S	31	14.35	*S* = 1580 $Å^2$
	7.1	halo I	broad		
	4.6	halo II	broad		
	3.5	halo III	broad		

It is remarkable that our vanadyl phthalocyanines display a columnar phase with a rectangular 2D symmetry, a rather rare example in phthalocyanine compounds [Ser96]. Indeed, due to their almost perfect disc-shape, octa-alkoxy substituted phthalocyanine compounds mainly stack into cylindrical columns which self-organise to form hexagonal columnar phase. A regular stacking along the columnar axis favoured by means of V=O interactions was also expected due to the net dipole moment along the small molecular axis as in the case of the structurally related alkylthio 2,3,9,10,16,17,23,24-octa(octadecylthio)phthalo-cyaninato oxovanadium(IV) [TanSug98] (or oxotitanium(IV) complexes [SanSug98]) which

showed a hexagonal columnar mesophase only. In the present case, it is clear that the presence of the dipole affects strongly the packing, the only structural difference, with respect to other metallophthalocyanines with alkoxy chains [Ser96].

Table 45 - X-ray diffraction data for the octa(hexadecyloxy)-substituted vanadyl phthalocyanine complex (same legend as Table 43)

Temperature (°C)	d_{obs} (Å)	I	hk	d_{calc} (Å)	Parameters
100	31.7	VS	11	31.7	Col_r-*C2mm*
	27.8	S	20	27.8	a = 55.6 Å
	19.0	W	02	19.3	b = 38.6 Å
	16.5	S	31	16.7	S = 2141 Å^2
	13.9	M	40	13.9	
	7.0	halo I	broad		
	4.5	halo II	broad		
	3.5	halo III	broad		
150	31.4	VS	11	31.4	Col_r-*C2mm*
	28.0	S	20	28.0	a = 56.0 Å
	18.9	W	02	19.0	b = 37.9 Å
	16.8	S	31	16.7	S = 2124 Å^2
	7.1	halo I	broad		
	4.6	halo II	broad		
	3.6	halo III	broad		
200	30.9	VS	11	30.9	Col_r-*C2mm*
	28.1	S	20	28.1	a = 56.2 Å
	18.6	W	02	18.5	b = 37.0 Å
	16.8	S	31	16.7	S = 2080 Å^2
	7.1	halo I	broad		
	4.6	halo II	broad		
	3.6	halo III	broad		

In order to propose a suitable packing mode taking into account both the molecular shape and the phase symmetry, the cell parameters a and b and the rectangular lattice area, $S = a \cdot b$, were studied as a function of both the chain length n and the temperature T. Figure 56 shows, as expected, the increase of both the parameters a

and *b* with chain length, although the variation of *a* is somewhat more pronounced than that of *b* (the *a*/*b* ratio increases). The rectangular lattice, in the studied temperature range, does not evolve towards a pseudo-hexagonal symmetry i.e. the *a*/*b* ratio does not converge to v3 [WebGui91, BanNis01].

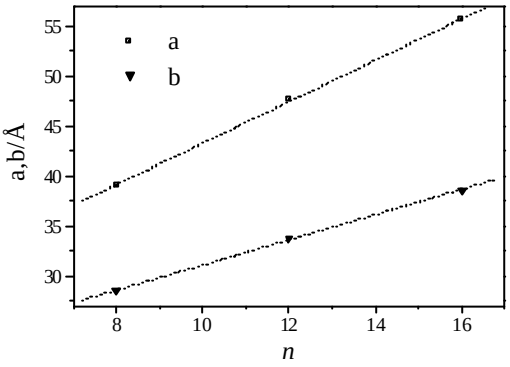

Figure 56 - The variation of the lattice parameters a *and* b *as a function of the alkoxy chain-length* n *at 100°C*

Moreover, *a* and *b* are almost constant with temperature. Consequently, *S* increases with *n* (Figure 57, top), in agreement with the incremental increase of the chain-lengths, but is also almost temperature-independent (Figure 57, bottom). The two stacking periodicities do not change either with *T* or with *n*. These results support the idea that the thermal expansion of the chains occur on average in the plane perpendicular to the columnar axis, with a tendency of the chain-lengthening to occur preferentially along the *a*-direction.

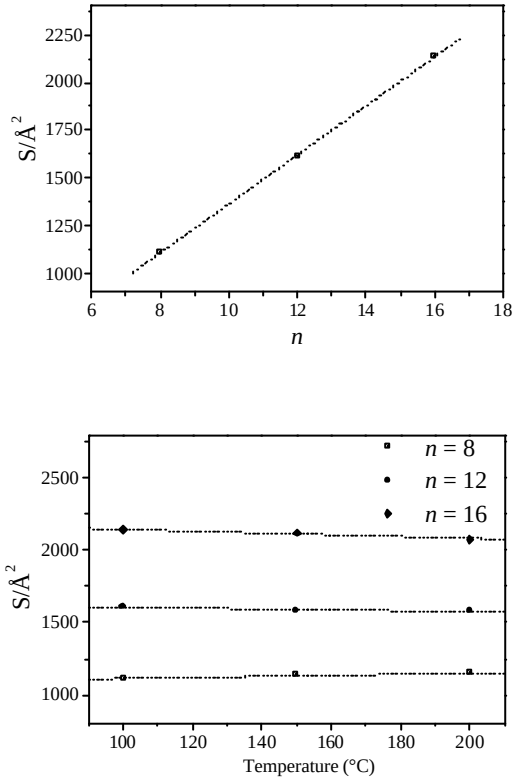

Figure 57 - The variation of the rectangular lattice area S *with the chain length* n *(top) and the temperature* T *(bottom)*

It is also interesting to compare the values found for the rectangular columnar cross-section (*S*/2), with the values of the cross-sections of the hexagonal columnar phases calculated for related octa-alkoxy phthalocyanine complexes. On average, the columnar cross-section is 800 $Å^2$ for n = 8, 900-1000$Å^2$ for n = 12, and 1200 $Å^2$ for n = 16 [SauWeg88, vanNee88, vanNee89, VacDop92, HaiKne95, this work]. These values are slightly higher than those found here (Tables 31-33), suggesting therefore a tilt. This tilt should occur along the *b* direction in order to

keep the elliptical shape of the column, in agreement with the symmetry of the two-dimensional rectangular lattice. The formation of the latter may thus be explained by the antiparallel stacking of two molecules, and by the subsequent tilt of the core with respect to the columnar axis along the short elliptical axis as shown in Figure 58.

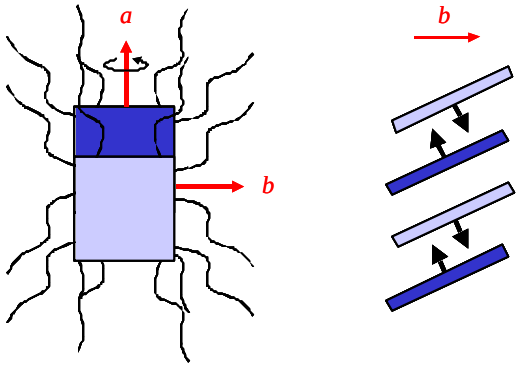

Top view of the column Side view of the column

Figure 58 - Schematic representation of the stacking of the phthalocyanine molecules along the columnar axis

Such a dimeric structure has already been determined in the case of phthalocyanine of lead [WebGui87], and demonstrated by EXAFS spectroscopy on a related platinum(II) phthalocyanine complex [ChaCho94]. Furthermore, the stacking periodicity of about 7Å is observed in phthalocyanine complexes of the trivalent lanthanides, which are known to possess a double-decker structure. It is clear that the dipole moment will contribute to such an antiferroelectric stacking, although the reason to favour such an arrangement with respect to the alkythio analogues is not clear. They may result from the differences in the electronic behaviour of the terminal chains: the alkoxy groups are electron donating to the phthalocyanine ring, whereas the alkylthio groups are to a first approximation neither electron donating or electron withdrawing. The position of the V=O stretching vibrations in

the IR spectrum (992-995 cm^{-1}) indicates that no linear chains of vanadyl groups via V=O···V=O interactions are present. Linear chain formation produces shifts to smaller wavenumbers (ca. 850-870 cm^{-1}) [SerCar92].

The lower thermal stability of the alkoxysubstituted phthalocyanines compared to that of the alkylthio substituted analogue for which the clearing point could be observed might be attributed to this less efficient packing (although it should be mentioned that the higher thermal stability of compound synthesised by Tantrawong *et al*. [TanSug98] can be related to the longer chain length i.e. octadecylthio).

5.3.2 Octa-alkyl phthalocyanine transition metal complexes

5.3.2.1 Influence of the chain length: homologous series for Co^{2+}, Ni^{2+}, Cu^{2+}, Zn^{2+}

Table 46 gives an overview of the thermal properties of the synthesised octa-alkyl substituted cobalt(II) complexes. Figure 59 shows the graphical representation of the mesomorphic data for this limited homologous cobalt(II) series we measured. As for the alkoxy compounds and the alkyl ligands, the melting and clearing points demonstrate a decreasing trend on going to longer chain lengths.

The clearing points of the cobalt(II) phthalocyanines are distinctively higher than the corresponding metal-free phthalocyanines. The melting points of the cobalt(II) phthalocyanines are lower than the corresponding ligands as opposed to the effect noticed for the octa-alkoxy Co(II) Pc's. Thus, the metal ion in the central cavity of the phthalocyanine ring has a stabilising effect on the mesophase. For instance for the metal-free phthalocyanine with $C_{14}H_{29}$ chains, the mesophase behaviour is Cr 128 Col_h 210 I, whereas for the corresponding cobalt(II) complex it is Cr 100 Col_h 260 I.

Since this is the first work that presents octa-alkyl substituted phthalocyanines containing a cobalt(II) ion, no comparison can be made with other reported values.

Table 46 - Peak values for the melting and clearing points of the synthesised octa-alkyl substituted phthalocyanine cobalt (II) complexes (Dec = decomposition of the sample before clearing to the isotropic liquid)

	Melting point			Clearing point
Compound	Transition temperature (°C)	ΔH_m ($kJmol^{-1}$)	ΔS_m ($JK^{-1}mol^{-1}$)	Transition temperature (°C)
$(C_7H_{15})_8PcCo$	163	6	14	Dec
$(C_8H_{17})_8PcCo$	158	15	35	Dec
$(C_{12}H_{25})_8PcCo$	112	35	91	290
$(C_{14}H_{29})_8PcCo$	100	97	260	288
$(C_{16}H_{33})_8PcCo$	74	136	392	272
$(C_{18}H_{37})_8PcCo$	76	239	685	245

A homologous series was prepared for the copper(II) ions, which showed markedly higher melting points [NisAzu92, EngBas93]. The clearing points were not reported on or could not be measured before decomposition. The next paragraph will take a closer look at the influence of the central metal ion.

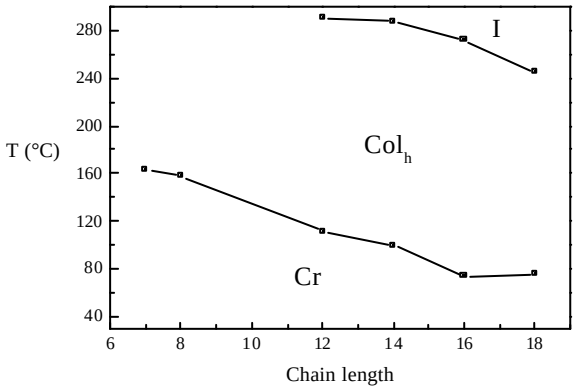

Figure 59 - Influence of the alkyl chain length on the transition temperatures of the substituted cobalt(II) phthalocyanines (Cr = crystalline solid, Col_h = hexagonal columnar mesophase, I = isotropic liquid)

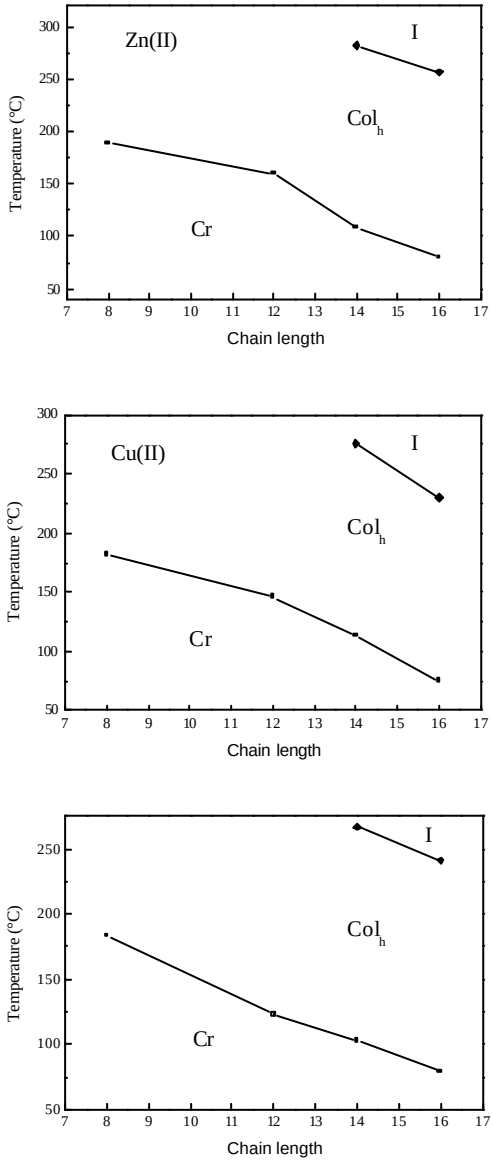

Figure 60 - Influence of the alkyl chain length on the transition temperatures of the substituted Zn^{2+} (top), Cu^{2+}(middle) and Ni^{2+} (bottom) phthalocyanines (Cr = crystalline solid, Col_h = hexagonal columnar mesophase, I = isotropic liquid)

For the homologous series of the Zn^{2+}, Cu^{2+} and Ni^{2+} complexes the data are given in the next paragraph (Table 47). Figure 60 gives the graphical representation for the three series. The same trends as for the cobalt(II) complexes were observed.

5.3.2.2 Influence of the central metal ion: Co(II), Ni(II), Cu(II), Zn(II)

Table 47 gives an overview of the thermal properties of the synthesised octa-alkyl substituted transition cobalt(II) complexes. For a number of compounds, the transition enthalpies could not be deduced due to the low sensitivity because we only had a limited amount of sample.

Table 47 - Peak values for the melting and clearing points of the synthesised octa-alkyl substituted phthalocyanine transition metal complexes (Dec = decomposition of the sample before clearing to the isotropic liquid; / = no values could be reported)

	Melting point			Clearing point
Compound	Transition temperature (°C)	ΔH_m ($kJmol^{-1}$)	ΔS_m ($JK^{-1}mol^{-1}$)	Transition temperature (°C)
$(C_8H_{17})_8PcZn$	189	11	24	Dec
$(C_8H_{17})_8PcCu$	182	12	26	Dec
$(C_8H_{17})_8PcNi$	183	15	33	Dec
$(C_8H_{17})_8PcCo$	158	15	35	Dec
$(C_{12}H_{25})_8PcZn$	160	42	97	Dec
$(C_{12}H_{25})_8PcCu$	146	32	76	Dec
$(C_{12}H_{25})_8PcNi$	123	/	/	Dec
$(C_{12}H_{25})_8PcCo$	112	35	91	290
$(C_{14}H_{29})_8PcZn$	109	45	118	282
$(C_{14}H_{29})_8PcCu$	113	/	/	276
$(C_{14}H_{29})_8PcNi$	103	/	/	267
$(C_{14}H_{29})_8PcCo$	100	97	260	288
$(C_{16}H_{33})_8PcZn$	80	109	309	257
$(C_{16}H_{33})_8PcCu$	75	40	115	230
$(C_{16}H_{33})_8PcNi$	79	162	460	241
$(C_{16}H_{33})_8PcCo$	74	136	392	272

Figure 61 depicts the graphical representations for the influence of the central metal ion (Co^{2+}, Ni^{2+}, $Cu^{2+}$and Zn^{2+}) for four different chain lengths: $-C_8H_{17}$, $-C_{12}H_{25}$, $-C_{14}H_{29}$, and $-C_{16}H_{33}$.

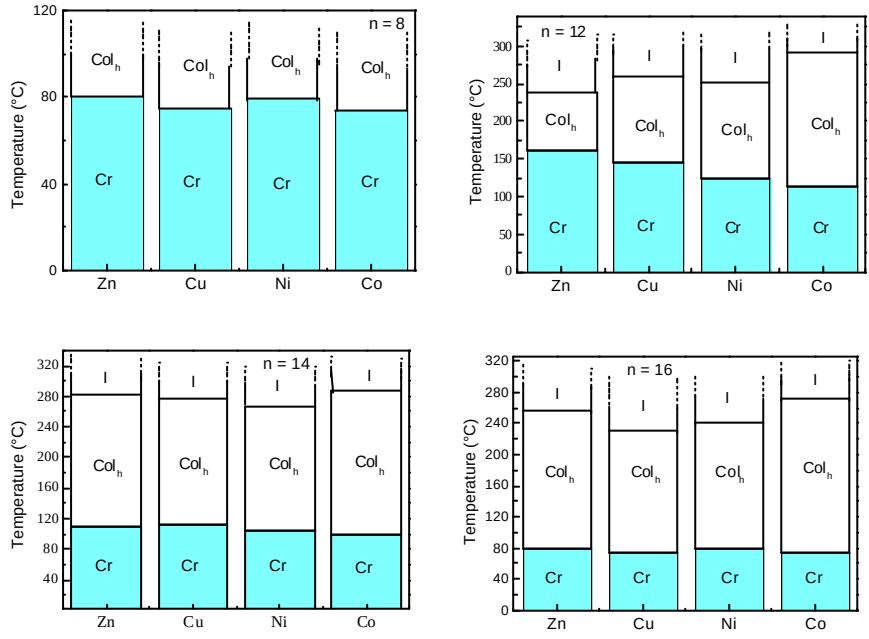

Figure 61 - Graphical representations of the influence of the central metal ion on (peak) transition temperatures for three different alkyl chain lengths: $-C_8H_{17}$ (top left), $-C_{12}H_{25}$ (top right), $-C_{14}H_{29}$ (bottom left) and $-C_{16}H_{33}$ (bottom right) (Cr = crystalline solid, Col_h = hexagonal columnar mesophase, I = isotropic liquid, the dotted lines indicate decomposition of the sample)

The melting point stays relatively constant with decreasing ion radius, whereas for the melting points no clear trend is visible. The Co(II) complexes exhibit for all chain lengths the widest mesophase stability range. Compared to the metal-free ligands, also no clear tendency is visible: the complexes with chain length C_8H_{17}

melt slightly higher than the corresponding ligand, whereas the other chain lengths have significantly lower melting points. The only synthesized complexes so far are Ni(II) and Cu(II) complexes as is clear from Appendix B. Our mesomorphic data are in good agreement with those values [NisUen89, NisAzu92, EngBas93].

The mosaic textures we observed with POM for the Cu^{2+}, Ni^{2+}, Co^{2+} and Zn^{2+} complexes were all identified as the hexagonal columnar mesophase (Col_h). The texture of the $(C_{16}H_{33})_8PcCo$ is shown in Figure 62.

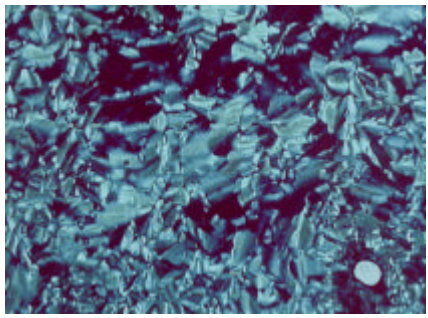

Figure 62 - Texture of the $(C_{16}H_{33})_8PcCo$ at 250 °C at 140 °C (right) between crossed polarisers at 320 °C (x 200)

5.3.2.3 The octa-alkyl phthalocyanine oxovanadium complexes

Table 48 gives an overview of the thermal properties of the synthesised octa-alkyl substituted transition vanadyl(II) complexes. The vanadyl complexes have noticeably lower melting and clearing temperatures than the corresponding Zn(II), Cu(II), Ni(II) and Co(II) complexes.

The VO^{2+} complexes showed a different texture under the microscope. The texture of the $(C_{16}H_{33})_8PcVO$ complexes is shown in Figure 63.

Table 48 - Mesophase behaviour of the octa(alkyl)-substituted vanadyl phthalocyanine complexes

	Melting point			Clearing point
Compound	Transition temperature (°C)	ΔH_m ($kJmol^{-1}$)	ΔS_m ($JK^{-1}mol^{-1}$)	Transition temperature (°C)
$(C_{14}H_{29})_8PcVO$	67	59	174	153
$(C_{16}H_{33})_8PcVO$	44	106	334	159

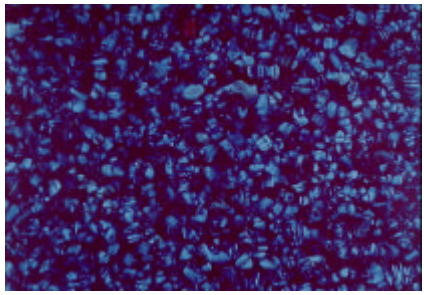

Figure 63 - Texture of the $(C_{16}H_{33})_8PcVO$ at 140 °C between crossed polarisers at 320 °C (x 200)

A first measurement by XRD indicated the presence of a Col_r mesophase, as for the octa-alkoxy vanadyl complexes (Table 49). Since we only observed two reflections and a halo, this structure will have to be confirmed later by further XRD-experiments.

Table 49 - X-ray diffraction data at 150°C for the octa(hexadecyl)-substituted vanadyl phthalocyanine complex (same legend as Table 43)

Temperature (°C)	d_{obs} (Å)	I	hk
150	27.8	VS	11
	25.6	S	20
	4.6	broad	halo

5.3.3 Octa-alkoxy methyl phthalocyanines transition metal complexes

Table 50 shows the thermodynamic data gathered for the synthesised octa-alkoxymethyl phthalocyanines transition metal complexes. All complexes showed a single mesophase by investigation with DSC and polarising optical microscopy. The melting points all were in the region between 50 and 90°C. Clearing points could not be detected due to the decomposition of the samples before reaching the isotropic phase. Textures from polarising optical microscopy indicated once more the presence of a hexagonal columnar mesophase (Col_h).

Table 50 - Peak values for the melting and clearing points of the synthesised octa-alkoxymethyl substituted phthalocyanine transition metal complexes (Dec = decomposition of the sample before reaching the clearing point)

	Melting point			Clearing point
Compound	Transition temperature (°C)	ΔH_m ($kJmol^{-1}$)	ΔS_m ($JK^{-1}mol^{-1}$)	Transition temperature (°C)
$(C_8H_{17}OCH_2)_8PcZn$	88	52	149	Dec
$(C_8H_{17}OCH_2)_8PcCu$	82	65	183	Dec
$(C_8H_{17}OCH_2)_8PcNi$	63	48	143	Dec
$(C_8H_{17}OCH_2)_8PcCo$	73	47	136	Dec
$(C_{12}H_{24}OCH_2)_8PcZn$	70	24	70	Dec
$(C_{12}H_{24}OCH_2)_8PcCu$	64	98	291	Dec
$(C_{12}H_{24}OCH_2)_8PcNi$	58	78	236	Dec
$(C_{12}H_{24}OCH_2)_8PcCo$	71	83	241	Dec
$(C_{16}H_{33}OCH_2)_8PcZn$	57	93	282	Dec
$(C_{16}H_{33}OCH_2)_8PcCu$	53	102	313	Dec
$(C_{16}H_{33}OCH_2)_8PcNi$	51	77	238	Dec
$(C_{16}H_{33}OCH_2)_8PcCo$	58	88	266	Dec

Only three octa-alkoxymethyl substituted phthalocyanine transition metal complexes ($(C_{12}H_{24}OCH_2)_8PcCu$, $(C_{12}H_{24}OCH_2)_8PcZn$ and $(C_{12}H_{24}OCH_2)_8PcMn$)

were synthesised prior to this research, as is evident from appendix B [PieSim82, GuiWeb85]. Our data are in reasonable good agreement with those reported in the references, taking into account the fact that we report on peak positions rather than onset positions. Nevertheless, we could not confirm the presence of two mesophases (Col_x and Col_h), as did Guillon *et al*. We will discuss the influence of the chain length and the central metal ion in the next paragraphs.

5.3.3.1 Influence of the chain length: homologous series

The influence of the chain length on the melting points is represented for the four transition metals in Figure 64. All complexes show a decreasing trend for the melting point with increasing chain length.

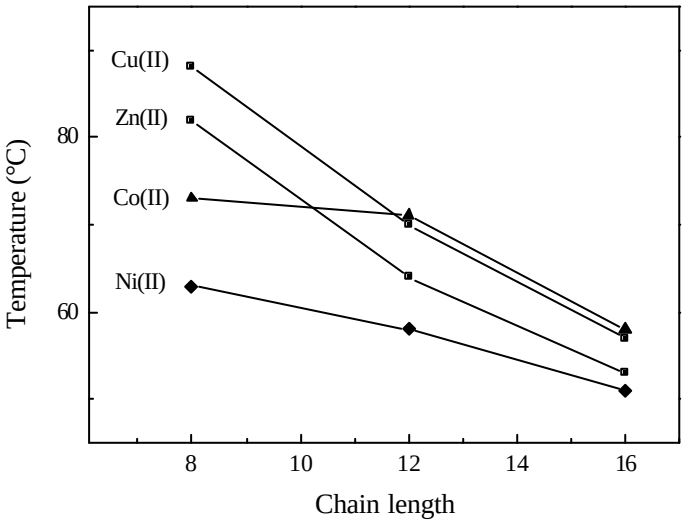

Figure 64 - Influence of the alkoxymethyl chain length on the melting temperature of Zn^{2+}, Cu^{2+}, Ni^{2+} and Co^{2+} octa-alkoxymethyl substituted phthalocyanine complexes

The decrease is more pronounced on going from $-CH_2-OC_8H_{17}$ to $-CH_2-OC_{12}H_{25}$ for the Cu(II) and Zn(II) complexes, whereas for the Ni(II) and Co(II) complexes

the decline is more pronounced on going from -CH_2-$OC_{12}H_{25}$ to the -CH_2-$OC_{16}H_{33}$ chain length.

Table 51 shows the XRD-data for the octa(dodecyloxymethyl) phthalocyanine cobalt(II) complex at 100 and 150°C, confirming the hexagonal columnar mesophase (Col_h). The broad halo at 4.6 Å corresponds to the molten aliphatic chains. Since no well-defined halo for was found corresponding to an intracolumnar order, we can assume that the Pc cores within the columns are disordered. The remarkably smaller *a* and *S* parameters (compared to the alkoxy variant) give support to the idea that the chains are not coplanar with the Pc core. No further systematic XRD-experiments were conducted.

Table 51 - X-ray diffraction data for the octa(dodecyloxymethyl) phthalocyanine cobalt(II) complex (same legend as Table 35)

Temperature (°C)	d_{obs} (Å)	I	hk	d_{calc} (Å)	Mesophase and parameters
100	26.8	VS	10	26.9	Col_h-*p6mm*
	15.5	S	11	15.5	*a* = 30.9 Å
	13.4	M	20	13.4	*S* = 829 $Å^2$
	10.2	W	21	10.2	
	4.6	halo	broad		
150	26.85	VS	10	26.9	Col_h-*p6mm*
	15.55	S	11	15.5	*a* = 31.0Å
	13.45	M	20	13.5	*S* = 832 $Å^2$
	10.2	W	21	10.2	
	4.6	halo	broad		

5.3.3.2 Influence of the central metal ion: Co(II), Ni(II), Cu(II), Zn(II)

As for the octa-alkoxy complexes and some of the chain lengths of the octa-alkyl substituted transition metal complexes, the melting points depend on the central metal ion: Ni^{II} < Cu^{II} < Zn^{II} (Figure 65). The melting points of the Co^{II} complexes show a less consequent behaviour.

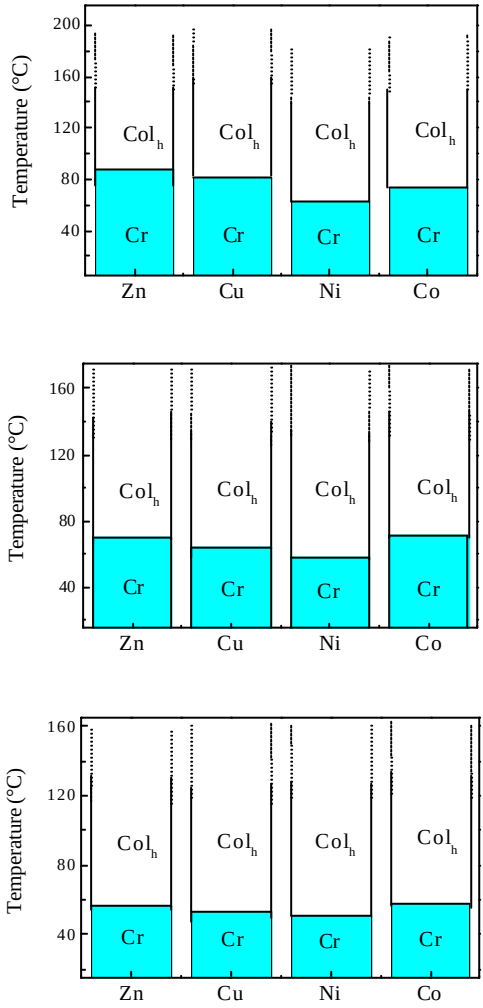

Figure 65 - Graphical representations of the influence of the central metal ion on (peak) transition temperatures for three different alkyl chain lengths: -$CH_2OC_8H_{17}$ (top), -$CH_2OC_{12}H_{25}$ (middle) and -$CH_2OC_{16}H_{32}$ (bottom) (Cr = crystalline solid, Col_h = hexagonal columnar mesophase, I = isotropic liquid, the dotted lines indicate decomposition of the sample)

5.4 Lanthanide complexes

For all bis(octa-alkoxy phthalocyanine) lanthanide complexes, the transition enthalpies are not given because the transition of these compounds are sometimes difficult to detect by DSC (no clearing peaks).

5.4.1 Influence of the chain length: homologous series for erbium(III)

Table 52 gives an overview of the thermal properties of the synthesised bis(octa-alkoxyphthalocyaninato) erbium(III) complexes. Figure 66 shows the graphical representation of these data.

Table 52 - Mesophase behaviour of the bis(octa-alkoxyphthalocyaninato) erbium complexes (peak values); Dec = decomposition before clearing to the isotropic liquid, Cr = crystal, Col_h = hexagonal columnar mesophase, I = isotropic liquid, †: determined by optical polarising microscopy)

Compound	Transition temperatures (°C)				
$[(C_4H_9O)_8Pc]_2Er$	Cr	202	Col_h	Dec	I
$[(C_5H_{11}O)_8Pc]_2Er$	Cr	174	Col_h	Dec	I
$[(C_6H_{13}O)_8Pc]_2Er$	Cr	147	Col_h	Dec	I
$[(C_8H_{17}O)_8Pc]_2Er$	Cr	137	Col_h	263	I
$[(C_9H_{19}O)_8Pc]_2Er$	Cr	93	Col_h	239	I
$[(C_{10}H_{21}O)_8Pc]_2Er$	Cr	71	Col_h	180†	I
$[(C_{12}H_{25}O)_8Pc]_2Er$	Cr	68	Col_h	174†	I
$[(C_{14}H_{29}O)_8Pc]_2Er$	Cr	58	Col_h	180†	I
$[(C_{15}H_{31}O)_8Pc]_2Er$	Cr	44	Col_h	170†	I
$[(C_{16}H_{33}O)_8Pc]_2Er$	Cr	43	Col_h	163	I
$[(C_{18}H_{37}O)_8Pc]_2Er$	Cr	65	Col_h	151	I
$[(C_{19}H_{39}O)_8Pc]_2Er$	Cr	66	Col_h	105†	I

The transition temperatures for the octa-decyl, -dodecyl and -octadecyl complexes are in generally higher in this table than in a previously published paper

[SleGör01], because we give peak positions as measured by DSC, whereas the article reports on data gathered by polarising microscopy.

As for the other compounds, the melting and clearing points demonstrate in general a decreasing trend on going to longer chain lengths. Yet, the decline for the clearing points is more pronounced than for the homologous series discussed above. Another remarkable fact is the small increase of the melting point for the two longest chain lengths.

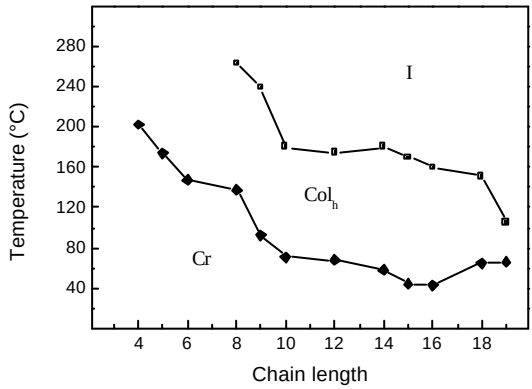

Figure 66 - Graphical representation of the mesophase behaviour of the bis[octa(alkoxy)-substituted phthalocyaninato] erbium complexes

The only liquid crystalline complex that was reported prior to our work is the $[(C_{12}H_{25}O)_8Pc]_2Lu$ compound by with a melting point of 85°C and a clearing point of 189°C [BelSir89, NaiOht01]. For the chain length -$C_{12}H_{25}O$ these values agrees with our erbium complex. We could not confirm the presence of a second mesophase for our complexes as did van de Craats *et al.* in 1997 for the $[(C_{12}H_{25}O)_8Pc]_2Lu$ complex between 61 and 90°C [vanWar97]. Later on, this unidentified mesophase was verified as a novel type of Col_{ro} [NaiOht01].

Based on POM studies and the thermodynamic data obtained by DSC it was decided to do XRD-measurements at 100 and 150 °C for the erbium(III) complexes

(Guinier setup). For the $[(C_{10}H_{21}O)_8P]_2Er$ a set of diffraction patterns was also registered with the curved counter "Inel CPS 120" by measuring every 10°C between 30 and 200°C as shown in Figure 67 (top). Figure 67 (bottom) gives the diffractogram at 150°C.

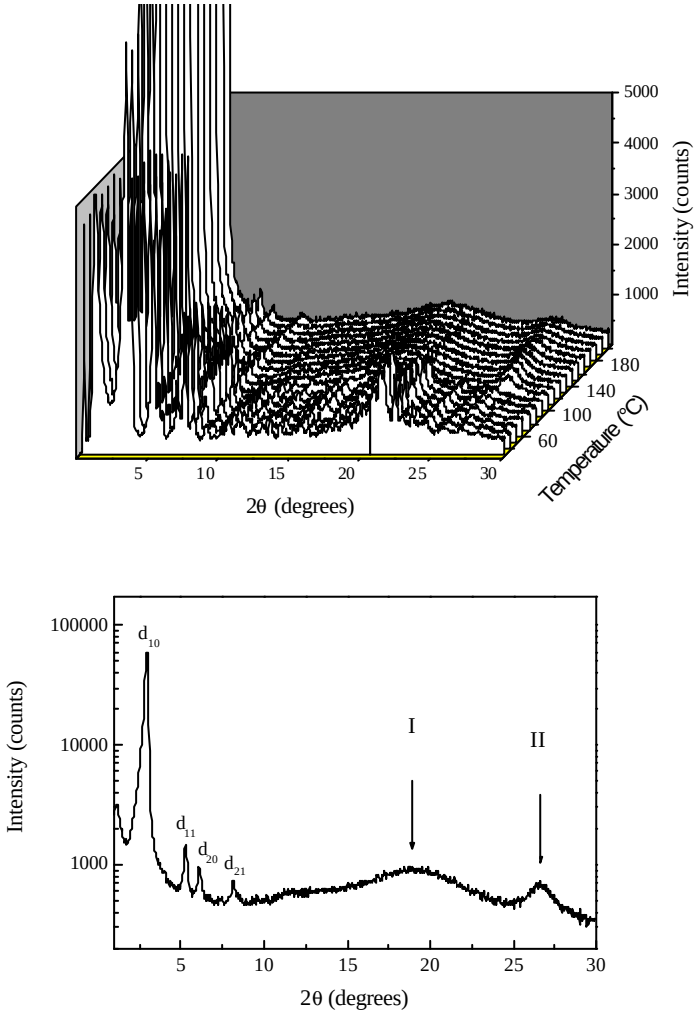

Figure 67 - X-ray diffraction patterns for the $[(C_{10}H_{21}O)_8Pc]_2Er$ complex every 10°C between 30°C and 200°C (top) and indexed diffractogram at 150 °C (bottom)

Table 53 gives an overview of the detailed indexation that was carried out for the $[(C_{10}H_{21}O)_8Pc]_2Er$ complex. Again, the hexagonal columnar (Col_h) mesophase was confirmed for all complexes.

Table 53 - Detailed indexation at a given temperature (T) of the $[(C_{10}H_{21}O)_8Pc]_2Er$ complex (d_{obs} and d_{calc} are the diffraction spacings which are observed and calculated respectively; I is the intensity of the diffraction signal (VS: very strong, S: strong, M: medium, W: weak, VW: very weak); hk is the indexation of the two-dimensional lattice; a_o is the lattice parameter, s_o is the lattice area and p6mm is the 2D space groups of the hexagonal (Col_h) columnar phase)

Temperature (°C)	d_{obs} (Å)	I	hk	d_{calc} (Å)	Mesophase and parameters
100	26.9	VS	10	26.9	Col_h-*p6mm*
	16.2	S	11	15.5	a = 33.0 Å
	14.1	S	20	13.5	S = 943 Å^2
	10.1	M	21	10.2	
	4.5	halo I	broad		
	3.4	halo II	broad		
150	26.5	VS	10	26.5	Col_h-*p6mm*
	16.1	S	11	15.3	a = 30.6 Å
	13.9	S	20	13.3	S = 811 Å^2
	10.3	M	21	10.0	
	4.6	halo I	broad		
	3.4	halo II	broad		

In the wide-angle region, we observed two halos for all of our compounds. The broad halo around 4.5 Å corresponds to the liquid-like order of the aliphatic chains. The less broad halo around 3.4 Å is the stacking distance between the Pc cores. This is not in accordance with the staggered and convex structure of the double-deckers, which would suggest a stacking distance of about 7 Å. *Belarbi et al.* [BelSIr89] subscribed this observed stacking distance to the presence of ligand molecules, but Naito *et al.* later on suggested on observing the same phenomena that the two Pc macrocycles are no longer staggered and convex but swing and

rotate at the same time to extinguish both configurations on time average [NaiOht01]. Figure 68 gives a schematic representation of the suggested molecular stacking of the $PcLn_2$ complexes.

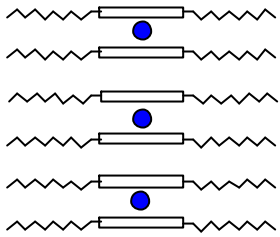

Figure 68 - Side-view of the ordered packing in the hexagonal columnar mesophase for the bis(octa-alkoxy phthalocyaninato) lanthanide complexes

Notice from Figure 67 (top) that the halo's become less intense and also shift to lower angles with increasing temperature. This is emphasised in Figure 69, where XRD-diffractograms of the $[(C_{10}H_{21}O)_8Pc]_2Er$ at 110°C and 180°C are shown.

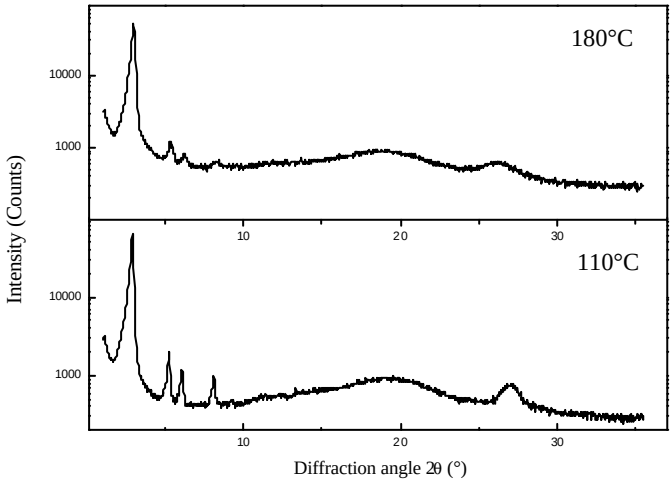

Figure 69 - XRD-diffractograms of $[(C_{10}H_{21}O)_8Pc]_2Er$ at 110°C and 180°C

Figure 70 shows the graphical representation of the first order reflection d_{10} (top) and the columnar section S (bottom) versus the chain length. As expected the parameter d_{10} (and the lattice parameters as well) increases linearly with longer chains. They are almost constant with temperature. Extrapolating to chain length 0, again yields a fairly good approximation (± 122 Å^2) of the Pc core diameter with 8 peripherally oxygen atoms attached to it. So no tilt within the columns is predicted.

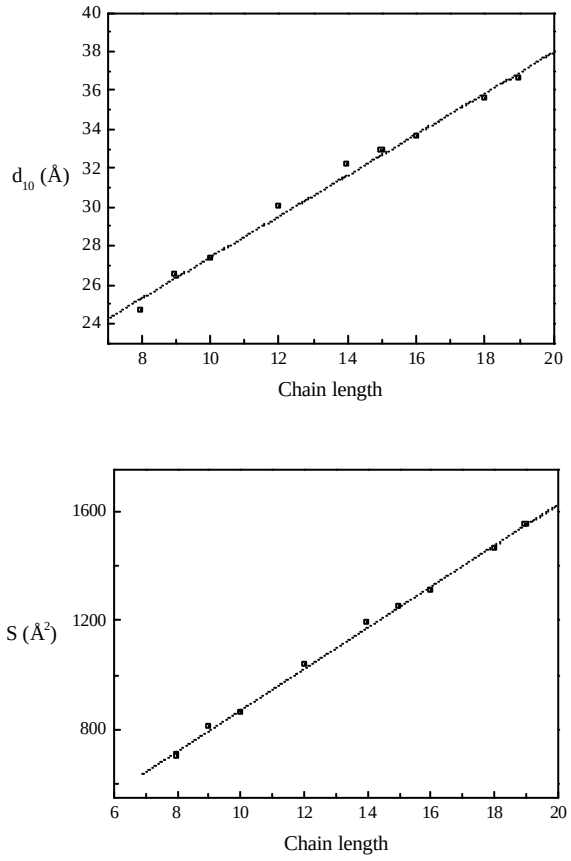

Figure 70 - First-order reflection d_{10} and columnar section S for the $[[(C_nH_{2n+1}O)_8Pc]_2Er$ complexes in function of the chain length

5.4.2 Influence of the central metal ion

Table 54 gives an overview of the thermal properties of the synthesised bis(octa-alkoxy phthalocyaninato) erbium(III) complexes. Figure 71 shows the graphical representation of these data. The transition temperatures for the neodymium, europium, erbium and lutetium complexes we reported earlier on [SleGör01] are in generally higher in this table than in the reference article, because here we give peak positions (as far as possible) whereas the article reports on data gathered by polarising microscopy.

Table 54 - Mesophase behaviour of the bis(octa-dodecyloxyphthalocyaninato) lanthanide(III) complexes (peak values, Cr = crystal, Col_h =hexagonal columnar mesophase, I = isotropic liquid, †: determined by optical microscopy)

Compound	Transition temperatures (°C)				
$[(C_{12}H_{25}O)_8Pc]_2Pr$	Cr	74	Col_h	208†	I
$[(C_{12}H_{25}O)_8Pc]_2Nd$	Cr	66	Col_h	206	I
$[(C_{12}H_{25}O)_8Pc]_2Eu$	Cr	65	Col_h	203	I
$[(C_{12}H_{25}O)_8Pc]_2Gd$	Cr	68	Col_h	218†	I
$[(C_{12}H_{25}O)_8Pc]_2Tb$	Cr	72	Col_h	205	I
$[(C_{12}H_{25}O)_8Pc]_2Dy$	Cr	83	Col_h	205	I
$[(C_{12}H_{25}O)_8Pc]_2Ho$	Cr	85	Col_h	190†	I
$[(C_{12}H_{25}O)_8Pc]_2Er$	Cr	68	Col_h	180†	I
$[(C_{12}H_{25}O)_8Pc]_2Tm$	Cr	68	Col_h	182†	I
$[(C_{12}H_{25}O)_8Pc]_2Yb$	Cr	84	Col_h	192†	I
$[(C_{12}H_{25}O)_8Pc]_2Lu$	Cr	92	Col_h	188	I

All compounds show wide mesomorphic range (>100°C). Nevertheless, the mesophase stability seems to decrease slightly when going to smaller ionic radii. Although more pronounced, this trend has been observed before for other lanthanide containing liquid crystals [BinVan99]. As can be deduced from appendix C, the data are consistent with the only prior observed by Belarbi *et al.*

bis(octa-alkoxy phthalocyaninato) lanthanide(III) complex, $[(C_{12}H_{25}O)_8Pc]_2Lu$, [BelSir89].

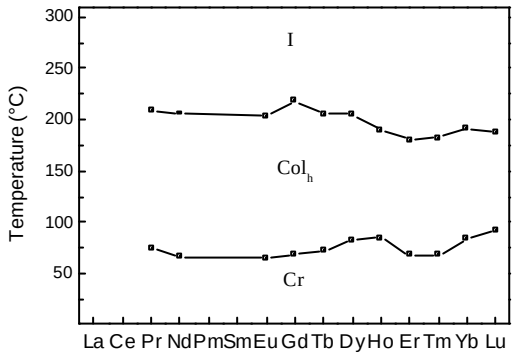

Figure 71 - Graphical representation of the mesophase behaviour of the bis(octadodecyloxyphthalocyaninato) lanthanide(III) complexes

Polarising microscopy experiments indicated yet again the presence of the Col_h mesophase. This is confirmed by X-ray diffraction for all the lanthanide complexes.

Based on the thermodynamic data obtained by Differential Scanning Calorimetry it was decided to do XRD-measurements at 100, 150 and 200 °C for the bis(octa-dodecyloxyphthalocyaninato) lanthanide complexes. Figure 72 depicts the Image Plate as recorded for the $[(C_{12}H_{25}O)_8Pc]_2Nd$ complex at 100°C. Table 55 gives an overview of the detailed indexation that was carried out for the $[(C_{12}H_{25}O)_8Pc]_2Nd$ complex. The diffraction pattern consists of four sharp reflections in the small angle region, with the squared reciprocal spacings in the ratio 1, $\sqrt{3}$, $\sqrt{4}$, $\sqrt{7}$, corresponding to the indexation [hk] = [10], [11], [20], [21] indicating a two-dimensional hexagonal packing of columns.

We were not able to observe polymorphism for our complexes, as was noticed by Naito *et al*. [NaiOht01] for the $[(C_{12}H_{25}O)_8Pc]_2Lu$ complex that was first reported

by Belarbi *et al*. [BelSir89]. By measuring XRD diffraction patterns at 3°C intervals from 28 to 190°C, they reported on a second, unidentified mesophase Col_x between the crystalline phase and the hexagonal columnar mesophase (61-90°C).

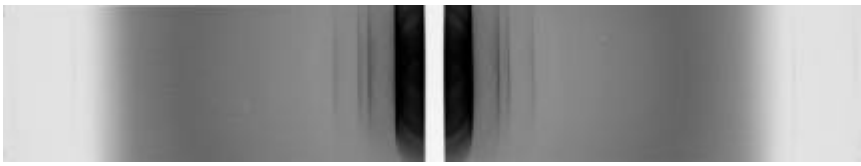

Figure 72 - Image Plates recorded for the $[(C_{12}H_{25}O)_8Pc]_2Nd$ complex at 100 °C (upper), 150 °C (middle) and 200 °C (lower)

Table 55 - Detailed indexation at a given temperature (T) of the $[(C_{12}H_{25}O)_8Pc]_2Nd$ complex (same legend as table 42)

Temperature (°C)	d_{obs} (Å)	I	hk	d_{calc} (Å)	Mesophase and parameters
100	29.6	VS	10	29.6	Col_h-*p6mm*
	17.1	S	11	17.1	a = 34.2 Å
	14.8	M	20	14.8	S = 1012 Å^2
	4.5	halo	broad		
	3.5	halo	broad		
150	29.6	VS	10	29.7	Col_h-*p6mm*
	17.2	S	11	17.1	a = 34.2 Å
	4.5	halo	broad		S = 1012 Å^2
	3.5	halo	broad		
200	29.4	VS	10	29.4	Col_h-*p6mm*
	16.9	S	11	16.9	a = 33.9 Å
	14.7	M	20	14.7	S = 998 Å^2
	4.6	halo	broad		
	3.5	halo	broad		

Since the mesophases were identified as being columnar hexagonal, d_{10} reflection was used to calculate the unit cell parameters a and S. These measurements were

done at 100, 150 and 200°C. From the observed first-order reflections, the spacings corresponding to the (10) reflections in the columnar phase as a function of the central lanthanide ion were considered. From this reflection, the lattice parameter *a* and the columnar section *S* could be calculated. As can be seen from Figure 73, the central lanthanide ion had only minor influence on these parameters. Moreover, these parameters are relatively constant with temperature.

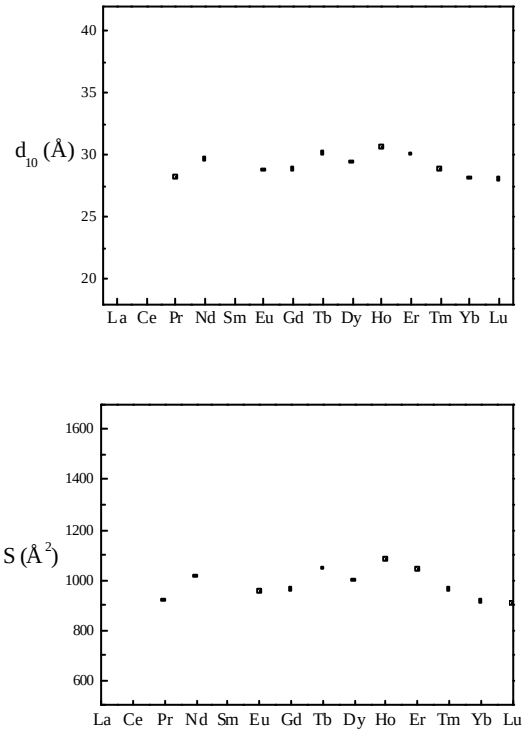

Figure 73 - Lattice parameter a (top) and columnar section S (bottom) in function of the lanthanide ion for the $[[(C_{12}H_{25}O)_8Pc]_2Ln$ complexes (at 100°C)

5.5 Conclusions

We investigated the thermal properties of three different peripherally octa-substituted phthalocyanines and metallophthalocyanines. All of the discussed compounds exhibit a relatively wide mesomorphic range. The smallest mesophase range was the one observed for the $[(C_{19}H_{39}O)_8Pc]_2Er$ complex: Cr 66 Col_h 105 I. Moreover, all compounds show enantiotropic behaviour, although it was hard sometimes to detect the clearing point because of simultaneous decomposition of the sample. Except for some examples mentioned in literature [GuiSko83, DulGut92, vanWar97, NaiOht01], the absence of polymorphism seems to be typical for our discotic liquid-crystalline peripherally octa-substituted phthalocyanines and metallophthalocyaninato complexes. As confirmed by polarising microscopy and XRD-diffraction experiments, the mesophase observed is the hexagonal columnar mesophase (Col_h) for all but the vanadyl complexes. The phthalocyaninato complexes formed by reacting the phthalonitrile with vanadium(II)chloride exhibit the rectangular columnar (Col_r) mesophase.

A minimum side-chain length is required for mesomorphic behaviour: for the octa-alkoxy substituent-type, we noticed that side-chains with a length of fewer than four carbon atoms did not demonstrate a mesophase. For all investigated homologous series, the melting point generally decreases with increasing chain length. The decrease is more relevant for shorter chain lengths. At longer chain lengths, the relationship is less obvious for some types of compounds (lanthanide complexes). The clearing points decrease more drastically with increasing chain length. This trend is more pronounced for the octa-alkoxy side-chains.

The type of side chain has a great influence on how the side chains are ordered around the Pc core. The melting points are in general much higher for the octa-alkyl complexes than for the octa-alkoxy and the octa-alkoxymethyl compounds (order: octa-alkyl >> octa-alkoxy > octa-alkoxymethyl). Due to specific steric interactions, the side-chains determine the way neighbouring columns are oriented

and also they strongly influence the order within the columns. We define the linking group as the first two atoms of the side chain to the central Pc core (hence we have: -OCH_2, -CH_2CH_2 and -CH_2O). The alkoxy linking group allows the chain to reside in the plane of the Pc macrocycle (as can be decided based on the measured and tabulated d_{10} reflections). For both the alkyl and alkoxymethyl linking groups the steric hindering yields out-of-plane side chains. This is consistent with the observed greater mesomorphic range for the octa-alkoxy compounds. These compounds all show a regular stacking periodicity of ± 3.4 Å. For both the other linking groups, the order within the columns is less pronounced, as is clear from literature XRD-data.

We also compared the influence on the mesophase behaviour from various central metal ions. For the octa-alkoxy and octa-alkyl compounds, the vanadyl ions have the strongest stabilising effect on the mesophase compared to the metal-free ligand ($\Delta T_m \approx 30°C$). They have lower melting temperatures than the ligands. For the other transition metals (Zn^{2+}, Cu^{2+}, Ni^{2+}, Co^{2+}) the melting temperatures increases but in the whole the mesophase is stabilised due to the strong increase of the clearing point. The strongest increase of the melting point is found for Zn^{2+} (order: $Ni^{2+} < Cu^{2+} \approx Co^{2+} < Zn^{2+}$). The clearing points could often not be detected because of the decomposition of the sample, so it is hard to predict the stabilising properties for the different cations. For the alkyl-type substituents the correlation between the central metal ion and the mesophase stability is somewhat less clear. Liquid-crystalline lanthanide complexes were not thoroughly reported on prior to our research [BinGör02], as can be seen in Appendix C. Incorporation of lanthanide ions reduced the mesophase range by both increasing the melting point and a decrease of the clearing point.

5.6 References

[BanNis01] K. Ban, K. Nishizawa, K. Ohta, A.M. van de Craats, J.M. Warman, I. Yamamoto, H. Shirai, *J. Mater. Chem.*, **11**, 321, 2001.

[BarRak98] J. Barberá, O.A. Rakitin, M.B. Ros, T. Torroba, *Angew. Chem. Int. Ed*., **37**, 3, 1998.

[BinGör02] K. Binnemans, C. Görller-Walrand, *Chem. Rev.*, **102**, 2303, 2002.

[BinVan99] K. Binnemans, R. Van Deun, D.W. Bruce, Y.G. Galyametdinov *Chem. Phys. Lett.*, **300**, 509, 1999.

[ChaCho94] Y.H. Chang, K.H. Choi, W.T. Ford, S.J. Cho, R. Ryooo, *J. Chem. Soc., Chem. Commun*. 785, 1994.

[ClaMcK95] G.J. Clarkson, N.B. McKeown and K.E. Treacher, *J. Chem. Soc. Perkin Trans. I*, 1817, 1995.

[EngBas93] M.K. Engel, P. Bassoul, L. Bosio, H. Lehmann, M. Hanack and J. Simon, *Liq. Cryst*., **15**, 709, 1993.

[ForSum94] W.T. Ford, L. Sumner, W.M. Zhu, Y.H. Chang, P.J. Um, K.H. Choi, P.A. Heiney, N.C. Maliszewskyj, *New. J. Chem.*, **18**, 495, 1994.

[GuiSko83] D. Guillon, A. Skoulios, C. Piechocki, J. Simon, P. Weber, *Mol. Cryst. Liq. Cryst*., **100**, 275, 1983.

[GuiWeb85] D. Guillon, P. Weber, A. Skoulios, C. Piechocki, J. Simon, *Mol. Cryst. Liq. Cryst*., **130**, 223, 1985.

[HaiKne95] P. Haisch, U. Knecht, L.R. Subramanian, M. Hanack, *Mol. Cryst. Liq. Cryst*., **270**, 7, 1995.

[NaiOht01] R. Naito, K. Ohta, H. Shirai, *J. Porph. Phthalocya*., **5**, 44, 2001.

[NisAzu92] H. Nishi, N. Azuma, K. Kitahara, *J. Heterocycl. Chem.*, **29**, 475, 1992

[NisUen89] H. Nishi, S. Ueno, *Nippon Kagaku Kaishi*, 983, 1989.

[OhtJac88] K. Ohta, L. Jacquemin, C. Sirlin, L. Bosio, J. Simon, *New. J. Chem.*, **12**, 751, 1988.

[PieSim82] C. Piechocki, J Simon, A. Skoulios, D. Guillon, P. Weber, *J. Am. Chem. Soc.*, **104**, 5245, 1982.

[SanSug98] J. Santiago, T. Sugino, Y. Smimizu, *Chem. Lett*. 661, 1998.

[SauWeg88] T. Sauer, G. Wegner, *Mol. Cryst. Liq. Cryst*., 162B, 97, 1988.

[Ser96] Serrano, J. L. (ed.), 1996, *Metallomesogens* (Weinheim: VCH).

[SerCar92] A. Serrette, P.J. Carroll, M. Swager, *J. Am. Chem. Soc.*, **114**, 1887, 1992.

[SevUnd93] L.M. Severs, A.E. Underhill, D. Edwards, P. Wight, D. Thetford, *Mol. Cryst. Liq. Cryst.*, **234**, 235, 1993.

[SimBas93] J. Simon, P. Bassoul, "Phthalocyanine based Liquid Crystals: Towards Submicronic Devices" in *Phthalocyanines, Properties and Applications*, eds. C.C. Leznoff en A.B.P. Lever, VCH Weinheim, Volume 2, 1993.

[SleGör01] J. Sleven, C. Görller-Walrand, K. Binnemans, *Mater. Sci. Eng. C*, **18**, 229, 2001.

[TanSty93] S. Tantrawong, P. Styring, J.W. Goodby, *J. Mater. Chem.*, **3**, 1209, 1993.

[TanSug98] S. Tantrawong, T. Sugino, Y. Shimizu, A. Takeuchi, S. Kimura, T. Mori, H. Takezoe, *Liq. Cryst*., **24**, 783, 1998.

[Tou95] T. Toupance, PhD thesis, Université de Paris VI, Paris, 1995.

[VacDop92] J. Vacus, P. Doppelt, J. Simon, G. Memetzidis, *J. Mater. Chem.*, **2**, 1065, 1992.

[vanNee88] J.F. van der Pol, E. Neeleman, J.W. Zwikker, R.J.M. Nolte, W. Drenth, *Recl. Trav. Chim. Pays-Bas*, **107**, 615, 1988.

[vanNee89] J.F. van der Pol, E. Neeleman, J.W. Zwikker, R.J.M. Nolte, W. Drenth, J. Aerts, R. Visser, S.J. Picken, *Liq. Cryst*., **6**, 577, 1989.

[vanWar97] A.M. van de Craats, J.M. Warman, H. Hasebe, R. Naito, K. Ohta, *J. Phys. Chem. B*, **101**, 9224, 1997.

[WebGui87] P. Weber, D. Guillon, A. Skoulios, *J. Phys. Chem.*, **91**, 2242, 1987.

[WebGui91] P. Weber, D. Guillon, A. Skoulios, *Liq. Cryst.*, **9**, 369, 1991.

Chapter 6

OPTICAL PROPERTIES

6.1 Introduction

The purity and the depth of the blue and green colour of the phthalocyanine compounds arise from the unique property of these molecules of having an isolated, single absorption band located in the far red end of the visible spectrum near 670 nm, with a molar absorptivity ε often exceeding 10^5 mol^{-1} cm^{-1}. This absorption band is called the *Q-band* and is responsible for the colour of the compound.

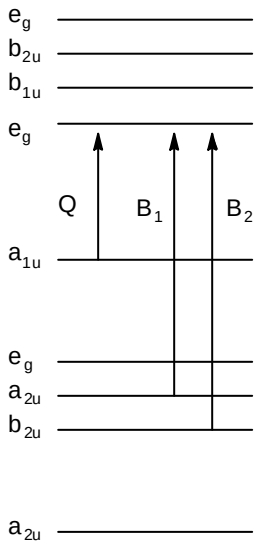

Figure 74 - Gouterman's orbital model for the metallophthalocyanine p® p transitions*

Unlike many other molecules, the next most energetic set of transitions is generally much less intense, lying just to the blue of the visual region near 340 nm. The absorption at about 340 nm is called the *B-band*. The *Q-band* as well as the *B-band* are $\pi \rightarrow \pi^*$ transitions [HolSti78, vanNee89]. Figure 74 represents Gouterman's four-orbital model for metallophthalocyanine molecules [StiNyo93a, MacSti01].

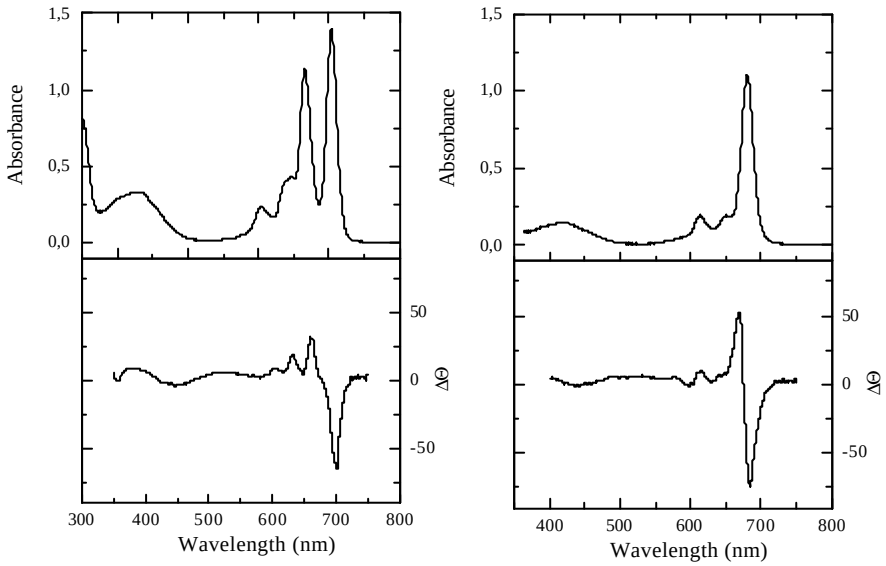

Figure 75 - UV/VIS (upper) and MCD (lower) spectra for the $(C_{12}H_{25}O)_8$Pc ligand (left) and $(C_{12}H_{25}O)_8$PcCu complex (right)

The *Q-band* absorption is assigned to a transition from the HOMO of a_{1u} symmetry to the LUMO of e_g symmetry. The first excited state is a doubly degenerate ^1E_u. In H_2Pc the Q-band is split up because of the lower symmetry (D_{2h}) and the consequent loss of degeneracy of the LUMO orbital to produce Q_y and Q_x. The splitting of the Q-band of H_2Pc disappears on deprotonation to form the Pc^{2-} anion, which has D_{4h} symmetry. The metallophthalocyanines also have D_{4h} symmetry and this splitting is no longer present since the excited state of the Q-band is

degenerate. This is emphasised when comparing the MCD spectra of the complex and the ligand. For the complex an A-term is centred on the maximum of the Q-absorption peak. This is illustrated in Figure 75 for the octa-dodecyloxy phthalocyanine ligand and its copper(II) complex.

The Q- and the B-bands are similar for different metallophthalocyanines though there can be differences in the peak positions and fine structure. The absorption bands often show a vibrational fine structure, due to vibronic couplings. The region between the peaks (about 500 nm) is called an optical window, because there is almost no light absorption. When additional bands are introduced in the window region for example from charge transfer transitions between the central metal ion and the π ring, the colour of the complex changes.

The spectral properties of the lanthanide dimers are more complicated than for the metal phthalocyanines with only one Pc-ring. Furthermore, oxidation and reduction of the Pc ring produces π cationic or π anionic species, which have both of them characteristic spectroscopic properties [StiNyo93b]. The neutral Pc_2Ln complex is characterised by a band at 655 nm, the reduced π anion exhibits two bands near 620 and 700 nm. The cationic complex displays an absorption band at 700 nm and one at 855 nm. In addition, the neutral Pc_2Ln shows two absorption regions in the infrared at 904 and 1382 nm that are not present in the case of the oxidised and the reduced species. The band at 904 nm is linked to the radical part of the complex. The band at 1382 nm is connected to an intramolecular charge transfer: the dianion Pc^{2-} behaves as an electron donor and the $Pc^{-\bullet}$ radical as an electron acceptor. An additional absorption at 450-460 nm is measured for the Pc_2Lu and Pc_2Lu^+ compounds, due to the radical ($e_g \rightarrow a_{1u}$, due to the missing electron). Figure 76 illustrates this, showing the UV/VIS spectrum of the $[(C_{12}H_{25}O)_8Pc]Gd$ complex. A graphical summary of the above is presented in Figure 77. Because of the intensity of the ligand transitions, the lanthanide ion spectra are not visible.

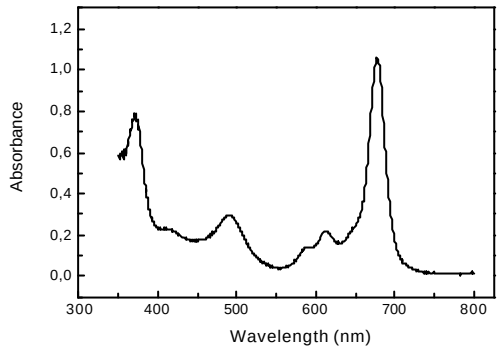

Figure 76 - UV/VIS spectrum for the [$(C_{12}H_{25}O)_8$Pc]Gd complex

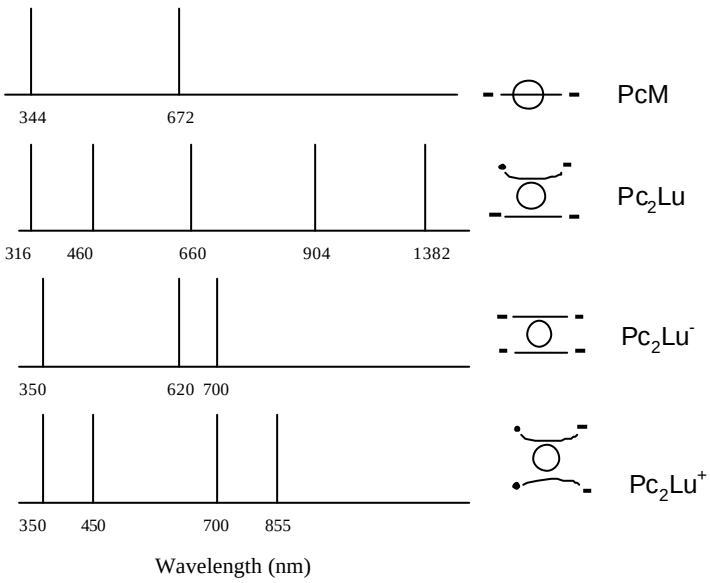

Figure 77 - Schematic representation of the absorption bands between 300 and 1800 nm for different metallophthalocyanines (after: [MarTra87])

Addition of substituents to the phthalocyanine core and different central metal ions often cause a shift of the Q-band. Since the Q-band is determined by the HOMO-

LUMO frontier orbitals, the tuning of this transition is of interest for increasing the conductivity of phthalocyanines. We investigated our compounds by both UV/VIS and MCD in order to gain some insight into the way the different linking groups, chain lengths and metal ions influence the spectroscopic properties. All spectra were recorded in chloroform (spectroscopic grade).

6.2 Ligands

6.2.1 Octa-alkoxy phthalocyanines

We observed no significant influence of the chain length on the peak positions (B, $Q_{x,y}$) in the UV/VIS spectra for the metal-free phthalocyanines (Table 56). Compared to the unsubstituted phthalocyanine compound, a small bathochromic (red) shift is observed for the most intense absorption peaks ($Q_{x,y}$: 655, 699 nm).

Table 56 - Peak positions and absorptivities for the $Q_{x,y}$, B-bands for the octa-alkoxy substituted phthalocyanines

Compound	λ_{max} Q_y-band (nm)	log e	λ_{max} Q_x-band (nm)	log e	λ_{max} B-band (nm)	log e
$(C_4H_9O)_8PcH_2$	666	2.13	703	2.04	350	1.88
$(C_5H_{11}O)_8PcH_2$	665.5	2.00	703.5	1.91	349.5	1.76
$(C_6H_{13}O)_8PcH_2$	665.5	2.11	704	2.02	348	1.87
$(C_7H_{15}O)_8PcH_2$	666	2.23	703.5	2.14	350	1.98
$(C_8H_{17}O)_8PcH_2$	666	2.14	704	2.06	349.5	1.90
$(C_9H_{19}O)_8PcH_2$	666.5	2.01	703.5	1.93	349.5	1.78
$(C_{10}H_{21}O)_8PcH_2$	666	2.05	704	1.96	349	1.77
$(C_{11}H_{23}O)_8PcH_2$	666.5	1.97	704	2.11	348	1.95
$(C_{12}H_{25}O)_8PcH_2$	666.5	2.12	704	2.03	350	1.88
$(C_{13}H_{27}O)_8PcH_2$	665	2.04	703.5	1.90	349	1.84
$(C_{14}H_{29}O)_8PcH_2$	666	2.02	703.5	1.93	348.5	1.81
$(C_{15}H_{31}O)_8PcH_2$	665.5	2.02	703	1.94	344	2.01
$(C_{16}H_{33}O)_8PcH_2$	666	1.98	704	1.89	346.5	1.97
$(C_{18}H_{37}O)_8PcH_2$	666	1.87	704	1.79	346	1.97
$(C_{19}H_{39}O)_8PcH_2$	666	1.98	703.5	1.96	345	1.92
$(C_{20}H_{41}O)_8PcH_2$	666	2.01	704	1.99	348.5	1.87

6.2.2 Octa-alkyl phthalocyanines

Table 57 gives the peak positions for the $Q_{x,y}$ and B-bands for the octa-alkyl substituted phthalocyanines. No absorptivities were calculated because of the low yields no absolute concentrated solutions were measured. Again, no significant influence of the chain length is observed. When compared with the octa-alkoxy analogues, the Q-absorption bands are slightly red-shifted.

Table 57 - Peak positions for the $Q_{x,y}$, B-bands for the octa-alkoxy substituted phthalocyanines

Compound	λ_{max} Q_y-band (nm)	λ_{max} Q_x-band (nm)	λ_{max} B-band (nm)
$(C_7H_{15})_8PcH_2$	674	707	345.5
$(C_8H_{17})_8PcH_2$	673	708	346
$(C_{12}H_{25})_8PcH_2$	672	708	348
$(C_{14}H_{29})_8PcH_2$	674	707.5	346
$(C_{16}H_{33})_8PcH_2$	674.5	706.5	346
$(C_{18}H_{37})_8PcH_2$	673	707	346.5

6.2.3 Octa-alkoxymethyl phthalocyanines

Also no absorptivities were calculated because of the low yields no absolute concentrated solutions were measured. Again, no significant effect of the chain length on the peak positions (B, $Q_{x,y}$) in the UV/VIS spectra was found (Table 58). A small bathochromic (red) shift is observed for the most intense absorption peaks, when compared to the unsubstituted phthalocyanine.

Table 58 - Peak positions and absorptivities for the $Q_{x,y}$, B-bands for the octa-alkoxymethyl substituted phthalocyanines

Compound	λ_{max} Q_y-band (nm)	λ_{max} Q_x-band (nm)	λ_{max} B-band (nm)
$(C_8H_{17}OCH_2)_8PcH_2$	666	700.5	345.5
$(C_{12}H_{24}OCH_2)_8PcH_2$	667	701	347
$(C_{16}H_{33}OCH_2)_8PcH_2$	666.5	702	346

6.3 Transition metal complexes

6.3.1 Octa-alkoxy phthalocyanines

6.3.1.1 Influence of the chain length: homologous series for cobalt(II)

The chain length has hardly any influence on the position of the Q-band. Table 59 shows the peak positions and absorptivities for the Q-band for the octa-alkoxy substituted phthalocyanine cobalt(II) complexes. The graphical representation is given in Figure 78.

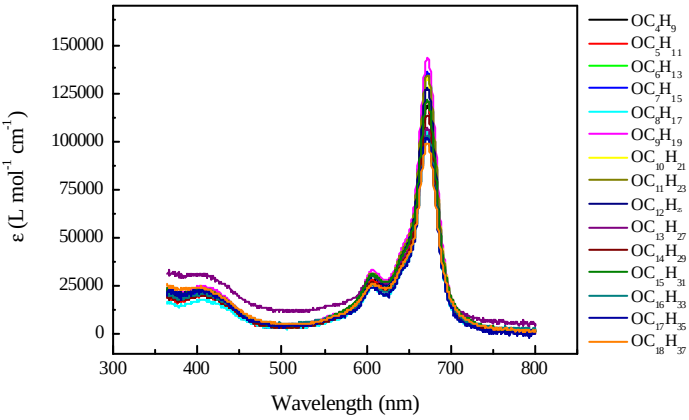

Figure 78 - UV/VIS-spectra for the octa-alkoxy substituted Pc cobalt(II) complexes

Table 59 - Peak positions and absorptivities for the Q-bands for the octa-alkoxy substituted phthalocyanine cobalt(II) complexes

Compound	λ_{max} Q-band (nm)	log ε
$(C_4H_9O)_8PcCo$	672.0	5.07
$(C_5H_{11}O)_8PcCo$	672.0	5.08
$(C_6H_{13}O)_8PcCo$	672.0	5.13
$(C_7H_{15}O)_8PcCo$	672.0	5.13
$(C_8H_{17}O)_8PcCo$	672.0	5.01
$(C_9H_{19}O)_8PcCo$	672.0	5.16
$(C_{10}H_{21}O)_8PcCo$	672.0	5.12
$(C_{11}H_{23}O)_8PcCo$	672.0	5.13
$(C_{12}H_{25}O)_8PcCo$	672.0	5.10
$(C_{13}H_{27}O)_8PcCo$	672.0	5.03
$(C_{14}H_{29}O)_8PcCo$	672.0	5.05
$(C_{15}H_{31}O)_8PcCo$	672.0	5.08
$(C_{16}H_{33}O)_8PcCo$	672.0	5.01
$(C_{17}H_{35}O)_8PcCo$	672.0	5.01
$(C_{18}H_{37}O)_8PcCo$	672.0	4.99

6.3.1.2 Influence of the central metal ion: Cu(II), Co(II), Ni(II), Cu(II), Zn(II), V(IV)O

The UV/VIS data are summarised in Table 60, and are graphically illustrated for $C_{16}H_{33}O$ terminal chain in Figure 79. The Q-band is more intense for the vanadyl and copper(II) phthalocyanines than for the other metallophthalocyanines. The lowest intensity is observed for the cobalt(II) phthalocyanines, but the position of the zinc(II) and nickel(II) complex is more difficult to establish. The Q-band was found to shift to the red in the order $Co^{II} \approx Ni^{II} < Zn^{II} < Cu^{II} < V^{IV}O$. The total shift between the cobalt(II) and the copper(II) phthalocyanines is about 10 nm. The vanadyl compounds are shifted another 20 nm. The reason for this large shift remains yet unclear. The variation in intensity for the vanadyl complexes can be

explained by means of a tentative model. The relative intensity of the Q-band is determined by configuration-interaction between the $a_{1u} \rightarrow e_g$ en $a_{2u} \rightarrow e_g$ transitions and is very sensitive to small disturbances of these orbitals. The $4p_z$ orbital of vanadium can interact with the occupied a_{2u} orbital of the Pc, while no orbitals with a_{1u} symmetry are present in the valence shell of the metal. This would lead to an orbital mechanism for the observed change in intensity (the $4p_z$ orbital of the V(IV)O has a strong influence on the complex in this model). Nevertheless, further (computational) investigations might be required to fully explain the observed spectra.

Table 60 - Peak positions and absorptivities for the Q-bands for the octa-alkoxy substituted phthalocyanine Zn(II), Cu(II), Ni(II), Co(II) and V(IV)O complexes

Compound	λ_{max} Q-band (nm)	log ε
$(C_8H_{17}O)_8PcZn$	679.0	5.19
$(C_8H_{17}O)_8PcCu$	681.5	5.29
$(C_8H_{17}O)_8PcNi$	672.5	5.25
$(C_8H_{17}O)_8PcCo$	672.0	5.01
$(C_8H_{17}O)_8PcVO$	702.5	5.33
$(C_{12}H_{25}O)_8PcZn$	679.0	5.18
$(C_{12}H_{25}O)_8PcCu$	681.5	5.34
$(C_{12}H_{25}O)_8PcNi$	673.0	5.24
$(C_{12}H_{25}O)_8PcCo$	672.0	5.10
$(C_{12}H_{25}O)_8PcVO$	703.0	5.36
$(C_{16}H_{33}O)_8PcZn$	680.5	5.16
$(C_{16}H_{33}O)_8PcCu$	681.5	5.28
$(C_{16}H_{33}O)_8PcNi$	672.5	5.10
$(C_{16}H_{33}O)_8PcCo$	672.0	5.01
$(C_{16}H_{33}O)_8PcVO$	702.5	5.34

After standing for several days, the blue green solutions of the zinc(II) phthalocyanines turned yellow. The reason for this behaviour is that

phthalocyanines containing diamagnetic metal ions such as zinc(II) and aluminium(III) form derivatives that are photosensitisers, producing singlet-oxygen under the influence of light, and so tend to oxidise and decompose [Ros91]. Paramagnetic metals such as copper(II) form phthalocyanines in which the residence time in the excited state produced by absorption of a photon is too short to allow singlet oxygen formation and so are more photostable.

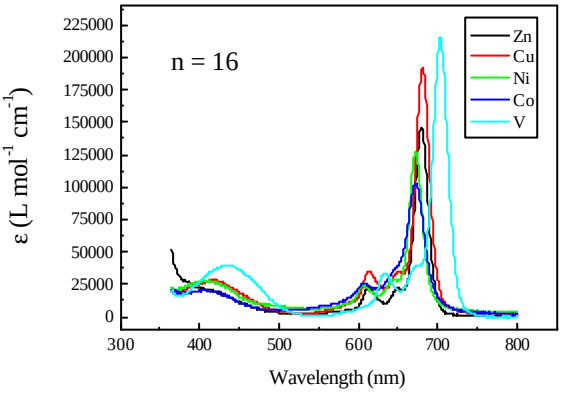

Figure 79 - UV/VIS-spectra for the Co(II), Cu(II), Zn(II), Ni(II) and V(IV)O complexes with -$C_{16}H_{33}O$ terminal chain

6.3.2 Octa-alkyl phthalocyanines

6.3.2.1 Influence of the chain length: homologous series for cobalt(II)

Because of the low yields for the synthesis, not all complexes could be measured. From Table 61 it is clear that there is no significant change for the Q-band position on going to longer chain lengths. The position of the Q-band is shifted by about 10 nm into the red, relative to the octa-alkoxy cobalt(II) complexes. The difference in absorptivity is negligible.

Table 61 - Peak positions and absorptivities for the Q-bands for the octa-alkyl substituted phthalocyanine Co(II) complexes

Compound	λ_{max} Q-band (nm)	log ε
$(C_7H_{15})_8PcCo$	680	5.30
$(C_8H_{17})_8PcCo$	/	/
$(C_{12}H_{25})_8PcCo$	684	5.26
$(C_{14}H_{29})_8PcCo$	/	/
$(C_{16}H_{33})_8PcCo$	680	5.17
$(C_{18}H_{37})_8PcCo$	680.5	5.27

6.3.2.2 Influence of the central metal ion: Cu(II), Co(II), Ni(II), Cu(II), Zn(II), V(IV)O

The UV/VIS data that were collected are given in Table 62. For the octa-hexadecyl phthalocyanine complexes, the data are graphically represented in Figure 80. Some of the compounds could not be measured because of the low yields of the reactions. No significant differences in absorptivities between the different metal complexes are observed.

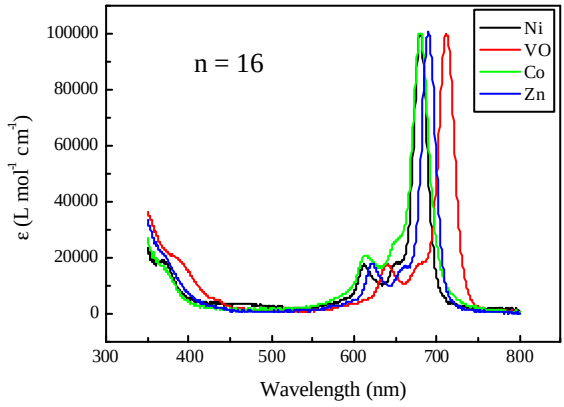

Figure 80 - UV/VIS-spectra for the Co(II), Zn(II), Ni(II) and V(IV)O complexes with -$C_{16}H_{33}$ terminal chain

The Q-band shift to the red was in the same order as for the alkoxy analogues: Co^{II} ≈ Ni^{II} < Zn^{II} < $V^{IV}O$. The total shifts also compare: 10 nm between the cobalt(II) and the copper(II) phthalocyanines and a further 20 nm for the vanadyl compounds. The bleaching of the blue green solutions of the zinc(II) phthalocyanines was also observed.

Table 62 - Peak positions and absorptivities for the Q-bands for the octa-alkyl substituted phthalocyanine Zn(II), Cu(II), Ni(II), Co(II) and V(IV)O complexes

Compound	λ_{max} Q-band (nm)	log ε
$(C_8H_{17})_8PcZn$	/	/
$(C_8H_{17})_8PcCu$	688.5	5.31
$(C_8H_{17})_8PcNi$	/	/
$(C_8H_{17})_8PcCo$	/	/
$(C_{12}H_{25})_8PcZn$	/	/
$(C_{12}H_{25})_8PcCu$	689	5.33
$(C_{12}H_{25})_8PcNi$	680	5.31
$(C_{12}H_{25})_8PcCo$	688	5.26
$(C_{14}H_{29})_8PcZn$	/	/
$(C_{14}H_{29})_8PcCu$	688	5.38
$(C_{14}H_{29})_8PcNi$	679.5	5.38
$(C_{14}H_{29})_8PcCo$	/	/
$(C_{14}H_{29})_8PcVO$	/	/
$(C_{16}H_{33})_8PcZn$	689.5	5.33
$(C_{16}H_{33})_8PcCu$	/	/
$(C_{16}H_{33})_8PcNi$	680.5	5.04
$(C_{16}H_{33})_8PcCo$	680	5.17
$(C_{16}H_{33})_8PcVO$	711.5	5.34

6.3.3 Octa-alkoxymethyl phthalocyanines

The UV/VIS data that were collected are given in Table 63. The data are graphically represented in Figure 81. No absorptivities were measured because no

quantitative solutions could be prepared due to the micro-scale synthesis of the complexes. We collected spectra having an absorption of about 1.

6.3.3.1 Influence of the chain length

As can be deduced from Table 63, the chain length did not significantly influence the spectral properties of the octa-alkoxymethyl transition metal complexes.

Table 63 - Peak positions for the Q-bands for the octa-alkoxymethyl substituted phthalocyanine transition metal complexes

Compound	λ_{max} Q-band (nm)
$(C_8H_{17}OCH_2)_8PcZn$	681.5
$(C_8H_{17}OCH_2)_8PcCu$	680.5
$(C_8H_{17}OCH_2)_8PcNi$	672
$(C_8H_{17}OCH_2)_8PcCo$	672.5
$(C_{12}H_{24}OCH_2)_8PcZn$	681.5
$(C_{12}H_{24}OCH_2)_8PcCu$	680.5
$(C_{12}H_{24}OCH_2)_8PcNi$	672.5
$(C_{12}H_{24}OCH_2)_8PcCo$	673.5
$(C_{16}H_{33}OCH_2)_8PcZn$	681.5
$(C_{16}H_{33}OCH_2)_8PcCu$	681
$(C_{16}H_{33}OCH_2)_8PcNi$	671.5
$(C_{16}H_{33}OCH_2)_8PcCo$	672

6.3.3.2 Influence of the central metal ion: Cu(II), Co(II), Ni(II), Cu(II), Zn(II)

The Q-band was found to shift bathochromically in the order $Co^{II} \approx Ni^{II} < Zn^{II} \approx Cu^{II}$. The total shift between the cobalt(II) and the copper(II) phthalocyanines is about 10 nm. For the octa-alkoxymethyl transition metal complexes the blue green solutions of the zinc(II) phthalocyanines also shifted colour after a period of standing in air.

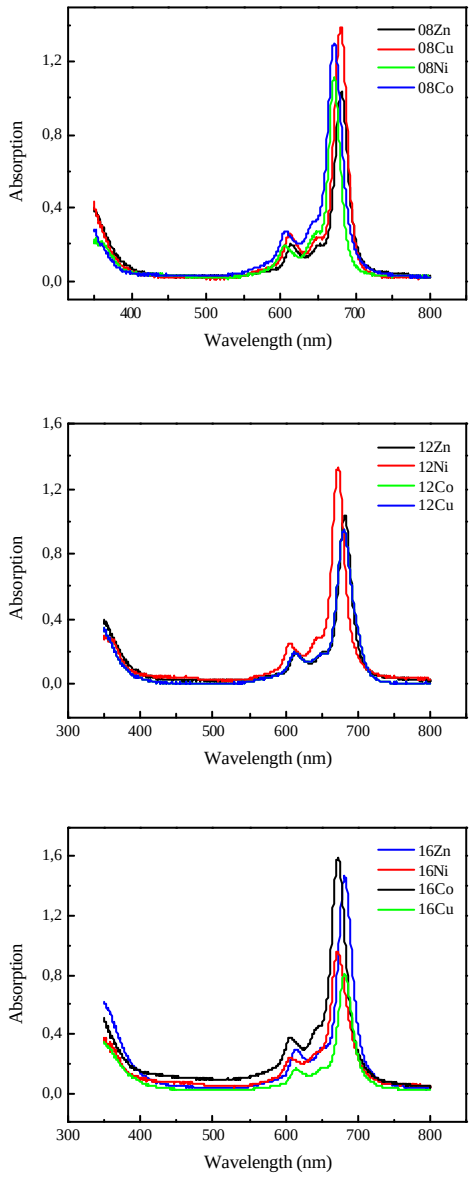

Figure 81 - UV/VIS-spectra for the Co(II), Zn(II) and Ni(II) complexes with -$CH_2OC_8H_{17}$ (top), -$CH_2OC_{12}H_{25}$ (middle) and -$CH_2OC_{16}H_{33}$ (bottom) terminal chain

6.4 Lanthanide complexes

Because of the low yields no quantitative solutions could be prepared and hence no absorptivities were measured. We collected spectra having an absorption of about 1. From these spectra it was possible to draw conclusions on the influence of the chain length and the lanthanide(III) ion on the positions of the main absorption bands.

6.4.1 Influence of the chain length: homologous series for erbium(III)

As mentioned in the introduction, the spectra for the lanthanide complexes show three main absorption bands: the Q-band, the B-band and a band due to the radical electron. Table 64 gives the peak positions for those bands. As for the ligands and the transition metal complexes, the chain length has no significant influence on the spectral positions.

Table 64 - Peak positions for the B-band, the radical band and the Q-band of the bis(octa-alkoxy substituted phthalocyaninato) erbium(III) complexes in chloroform

Compound	λ_{max} B-band (nm)	λ_{max} radical band (nm)	λ_{max} Q-band (nm)
$[(C_4H_9O)_8Pc]_2Er$	369.5	484.5	672
$[(C_5H_{11}O)_8Pc]_2Er$	369.5	481.5	671
$[(C_6H_{13}O)_8Pc]_2Er$	370.5	480.5	671.5
$[(C_8H_{17}O)_8Pc]_2Er$	369	481.5	672
$[(C_9H_{19}O)_8Pc]_2Er$	368	482	671.5
$[(C_{10}H_{21}O)_8Pc]_2Er$	367	482	672
$[(C_{12}H_{25}O)_8Pc]_2Er$	369.5	482.5	673
$[(C_{14}H_{29}O)_8Pc]_2Er$	370.5	483.5	672.5
$[(C_{15}H_{31}O)_8Pc]_2Er$	369.5	482.5	671.5
$[(C_{16}H_{33}O)_8Pc]_2Er$	367.5	483	672.5
$[(C_{18}H_{37}O)_8Pc]_2Er$	369	485	672
$[(C_{19}H_{39}O)_8Pc]_2Er$	370	484.5	672

6.4.2 Influence of the central metal ion: La(III)-Lu(III)

The UV/VIS data are summarised in Table 65, and is graphically illustrated for the Q-band positions in Figure 82. The position of the most intense absorption maximum (Q-band) for the bis(octa-dodecyloxy substituted phthalocyaninato) lanthanide(III) complexes depends directly on the atomic number of the lanthanide. The same decrease in peak position with smaller ionic radii is observed for the band round 480 nanometer as clear from Table 65. For the B-band no clear relationship could be established. Kirin *et al*. were the first to observe such a hypsochromic shift for the unsubstituted bisphthalocyanine lanthanide complexes in methanol solutions [KirMos67]. They explained the displacement to shorter wavelengths with decrease in the radius of the lanthanide by an increase in the strength of the metal-nitrogen bond.

Table 65 - Peak positions for the B-band, the radical band and the Q-band of the bis(octa-dodecyloxy substituted phthalocyaninato) lanthanide(III) complexes in chloroform

Compound	λ_{max} B-band (nm)	λ_{max} radical band (nm)	λ_{max} Q-band (nm)
$[(C_{12}H_{25}O)_8Pc]_2Ce$		503	686
$[(C_{12}H_{25}O)_8Pc]_2Pr$	375	500	684.5
$[(C_{12}H_{25}O)_8Pc]_2Nd$	373	497.5	684
$[(C_{12}H_{25}O)_8Pc]_2Sm$	373	494.5	681
$[(C_{12}H_{25}O)_8Pc]_2Eu$		492	679.5
$[(C_{12}H_{25}O)_8Pc]_2Gd$	370	490	678
$[(C_{12}H_{25}O)_8Pc]_2Tb$	370	487	676.5
$[(C_{12}H_{25}O)_8Pc]_2Dy$		485	675
$[(C_{12}H_{25}O)_8Pc]_2Ho$		484	674
$[(C_{12}H_{25}O)_8Pc]_2Er$	369.5	482.5	673
$[(C_{12}H_{25}O)_8Pc]_2Tm$	367.5	480.5	671
$[(C_{12}H_{25}O)_8Pc]_2Yb$	369.5	478	669.5
$[(C_{12}H_{25}O)_8Pc]_2Lu$		476	667.5

More precisely, the blue-shift occurs due to the decreased distance between the Pc rings with smaller radius of the lanthanide(III) ion. This was deduced from the Walsh diagram for the interplanar distance as calculated by Rousseau *et al.* for the unsubstituted Pc_2Ln complexes [RouAro95].

Compared to the unsubstituted complexes, the position of the Q-band is shifted by about 50 nanometers. This is illustrated in Figure 82. This is probably mainly due to the solvent, because Kirin et al. measured their samples in methanol. We measured the main transition bands complexes in chloroform for the unsubstituted Pc_2Ln that we synthesised. These data are shown in the middle of Figure 82. For these data, only an offset of ± 10 nm with the octa-alkoxy substituted complexes was found.

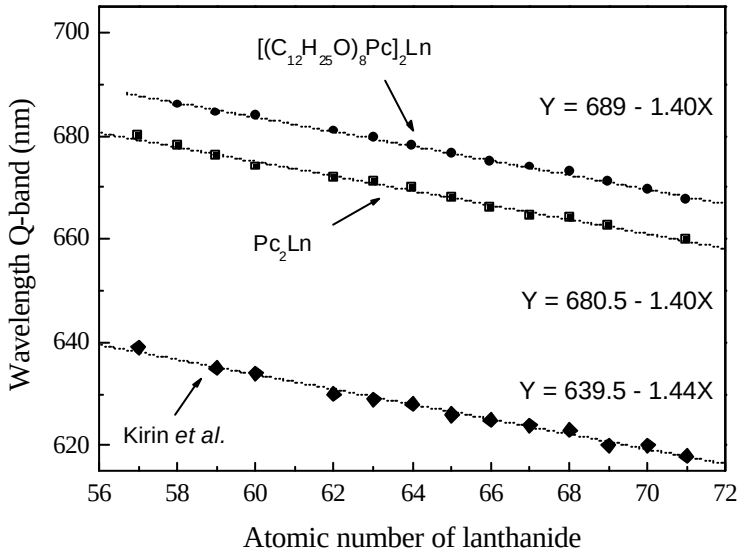

Figure 82 - Influence of the lanthanide(III) ion on the position of the Q-band absorption maxima: bis(octa-dodecylphthalocyaninato) lanthanide(III) complexes in chloroform (●), Pc_2Ln complexes in methanol (■) and Pc_2Ln complexes in methanol (◆, [KirMos67])

The (pronounced) change in position of an electronic absorption or emission band, accompanying a change in the polarity of the medium is called *solvatochromism*. Negative (positive) solvatochromism corresponds to a hypsochromic (bathochromic) shift with increasing solvent polarity. Comparing our data for the unsubstituted Pc_2Ln complexes with the observations by Kirin et al., we can conclude a negative solvatochromism is noted.

In conclusion, we can state that peripheral substitution leads to bathochromic shifts of the Q-band absorption maxima. Tomilova *et al*. performed measurements in o-dichlorobenzene and found an intercept of 688 and a slope of 1.77 for the linear regression curve their series of octa-4-tert-butyl Pc_2Ln (Ln = La, Pr, Nd, Sm, Gd, Er, Lu) complexes [TomChe84].

6.5 Conclusions

The phthalocyanine compounds we synthesized all show a strong light absorption. In comparison to alkoxy and alkoxymethyl substituted phthalocyanines, the solubility of alkyl-substituted phthalocyanines is lower. The reason for this is the better interaction of solvent molecules and the oxygen atom in the side chain of the former (we made this observation qualitatively, while preparing the solutions for the UV/VIS spectra).

As expected, the chain length does not have any influence on the optical properties. This is because the electronic effect of the linking group does not depend on the length, but rather to the atoms closely attached to the aromatic structure (linking group).

For the three types of chains we considered, the electronic effects on the Pc core are different. The alkoxymethyl chains are strongly withdraw electrons, whereas the alkoxy and alkyl chains are strongly and weakly electron donating, respectively. Yet, these considerations are not strongly reflected in the UV/VIS spectra. Compared to the unsubstituted compounds only a small bathochromic shift is evident. The shift is caused by a disturbance of the frontier orbitals by the substituents [RouAro95].

The central metal ion (both transition metals and lanthanides) does strongly affect the position of the Q-band. For the transition metals there is no obvious relationship between the metal ion and the Q-transition maximum. The most dramatic shift is noticed for the vanadyl compounds. Further research and modelling (e.g. *ab initio* methods) might bring insight into the observed phenomena.

On the whole we can conclude that peripheral substitution has a minor effect on the Q-band position. The choice of the central metal ion nevertheless can influence the optical spectra. This is most obvious for the vanadyl and lanthanide complexes.

6.6 References

[HolSti78] B.R. Hollebone, M.J. Stillman, *J. Chem. Soc. Faraday Trans.*, **74**, 2107, 1978.

[LezLev96] C.C. Leznoff, A.B.P Lever , *Phthalocyanines, Properties and Applications*, Vols 1-4, VCH Weinheim, 1989.

[KirMos67] I.S. Kirin, P.N. Moskalev, Y.A. Makashev, *Russ. J. Inorg. Chem.*, **12**, 369, 1967.

[MacSti01] J. Mack, J. Stillman, *J. Porphyr. Phthalocya*., **5**, 67, 2001.

[MarTra87] D. Markovitsi, T. Tran-Hi, R. Even, J. Simon, *Chem. Phys. Lett.*, **137**, 107, 1987.

[Ros91] Rosanthal, I., *Photochem. Photobiol*., 53**,** 859, 1991.

[RouAro95] R. Rousseau, R. Aroca, M.L. Rodriguez-Mendez, *J. Mol. Struct*., **356**, 49, 1995.

[StiNyo93a] M.J. Stillman, T. Nyokong, "Absorption and magnetic circular dichroism spectral properties of phthalocyanines. Part 1: complexes of the dianion Pc^{2-}" in *Phthalocyanines, Properties and Applications*, Vol 1, eds. C.C. Leznoff and A.B.P. Lever, VCH Weinheim, 1996.

[StiNyo93b] M.J. Stillman, T.J. Nyokong, "Absorption and magnetic circular dichroism spectral properties of phthalocyanines. Part 2: Ring-Oxidised and Ring-Reduced Complexes" in *Phtalocyanines, Properties and Applications*, Vol 4, eds. C.C. Leznoff and A.B.P. Lever VCH Weinheim, 1996.

[TomChe84] L.G. Tomilova, E.V. Chernykh, N.T. Ioffe, E.A. Luk'yanets, *J. Gen. Chem. USSR*, **53**, 2339, 1984.

[vanNee89] J.F. van der Pol, E. Neeleman, J.W. Zwikker, R.J.M. Nolte, W. Drenth, J. Aerts, R. Visser, S.J. Picken, *Liq. Cryst*., **6**, 577, 1989.

General summary

Phthalocyanines form a colourful class of macrocyclic compounds, attracting the attention of many scientists. Some of these compounds – especially the metal containing phthalocyanines – play an important role in industrial activity and in society. Applications for phthalocyanines are found in the fields of non-linear optics, catalysis, electronic (bio)sensors, photovoltaic solar cells, optical data storage, lubricants, photo- and radiosensitizers for treatment of cancer, protein inhibitors …

When substituents are placed on the Pc-ring, not only the solubility of the compounds increases, also liquid-crystalline phthalocyanines can be obtained. The columnar architecture of the mesophase suggests the possibility to use them as anisotropic electric conductors. Various mesogenic phthalocyanines have been prepared, but with a limited variation for the central metal ion: mainly the copper(II) ion was used as a transition metal and most studies of liquid-crystalline Pc_2Ln compounds have been restricted to lutetium(III) as the metal ion.

We synthesised three different peripherally octa-substituted phthalocyanines and their complexes with different transition metal and lanthanide ions. We were interested in the influence of the central metal ion, the substituent type and the chain length on the thermal behaviour and optical properties. Three types of substituents were examined: alkoxy, alkyl and alkoxymethyl chains. We investigated the metal-free compounds, a selection of transition metal complexes (Zn(II), Cu(II), Ni(II), Co(II), V(IV)O) and the octa-alkoxy substituted lanthanide(III) complexes.

In a first part of this thesis the synthesis of the various compounds was discussed. A major problem was the purity check of the synthesised complexes. The elemental analysis did only in rare cases yield satisfactory results and adding a combustion catalyst to the CHN-sample did not improve this outcome. This is a

well-known problem for these types of macrocyclic compounds. The problem was overcome by judging the purity based on the compound's MALDI-TOF, IR and UV/VIS spectra. The overall yield for the octa-substituted synthesised ligands and complexes via the traditional pathways was in general rather low. Nevertheless, we succeeded in obtaining the unsubstituted phthalocyanine lanthanide complexes in higher yields with a recent technique that uses microwave radiation as the energy source. A further refinement of this synthesis method is desired because of the irreproducible yields and lack of control of the parameters of the (commercial) microwave oven that was used. Attempts in synthesising peripherally substituted metallophthalocyanines with this technique were unsuccessful.

The thermal behaviour of the synthesised compounds was discussed in the second section of this thesis. Polarising optical microscopy, DSC, TGA-DTA and high-temperature X-ray diffraction were used to study the products. All of the discussed compounds exhibited a relatively wide mesomorphic range and they all showed enantiotropic behaviour, although it was sometimes hard to detect the clearing point because of simultaneous decomposition of the sample. The absence of polymorphism was found for all of our discotic liquid-crystalline peripherally octa-substituted phthalocyanines and metallophthalocyaninato complexes. As confirmed by polarising microscopy and XRD-diffraction experiments, the mesophase observed was the hexagonal columnar mesophase (Col_h) for all but the vanadyl complexes, which exhibited the rectangular columnar (Col_r) mesophase. Side-chains with a length of fewer than four carbon atoms did not demonstrate a mesophase. For all investigated homologous series, the melting point generally decreased with increasing chain length. The decrease was more relevant for shorter chain lengths. At longer chain lengths, the relationship was less obvious for some types of compounds (lanthanide complexes). The clearing points decreased more drastically with increasing chain length. This trend was more pronounced for the octa-alkoxy side-chains.

The melting points were in general much higher for the octa-alkyl phthalocyanines than for the octa-alkoxy and the octa-alkoxymethyl compounds (order: octa-alkyl >> octa-alkoxy > octa-alkoxymethyl). Due to specific steric interactions, the side-chains determine the way neighbouring columns are oriented and also they strongly influence the order within the columns.

For the octa-alkoxy and octa-alkyl compounds, the vanadyl ions showed the strongest stabilising effect on the mesophase compared to the metal-free ligand ($\Delta T_m \approx 30°C$). They had lower melting temperatures than the ligands. For the other transition metals (Zn^{2+}, Cu^{2+}, Ni^{2+}, Co^{2+}) the melting temperatures increased, but in the whole the mesophase was stabilised due to the strong increase of the clearing point. The strongest increase of the melting point was found for Zn^{2+} (order: $Ni^{2+} < Cu^{2+} \approx Co^{2+} < Zn^{2+}$). For the alkyl-type substituents the correlation between the central metal ion and the mesophase stability was somewhat less clear. Incorporation of lanthanide ions reduced the mesophase range by both increasing the melting point and a decrease of the clearing point.

The third part of this work investigated the optical properties by absorption and MCD-spectroscopy. The phthalocyanine compounds we synthesized all show a strong light absorption. On the whole we can conclude that peripheral substitution has a minor effect on the Q-band position. The choice of the central metal ion nevertheless can influence the optical spectra. This is most obvious for the vanadyl and lanthanide complexes.

Algemene samenvatting

Ftalocyanines vormen een kleurrijke klasse van macrocyclische verbindingen, die de aandacht trekken van vele wetenschappers. Bepaalde (metallo)ftalocyanine verbindingen spelen een belangrijke rol in de industrie en de samenleving in zijn geheel. Ftalocyanines worden aangewend in verschillende gebieden: niet-lineaire optica, katalyse, electronische (bio)sensoren, fotovoltaïsche cellen, optische data-opslag, smeermiddelen, foto- en radiotherapie voor de behandeling van kanker, proteïne inhibitie …

Als er substituenten op de Pc-ring geplaatst worden, zal niet enkel de oplosbaarheid van de verbindingen toenemen, maar kunnen ook vloeibaar-kristallijne ftalocyanines bekomen worden. De kolomvormige architectuur van de mesofase maakt de verbindingen interessant als mogelijke anisotrope elektrische halfgeleiders. Verschillende mesogene ftalocyanines werden reeds gesynthetiseerd, doch er werd slechts een beperkt aantal centrale metaalionen bestudeerd. Voor de transitiemetaalcomplexen werden vooral koper(II) ionen gebruikt en de meeste studies over vloeibaar-kristallijne Pc_2Ln verbindingen handelen over lutetium(III) complexen.

Deze thesis handelt over drie verschillende types van perifeer octa-gesubstitueerde ftalocyanines en metalloftalocyanines met transitiemetalen en lanthaniden als centrale metaalionen. Het doel was om meer inzicht te verkrijgen op de invloed van het type van keten, de lengte van de keten en het centraal metaalion op de thermische en optische eigenschappen van onze verbindingen. De drie onderzochte ketentypes waren alkoxy, alkyl en alkoxymethyl ketens. We bereidden en onderzochten de metaalvrije verbindingen, een selectie transitiemetaalcomplexen Cu(II), Ni(II), Co(II), V(IV)O) en de octa-alkoxy gesubstitueerde lanthanide(III) complexen.

In een eerste deel wordt de synthese van de verbindingen uitvoerig besproken. Een belangrijk probleem was de controle van de zuiverheid van de gesynthetiseerde verbindingen. De resultaten van CHN elementaire analyse zijn voor deze verbindingen onbetrouwbaar. We beoordeelden de zuiverheid van de bekomen verbindingen dan ook louter op de MALDI-TOF, IR en UV/VIS spectra. De globale opbrengsten voor de octa-gesubstitueerde liganden en complexen waren in het algemeen vrij laag via de traditionele synthesepaden. We slaagden er wel in om betere rendementen te bekomen voor de ongesubstitueerde ftalocyanine lanthanide complexen met behulp van een vrij recente techniek die microgolven gebruikt als energiebron tijdens de synthese. Deze methode dient echter nog op punt gesteld te worden omdat de resultaten slecht reproduceerbaar waren en we geen controle hadden over de instrumentele parameters van de (commerciële) microgolfoven. Pogingen om gesubstitueerde (metallo)ftalocyanines te bereiden waren niet succesvol met deze techniek.

Het thermisch gedrag van onze producten werd bestudeerd met behulp van optische microscopie, DSC, TGA-DTA en hoge-temperatuur X-stralen diffractie. Al onze verbindingen hadden een relatief breed mesofasegebied. Bovendien vertoonden alle producten een enantiotroop vloeibaar-kristallijn gedrag, hoewel het soms moeilijk was om het klaarpunt te detecteren omwille van gelijktijdige ontbinding van het staal. Polymorfisme was voor geen enkele verbinding waarneembaar. Via optische polarisatiemicroscopie en XRD-diffractie experimenten werd voor de meeste verbindingen de hexagonale kolomvormige mesofase (Col_h) vastgesteld, enkel de vanadylcomplexen vertoonden een rechthoekige kolomvormige mesofase (Col_r). Zijketens met minder dan vier koolstofatomen vertoonden geen mesofase. Voor alle onderzochte homologe reeksen kende het smeltpunt een dalende trend met toenemende ketenlengte. De afname was drastischer voor de kortere ketenlengtes. Voor de langere ketenlengtes was er geen rechtstreeks verband waarneembaar voor de lanthanidecomplexen. De

klaarpunten vertoonden een sterkere daling dan de smeltpunten met toenemende ketenlengte. Dit was het meest uitgesproken voor de octa-alkoxy ketens.

De smelttemperaturen lagen in het algemeen hoger voor de octa-alkyl gesubstitueerde ftalocyanines dan voor beide andere types (octa-alkyl >> octa-alkoxy > octa-alkoxymethyl). De zijketens bepalen de manier waarop naburige kolommen georiënteerd zijn en zij bepalen ook grotendeels de orde binnenin de kolommen ten gevolge van specifieke sterische.

De vanadylcomplexen vertoonden het sterkst stabiliserende effect op de mesofase voor de octa-alkoxy en octa-alkyl verbindingen in vergelijking met het metaalvrije ligand ($\Delta T_m \approx 30°C$). Deze complexen smolten bij lagere tempraturen dan de liganden. Voor de andere transitiemetaalcomplexen (Zn^{2+}, Cu^{2+}, Ni^{2+}, Co^{2+}) namen de smeltpunten toe, maar werd de mesofase toch gestabiliseerd door de sterke toename van het klaarpunt. De sterkste toename van het smeltpunt werd genoteerd voor de Zn^{2+} complexen (volgorde: $Ni^{2+} < Cu^{2+} \approx Co^{2+} < Zn^{2+}$). Voor de alkyl-type verbindingen was de correlatie tussen het centraal metaalion en de transitietemperaturen minder uitgesproken. Lanthanide-ionen verkleinden het mesofasegebied door zowel een toename van het smeltpunt als een afname van het klaarpunt.

Het derde deel van deze thesis onderzocht de optische eigenschappen van de verbindingen met behulp van absorptie en MCD-spectroscopie. Al onze producten vertoonden een sterke lichtabsorptie. Het effect van perifere substitutie op de optische eigenschappen is minimaal. De keuze van het centraal metaalion daarentegen, beïnvloed de spectrale eigenschappen wel degelijk. Dit is vooral zo voor de vanadyl en lanthanide complexen.

List of publications and communications at conferences

Publications

"Synthesis, Spectral and Mesomorphic Properties of Octa-alkoxy Substituted Phthalocyanine Ligands and Lanthanide Complexes", Materials Science and Engineering C 18, 229-238, 2001.

"Synthesis, Structural and Mesomorphic Properties of a Homologeous Series of Octa-alkoxy Substituted Phthalocyanines Complexed with Cobalt(II)", Journal of Material Chemistry, accepted.

"Thermal and optical behavior of octa-alkoxy substituted phthalocyaninatovanadyl complexes", Liquid Crystals, accepted.

"Liquid-Crystalline Octa-alkoxy Substituted Phthalocyanines Complexed with Transition Metals", Liquid Crystals, submitted.

"Mesomorphism and Optical Properties of Octa-alkoxy Substituted Phthalocyanine Lanthanide Complexes: Influence on Peripheral Chain Length and Central Metal Ion", Chemical Materials, submitted.

Communications at conferences

"Lanthanidecomplexen van Octa-alkyloxy Gesubstitueerde Ftalocyanines : Invloed van de Alkoxyketenlengte en het Centraal Metaalion op de Thermische en Optische Eigenschappen", 5e Vlaams Jongerencongres van de Chemie", Brussel, 11 april 2000 (poster & lecture)

"Lanthanide Complexes of Octa-alkyloxy Substituted Phthalocyanines : Influence of the Alkoxy Chain Length and the Central Metal Ion on Thermal and Optical Properties", First International Conference on Porphyrins and Phthalocyanines", Dijon, Frankrijk, 25-30 juni 2000 (poster)

"Octa-alkyloxy substituted Phthalocyanines : Influence of the Alkoxy Chain Length and the Central Metal Ion on Thermal Properties", 2nd International Conference on Supramolecular Science & Technology", Leuven 10-14 september 2000 (poster)

"Peripheral substituted octa-alkoxy Phthalocyanines: Influence of the Alkoxy Chain Length and the Central Metal Ion on Thermal and Optical Properties", 4th International Conference on f-elements", Madrid, Spanje, 17-21 september 2000 (poster)

"Vloeibaar-kristallijne octa-alkoxy gesubstitueerde ftalocyanines gecomplexeerd met transitiemetalen: thermische en optische eigenschappen", 6e Vlaams Jongerencongres van de Chemie, Antwerpen, 9 april 2002 (poster)

Appendix A

MESOMORPHIC METAL-FREE, PERIPHERALLY OCTA-SUBSTITUTED PHTHALOCYANINES, SYNTHESISED PRIOR TO THIS WORK

Substituent	Ion	Range	Mesophase	Reference
$-C_5H_{11}$	H_2	323-379	Col_{hd}	[EngBas93]
$-C_6H_{13}$	H_2	250-363	Col_{hd}	[EngBas93]
$-C_7H_{15}$	H_2	185 - …	Col_{hd}	[NisAzu92]
$-C_8H_{17}$	H_2	186-325	Col_{hd}	[EngBas93]
$-C_9H_{19}$	H_2	159 - …	Col_{hd}	[NisAzu92]
$-C_{10}H_{21}$	H_2	163-282	Col_{hd}	[EngBas93]
$-C_{11}H_{23}$	H_2	130 - …	Col_{hd}	[NisAzu92]
$-C_{12}H_{25}$	H_2	120-252	Col_{hd}	[OhtJac88]
$-C_{13}H_{27}$	H_2	119 - …	Col_{hd}	[NisAzu92]
$-C_{14}H_{29}$	H_2	121 - …	Col_{hd}	[NisUen89]
$-C_{16}H_{33}$	H_2	108-196	Col_{rd}, (170) Col_{hd}	[ClaMcK95]
$-OC_6H_{13}$	H_2	119 to > 350	Col_{ho}	[vanNee89]
$-OC_7H_{15}$	H_2	104 to > 350	Col_{ho}	[vanNee89]
$-OC_8H_{17}$	H_2	94 to > 350	Col_{ho}	[vanNee89, ForSum94]
$-OC_9H_{19}$	H_2	101 to > 350	Col_{ho}	[vanNee89]
$-OC_{10}H_{21}$	H_2	94 to > 350	Col_{ho}	[vanNee89]
$-OC_{11}H_{23}$	H_2	83 to > 350	Col_{ho}	[vanNee89]
$-OC_{12}H_{25}$	H_2	83 to > 350	Col_{ho}	[vanNee89, ForSum94]
$-OC_{18}H_{37}$	H_2	98-247	Col_h	[SchWar94, ForSum94]
$-CH_2OC_8H_{17}$	H_2	67-320	Col_{hd}	[SimBas93]
$-CH_2OC_{12}H_{25}$	H_2	79-260	Col_x, (185) Col_{hd}	[GuiSko83]
$-CH_2OC_{18}H_{37}$	H_2	62-193	Col_{hd}	[SimBas93]

[ClaMcK95] G.J. Clarkson, N.B. McKeown and K.E. Treacher, *J. Chem. Soc. Perkin Trans. I*, 1817, 1995.

[EngBas93] M.K. Engel, P. Bassoul, L. Bosio, H. Lehmann, M. Hanack and J. Simon, *Liq. Cryst.*, **15**, 709, 1993.

[ForSum94] W.T. Ford, L. Sumner, W. Zhu, Y.H. Chang, PJ. Um, K.H. Choi, P.A. Heiney, N.C. Maliszewskyj, *New J. Chem.*, **18**, 495, 1994.

[GuiSko83] D. Guillon, A. Skoulios, C. Piechocki, J. Simon, P. Weber, *Mol. Cryst. Liq. Cryst.*, **100**, 275, 1983.

[NisAzu92] H. Nishi, N. Azuma, K. Kitahara, *J. Heterocycl. Chem.*, **29**, 475, 1992.

[NisUen89] H. Nishi, S. Ueno, *Nippon Kagaku Kaishi*, 983, 1989.

[OhtJac88] K. Ohta, L. Jacquemin, C. Sirlin, L. Bosio and J. Simon, *New. J. Chem.*, **12**, 751, 1988.

[SchWar94] P.G. Schouten, J.W. Warman, M.P. de Haas, C.F. van Nostrum, G.H. Gelinck, R.J.M. Nolte, M.J. Copyn, J.W. Zwikker, M.K. Engel, M. Hanack, Y.H. Chang and W.T. Ford, *J. Am. Chem. Soc.* **116**, 6880, 1994.

[SimBas93] J. Simon, P. Bassoul, "Phthalocyanine based Liquid Crystals: Towards Submicronic Devices" in *Phthalocyanines, Properties and Applications*, eds. C.C. Leznoff en A.B.P. Lever, VCH Weinheim, Volume 2, 1993.

[vanNee89] J.F. van der Pol, E. Neeleman, J.W. Zwikker, R.J.M. Nolte, W. Drenth, J. Aerts, R. Visser, S.J. Picken, *Liq. Cryst.*, **6**, 577, 1989.

Appendix B

MESOMORPHIC PERIPHERALLY OCTA-SUBSTITUTED PHTHALOCYANINE TRANSITION METAL COMPLEXES, SYNTHESISED PRIOR TO THIS WORK

Substituent	Ion	Range	Mesophase	Reference
$-C_5H_{11}$	Cu	342 to >380	Col_{hd}	[EngBas93]
$-C_6H_{13}$	Cu	259 to > 380	Col_{hd}	[EngBas93]
$-C_6H_{13}$	Ni	260 to >380	Col_{hd}	[EngBas93]
$-C_7H_{15}$	Cu	191 -…	Col_{hd}	[NisAzu92]
$-C_8H_{17}$	Cu	180 to > 380	Col_{hd}	[EngBas93]
$-C_8H_{17}$	Ni	190-373	Col_{hd}	[EngBas93]
$-C_9H_{19}$	Cu	175 - …	Col_{hd}	[NisAzu92]
$-C_{10}H_{21}$	Cu	169-351	Col_{hd}	[EngBas93]
$-C_{10}H_{21}$	Ni	168-333	Col_{hd}	[EngBas93]
$-C_{11}H_{23}$	Cu	155 - …	Col_{hd}	[NisAzu92]
$-C_{12}H_{25}$	Cu	150 - …	Col_{hd}	[NisUen89]
$-C_{13}H_{27}$	Cu	117 - …	Col_{hd}	[NisAzu92]
$-C_{14}H_{29}$	Cu	115 - …	Col_{hd}	[NisUen89]
$-OC_6H_{13}$	Cu	120 to > 350	Col_{ho}	[vanNee89]
$-OC_7H_{15}$	Cu	110 to > 350	Col_{ho}	[vanNee89]
$-OC_8H_{17}$	Cu	112 to > 350	Col_{ho}	[vanNee89, ForSum94]
$-OC_9H_{19}$	Cu	106 to > 350	Col_{ho}	[vanNee89]
$-OC_{10}H_{21}$	Cu	104 to > 350	Col_{ho}	[vanNee89]
$-OC_{10}H_{21}$	Ni	87 - 111		[HaiKne95]
$-OC_{11}H_{23}$	Cu	92 to > 350	Col_{ho}	[vanNee89]
$-OC_{12}H_{25}$	Cu	95 to > 300	Col_{ho}	[vanNee89, ForSum94]
$-OC_{12}H_{25}$	Pt	77 to > 350	Col_{ho}	[VacDop92]
$-OC_{12}H_{25}$	Co	85 - 345	Col_{ho}	[SevUnd93]
$-OC_{12}H_{25}$	Zn	99 to > 350	Col_{ho}	[SevUnd93]
$-OC_{12}H_{25}$	Ni	96 - 254	Col_{ho}	[SevUnd93]
$-OC_{18}H_{37}$	Cu	52 - 257	Col_{ho}	[ForSum94]
$-CH_2OC_{12}H_{25}$	Cu	53 to >300	Col_{hd}	[PieSim82]
$-CH_2OC_{12}H_{25}$	Zn	78 to >300	Col_x, (?) Col_{hd}	[GuiWeb85]
$-CH_2OC_{12}H_{25}$	Mn	44-280	Col_x, (?) Col_{hd}	[GuiWeb85]
$-CH_2OC_8H_{17}$	Co	72		[HanBec87]
$-CH_2OC_8H_{17}$	Ni	68		[HanBec87]

[EngBas93] M.K. Engel, P. Bassoul, L. Bosio, H. Lehmann, M. Hanack and J. Simon, *Liq. Cryst.*, **15**, 709, 1993.

[ForSum94] W.T. Ford, L. Sumner, W. Zhu, Y.H. Chang, PJ. Um, K.H. Choi, P.A. Heiney, N.C. Maliszewskyj, *New J. Chem.*, **18**, 495, 1994.

[NisAzu92] H. Nishi, N. Azuma, K. Kitahara, *J. Heterocycl. Chem.*, **29**, 475, 1992.

[NisUen89] H. Nishi, S. Ueno, *Nippon Kagaku Kaishi*, 983, 1989.

[PieSim82] C. Piechocki, J. Simon, A. Skoulios, D. Guillon, P. Weber, *J. Am. Chem. Soc.*, **104**, 5245, 1982.

[SevUnd93] L.M. Severs, A.E. Underhill, D. Edwards, P. Wight, D. Thetford, *Mol. Cryst. Liq. Cryst.*, **234**, 235, 1993.

[VacDop92] J. Vacus, P. Doppelt, J. Simon, G. Memetzidis, *J. Mater. Chem.*, **2**, 1065, 1992.

[vanNee89] J.F. van der Pol, E. Neeleman, J.W. Zwikker, R.J.M. Nolte, W. Drenth, J. Aerts, R. Visser, S.J. Picken, *Liq. Cryst.*, **6**, 577, 1989.

[WebGui87] P. Weber, D. Guillon, A. Skoulios, *J. Phys. Chem.*, **91**, 2242, 1987.

Appendix C

MESOMORPHIC PERIPHERALLY OCTA-SUBSTITUTED PHTHALOCYANINE LANTHANIDECOMPLEXES, SYNTHESISED PRIOR TO THIS WORK

Substituent	Ion	Range	Mesophase	Reference
$-C_8H_{17}$	Lu	79-82	Col_{hd}	[KomOht94]
$-C_{12}H_{26}$	Lu	32-44	Col_{hd}	[KomOht94]
$-C_{16}H_{33}$	Lu	30-40	Col_{hd}	[KomOht94]
$-C_{18}H_{37}$	Lu	30-43	Col_{hd}	[KomOht94]
$-OC_{12}H_{25}$	Lu	85-185	Col_h	[BelSir89]
$-CH_2OC_{18}H_{37}$	Lu	51-56	Col_h	[PieSim85]

[BelSir89] Z. Belarbi, C. Sirlin, J. Simon, JJ. Andre, *J. Phys. Chem.*, **93**, 8105, 1989.

[KomOht94] T. Komatsu, K. Ohta, T. Fujimoto, I. Yamamoto, *J. Mater. Chem.*, **4**, 533, 1994.

[PieSim85] C. Piechocki, J. Simon, J.J. André, D. Guillon, P. Petit, A. Skoulios, P. Weber, *Chem. Phys. Lett.*, **122**, 124, 1985.

Appendix D

X-RAY EQUIPMENT USED

The recognition of textures by the use of POM requires experience and it often only gives a first indication of the actual mesophase. By means of X-ray diffraction experiments, mesophases can be unambigously identified.

The periodic structures (the electron clouds to be precise) in the liquid-crystalline phase give the (diffracted) beam information on the type of the phase. The electromagnetic radiation that is used (X-rays) have a wavelength of the same order as the interatomar distances. Every atom produces a diffracted wave and these waves of different sources can interfere.

The possible diffraction directions are well defined. Consider a set of planes *hkl* with parallel planes that are equidistant to each other. These planes are defined by the Miller indices *h, k* and *l* in a way that *a/h* represents the distance between two consecutive planes *(h, k, l)* in the direction of *a* (idem for *b/k* en *c/l*). In this way the directions of the diffracted beams match the directions of the set of planes in accord with Bragg's law:

$$n \cdot \lambda = 2 \cdot d \cdot \sin\theta$$

where

λ: wavelength of the radiation

d: distance between the plains

θ: angle of diffraction

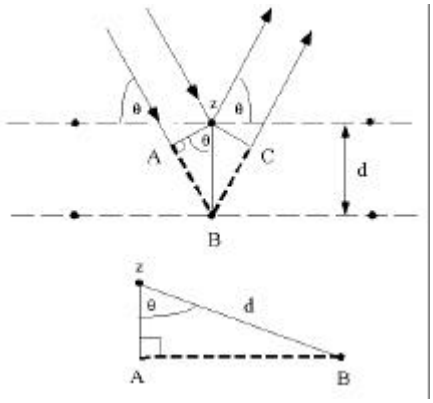

Everey atoms has his own “diffractive power”, quantified in the (atomic) scattering factor *f.* For a diffraction plane *(hkl)* the intensity of the diffracted beam, determined by the position of each atom, is given by the structure factor *F(hkl)*:

$$F(hkl) = \sum_{i=1}^{n} f_i e^{2\pi j(hx_i + ky_i + lz_i)}$$

The structure factors *F(hkl)* are directly related to the Intensity I *(hkl)* of the corresponding reflection *h,k,l*:

$$I_{hkl} \propto |F_{hkl}|^2$$

Hence, by measuring diffraction angles and intensities we obtain information on the way the atoms are arranged within the network. Note that we cannot calculate *F* from the intensity; only the scalar magnitude of F, |F|, and not the complex scattering factor F itself is available to us directly from the experiment. This is the root cause of the so-called ‘phase problem’, which we will not discuss here.

The X-ray diffraction patterns were obtained with 3 different experimental setups. In all cases, the crude powders were measured in Lindemann cappilaries of 1 mm diameter. The XRD patterns were obtained with two different experimental set-ups, the crude powder was filled in Lindemann capillaries of 1 mm diameter. A

linear monochromatic Cu-Kα_1 beam (λ = 1.5405Å) was obtained using a Guinier camera with a sealed-tube generator (900 W) and a Debye-Scherrer camera equipped with a bent quartz monochromator and an electric oven. A first set of diffraction patterns was registered with a gas curved counter "Inel CPS 120" associated with a data acquisition computer system; periodicities up to 60 Å can be measured, and the sample temperature is controlled within ±0.05°C. The two other sets of diffraction patterns were registered on image plate. With the Guinier camera, periodicities up to 90 Å can be measured and the phase symmetry was determined (the sample temperature is controlled within ±0.3°C). The other set up, periodicities up to 300Å can be measured, and the cell parameters were calculated from the position of the reflection at the smallest Bragg angle, which was in all cases the most intense.

Guinier type: 0 to 70 Å, used for determining the symmetry by indexation of the reflections and calculating the ratio's

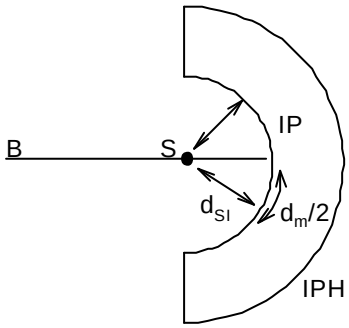

B: incoming X-ray beam
S: sample
IPH: Image Plate Holder
IP: image plate
d_{SI}: distance sample and Image Plate (12.5 cm)
d_m: measured distance of reflection on Image Plate

formula to determine d (distance between reflection planes):

$$d = \lambda/(2\cdot\sin\theta) = \lambda/(2\cdot\sin(d_m/2))$$

(where d_m is expressed in degrees by multiplying by $180/\pi$)

Inel linear: 0-5 ° (2θ), determination of d_{10} (exact), d_{10} in function of chain length and temperature

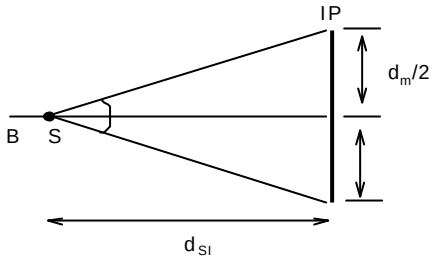

B: incoming X-ray beam
S: sample
IP: image plate
d_{SI}: distance sample and Image Plate (38.4 cm)
d_m: measured distance of reflection on Image Plate

formula to determine d (distance between reflection planes):

$$\theta = 0.5 \cdot \text{artg}(d_m/2 \cdot d_{SI})$$

$$d = \lambda/(2 \cdot \sin\theta) = \lambda/[2 \cdot \sin(0.5 \cdot \text{artg}(d_m/2 \cdot d_{SI})]$$

Inel courbe: small angles + diffuse regions (melting of the chains, periodicity, …)

The setup can be compared with the Guinier chambers, except the detection system which is fully automated; the data are collected as ASCII-files and treated with the aid of ORIGIN software.

Appendix E

MAGNETIC CIRCULAR DICHROISM

Besides the classical absorption spectroscopy also magnetic circular dichroism (MCD) measurements can be done. MCD measures a sample's differential electronic absorption of left and right circularly polarized light in a longitudinal magnetic field i.e. the light beam is parallel to the magnetic field lines. The MCD-signal is the difference in absorption ΔA between the two light beams.

$$\Delta A = A_{lcp} - A_{rcp} \qquad (A = \text{absorbance})$$

MCD-spectroscopy is based on the so-called Zeeman-effect: in a magnetic field every electronic degeneracy is removed.

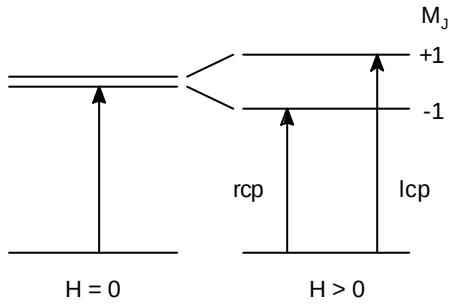

MCD is an optical probe of paramagnetism that details the electronic and magnetic properties of the ground states of metal centres. It can be used also to identify and assign optical transitions from metal sites.

From the spectra electronic excited state properties and assignments (metal d-d and CT transitions and ligand π-π^* transitions) can be made and ground state magnetic properties (g-values, spin state, zero-field splittings, magnetic couplings) can be studied. As an example, it can be deduced whether an electronic transition takes

place to a degenerate or a non-degenerate state. By using MCD the metal centre oxidation state and spin state can be determined. It is also possible to study the effects of inhibitors/substrate/mutations on the electronic and magnetic properties of the metal centre(s). Another possibility is to study the axial ligands on low-spin ferric heme centres and selective determination of the electronic properties of *paramagnetic* metal centres via temperature-dependent studies.

MCD is an advantageous technique because all matter exhibits MCD. Moreover, improved resolution of electronic transitions compared to absorption measurements is common.

Selective investigation of magnetic properties of individual metal centres via temperature and magnetic field dependence studies of discrete transitions

MCD does not give any information on the metal coordination environment (this can only be inferred indirectly from the observed electronic and magnetic properties). Furthermore, detailed electronic assignments are difficult for low-symmetry metal centres and the technique is not useful for investigating non-chromophoric metal centres (e.g. Zn^{2+}). MCD is also insensitive to weak magnetic interactions that are smaller than the Zeeman interaction.

Other disadvantages are the difficulties in interpreting the signs and relative intensities of MCD bands for low-symmetry chromophores and the analysis of variable-temperature/variable-field MCD data in terms of magnetic ground state properties (explicitly consideration of the transition polarization is necessary) .